



**UCL**

# **Technologies to improve the performance of Wireless Sensor Networks in high-traffic applications**

A thesis submitted for the degree of Doctor of Philosophy  
in Electronic and Electrical Engineering

Jan. 2012

QIN, Fei

Department of Electronic and Electrical Engineering  
University College London

## Statement of Originality

I, QIN, Fei, confirm that the work presented in this thesis is my own. Where information has been derived from other sources, I confirm that this has been indicated in the thesis

Signed \_\_\_\_\_

Date \_\_\_\_\_

---

## Abstract

The expansion of wireless sensor networks to advanced areas, including structure health monitoring, multimedia surveillance, and health care monitoring applications, has resulted in new and complex problems. Traditional sensor systems are designed and optimised for extremely low traffic loads. However, it has been witnessed that network performance drops rapidly with the higher traffic loads common in advanced applications. In this thesis, we examine the system characteristics and new system requirements of these advanced sensor network applications. Based on this analysis, we propose an improved architecture for wireless sensor systems to increase the network performance while maintaining compatibility with the essential WSN requirements: low power, low cost, and distributed scalability.

We propose a modified architecture deriving from the IEEE 802.15.4 standard, which is shown to significantly increase the network performance in applications generating increased data loads. This is achieved by introducing the possibility of independently allocating the sub-carriers in a distributed manner. As a result, the overall efficiency of the channel contention mechanism will be increased to deliver higher throughput with lower energy consumption. Additionally, we develop the concept of increasing the data transmission efficiency by adapting the spreading code length to the wireless environment. Such a modification will not only be able to deliver higher throughput but also maintain a reliable wireless link in the harsh RF environment. Finally, we propose the use of the battery recovery effect to increase the power efficiency of the system under heavy traffic load conditions.

These three innovations minimise the contention window period while maximising the capacity of the available channel, which is shown to increase network performance in terms of energy efficiency, throughput and latency. The proposed system is shown to be backwards compatible and able to satisfy both traditional and advanced applications and is particularly suitable for deployment in harsh RF environments. Experiments and analytic

techniques have been described and developed to produce performance metrics for all the proposed techniques.

---

## Acknowledgements

Obtaining a PhD is never an easy task. Throughout my time I was lucky enough to be supervised by Dr. John E. Mitchell who guided me during my research, teaching me the methodology to solve research problems, which I hope will prove invaluable for my career. To John, I express my sincerest gratitude.

I extend my thanks to the knowledgeable and friendly academics of the Telecommunications Research Group: Prof. Yang Yang, Dr. Ioannis Andreopoulos, and Prof. Izzat Darwazeh for their advice, understanding and encouragement in my work. Deepest thanks go to Prof. Teng Long and Prof. Yong Ma for their guidance at different stages of my life.

I would also like to thank my friends, with whom I carried out research: Bing Xia, Bowen Cao, Dr. Xuewu Dai and Dr. Manoj Thakur for their support. I would also like to thank all the members of the group: Oluyemi Omomukuyo, George Konstantinou, Haixia Chen, Yu Chen, Dujdow Buranapanichkit, George Smart, Safa Ahmed, Ryan Grammenos, and Marcus Perrett for the memorable times that we shared together.

As well as my colleagues, I am indebted to my wife, Huiling Chen, without whose enduring support, understanding and encouragement, I would never have achieved this PhD. I thank my parents for their constant support and invaluable advice.

Finally, I express my sincere appreciation to the Dorothy Hodgkin Postgraduate Award (DHPA) co-funded by the British Telecom and EPSRC for financially sponsoring my research.

---

## Table of content

Statement of Originality.....	2
Abstract .....	3
Acknowledgements.....	5
Table of content.....	6
List of Figures .....	9
List of Tables .....	11
List of Acronyms.....	12
Chapter 1. Introduction .....	15
1.1 Aim and Scope .....	15
1.2 Contributions and Publications.....	20
1.3 Thesis Organisation.....	22
Chapter 2. Wireless Sensor Network.....	24
2.1 WSN: From Traditional to Advance.....	24
2.2 IEEE802.15.4 Technology.....	27
2.2.1 Physical layer of IEEE 802.15.4.....	28
2.2.2 MAC layer of IEEE 802.15.4.....	29
2.3 Related Works.....	30
2.4 Summary.....	36
Chapter 3. Increase the Efficiency of Channel Contention using a Multi-carrier	
Architecture .....	37
3.1 Introduction .....	37
3.2 System architecture .....	42
3.2.1 CFO problem in multi-carrier system.....	42
3.2.2 PAPR problem .....	50
3.3 Low cost solution for WSN.....	51
3.4 Experiment Validation .....	59
3.5 Performance Evaluation .....	62
3.5.1 Renewal process of Slotted Aloha.....	63
3.5.2 Analytic Model under ideal channel conditions.....	65
3.5.3 Model Extension.....	69

---

3.5.4	Performance Analyses.....	71
3.6	Conclusion.....	77
Chapter 4.	Error Performance Estimation for Adaptive Spreading Code Length based WSN .....	79
4.1	Introduction .....	79
4.2	Adaptive Spreading Code Length in IEEE 802.15.4 System .....	81
4.3	Error Performance Estimation Model for Adaptive Spreading Code Length in IEEE 802.15.4 .....	84
4.4	Empirical Validation of the Model .....	88
4.4.1	Experiment setup .....	88
4.4.2	Validation of error performance estimation model.....	90
4.4.3	Analysis of throughput Performance .....	93
4.4.4	Power efficiency.....	99
4.5	Conclusion.....	100
Chapter 5.	Effective-SNR Estimation for Wireless Sensor Network Using Kalman Filter	102
5.1	Introduction .....	102
5.2	Problem Formulation .....	105
5.2.1	Notation .....	105
5.2.2	Propagation Model in the Harsh RF Environment .....	106
5.2.3	Effective-SNR model.....	109
5.3	Kalman Filter Design .....	113
5.3.1	Linearisation of the measurements .....	115
5.3.2	Kalman Filter Design.....	116
5.3.3	Estimating the covariance matrices .....	119
5.3.4	Simplified implementation of Kalman filter.....	122
5.4	Experiment Results .....	123
5.5	Conclusion.....	130
Chapter 6.	Utilising the Adaptive Spreading Code Length for the MAC Protocol Design of WSNs .....	131
6.1	Introduction .....	131
6.2	Design of AS-MAC protocol.....	134
6.2.1	Modifications to Carrier Sense.....	134
6.2.2	Packets Aggregation.....	139
6.2.3	Optimisation of the spreading code length .....	141

---

6.2.4	Overall protocol architecture .....	144
6.3	Performance Evaluation using Experimental approach.....	146
6.3.1	Throughput performance.....	147
6.3.2	Throughput performance with variable environment noise .....	151
6.3.3	Energy efficiency .....	157
6.4	Conclusion.....	162
Chapter 7.	Utilising the battery recovery effect in WSN with high traffic load applications. .....	164
7.1	Introduction .....	164
7.2	Experiment demonstration of battery recovery effect in WSN platforms .....	166
7.3	Lifetime and latency trade-off in large scale sensor network .....	170
7.3.1	Introduction of the simplified battery model .....	170
7.3.2	Battery recovery awareness design in large scale WSN .....	171
7.3.3	Analysis of simulation results.....	172
7.4	Conclusion.....	181
Chapter 8.	Conclusion and Future Work.....	183
8.1	Conclusion.....	183
8.2	Suggestion for Future Works .....	186
References List	.....	188

## List of Figures

FIGURE 1.1. TRANSMISSION SCHEME IN WSN SYSTEM .....	16
FIGURE 1.2. EXPECTED SYSTEM ARCHITECTURE .....	19
FIGURE 2.1. ENGINE SECTION IN THE BP TRAIL SITE [14] .....	25
FIGURE 2.2. MODULATION PROCESS OF IEEE802.15.4 .....	28
FIGURE 2.3. O-QPSK MODULATION WITH HSPTS FILTER [16]. .....	29
FIGURE 2.4. PACKET CONSIST OF IEEE802.15.4 .....	29
FIGURE 3.1. ADAPTIVE BANDWIDTH SYSTEM ARCHITECTURE .....	40
FIGURE 3.2. TRAFFIC DIRECTION IN WSN SYSTEM .....	41
FIGURE 3.3. AMBIGUITY FUNCTION OF RECTANGLE FUNCTION .....	46
FIGURE 3.4. CFO IN DIFFERENT SCENARIOS OF MULTI-CARRIER BASED SYSTEMS .....	48
FIGURE 3.5. PAPR PROBLEM .....	51
FIGURE 3.6. AMBIGUITY FUNCTION OF GAUSSIAN PULSE SHAPING FILTER .....	52
FIGURE 3.7. ROTATION EFFECT ON DIFFERENT SUB-CARRIERS .....	55
FIGURE 3.8. GAUSSIAN AMBIGUITY FUNCTION. ....	56
FIGURE 3.9. MODIFIED MULTI-CARRIER BASED SYSTEM ARCHITECTURE.....	57
FIGURE 3.10. TWO DIMENSION POWER SCALABILITY .....	59
FIGURE 3.11. EXPERIMENT SETUP OF THE MULTI-CARRIER BASE WSN ARCHITECTURE .....	60
FIGURE 3.12. PHOTO OF THE MULTI-CARRIER BASE WSN EXPERIMENT .....	61
FIGURE 3.13. SIGNAL SPECTRUM IN EXPERIMENT, CAPTURED FROM FSQ40 .....	61
FIGURE 3.14. ERROR PERFORMANCE RESULT OF THE MULTI-CARRIER BASED SYSTEM .....	62
FIGURE 3.15. CHANNEL REGULATION FOR MULTI-CARRIER BASED SYSTEM .....	63
FIGURE 3.16. RENEWAL PROCESS OF SLOTTED ALOHA .....	64
FIGURE 3.17. SIMULATION RESULT VERSUS ANALYTIC RESULT ( $W=8, M=4, Q=0.1, B=4$ ) .....	72
FIGURE 3.18. AVERAGE SERVICE DELAY .....	73
FIGURE 3.19. AVERAGE ENERGY CONSUMPTION EVERY LEVEL 2 CYCLE .....	75
FIGURE 3.20. PERFORMANCE FOR SIMILAR THROUGHPUT .....	76
FIGURE 4.1. MODIFICATION IN THE MAPPING SCHEME OF IEEE 802.15.4 STANDARD .....	82
FIGURE 4.2. THEORETIC BER PERFORMANCE ESTIMATED USING HAMMING DISTANCE METHOD .....	84
FIGURE 4.3. HISTOGRAM OF MAXIMUM TOLERANT NUMBER OF THE ERROR CHIP .....	86
FIGURE 4.4. EXPERIMENT ARCHITECTURE TO DETERMINE THE ERROR PERFORMANCE IN AN AWGN CHANNEL .....	89
FIGURE 4.5. PHOTO OF EXPERIMENT SETUP TO DETERMINE THE ERROR PERFORMANCE IN AN AWGN CHANNEL.....	90
FIGURE 4.6. IEEE 802.15.4 UN-SLOTTED MAC SCHEME .....	90
FIGURE 4.7. RECOVERED PACKET RECEIVED RATE FROM EXPERIMENT RESULTS.....	92
FIGURE 4.8. ERROR PERFORMANCES OF DIFFERENT SPREADING CODE LENGTHS .....	92
FIGURE 4.9. THROUGHPUT PERFORMANCE WITH VARIABLE SIGNAL STRENGTHS .....	95
FIGURE 4.10. THROUGHPUT PERFORMANCE WITH VARIABLE NOISE LEVELS.....	95
FIGURE 4.11. THROUGHPUT PERFORMANCE WITH VARYING PACKET LENGTHS.....	96
FIGURE 4.12. EFFECT OF BACKOFF WINDOW SIZE $BE=4$ .....	97
FIGURE 4.13. EFFECT OF BACKOFF WINDOW SIZE $BE=5$ .....	98
FIGURE 4.14. THROUGHPUT VERSUS DISTANCE .....	99
FIGURE 4.15. POWER CONSUMPTION FOR DIFFERENT SPREADING MODES .....	100
FIGURE 5.1. PER-LQI EMPIRICAL RESULT .....	110
FIGURE 5.2. AVERAGE LQI VS INSTANTANEOUS LQI .....	112
FIGURE 5.3. ARCHITECTURE OF KALMAN FILTER.....	114
FIGURE 5.4. MEASUREMENT NOISE .....	120

FIGURE 5.5. TRAINING SEQUENCE OF PRR .....	122
FIGURE 5.6. CONVERGE PROCESS OF K .....	122
FIGURE 5.7. FREQUENCY SELECTIVE CHANNEL FOR EFFECTIVE-SNR ESTIMATION EXPERIMENT .....	124
FIGURE 5.8. EXPERIMENT RESULT IN TIME SEQUENCE UNDER INDOOR ENVIRONMENT WITH VARYING ENVIRONMENT NOISE .....	125
FIGURE 5.9. EXPERIMENT RESULT IN VARYING NOISE STRENGTHS UNDER INDOOR ENVIRONMENT .....	126
FIGURE 5.10. CORRELATION RESULTS UNDER INDOOR ENVIRONMENT WITH VARYING ENVIRONMENT NOISE .....	127
FIGURE 5.11. EXPERIMENT RESULT IN TIME SEQUENCE WITH VARYING TRANSMITTING SIGNAL STRENGTHS .....	127
FIGURE 5.12. EXPERIMENT RESULT IN VARYING TRANSMITTING SIGNAL STRENGTHS .....	128
FIGURE 5.13. EXPERIMENT RESULT UNDER INDOOR ENVIRONMENT WITH VARYING TRANSMIT POWER .....	128
FIGURE 6.1. IEEE 802.15.4 MAC PROTOCOL .....	132
FIGURE 6.2. FOUR WAY HAND-SHAKE BASED PROTOCOL .....	133
FIGURE 6.3. EFFECT OF CARRIER SENSE .....	135
FIGURE 6.4. TIME CONSTRAINTS OF THE CARRIER SENSE OPERATION .....	136
FIGURE 6.5. CARRIER SENSE MODIFICATION IN AS-MAC .....	138
FIGURE 6.6. MODIFICATION OF THE PACKET STRUCTURE IN AS-MAC .....	140
FIGURE 6.7. BASIC SCHEME OF AS-MAC .....	141
FIGURE 6.8. ALGORITHM FOR TRANSMISSION OPERATION .....	144
FIGURE 6.9. ALGORITHM FOR RECEIVING OPERATION .....	145
FIGURE 6.10. PHOTO OF THE AS-MAC EXPERIMENT SETUP .....	146
FIGURE 6.11. CAPACITY COMPARISON BETWEEN THE PROPOSED AS-MAC AND STANDARD IEEE 802.15.4 MAC .....	147
FIGURE 6.12. THROUGHPUT PERFORMANCE IN STAR TOPOLOGY .....	148
FIGURE 6.13. TWO FLOW TOPOLOGY. NODE 1 AND 3 ARE EXPOSED TERMINALS .....	149
FIGURE 6.14. THROUGHPUTS IN EXPOSED TERMINAL SCENARIO .....	150
FIGURE 6.15. TWO FLOW TOPOLOGY. NODE 3 IS THE HIDDEN TERMINAL OF NODE 0 .....	150
FIGURE 6.16. THROUGHPUTS IN THE HIDDEN TERMINAL SCENARIO .....	151
FIGURE 6.17. THROUGHPUT PERFORMANCE OF AS-MAC WITH VARIABLE ENVIRONMENT NOISE .....	152
FIGURE 6.18. THROUGHPUT PERFORMANCE OF AS-MAC WITH ENVIRONMENT NOISE UNDER STAR TOPOLOGY .....	153
FIGURE 6.19. EXPERIMENT SETUP FOR PROTOCOL COMPARISON WITH VARIABLE ENVIRONMENT NOISE .....	154
FIGURE 6.20. EXPERIMENT PHOTO FOR PROTOCOL COMPARISON WITH VARIABLE ENVIRONMENT NOISE .....	154
FIGURE 6.21. THROUGHPUT PERFORMANCE WITH ENVIRONMENT NOISE IN THE MULTI-FLOW SCENARIO .....	156
FIGURE 6.22. POWER CONSUMPTION OF IEEE802.15.4 MAC .....	158
FIGURE 6.23. POWER CONSUMPTION OF AS-MAC .....	158
FIGURE 6.24. POWER CONSUMPTION WITH INCREASED PACKETS ARRIVAL RATE FOR 10 MIN .....	159
FIGURE 6.25. POWER CONSUMPTION WITH INCREASED NODE NUMBER, 20 PPS FOR 10 MIN .....	161
FIGURE 6.26. POWER CONSUMPTION WITH INCREASED NODE NUMBER, 80 PPS FOR 10 MIN .....	162
FIGURE 7.1. THE EXPERIMENT SETUP OF BATTERY RECOVERY EFFECT .....	166
FIGURE 7.2. THE NORMALISED LIFETIME GAIN WITH CONSTANT ACTIVE TIME .....	167
FIGURE 7.3. THE NORMALISED LIFETIME GAIN WITH CONSTANT SLEEP TIME .....	167
FIGURE 7.4. THE NORMALISED LIFETIME GAIN OF IMOTE2 WITH CONSTANT ACTIVE TIME .....	168
FIGURE 7.5. THROUGHPUT PERFORMANCE OF SINGLE TRANSMISSION PAIR .....	172
FIGURE 7.6. ENERGY PERFORMANCE OF THE BATTERY RECOVERY AWARE ALGORITHM .....	174
FIGURE 7.7. LATENCY PERFORMANCE OF THE BATTERY RECOVERY AWARE ALGORITHM .....	175
FIGURE 7.8. NETWORK TOPOLOGY OF THE MULTI-HOP SIMULATIONS .....	176
FIGURE 7.9. THROUGHPUT PERFORMANCE OF MULTI-HOP SCENARIO .....	177
FIGURE 7.10. LIFETIME PERFORMANCE OF MULTI-HOP SCENARIO .....	178
FIGURE 7.11. NORMALISED LIFETIME GAIN OF MULTI-HOP SCENARIO .....	178
FIGURE 7.12. NORMALISED LATENCY OF MULTI-HOP SCENARIO .....	179
FIGURE 7.13. PERFORMANCE CHANGE WITH VARIED $B_{MAX}$ .....	180

---

## List of Tables

TABLE 2.1 SPREADING CODE SET USED BY IEEE802.15.4.....	29
TABLE 3.1 POWER CONSUMPTION SETTINGS .....	74
TABLE 4.1 SPREADING CODE SETS EMPLOYED BY AT86RF231 IN MSK FORMAT.....	87
TABLE 4.2 RMS/STD OF ANALYTIC MODEL.....	93
TABLE 4.3 CALCULATION COMPLEXITY.....	93
TABLE 5.1 RMS/STD OF THE DIFFERENT RESIDUALS.....	129
TABLE 6.1 PSEUDO CODE OF THE OPTIMISATION PROCESS .....	142
TABLE 6.2 POWER CONSUMPTION FOR 1 HOUR IN EXTREMELY LOW TRAFFIC LOAD, .....	160

---

## List of Acronyms

ACK	Acknowledgement
ADC	Analog to Digital Convertor
AWGN	Additive White Gaussian Noise
BEB	Binary Exponential Backoff
BER	Bit Error Rate
CCA	Clear Channel Assessment
CDF	Cumulative Distribution Function
CDMA	Code Division Multiple Access
CER	Chip Error Rate
CFO	Carrier Frequency Offset
CG	Coding Gain
CLK	Clock
COTS	Commercial Off-The-Shelf
CRC	Cyclic Redundancy Check
CSMA	Carrier Sense Multiple Access
DAC	Digital to Analog Convertor
DSSS	Direct Sequence Spread Spectrum
EKF	Extended Kalman Filer
FCF	Frame Control Field
GB	Geometric Backoff
HSPS	Half Sin Pulse Shaping
ICI	Inter Chip Interference
ISI	Inter Symbol Interference
LNA	Low Noise Amplifier

---

LQI	Link Quality Indicator
LR-WPAN	Low-Rate Wireless Personal Area Networks
LTE	Long Term Evolution
MAC	Medium Access Control
ML	Maximum Likelihood
MSK	Minimum-Shift Keying
MUI	Multi User Interference
NiCd	Nickel-cadmium
NiMH	Nickel-metal hydride
OFDMA	Orthogonal Frequency Division Multiple Access
O-QPSK	Offset Quadrature Phase Shift Keying
PA	Power Amplifier
PAPR	Peak to Average Power Ratio
PDF	Probability Distribution Function
PER	Packet Error Rate
PN	Pseudorandom Number
PPM	Parts per Million
PPS	Packet per Second
PRR	Packet Receive Rate
QoS	Quality of Service
QoI	Quality of Information
RF	Radio Frequency
RMS	Root Mean Square
RSS	Received Signal Strength
RSSI	Received Signal Strength Indicator
SCFDMA	Single Carrier Frequency Division Multiple Access

SDR	Software Defined Radio
SER	Symbol Error Rate
SNR	Signal to Noise Ratio
SQD	Signal Quality Degradation
STD	Standard Deviation
TDMA	Time Division Multiple Access
UB	Uniform Backoff
WSNs	Wireless Sensor Networks

# Chapter 1. Introduction

## 1.1 Aim and Scope

Wireless Sensor Networks (WSNs), which have been widely promoted over the last decade, are designed to monitor environmental parameters [1;2], e.g. temperature, light, and humidity in an intelligent, multi-hop style. Regardless of the scenarios and applications, WSNs are expected to last for long periods, usually years, without any maintenance, which means the system should be highly energy efficiency. To achieve this target, WSNs usually operate with extremely low duty cycles, i.e. they sleep between samples before waking up to send one sample. This configuration is reasonable, because the physical parameters monitored are slowly changing and do not require high sample rates to reconstruct the characteristics of the system. However, over time, although the essential characteristics of WSNs remain the same: power efficiency, scalability, and low cost, applications have expanded to more advanced areas, for example, structure health monitoring systems [3], multimedia surveillance systems [4], human health care systems [5], and industry process and condition monitoring systems [6;7]. Consequently, the system requirements have become much more complex. In such applications, the offered traffic load is much higher due to higher sample rates, thus a WSN should be re-recognised as a data intensive network instead of the traditional view of a low duty cycle network. Therefore, researchers will need to increase the WSN system performance to satisfy new challenges brought by advanced applications while continuing to be compatible with the essential requirements.

Currently, most of WSN systems operated with Carrier Sense Multiple Access (CSMA) style network. With this architecture, the system can enter the sleep state to save energy and only wake up when there is information ready to be sent. As shown in Figure 1.1, the devices will first compete for the wireless channel before transmitting packets. The sensor devices will only access the network when they need to, and work in a duty cycled manner to reduce energy consumption. In traditional applications, because of

the low offered traffic load, the collision probability within the wireless channel is kept to a relatively low level. Therefore, the energy and time costs of channel competition can be kept low, which guarantees reasonable performance in the network. However, the performance will be quite different in advanced, high traffic load applications. As shown in Figure 1.1, since the channel collision probability increases due to higher traffic load (i.e. higher probability to access the channel), the channel contention process will be prolonged consuming more time and hence introducing increased delay and energy expenditure. As a consequent, not only the lifetime of network, but also other performance metrics including throughput and latency will all decreased significantly.

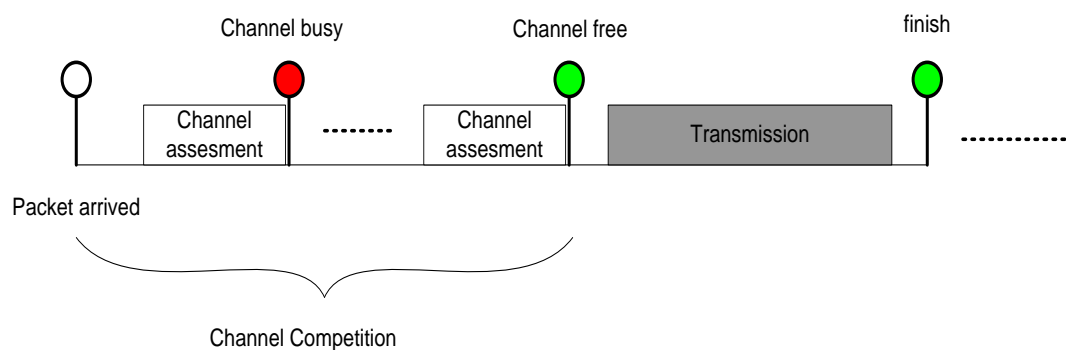


**Figure 1.1. Transmission scheme in WSN system**

The second inefficient scheme of the traditional WSN architecture is the transmission itself. To protect against harsh RF environments common in many WSN deployments, e.g. industrial plants, the modulation schemes of WSN systems have been designed for high reliability. In other words, the packets are typically transmitted with an unnecessarily slow datarate, while the wireless channel may support much higher datarate. Since the wireless channel is time varying, even WSN systems deployed in harsh locations can still utilise higher data-rates most of the time. It is easy to imagine that higher data-rate will lead to shorter transmission times and therefore inefficient, fixed-rate modulation schemes result in higher power consumption, higher collision probability and less delivered throughput.

The overall objective of this PhD thesis is to investigate the possibilities of increasing the potential performance of WSNs in advanced

applications where increased throughputs are required. Our solutions take as a base standard the IEEE 802.15.4 system and propose techniques to increase the system performance in two approaches, while still maintaining many of its primary features. The solutions offer improvements by improving efficiency at the channel contention stage and increasing datarate in the packet transmission stage.

In the channel competition stage, we propose the use of a multi-carrier based adaptive bandwidth scheme to increase the efficiency. It was noticed that in the multi-radio multi-channel system [8-10], high performance of system can be expected, due to the use of independent and simultaneously accessible radio transceivers. Since each transceiver can operate in different channels, simultaneous wireless communication with multiple devices will be enabled. In turn, this will significantly increase the efficiency of channel competition and provide the performance gain in the terms of minimising service delays as well as increasing network throughput. However, as expected, the performance gain obtained in this approach is at the expense of additional radio transceivers, which will increase both the power consumption and the system cost. We conjecture that the introduction of an OFDMA style multi-carrier scheme can achieve similar flexibility in the channel competition stage by allocating different number of sub-carriers<sup>1</sup> to different user competing for the channel without increasing the total channel bandwidth. The advantage of this scheme is that it can be based on the single radio architecture to save cost and power consumption, and can be easily integrated with the IEEE 802.15.4 transceiver design. Nonetheless, the standard multi-carrier system comes with several problems preventing its potential employment in WSN system, including Carrier Frequency Offset (CFO) and the high Peak to Average Power Ratio (PAPR). We have examined the cause of these problems, and propose a low-cost modification applicable for deployment in WSNs.

In the packet transmission stage, there is the potential to increase the system performance as well, since the existing IEEE 802.15.4 modulation scheme is designed for worst-case operation. To improve performance we

---

<sup>1</sup> In this context, sub-carrier could be equal to the channel in multi-radio architecture.

propose an adaptive coding scheme which matches transmission rates to the channel conditions. Similar schemes are common in cellular and WiFi systems and here we demonstrate that with very simple modifications in the physical layer, WSN systems can also be benefited by transmitting packets at a speed optimised to the SNR margin of wireless link. Within this modified architecture, the bandwidth and all other front-end components have been kept the same as required by the IEEE 802.15.4 standard, which means that the power consumptions for different data rate remain unchanged. Given the sensitivity to power consumption in WSNs, such an expansion should be able to increase the energy efficiency as well as the throughput, since a faster data rate will lead to a shorter active time. To fully utilise this feature, the system should be able to first determine the channel quality and then estimate the optimised matching spreading mode to transmit the packet. However, when this scheme is expanded to large-scale, multi-hop sensor networks, special considerations of the essential requirements of resource constraint WSNs are required. In such circumstance, we have examined these challenges, and propose corresponding solutions for deployment in WSNs, for example, how to evaluate the channel quality, how to estimate the optimised channel capacity, and how to implement such algorithm in a low complexity MAC protocol.

During the investigation of adaptive coding schemes, a very interesting phenomenon was noticed: the battery recovery effect. This refers to the process whereby the active chemical substances in a battery will replenish themselves if left idling for sufficient period of time, and hence, the deliverable energy of a battery can, to some extent, be recharged. This effect has been ignored in WSNs before, since in the extremely low duty cycle system this effect has already been automatically maximised. However, in the advanced applications considered here, due to the increase in offered traffic, additional design is required to take the advantage of this effect without the conflicting with the latency and throughput performances of the WSNs. Thus, we are motivated to exploit this battery recovery effect as an additional approach of energy efficiency to improve battery performance in sensor networks.

In conclusion, the proposed overall system architecture in the context of wireless sensor network system within advantage application should be able to adapt in both the frequency and spreading code dimension. A brief example has been illustrated in Figure 1.2, the wireless channel has been shared by three nearby devices, where each device only occupied partial channel after negotiation and adapted spreading code length with the channel quality to deliver robust service. The potential system is expected to have the following characters:

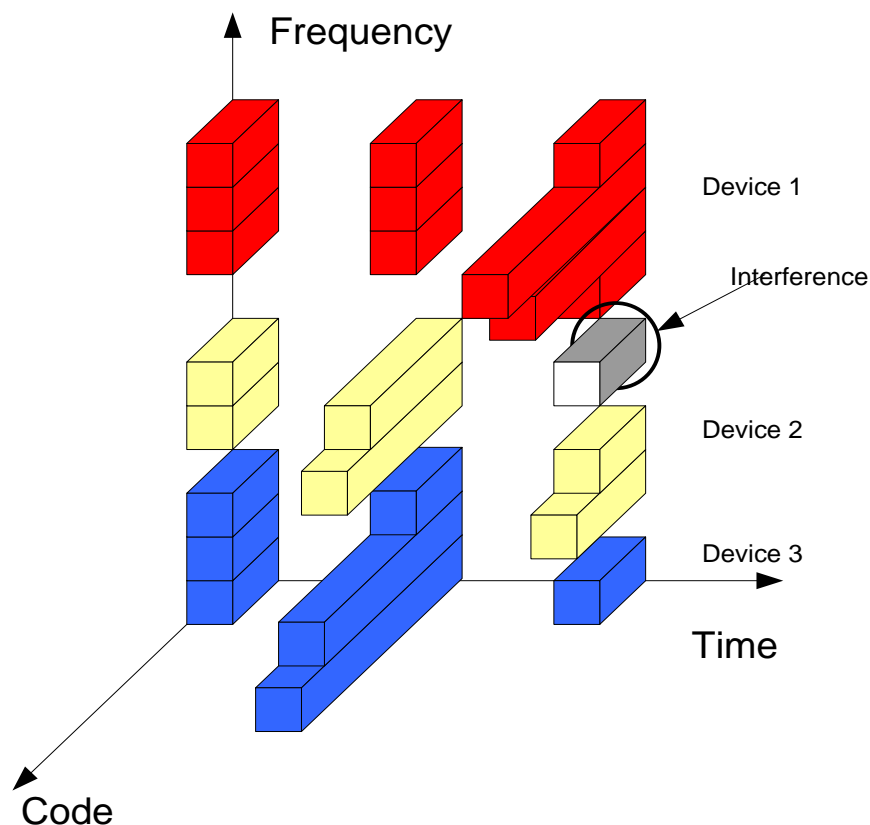


Figure 1.2. Expected system architecture

- Efficient channel management: dynamically assign bandwidth to different devices in the network to increase the channel competition efficiency.
- High channel utilisation: adapt the coding scheme for each sub channel to achieve higher data rate when the SNR margin of wireless channel permits.
- High speed and stable wireless link: monitor the environment noise and channel quality to enable the spreading code length adaptation accordingly.

- Co-existing with other networks: black list the corresponding bandwidth where RF interference is detected.
- Power efficiency: due to the efficient channel competition process and the fast data transmission.
- Increased battery lifetime: due to the understanding of battery recovery effect, the system is able to find an optimised trade-off between maximising battery life and minimising the service delay.
- Context aware services: provide prioritised QoS service for different data streams in advanced applications by assigning more sub-carriers and paths with better link conditions.

It should be noted that, due to the limitation of experiment equipment, we have not delivered a prototype system with all the features in this thesis. Instead, we have to demonstrate the performance of these proposed solutions in different aspects separately using theoretical analyses, experimental validation, and simulation. However, such an integrated prototype is designable using Software Defined Radio (SDR) platforms, for example the GNU radio, which may be considered in future work.

## 1.2 Contributions and Publications

The contributions of this thesis can be summarised as follows:

- First experimental demonstration of a low-cost modification to the IEEE 802.15.4 system to integrate with the multi-carrier architecture, which mitigated the multi-user interference caused by the multi-hop distributed nature of WSN systems. The proposed architecture is able to work within 125kHz frequency offset.
- First evaluation of the potential performance increase offered by the multi-carrier based adaptive bandwidth feature, which was validated by comparisons between results of analytic models and simulation.
- First experimental demonstration of the performance of spreading code length adaptation derived from the DSSS technology within IEEE802.15.4 system.

- Proposed and experimentally validated a new error performance estimation model for adaptive spreading code length with improved accuracy over existing techniques.
- Proposed a novel link indicator 'Effective-SNR' by utilising the redundancy between the standard link indicators in a two layer Kalman filter system, which enabled the resource constraint WSN platforms to estimate the channel capacity in a low-cost manner. The estimation accuracy of proposed method was 160% better than the raw SNR and 120% better than the instantaneous LQI.
- Designed a low-overhead MAC protocol utilising the adaptive spreading code length feature compatible with practical systems, and presented the first experimental evaluation of the network performance, which is able to deliver more than 200% of the throughput while saving more than 50% of the power consumption.
- First experimental demonstration of the battery recovery effect in wireless sensor systems, showing more than 25% potential lifetime increase.

The research work has resulted in the following publications within author's PhD period, as listed below:

- C. Chau, M. Wahab, **F. Qin**, Y. Wang, and Y. Yang, "Battery Recovery Aware Sensor Networks," in *Symposium on Modelling and Optimisation in Mobile, Ad Hoc, and Wireless Networks (WiOpt)*, 2008.
- **F. Qin**, Y. Yang, and J. Mitchell, "Performance Increase in WSN by the Adaptation of Spreading Code Length," in *London Communication Symposium (LCS)*, 2009.
- **F. Qin**, Y. Yang, and J. Mitchell, "Performance Increase Through the Use of Multiple Sub-carriers in WSN," in *7th ACM International Symposium on Mobility Management and Wireless Access (MobiWac)*, 2009.

- C. Chau, **F. Qin**, S. Samir, M. Wahab, and Y. Yang, "Harnessing Battery Recovery Effect in Sensor Networks", *IEEE Journal on Selected Areas in Communications (JSAC)*, Vol. 28, No. 7, 2010
- T. H. Lin, S. L. Hung, M. Chavali, R. J. Wu, H. N. Luk, and **F. Qin**, "Towards Development of Wireless Sensor System for Monitoring Anaesthetic Agents", *Sensor Letters*, Vol.8, Issue 6, 2010
- **F. Qin**, J. Mitchell, "Performance Estimation of Adaptive Spreading Code Length for Energy Efficient WSN", in *7th IEEE Wireless Advanced Conference(WiAd)*, 2011.
- **F. Qin**, J. Mitchell, "Analyses of MAC Performance for Multi-Carrier based Wireless Sensor Networks", in *11th IEEE International Workshop on Wireless Local Networks(WLN)*, 2011.
- H. Liu, S. Gao, T. H. Loh, **F. Qin**, "Low-Cost Intelligent Antenna with Low Profile and Broad Bandwidth", *IET Microwaves, Antennas & Propagation (accepted)*, 2011
- **F. Qin**, X. Dai, and J. Mitchell, "Effective-SNR Estimation for Wireless Sensor Network Using Kalman Filter", (*Submitted to Ad-Hoc Networks*), 2011.
- **F. Qin**, J. Mitchell, "AS-MAC: Utilising the Adaptive Spreading Code Length for the MAC Protocol Design of WSNs", (*Submitted to ACM Transactions on Sensor Networks*), 2011.

### 1.3 Thesis Organisation

This thesis is organised as follows:

Chapter 2 reviews the background and history of WSNs, introducing the most popular IEEE 802.15.4 standards, and addresses the motivation of our research project through a system requirement analyse of a real life case study. We also discuss related works in this chapter.

Chapter 3 introduces a low-cost, multi-carrier based architecture for WSNs. An emulation based experiment has been deployed to demonstrate the feasibility and performance of the proposed approach, followed by an

---

analysis of the potential improvements in network performance offered by such architecture using both analytic methods and simulation results.

Chapter 4 demonstrates a WSN with an adaptive spreading code length approach. To make it practically deployable, an accurate error estimation model has been proposed by examining the code set constitution and de-modulation process. Experiments with real life devices are used to validate the proposed error estimation model.

Chapter 5 utilises the redundancy of two standard channel indicators provided by the IEEE 802.15.4 system to generate a new, reliable link indicator: Effective-SNR. A two-layer based Kalman filter has been designed to estimate the Effective-SNR, defined as: the SNR to achieve the same error performance in an AWGN channel. The experiment results show that the proposed method is not only accurate by also fast converging with very low implementation cost.

Chapter 6 presents a MAC protocol design with adaptive spreading code length approach which is based on the error estimation model and Effective-SNR indication described in previous chapters. Experimental results have demonstrated significant performance increases in both energy efficiency and system throughput. The system performance in harsh RF environments has also been provided to show the ability of the proposed system to deliver a stable wireless link even in highly variable channel conditions.

Chapter 7 demonstrates the battery recovery effect, followed by a discussion of utilising such an effect in WSN applications with high traffic load to maximise the network life time by the carefully design the duty cycle of devices. Simulation based analysis has been provided to show the possibility of optimising the trade-off between battery recovery and service latency.

Chapter 8 presents the conclusions of this thesis, and proposes potential future work.

---

## Chapter 2. Wireless Sensor Network

### 2.1 WSN: From Traditional to Advance

A wireless sensor network consists of distributed wireless devices equipped with sensors, which can be utilised to collect information about physical parameters. A WSN system could be formed by tens or even hundreds of these devices, which cooperated to monitor a geographic area and transmit gathered data back to the base station in a wireless Ad-Hoc fashion. Such architectures could greatly simplify the deployment and maintainability of systems comparing with the wired sensor systems.

In the early days, such systems were always likely to be deployed for environment and habitat monitoring applications [1;2]. In these applications, WSN devices were equipped with temperature, humidity, or pressure sensors, and recorded data with low duty cycles, i.e. they woke up perhaps every hour to sample one measurement and transmit data via a wireless communication channel back to the base station. As a result, the offered traffic loads within the network in these applications were relatively small, usually with no QoS requirement (i.e. working in the 'best effort' model, as some applications are insensitive to lost of information). These systems usually needed to last a few months or even years without staff attending the deployment site, which means energy efficiency is the most important feature of a WSN system. Another attractive feature of WSNs is their scalability, which enables the system to be able to add and remove devices without reconfiguration or interrupting the work of network. Therefore, to fulfil this requirement, systems usually operate with a distributed multi-hop architecture. As expected, since there could typically be hundreds of these devices deployed in one system, the WSN devices have to be of a low-cost design, leading to constraints in the resource available in each device. As a result, the essential requirements of the sensor networks are: low cost, energy efficiency, and scalability. For instance, MintRoute [11] and S-MAC [12] have been proposed by academics to achieve these requirements in the routing and MAC layer respectively.

Recently, the flexibility of WSNs has attracted more interest from advanced applications, e.g. structure health monitoring systems [3], multimedia surveillance systems [4], human health care systems [5], and industry process and condition monitoring systems [6;7]. Accordingly, the offered traffic load inside the network has increased tens or even hundreds times over traditional applications and QoS is now a fundamental requirement [13]. As could be predicted, the traditional WSN architecture has failed to completely satisfy the requirements of these advanced applications. For instance, Kim et al. [3] deployed a multi-hop wireless sensor network to monitor the structural health of the Golden Gate Bridge. They reported that transferring 512 kB of data from 64 nodes required over 12 hours. Moreover, some of these applications require the nodes to be deployed in harsh radio environments (e.g. industry plants), thus the quality of the wireless link will suffer from the variable RF channel, which raises further challenges in the network design.



Figure 2.1. Engine section in the BP trial site [14]

To understand the new requirements posed and allow the deployment of advance sensor network applications in practice, a real life WSN project will be discussed here as an example. British Petrol (BP) has deployed a trial WSNs system in Loch Rannoch aiming to monitor the health status of a ship's engine to avoid the daily checks which requires regular staff attention. It is worth noting that this is a monitoring system rather than a detection

system, which means that the system is expected to work for several years not just for single events (the later one is less sensitive to energy usage).

This is a typical WSN application with high traffic load in a harsh RF environment. The engine itself also generates RF noise during operation, with other interference coming from the many electronic devices used in the ship including radar and communication systems, which operate with a random duty-cycle. Therefore, the wireless channel will suffer from time varying environment noise. Beside this, the engine area of Loch Rannoch consists of many metal surfaces and obstacles which may cause the heavy shadowing and fading effects (see Figure 2.1 for reference). These fading effects may come from the multi-path effect (e.g. the multiple reflection of metal surfaces). As a result the arrived signals through different paths in the receiver side may suffer from the frequency and time spreading, which will cause the signal quality degradation. However, since most of the WSN applications are statistic deployed, the degree of fading effect will be location dependant and be approximately constant for each deployed device. However, passing operators and vehicles may contribute to the varying channel. Without any doubt, all these effects will decrease the stability of the wireless link in the WSN system.

The system determines the health status of the engine by monitoring the vibration sensors attached to the engine body. In total 98 accelerometers have been deployed feeding data to 28 battery-powered WSN nodes. Each sensor captures at a raw sample rate of 100 kHz raw sample with an Analog-to-Digital Converter (ADC), which is then down-sampling to 3 kHz. Considering that each WSN node needs to transfer data from more than 3 sensors, the offered traffic load in the network will be much higher than the traditional WSNs system (around 60 packets per node per second when the payload length = 100 bytes). Furthermore, all the WSN nodes will be triggered at exactly the same time to start sampling, which will further increase the competition probability in the wireless channel and decrease the successful deliverable throughput. To summarise, in this system, the WSN network is working with extremely low duty cycle manner transmitting only operation and maintenance packets most of the time but will suffered congestion due

to the heavy traffic load and competition for the channel once the system has been triggered into the active stage. It should be noted that although these problems are discussed in the context of a structural health monitoring application, very similar problems also occurred in multi-media sensor networks and most of other advanced sensor network applications.

In summary, although the original essential requirements of WSNs have not changed (i.e. energy efficiency, scalability and low cost), advanced applications increase the offered traffic load and pose significant performance challenges, which requires the system to be able to deliver higher throughput with QoS requirements. As the current WSN architecture is optimised for low duty cycle scenarios, the system performance decreases rapidly in a heavy offered traffic load scenario, which limits the application of sensor networks in advanced fields. Therefore, our work is aiming to build a realisable architecture which is an evolution of current WSN architectures, to adapt WSNs for these types of advanced applications by providing increased performance within the resource constraints typically encountered.

## 2.2 IEEE802.15.4 Technology

Although any technology which does not rely on wires could be classified as a wireless technology and can be employed by WSNs e.g. acoustic communication for underwater WSNs [15], Radio Frequency (RF) technology is the default option to represent 'wireless' for WSNs. Moreover, in recent years, IEEE 802.15.4 [16] has become the most popular choice for most of the WSN platforms. The IEEE 802.15.4 standard also contributes to other standards including ZigBee [17], 6LoPAN [18], and Wireless Hart [19], which are different in higher layers but share the same physical layer and most of the MAC layer provided by IEEE 802.15.4. Without loss of generality, we narrowed our scope of research to IEEE 802.15.4 based technology which is most widely representation in the wireless sensor community. Therefore, a brief introduction on IEEE802.15.4 standard will be provided in this section to aid the future discussions in this thesis.

The IEEE 802.15.4 standard defines the characteristics for the PHY and MAC layers for applications named Low-Rate Wireless Personal Area

Networks (LR-WPAN), which shares the basic features of WSNs, i.e. easy deployment, extremely low cost, power efficiency, and acceptable data transfer.

### 2.2.1 Physical layer of IEEE 802.15.4

The IEEE 802.15.4 standard specifies three frequency bands: 868MHz, 915MHz, and 2.4GHz in the physical layer. As the first and second bands are not opened for un-licensed devices in all the countries, most IEEE802.15.4 compatible transceivers only support 2.4GHz [20;21].

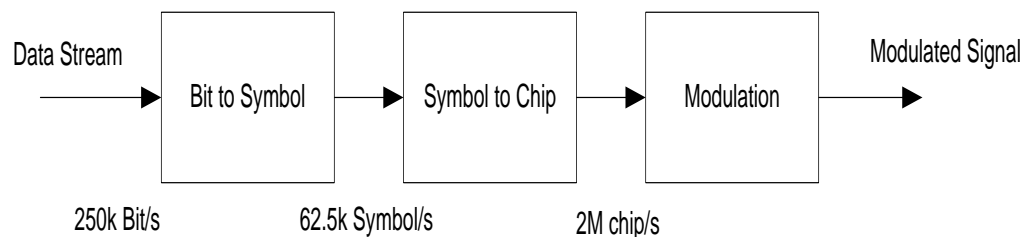


Figure 2.2. Modulation process of IEEE802.15.4

As regulated by the IEEE 802.15.4 standard, each 4 bits from the upper layers will be mapped into one symbol, giving  $2^4 = 16$  symbols. Each symbol shall be mapped into a 32 chip sequence, which is one of the pre-defined Pseudorandom Number (PN) code set. This processing is named Direct Sequence Spread Spectrum (DSSS) technology, which will increase the bandwidth but decrease the interference and noise effects. Since the code set are pseudo-orthogonal to each other, this system can also be treated as a 16-ary modulation system. In the 2.4GHz band the chip sequence is modulated using Offset Quadrature Phase Shift Keying (O-QPSK) technology with a Half Sine Pulse Shaping (HSPS) filter, while Binary Phase Shift Keying (BPSK) technology is employed in the 868MHz and 915MHz bands [16]. Recalling the discussion in section 2.1, to keep costs low most IEEE 802.15.4 transceivers employ non-coherent differential Minimum-Shift Keying (MSK) demodulation instead of coherent OQPSK demodulation to enable low cost and low complexity RFIC designs as discussed in [8,9]. The complexity of demodulation can be greatly simplified by removing the need for accurate frequency and phase synchronisation.

Table 2.1 Spreading Code Set used by IEEE802.15.4

symbol	Spreading code word
0000	11011001110000110101001000101110
0001	11101101100111000011010100100010
0010	00101110110110011100001101010010
0011	00100010111011011001110000110101
0100	01010010001011101101100111000011
0101	00110101001000101110110110011100
0110	11000011010100100010111011011001
0111	10011100001101010010001011101101
1000	10001100100101100000011101111011
1001	10111000110010010110000001110111
1010	01111011100011001001011000000111
1011	01110111101110001100100101100000
1100	00000111011110111000110010010110
1101	01100000011101111011100011001001
1110	10010110000001110111101110001100
1111	11001001011000000111011110111000

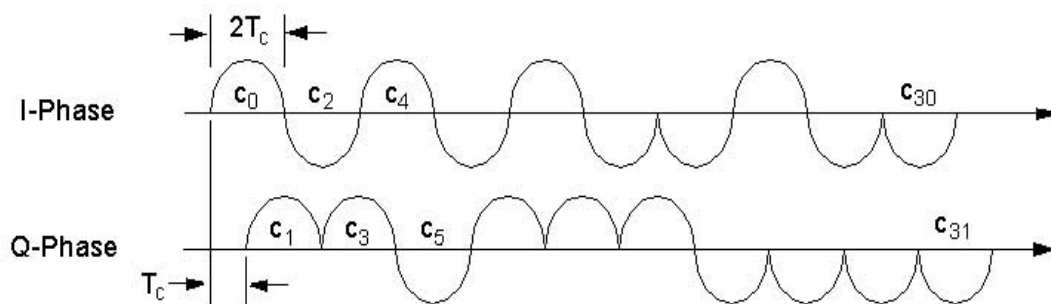


Figure 2.3. O-QPSK modulation with HSPS filter [16].

## 2.2.2 MAC layer of IEEE 802.15.4

All three bands share the same MAC layer which is a CSMA/CA protocol with a Binary Exponential Backoff (BEB) scheme. When a packet arrives at the MAC layer, a MAC header, a 2 byte CRC tail, one byte to indicate frame length, as well as a 6 bytes preamble will be added. The complete packet, which has been shown in Figure 2.4, is now ready to be transmitted.

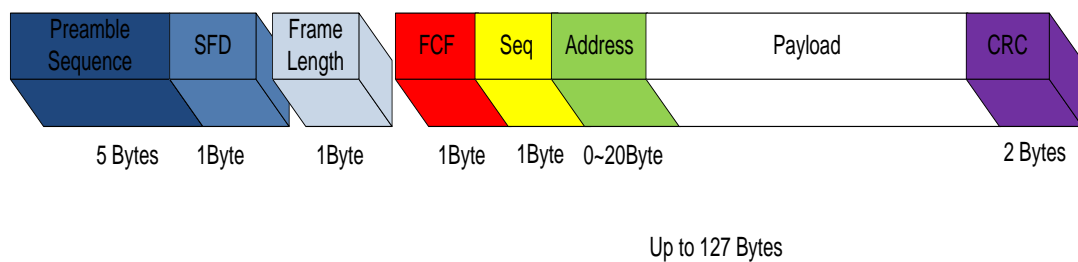


Figure 2.4. Packet consist of IEEE802.15.4

In CSMA/CA, the device will first start a back off period which is chosen from the set  $(0 \sim 2^{BE} - 1)$  with uniform probability, where  $BE$  is the Backoff Exponent which has a default value of 3 but can be configured. After the back off period, a node will perform a Clear Channel Assessment (CCA): if the channel is free then the packet will be sent directly, otherwise the node will increase the value of  $BE$  by 1, and back off again, repeating this process until the channel is free and the packet is sent, or if  $BE$  reaches the pre-set maximum retry value, which has default value of 5, the packet is discarded. The ACK scheme is optional in the standard IEEE802.15.4 MAC. The ACK.request bit in the FCF field can be enabled to ask the receiver to send an ACK packet after a short period denoting a successful transmission. If not, the transmission link will be working in a best effort mode.

### 2.3 Related Works

#### a) Existing approaches for high traffic loads in WSNs

Some research groups have noticed the increasing traffic load requirement in WSN and have tried to solve this problem by viewing it as a congestion control problem. CODA was the first solution proposed in [22], which is an energy efficient congestion control scheme with receiver based congestion detection, open-loop backpressure, and closed-loop source regulation. Hull et al. [23] examined the effect of three congestion control schemes (Hop by hop flow control, source rate control, and prioritised MAC protocol) in a real life WSN platform, and proposed a fusion algorithm to achieve the best effort. Ee et.al. [24] proposed a distributed congestion control algorithm for a common network architect in WSN. In [25], a source rate control scheme with further interference aware design has been proposed and validated in a 40 nodes WSN test bed. Nearly all these methods rely on the regulation of the packet generation rate, i.e. some packets will be drop if they exceed the buffer queue. Existing WSNs architectures lack the ability to allocate more resource to congested areas to aid faster transmission.

Some other groups are trying to improve network performance in this scenario with QoS support. Erol et.al. [26] treated the WSN as consisting of

tasks which are unlikely to have the same requirement, for instance, delay and priority. Their solution is based in the routing layer, which assigns the best route to the packets of a high priority task. Chewoo et.al. [27] proposed an enhanced MAC protocol for IEEE802.15.4 to support the service differentiation in WSNs. In [27], the network was treated as being constituted of rate-sensitive data flows. However, their algorithms can only adjust the parameters of the backoff window to meet network requirement. Danil et.al. [28] proposed a similar method of maintaining separate queues for different priorities packets and adjust contention and transmission power according to the priorities to guarantee the delivery of high priority packets.

Beside these, some researchers are trying to decrease the generated traffic load. Edith et.al. [29] proposed a method to reduce the redundant packets transferred in WSN based on an 'Information-Aware' scheme. The algorithm will drop packets when in the congested state according to the importance (decided by the application) of packets, trying to provide satisfactory Quality of Information (QoI) to the users. Although the term QoI has been proposed by Bisdikian [30] several years ago, up to now it is far from as well understood or as well accepted as QoS in communication networks or Quality of Images in computer vision. In other words, it is still lacking a universal judgement on which packets are less important and can be dropped. Moreover, this method does result in the loss of information and can only be applicable in specified applications.

As a conclusion, the increased traffic load in WSNs has been well recognised in the research community. However, these proposed approaches usually suffer from limitations in the technologies provided by existing WSNs architectures, and fail to contribute a significant performance increase for these scenarios.

#### b) Existing approaches to increase channel utilisation in WSNs

Opportunities do exist to increase the efficiency of the wireless sensor network performance within data intensive applications through other medium access technologies, such as Time Division Multiple Access (TDMA) [22] or Code Division Multiple Access (CDMA) [23]. In a TDMA style network,

the transmission is based on super-frames where each super-frame is divided into several time slots allocated to different users. Although this scheme can increase the channel utilisation efficiency, it requires additional time synchronisation and pre-allocated time slot. A CDMA based network will further require accurate power and time synchronisation to level the received power of all incoming signals to avoid interference, which could be overly complex for a low cost sensor network system.

Multi-channel based solutions are another popular approach in the research area of wireless networks, which allows transmission multiple channels to increase the network performance of WSNs. Nearly all proposed multi-channel protocols fall into one of the following two kinds: the first is scheduled access [31-34]. Protocols in this mode are a derivation of the TDMA style scheme, which usually divides each channel into slots, and assigns them to different devices in the network. However, this mode typically requires time synchronisation, global knowledge of the network topology, as well as of the traffic requirement for each device. The second type is more reasonable for WSN systems, the Random access [35-40]. Protocols in this mode are more flexible and compatible to traditional single channel system. But since the receiver can only switch between the channels, the system performance gain is limited. Some protocols simply assume the hardware to have the ability to listen to multiple frequencies at the same time [36-38], which is beyond the ability of any existing wireless transceiver in WSNs. Other protocols use low efficiency methods to solve these problems e.g. on demand channel switching, signal strength measurement based channel selection, or they assign channels randomly as in [39], which are easy to implemented but only have low performance gain.

As a comparison, the multi-radio multi-channel systems [8-10] usually have significant performance improvement. This is because these systems are equipped with multiple wireless transceivers, therefore the system is able to receive and transmit data concurrently over multiple channels at the same time. However, considering that the radio transceiver consume most of the energy in a WSN platform, multiple radio transceivers will certainly increase the power consumption. It must be noted that this performance increase is

obtained in the expense of increased power consumption and system cost. Therefore, such a solution is not suitable for the energy constrained and cost sensitive WSNs.

To summarise, the improvement of the wireless channel utilisation has been a focus of research for some time. Most of the proposed solutions are provide either high efficiency but low flexibility (centralised pre-organised solutions), or high flexibility but low efficiency (random and distributed solutions). However, in wireless sensor networks with high traffic load, it is important to achieve these two targets at the same time: i.e. high flexibility and high channel efficiency.

c) Transmission adaptation with varying channel quality in WSNs

The adaptation of data rate is inherent in the standards for IEEE802.11[41-45], Bluetooth [46;47] and some cellular systems [48;49]. Among these, IEEE 802.11 shows most similarity to the IEEE802.15.4 based WSNs system and provides helpful prior knowledge for our approach. The first data rate adaptation algorithm, the Autorate Fallback Algorithm (ARF) is proposed and implemented in [41], which is an SNR independent algorithm. ARF switched modes based on previous packet failures, which is simple to be implemented but provides relatively poor performance. The most famous data rate adaptation algorithm is the Receiver-Based Autorate Protocol (RBAR) [42], which demonstrated that a receiver based mechanism with SNR indication can achieve the best performance for an adaptation process. A more recent approach which included a practical implementation was proposed by Microsoft in [45], which further discussed interference effects in the network and proposed online calibration approaches based on their findings.

In the area of WSNs, rate adaptation can be achieved through the adjustment of the spreading code length of the IEEE802.15.4 architecture; one of the most popular physical layer solutions of wireless sensor network. In the IEEE 802.15.4 PHY layer, four information bits (a symbol) are used to select one of 16 code words from a nearly orthogonal code set to be transmitted during each data symbol period. Hence, the rate adoption will be

enabled by adjusting the length of these code words. Such operation will be an un-compliant IEEE 802.15.4 solution but shares most of the basic principles of IEEE 802.15.4. Lanzisera et al. have proposed an algorithm based on this solution to reduce the average power consumption of wireless sensor network [50;51]. To the best of our knowledge, this is the only work discussing this topic. The work of [50] successfully introduced the possibility of adaptive spreading code length and demonstrated the great potential of this technique through simulation but due to hardware limitations a full experimental demonstrated was not presented.

The most straightforward issue caused by harsh RF environments is interference, which consists of two types: interference from other devices intending to transmit signals including WiFi, communication radio, and radar device etc., or unintended radiation from devices that aren't supposed to transmit signals including sparks from motors or power generators, light dimmers and microwave oven. RF interference has been reported for industry locations in [52] and [53], and for hospital sites in [54]. A very special case has been reported in [55] for aviation equipment. The harsh RF environment can also be the result of multi-path effects which causes the fading channel of wireless transmissions. The channel performance with multi-path effects in various locations has been examined in [56;57]. All these investigations demonstrate that the harsh RF environment is not only time varying but also high enough to interrupt wireless communication.

Many groups are trying to develop better ways to indicate the time-varying, harsh RF channel. Several empirical studies have given us a better understanding of the complex correlation between SINR and link quality. For particular, Aguayo et. al. [58] have studied several packet loss related factors including SNR, interference, and multi-path fading effect. Based on the experiment results collected from an IEEE 802.11 mesh network, they argued that, SNR cannot be used as a reliable predictor of link quality. Son et.al. [59] experimentally studied the concurrent transmission performance using Mica2 and MicaZ platforms within the context of WSNs. They confirmed that the assumption proposed by [58] also exists in the low-power wireless links. Beyond these work, our analyses further studied why SINR

breaks the correlation with PRR in the fading channel, and propose the correspond compensation. Jamieson et.al. [44;60] proposed a more accurate link indicator for wireless network system named SoftPHY. SoftPHY uses a Maximum Likelihood (ML) based approach in the decoding step of physical layer to directly estimate the likelihood of error probability of tagged wireless link. However, their approach modified the core hardware of the RF transceiver, thus cannot be deployed on a COTS platforms. Murat et.al. [61] proposed a Kalman filter based link quality estimation scheme for wireless sensor network. However, their approach takes received signal strength as the only observer parameter, thus failing to consider signal distortion caused by multi-path and other harsh RF effects.

Adaptive transmission technology, which will automatically match the modulation and coding scheme with the channel quality, has been employed in wireless cellular and data networks for over a decade. Such approaches are expected to contribute to the network performance significantly for WSNs with high traffic loads in harsh RF environments.

#### d) Existing battery aware design in WSNs

Sensor networks commonly use rechargeable batteries, such as Nickel-cadmium (NiCd), Nickel-metal hydride (NiMH), Sealed lead-acid (SLA), Lithium-ion (Li-ion), and Lithium-polymer (similar to Li-ion). Different batteries have different properties. In particular, NiCd and NiMH are often used, because NiCd has a long cycle life, whereas NiMH has high energy density. There have been numerous studies about the performance of batteries in chemical engineering [62]. In networking, [63] carried out an empirical study to measure the performance of battery-powered sensors, but did not examine the saturation threshold. There are a number of approaches of energy management in sensor networks, examples include S-MAC, SEEDEX, RI-MAC, DW-MAC [12;64-66]. Commonly sensors, listening and reception can consume significant energy. There are other MAC protocols that consider battery characteristics for example BAMAC and Bel-MAC [67;68] rely on exchanging dynamic battery state information to optimise the use of batteries among sensors, but such information cannot be easily obtained without online measurement on the internal properties of a battery.

## 2.4 Summary

This chapter addressed the high traffic load demands resulting from the application layer in new WSN applications including structural health monitoring, multi-media surveillance and health care, which are significantly different to traditional WSN applications. It can be concluded that WSNs are facing new challenges to provide reliable and energy efficient transmission under heavy traffic loads. Furthermore, the literature review shows that this is an area beginning to attract attention from a number of academic groups but that accepted solutions are still not common due to the limitation of current WSN architectures. In the following chapters of this thesis, we will propose several approaches within this context, which aim to increase the performance of energy constraint WSNs and enable their extension to advanced applications.

## Chapter 3. Increase the Efficiency of Channel Contention using a Multi-carrier Architecture

### 3.1 Introduction

In this chapter, we attempt to improve the WSNs performance in advanced applications by increasing the efficiency of channel contention period. Currently, most of WSN systems operated with CSMA style network, where the devices compete for the wireless channel before the transmission of packets. As discussed in Chapter 1, when such system is posed with high traffic load in the advanced application, the WSN devices could consume more energy and time in the channel contention period than in the transmission period due the high collision and false channel assessment probability. This is because current WSN architecture is designed and optimised for the extremely low traffic network, which is no longer true for the WSN applications with high traffic load. As a consequent, the network performance including the energy efficiency, throughput and latency will all decreased significantly. This phenomenon has been witnessed not only in the pure CSMA based networks, i.e. IEEE 802.15.4 MAC, but also other specially designed protocols derived from CSMA like the famous S-MAC and B-MAC..

Figure 3.1 shows an ideal example in the channel contention period, where two devices are competing to access the wireless channel. In the standard IEEE802.15.4 MAC protocol, once a packet has arrived from the upper layer, the MAC/PHY layer will first asses the wireless channel to determine its status. If the channel is free, the device starts the data transmission immediately. During the data transmission process, if another device has a packet to be sent, its channel assessment will return a busy status. As a result, the second device will enter the backoff stage and attempts again after the backoff period. Obviously, since the channel assessment only determines whether the channel is free or busy, the second

device has no information about how long the packet transmission will last. Therefore, a random backoff scheme has to be adopted [16] and the backoff length is blindly selected. It may be longer than the data transmission, which results in a gap of free channel between two successive data transmissions. It may be shorter than the data transmission and a much longer backoff length is re-scheduled. In both cases, it is highly possible that a gap exists between two successive data transmission and the time in the gap is wasted in vain. This causes a low channel utilisation which is common in all CSMA-like protocols under heavy traffic load.

Opportunities do exist to increase the efficiency of the wireless sensor network performance within data intensive applications through other medium access technologies, such as Time Division Multiple Access (TDMA) [69] or Code Division Multiple Access (CDMA) [70]. In a TDMA style network, the transmission is based on super-frames where each super-frame is divided into several time slots allocated to different users. Although this scheme can increase the channel utilisation efficiency, we suggest that this technology may not be suitable for wireless sensor networks for the following reasons. Firstly, this method is a centralised, non-distributed algorithm. Secondly, the implementation of time synchronisation will cost communication overhead. Thirdly, the data traffic in a WSN system is not truly random as typically assumed in data networks, but correlated with the sensing events in the system. Therefore, pre-allocated, fixed time-slot allocation will lead to less flexibility and lower channel utilisation. A CDMA based network will further require accurate power and time synchronisation to level the received power of all incoming signals to avoid interference, which could be overly complex for a low cost based sensor network system. Therefore, the CSMA style network, in particularly the IEEE 802.15.4 system, is still the most popular choice of WSN systems, due to its scalability and flexibility. Multi-channel based solutions are another popular approach to increase the efficiency of wireless network, which allows transmission multiple channels to increase the network performance of WSNs. However, the multi-channel approaches are mainly increase the network performance by allowing concurrent transmission. Since the device can only switch

between channels, the receiver can only listen and receive from only one channel at the same time. Furthermore, in the multi-hop network, the multi-channel solution may face coordination problems, e.g. multi-channel hidden terminal problems and missing receiver problems [40]. To solve these problems, some protocols simply assume the hardware to have the ability to listen to multiple frequencies at the same time [36-38], which is beyond the ability of any existing wireless transceiver in WSNs. As a comparison, the multi-radio multi-channel approaches usually have significant performance improvement. This is because these systems are equipped with multiple wireless transceivers, therefore the system is able to receive and transmit data concurrently over multiple channels at the same time. However, considering that the radio transceiver consumes most of the energy in a WSN platform, multiple radio transceivers will certainly increase power consumption. It must be noted that this performance increase is obtained at the expense of increased power consumption and system cost. Therefore, such a solution is not suitable for the energy constrained and cost sensitive WSNs.

Therefore, we introduced an Orthogonal Frequency Division Multiple Access (OFDMA) liked multi-carrier architecture into WSN systems, in which the bandwidth of the shared wireless channel can be divided into several sub-channels and assigned to different nodes. Since the device can access the wireless channel using only part of the bandwidth, several nodes sharing the nearby wireless medium are allowed to transmit information concurrently (i.e. achieve similar performance gain with multi-radio multi-channel system). Thus the possibility of collision would be reduced, which will increase the efficiency of the channel contention period as well as the re-transmission rate. In other words, the system will have similar performance gain with the multi-radio multi-channel approaches, but realised with the existing bandwidth with a single transceiver design with is both cost and energy efficient. As a result, better network performance and energy efficiency of the CSMA based WSN systems could be expected. As illustrated in Figure 3.1, given each device only occupies a half of the bandwidth, when the first device is transmitting, the channel assessment operation of the second device will return the

information that another half of the channel is still available. Then the second device can utilise the rest of the channel to start its transmission immediately. Thus both devices transmit their data concurrently without backoff and collision. It should be noted that the bandwidth can be configured into more sub-channels. Therefore, more devices can transmit at the same time with further divided sub-channels. As a result, the efficiency of the contention period can be enhanced in data intensive applications.

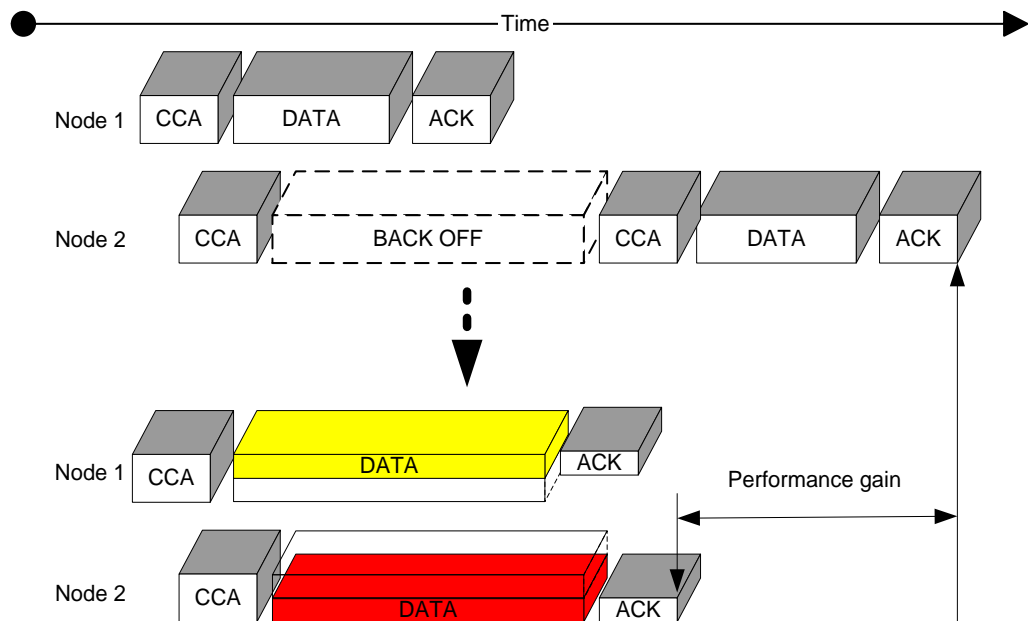


**Figure 3.1. Adaptive Bandwidth System Architecture**

Such a multi-carrier architecture will be similar to the OFDMA scheme, but can be applied with multi-hop distributed network. Although OFDMA system has the advantages of high channel utilisation which has been well studied and successfully deployed in cellular and data networks (e.g. LTE and WiMax system), its disadvantages of sensitivity to Carrier Frequency Offset (CFO) and the high Peak to Average Power Ratio (PAPR) pose challenges to its deployment in low cost, multi-hop sensor network. In particular, the adverse impacts of CFO and PAPR are much worse in the scenario of multi-senders, where the carrier frequency offset caused by frequency variations among different sender's Local Oscillators (LO) would cause significant Inter Channel Interference (ICI) and Multi User Interference (MUI) [71]. For example, in WiMax and LTE systems, OFDMA is deployed only in the down link mode where the base station is the only transmitter,



In this chapter, in order to avoid these disadvantages of OFDMA like multi-carrier system but benefit from its advantages (i.e. spectrum flexibility and resistant to multi-path effect), we will analytically examine the causes of these problems and demonstrate one possible modification of the multi-carrier architecture for WSNs. Unlike the widely used but complicated CFO estimation method, we propose a low cost solution for WSNs by integrating pulse shaping, differential modulation and chip spreading techniques to increase the CFO resistance and decrease the PAPR. The proposed physical layer design has been validated by the experiments, where a very good performance has been demonstrated in terms of against the CFO and PAPR problems.

In the later part of this chapter, we also investigate to what degree the WSNs can benefit from the proposed multi-carrier based architecture. In [72;73], researchers have argued that the simple increase of spectrum flexibility without an increase in overall bandwidth will not increase the throughput performance of a network. However, as we expected, the multi-carrier architecture can offer other benefits such as energy efficiency and service latency because of the increased efficiency of channel contention process. Due to experiment limitations in demonstration of the network performance, we present an analytical approach to demonstrate the performance of this multi-carrier system in the MAC layer and show that energy efficiency can be achieved while still maintaining high throughput when exposed to heavy offered traffic load, which is the general character of the advanced sensor network applications.

## **3.2 System architecture**

### **3.2.1 CFO problem in multi-carrier system**

In order to pave the way to mitigate the adverse effects of, the error performance of OFDMA subjected to frequency offset between carriers is first analysed and, a simple, low power and low cost modification of multi-carrier architecture is proposed, which is still compatible with the essential requirements of WSNs.

The transmit signal in a multi-carrier system can be defined as:

$$v(t) = \sum_{k=0}^{N_c-1} \sum_{n=-\infty}^{+\infty} C_{n,k} \times \Psi_{n,k}(t) \quad (3.1)$$

where  $N_c$  is the sub-carrier number,  $k$  is the sub-carrier index,  $n$  is the symbol index,  $C_{n,k}$  is the raw data.  $\Psi_{n,k}(t)$  is the up-converting base function given by:

$$\Psi_{n,k}(t) = g(t - nT_s) \times e^{j2\pi f_k t} \quad (3.2)$$

where  $g(t)$  is pulse shaping function,  $T_s$  is the transmission time interval,  $f_k$  is the carrier frequency of  $k$ -th sub-carrier.

The signal  $v(t)$  propagates through an Additive White Gaussian Noise (AWGN) channel, where an AWGN noise  $w_n$  is added to  $v(t)$  to give the received signal. It should be noted that the frequency offset will affect the error performance in both AWGN and fading channel. To simplify the analyses we only considered the AWGN channel in this chapter. Another consideration comes from the experimental limitations of validating the proposal, i.e. to replicate a controllable fading channel requires expensive channel emulators. Similar approaches have been adopted in many other research works [71;74] in the multi-carrier field. As with the standard multi-carrier system, the scheme proposed in this chapter may suffer further performance degradation from fading effects but still with significant performance improvement comparing to system without such a design.

At the receiver side, the demodulation process is implemented by projecting the received signal on the complex conjugates of the base function  $\Psi_{n,k}^*(t)$ :

$$\begin{aligned}
z_{n,k} &= \sum_{t=-\infty}^{+\infty} [v(t) + w_n] \times \Psi_{n,k}^*(t) \\
&= \sum_{t=-\infty}^{+\infty} \left[ \sum_{k=0}^{N_c-1} \sum_{n=-\infty}^{+\infty} C_{n,k} \times \Psi_{n,k}(t) + w_n \right] \times \Psi_{n,k}^*(t) \\
&= \sum_{t=-\infty}^{+\infty} \left[ \sum_{k=0}^{N_c-1} \sum_{n=-\infty}^{+\infty} C_{n,k} \times \Psi_{n,k}(t) \times \Psi_{n,k}^*(t) \right] + w'_n
\end{aligned} \tag{3.3}$$

In an ideal multi-carrier system scenario,  $\Psi_{n,k}(t) \times \Psi_{n,k}^*(t) = |\Psi_{n,k}(t)|^2 = 1$ . Therefore, the received signal can be successfully demodulated into  $z_{n,k} = C_{n,k} + w'_n$ .

Then, if we consider a situation where the multi-carrier scheme been employed in the downlink mode of a wireless system, the carrier frequency generated by the local oscillator in both the transmitter and receiver will be shifted from the ideal frequency<sup>2</sup>. To simplify the analysis, we normalise all frequency offsets to the transmitter side. In this case, the base function is rewritten as:

$$\Psi'_{n,k}(t) = g(t - nT_s) \times e^{j2\pi f_k t} \times e^{j2\pi \Delta f t} \tag{3.4}$$

where  $\Delta f$  is the frequency offset between the transmitter and receiver. It is worth noting that in this scenario  $\Delta f$  is same for all sub-carriers, since the  $\Delta f$  can only be introduced between the only transmitter and current receiver.

As the receiver has no information about the transmitter's parameters, the receiver has to use the predefined  $\Psi_{n,k}^*(t)$  to demodulate the incoming signal:

$$z_{n,k} = \sum_{t=-\infty}^{+\infty} \left[ \sum_{k=0}^{N_c-1} \sum_{n=-\infty}^{+\infty} C_{n,k} \times \Psi'_{n,k}(t) \times \Psi_{n,k}^*(t) \right] + w'_n \tag{3.5}$$

<sup>2</sup> In the mobile scenarios, the Doppler effect can also contribute to the carrier frequency offset.

$$\begin{aligned}
&= \sum_{t=-\infty}^{+\infty} \left[ \sum_{k=0}^{N_c-1} \sum_{n=-\infty}^{+\infty} C_{n,k} \times g(t - nT_s) \times e^{j2\pi f_k t} \times e^{j2\pi \Delta f t} \times g^*(t' \right. \\
&\quad \left. - nT_s) \times e^{-j2\pi f_k t} \right] + w'_n \\
&= \sum_{t=-\infty}^{+\infty} \left[ \sum_{k=0}^{N_c-1} \sum_{n=-\infty}^{+\infty} C_{n,k} \times g(t) \times g^*(t + \tau) \times e^{j2\pi \Delta f_{CF} t} \right] + w'_n
\end{aligned}$$

We can then define the ambiguity function, introduced in [74] as:

$$A(\tau, f) = \int_{-\infty}^{\infty} g(t) g^*(t + \tau) \times e^{j2\pi f t} dt \quad (3.6)$$

The ambiguity function describes the orthogonality performance of a multi-carrier system. In the ambiguity function,  $\tau$  defines the time offset which leads to the Inter Symbol Interference (ISI),  $f$  denotes the frequency offset which leads to the well known ICI effect. The ambiguity function can be understood as: for a certain sub-carrier, due to the time offset  $\tau$ ,  $t$  and frequency offset  $f$  existed between the up-converting base and the down-converting base, the affected output value will be equal to the ideal value multiplied by  $A(\tau, f)$ .

Figure 3.3 shows the rectangle based ambiguity function for standard OFDM, where

- $A(0,0) = 1$  : current sub-carrier's demodulation output is 100%;
- $A\left(0, \frac{n}{T_s}\right) = 0$   $n \in (1 \sim N_c)$  : other sub-carriers' effects on current sub-carrier is 0%.

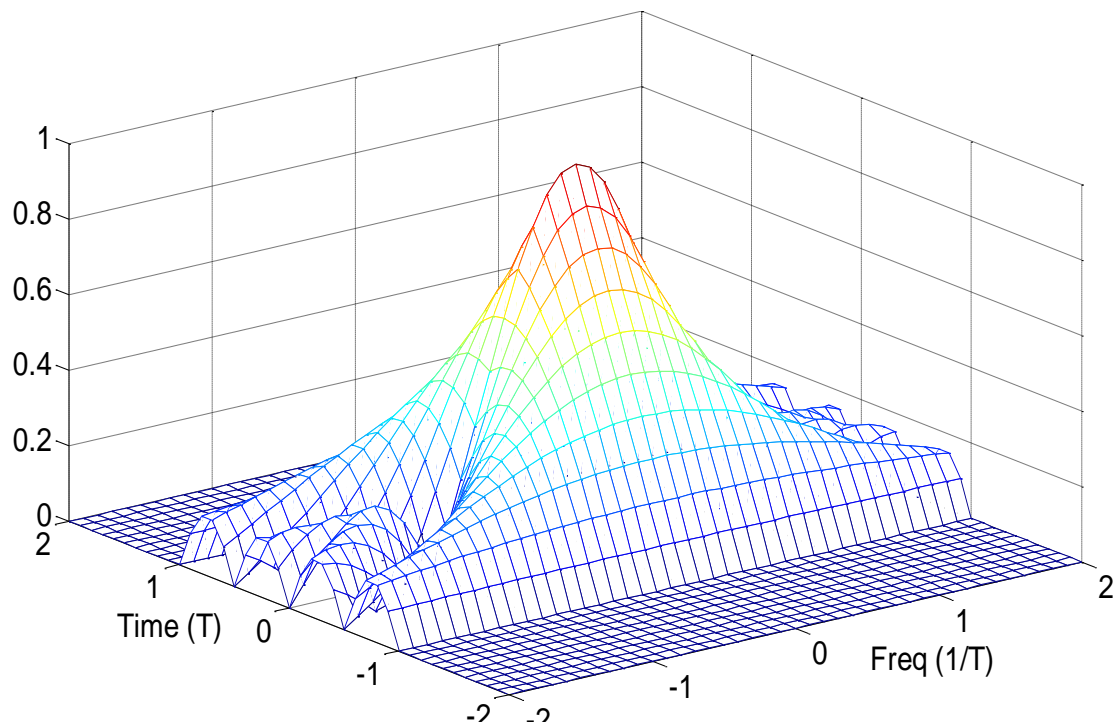


Figure 3.3. Ambiguity function of rectangle function

In an ideal demodulation process, no inter sub-carriers interference (ICI) exists, as each sub-carrier is exactly located on the zero points on all other sub-carriers. However, this is not true when CFO appears. Even a small amount of CFO between the transmitter and the receiver is able to make two adverse impacts on the system error performance.

First, due to the existence of  $\Delta f$ , all sub-carriers will suffer from an attenuation of the wanted output by  $A(0, 0 + \Delta f_{CFO})$  (i.e. shifted from the central point of Figure 3.3). Secondly, as we highlighted, each sub-carrier is laid exactly on the zero point  $(\frac{n}{T_s}, n \in (1 \sim N_c))$  of all other sub-carriers. Nonetheless, with the shifted carrier frequency, each sub-carrier will be located in  $\Delta f_{CFO} + \frac{n}{T_s}$ , instead of the zero point  $\frac{n}{T_s}, n \in (1 \sim N_c)$  of other sub-carriers. As a result, the amplitude of  $A(0, \Delta f_{CFO} + \frac{n}{T_s})$  increases very rapidly as shown in Figure 3.3, which contributes to the wanted signal being regarded as a noise component. In addition, each sub-carrier will have an effect on all others because of the infinite nature of the Sinc. function. In other words, each demodulated signal now depends on not only its own sub-carrier, but also on all other sub-carriers. When the number of sub-carriers is large, the accumulation of this effect will be very significant.

These explain why the multi-carrier system is very sensitive to frequency offset and why its tolerance to frequency offset is extremely small when compared with the frequency interval between sub-carriers. However, if the offset value of carrier frequency can be estimated using certain methods, e.g. Moose method [75] or schimdl-cox method [76], the adverse impacts of CFO can be significantly reduced by digitally modifying the down-converting base function  $\Psi_{n,k}^*(t)$  with the estimated frequency offset  $e^{j2\pi\Delta ft}$ . As a result, the received signal can be demodulated accurately. In fact, this is the most common method employed in cellular and WiFi system.

However, when the multi-carrier scheme was deployed in proposed WSNs with different sub-carriers allocated to different users to share the same wireless channel, the situation could be much worse than the downlink case just discussed. As illustrated in Figure 3.4, there are three transmitters each occupying two sub-carriers. Since all these devices have independent LO generating different carrier frequencies, different CFOs among sub-carriers can be expected. In this case, it is more appropriate to use the term MUI to describe the ICI effects, since the inter carrier interference is caused by the difference of carrier frequency of multiple users. With this consideration, equation (3.5) is now rewritten as:

$$z_{n,k} = \sum_{t=-\infty}^{+\infty} \left[ \sum_{k=0}^{N_c-1} \sum_{n=-\infty}^{+\infty} C_{n,k} \times g(t) \times g^*(t + \tau) \times e^{j2\pi \cdot \Delta f_{CFO}^k \cdot t} \right] + w'_n \quad (3.7)$$

where  $\Delta f_{CFO}^k$  is the carrier frequency offset at  $k$ -th sub-carrier, and may be different for sub-carriers.

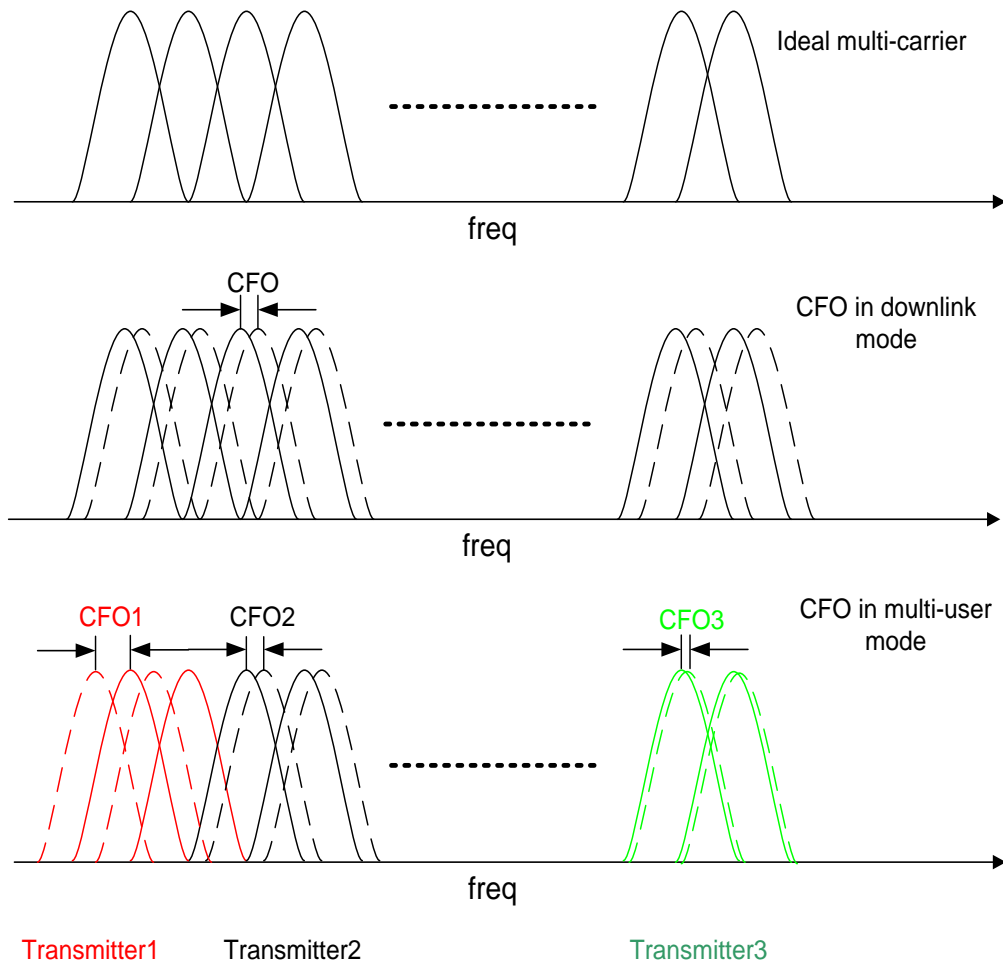


**Figure 3.4. CFO in different scenarios of multi-carrier based systems**

To give a detailed and clear image of the error performance under MUI effects, we derive the error performance function. For a given  $i$ -th sub-carrier, the error performance can be estimated by:

$$\mathfrak{E}(SNR) = \mathfrak{E}\left(\frac{P_s}{P_n + P_{MUI}}\right) \quad (3.8)$$

where  $P_s$  is the power of transmitted signal at  $k$ -th sub-carrier,  $P_n$  is the noise power added by the channel and  $P_{MUI}$  is the interference power caused by other sub-carriers. Here we use  $\mathfrak{E}$  as a function name, which could be referred to as the different error rate calculation function depending on the modulation<sup>3</sup>, e.g. BPSK, QPSK, or QAM etc.

<sup>3</sup> A practical error estimation model for IEEE 802.15.4 system can be found in chapter 4.

The CFO contributes to the decrease of the error performance in two ways: the decrease of  $P_s$ , and the increase of  $P_{MUI}$ . The decrease of  $P_s$  is calculated by

$$P_s = P_s \times A(\tau, \Delta f_{CFO}) \quad (3.9)$$

The calculation of the increase of  $P_{MUI}$  needs consider all contributions from other sub-carriers:

$$\begin{aligned} P_{MUI} &= \sum \text{all other sub-carrier's effect} \\ &= \sum_{n=1; n \neq i}^{N_c} P_s \times A(\tau, (f'_n - f_i)) \end{aligned} \quad (3.10)$$

where  $i$  is the sub-carrier index;  $N_c$  is the total number of sub-carriers; and

$$f'_n = \begin{cases} \frac{n}{T_s} & \text{sub-carrier } n \text{ with no CFO} \\ \frac{n}{T_s} + \Delta f_{CFO} & \text{sub-carrier } n \text{ with CFO} \end{cases} .$$

Then, equation (3.8) can be rewritten as:

$$\begin{aligned} &\mathfrak{E} \left( \frac{P_s}{P_n + P_{MUI}} \right) \\ &= \mathfrak{E} \left( \frac{P_s \times A(\tau, \Delta f_{CFO})}{P_n + \sum_{n=1; n \neq i}^{N_c} P_s \times A(\tau, (f'_n - f_i))} \right) \end{aligned} \quad (3.11)$$

Then it is easy to understand why a multi-carrier system is very sensitive to the CFO with the assistance of equation (3.11) and Figure 3.3. Obviously, even if we are able to estimate  $\Delta f_k$  for each sub-carrier, it still won't be able to avoid the MUI effect. The modification of  $\Delta f_k$  to the down-converting base function  $\Psi_{n,k}^*(t)$  can only cancel the attenuation of  $P_s$  component, and the error performance is still decreased by the interference component  $\sum_{n=1; n \neq i}^{N_c} P_s \times A(\tau, (f'_n - f_i))$  from other sub-carriers. This effect has been demonstrated in [71] and explains why WiMax and LTE systems only use OFDMA for downlink transmission but SCFDMA for uplink transmissions.

This effect can be mitigated by rebuilding the orthogonality of received signal [77] or by using a filter bank to separate all the sub-carriers [78]. All these approaches incur additional expense in terms of extremely high complexity to overcome non-orthogonality. Although this expense may be affordable in broadband or cellular wireless systems, it is not acceptable in WSNs where the computation resources and power consumption are very limited.

### 3.2.2 PAPR problem

Peak to average power ratio is another challenge in the implementation of multi-carrier systems. In a single carrier system, the modulated signals are almost variation of sinusoids with a low and constant peak to average power ratio. PAPR can be defined as:

$$PAPR = \frac{\max\{|s(t)|^2\}}{E\{|s(t)|^2\}}, \quad t \in [0, T_s] \quad (3.12)$$

where  $s(t)$  is the amplitude of the transmitted waveform.

Due to the low PAPR, the power amplifier for a single carrier system can be easily designed to guarantee the linearity and efficiency. However, due to the multi-carrier nature, various sub-carriers, each of them is similar to a single carrier signal, will be combined before being amplified at the power amplifier. As shown in Figure 3.5, the combined waveform exhibits pronounced envelope fluctuations in the time domain, resulting in a particularly high PAPR problem. As a result, the power amplifier for a multi-carrier system has to be highly linear over a large operating range to avoid any signal distortion caused by the saturation of power amplifier, which will greatly increase the cost and decrease the energy efficiency.

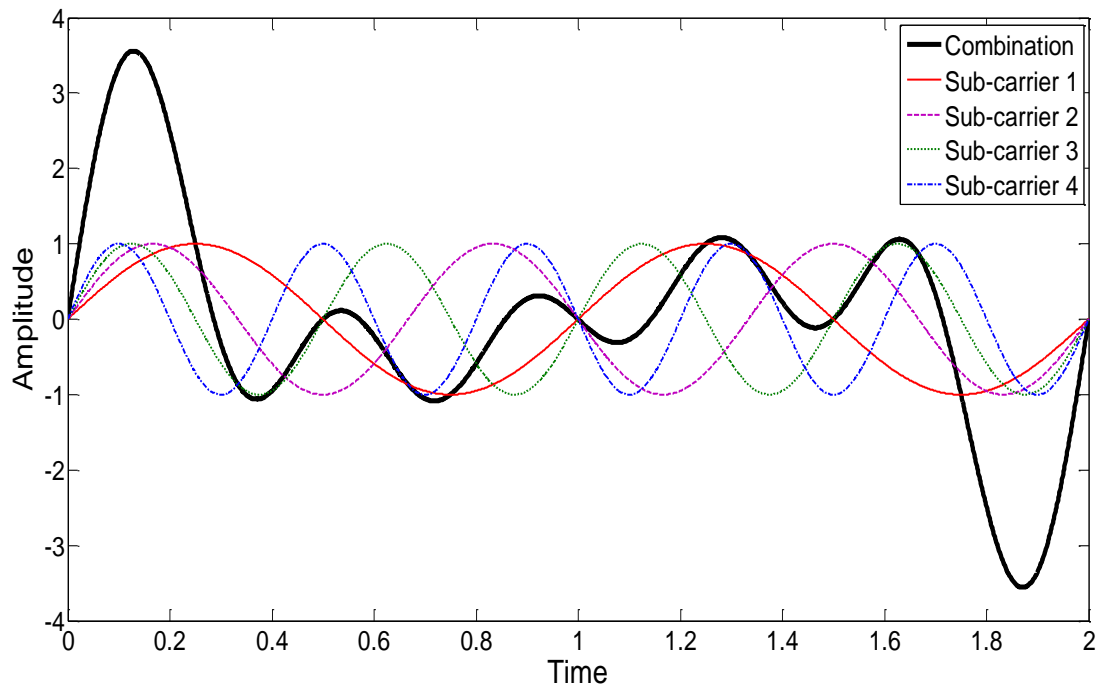
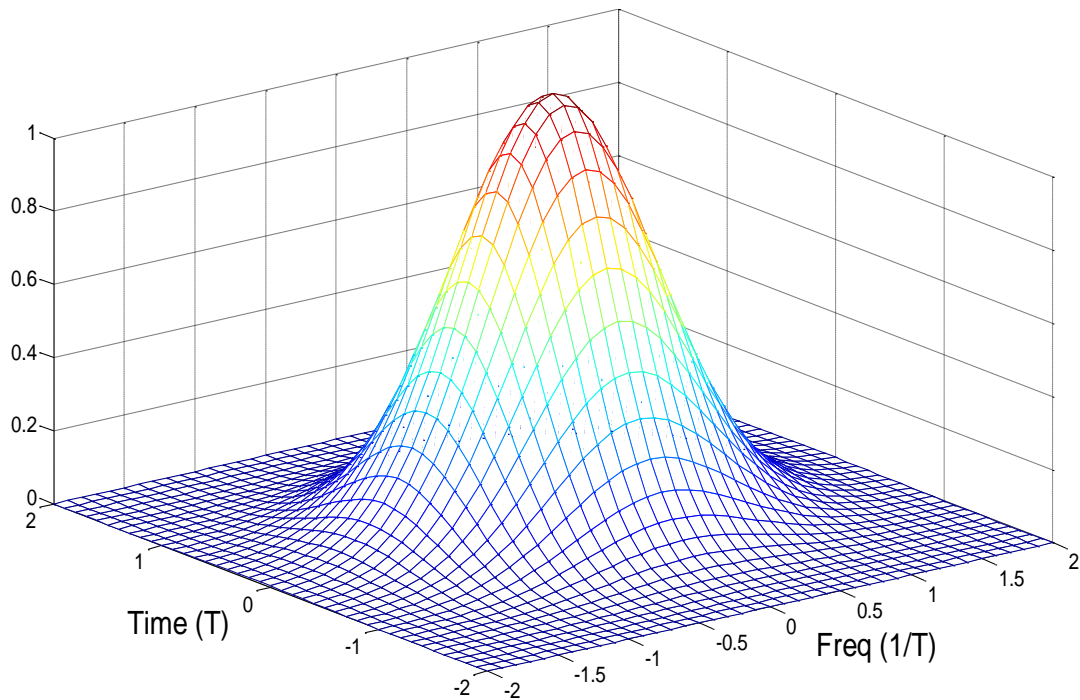


Figure 3.5. PAPR problem

### 3.3 Low cost solution for WSN

In this section, we propose to adopt pulse shaping as an approach to increase the resistance to CFO and time shifting instead of more expensive estimation methods. A number of works have demonstrated that using pulse shapes other than the simple square function can increase performance and counteract the effects of ISI/ICI [74;79-81]. This method is highly suitable for WSN because it only requires a simple modification of the pulse shaping function. Such a modification is very simple to implement in the digital processing part of the RFIC and therefore requires almost no increase in processing complexity or power consumption.



**Figure 3.6. Ambiguity function of Gaussian pulse shaping filter**

The performance of Ambiguity function can be significantly increased by the employment of pulse shaping filters rather than the simple gate function, e.g. Gaussian function or Raised Cosine function. Here, we implemented the Gaussian function based pulse shaping filter as an example, the performance of which has been shown in Figure 3.6. Since the Gaussian Function has no side bands in both the time and frequency domains, it is an appropriate choice for the pulse shaping function in our approach. The benefits of using the proposed Gaussian function for pulse shaping are threefold<sup>4</sup>:

- Only the adjacent sub-carriers will affect each other, leading to a lower accumulation of  $P_{MUI}$ .
- ICI between sub-carriers will not suffer from a rapid increase with increased CFO as no side bands exist, leading to a smaller increase of  $P_{MUI}$ .
- The function output decreases slowly with frequency shift around the ideal carrier frequency, leading to a smaller loss of  $P_s$ .

<sup>4</sup> It should be noted that the employ of Gaussian filter may not be the optimised solution. The comparison between different pulse shaping filters will be carried out in future work.

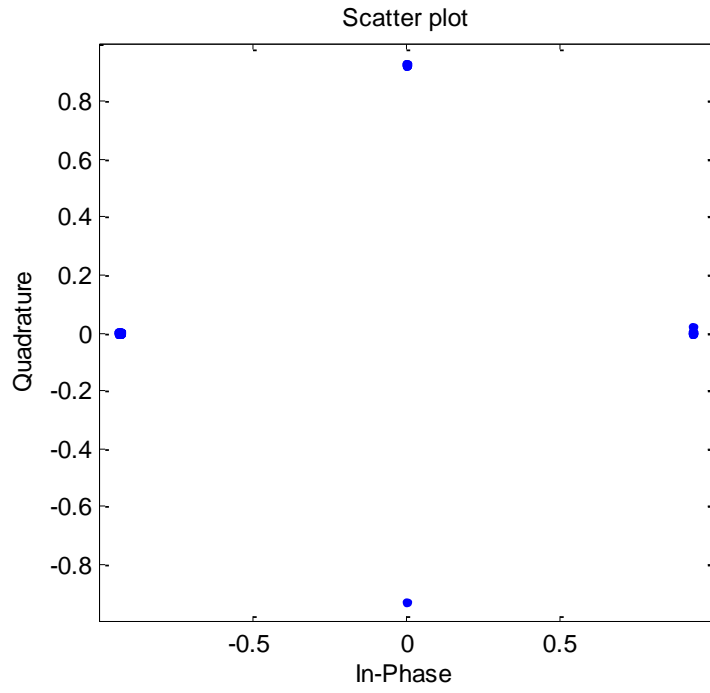
With these three factors, the error performance is expected to increase within CFO scenarios. In this case, equation (3.10) can be rewritten as:

$$\begin{aligned}
& \mathfrak{E} \left( \frac{P_s \times A(\tau, \Delta f_{CFO})}{P_n + \sum_{n=i-1, n \neq i}^{i+1} P_s \times A(\tau, (f'_n - f_i))} \right) \\
&= \mathfrak{E} \left( \frac{P_s \times A(\tau, \Delta f_{CFO})}{P_n + P_s \times A(\tau, (f'_{i-1} - f_i)) + P_s \times A(\tau, (f'_{i+1} - f_i))} \right) \\
&= \mathfrak{E} \left( \left[ \frac{P_n + P_s \times A(\tau, (f'_{i-1} - f_i)) + P_s \times A(\tau, (f'_{i+1} - f_i))}{P_s \times A(\tau, \Delta f_{CFO})} \right]^{-1} \right) \\
&= \mathfrak{E} \left( \left[ A(\tau, \Delta f_{CFO}) \times SNR^{-1} + \frac{A(\tau, (f'_{i-1} - f_i)) + A(\tau, (f'_{i+1} - f_i))}{A(\tau, \Delta f_{CFO})} \right]^{-1} \right)
\end{aligned} \tag{3.13}$$

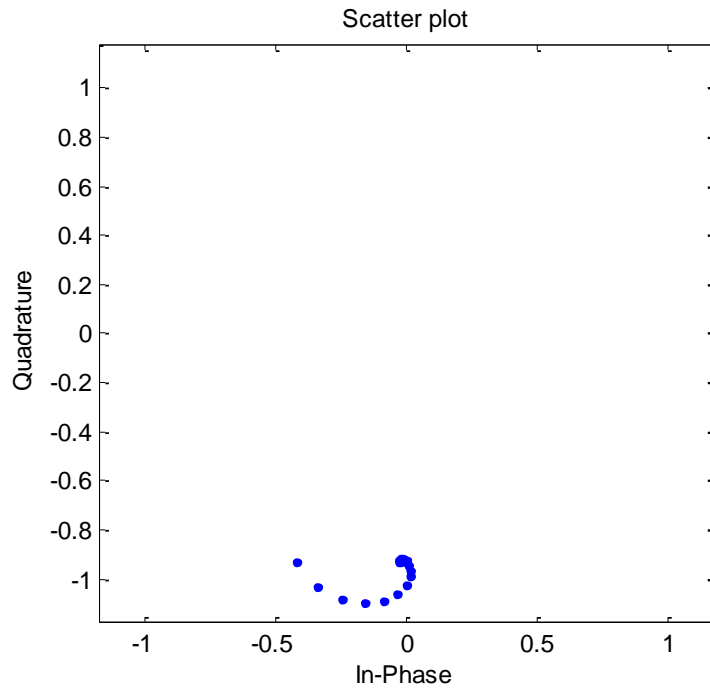
where the values of  $f'_{i-1}$  and  $f'_{i+1}$  depend on  $\Delta f_{CFO}$  representing the difference between two adjacent sub-carriers. We can see that the second term in equation (3.11) is reduced due to the use of the Gaussian ambiguity function.

In the implementation, it was noticed that the existence of  $\Delta f_{CFO}$  not only affects the output power of the sub-carrier but also the phase of the signal, which will rotate the demodulated data symbol.

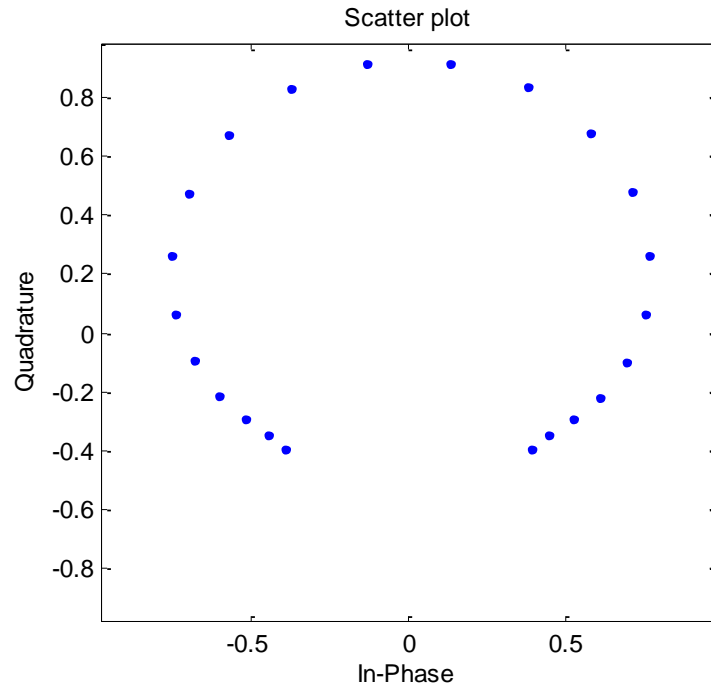
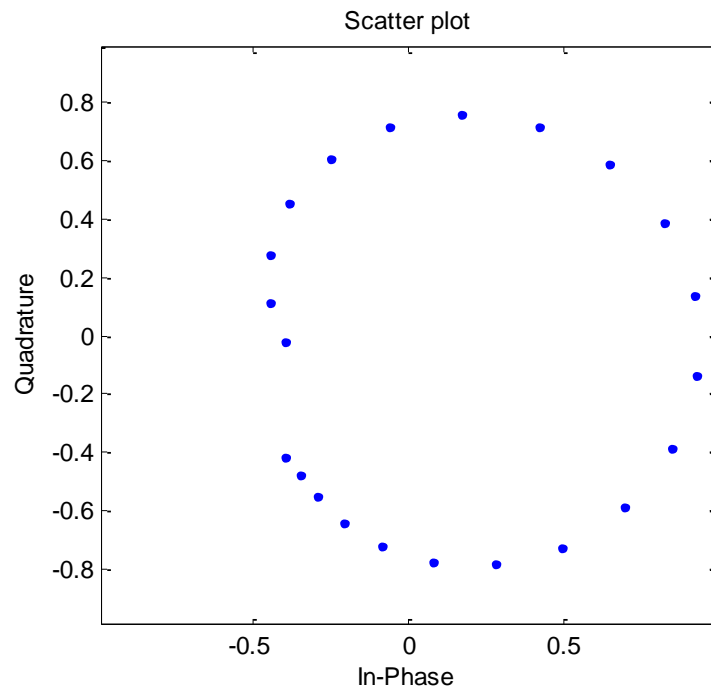
For example, in Figure 3.7, we captured the constellation diagrams from the output of a system with 16-subcarriers. The 1st to 8th sub-carriers belong to user one without  $\Delta f_{CFO}$ , while the 9th to 16th sub-carriers belong to another user with a small  $\Delta f_{CFO}$ . It is clear that only the 8th subcarrier has been affected by  $\Delta f_{CFO}$  of the second user, which confirms the results of equation (3.11). Likewise, all the effected sub-carriers of the second user are rotations of themselves, which will cause the decision errors in the demodulation process.



a).Sub-carriers 1st~7<sup>th</sup>



b).Sub-carrier 8<sup>th</sup>

c).Sub-carrier 9<sup>th</sup>

However, this problem can be easily solved. From Figure 3.8, it can be concluded that such rotation is linear with  $\Delta f_{CFO}$  within  $\pm \frac{1}{T}$ . The use of a differential demodulation scheme<sup>5</sup> can perfectly compensate this rotation effect, because the demodulation process in such systems is based on the correlation between the current symbol and the previous symbol.

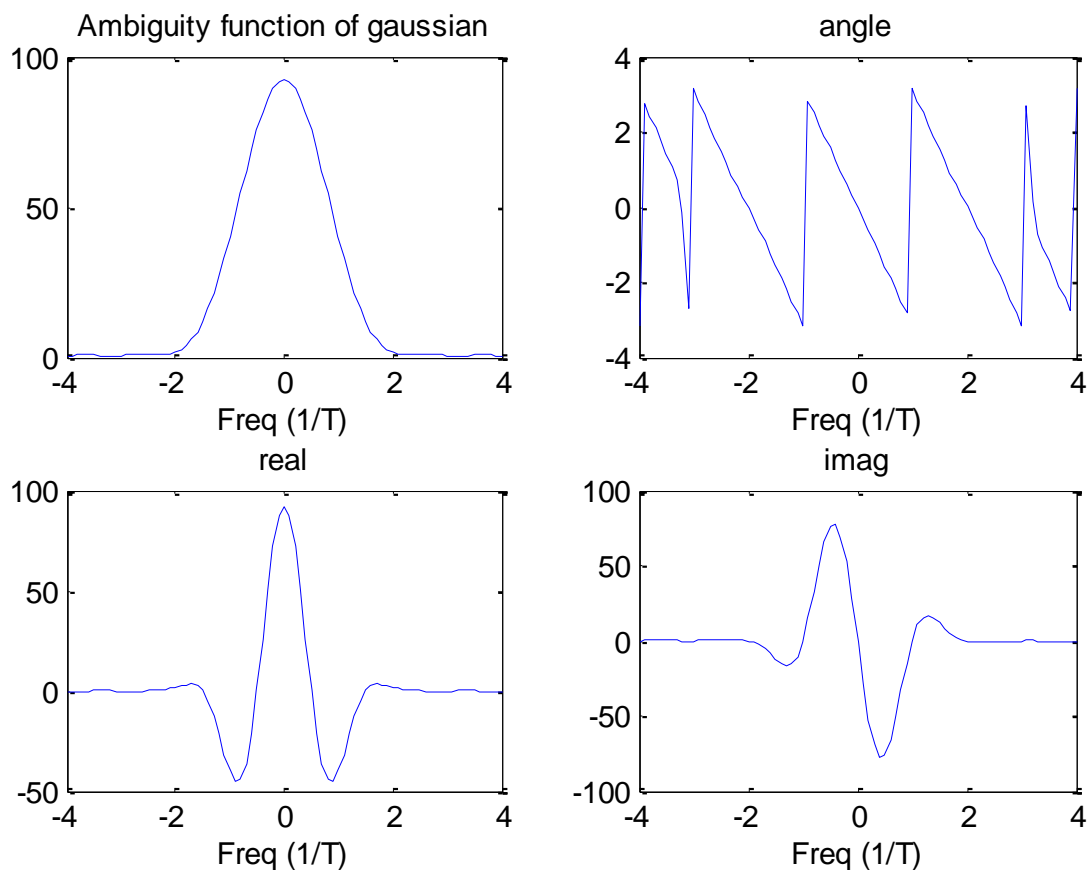


**Figure 3.8. Gaussian Ambiguity function.**

It can be assumed that  $\Delta f_{CFO}$  is constant within one symbol period. It is well known that the output frequency shift of a crystal oscillator is mainly due to the change of the temperature that is a very slowly changing physical parameter. Normally  $\Delta f_{CFO}$  is in a few unit Parts Per Million (PPM) every hour and therefore in one symbol period, which is typically several  $\mu s$ ,  $\Delta f_{CFO}$  can be approximated as a constant. Therefore, we are motivated to utilise this to solve the rotation problem. We propose to spread each symbol  $C_{n,k}$  into several chips (32 chips are used in our experiment), where the  $\Delta f_{CFO}$  will be

<sup>5</sup> In fact, most IEEE802.15.4 transceivers do employ non-coherent MSK demodulation, which is a kind of differential demodulation. Detail information can be found in Chapter4.

constant for each chips. The differential based demodulation of these chips can avoid the rotation effect. Although the first chip has a possibility of error, this only occurs when  $\Delta f_{CFO}$  changes with a time scale of hours. So that for all the other chips the error performance would be guaranteed.

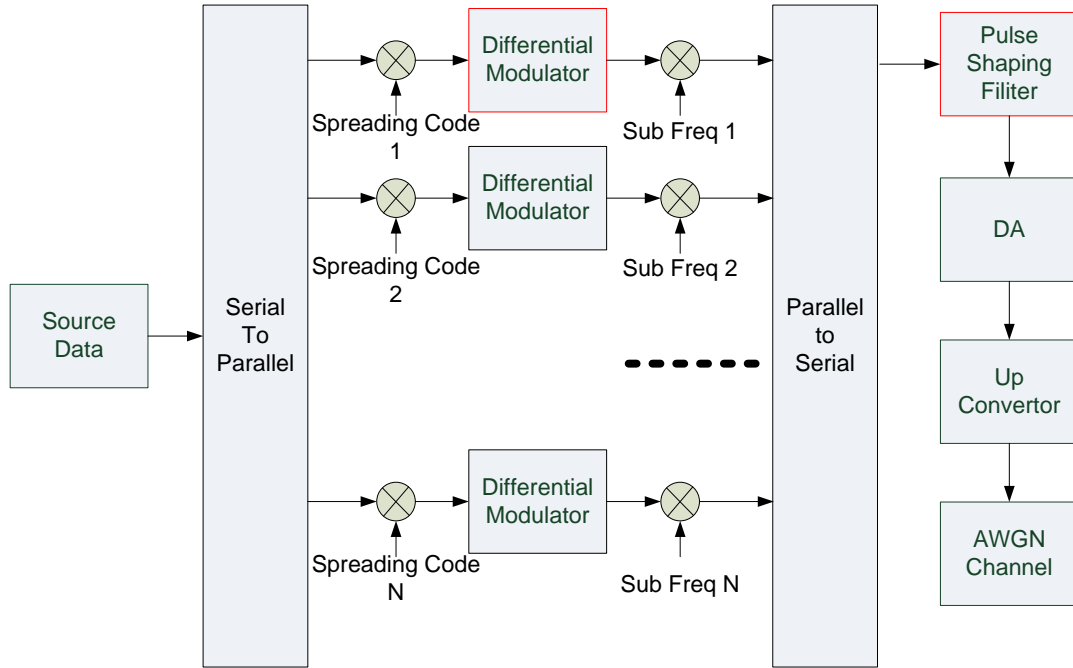


Figure 3.9. Modified Multi-carrier based System Architecture

In addition, as spread spectrum coding has been employed, the system can also take advantage of coding-gain by designing orthogonal spreading codes. This additional process does not increase the complexity of system. In theory, when all spreading codes are orthogonal, they will not interfere with each other and act as additional noise. However, in practice, it is not possible for all the spreading codes to be perfectly orthogonal. Thus some noise will remain. This effect will contribute a multiplicative coefficient<sup>6</sup> to the  $P_{MUI}$  calculated in equation (3.11), which will decrease according to the spreading code used.

$$\mathfrak{E}_s = \mathfrak{E} \left( \frac{P_s}{P_n + P_{MUI} * CG} \right) \quad (3.14)$$

<sup>6</sup> In fact, the coding gain works in a rather complex way, here we give only an approximation. Detailed information about the effect of coding gain can be found in Chapter 4.

$$= \mathfrak{E} \left( \left( \frac{[A(\tau, \Delta f_{CFO}) \times SNR^{-1} + [A(\tau, (f'_{i-1} - f_i)) + A(\tau, (f'_{i+1} - f_i))] * CG]}{A(\tau, \Delta f_{CFO})} \right)^{-1} \right)$$

where  $CG$  is the coding gain introduced by the demodulation process (for instance,  $CG$  is made up of two parts: processing gain and coding gain). From the empirical study, we found that the coding effect will make the second component negligible and in most cases this component can be roughly ignored.

$$\begin{aligned} \mathfrak{E}_s &= \mathfrak{E} \left( \frac{P_s}{P_n + P_{MUI} * CG} \right) \\ &\cong \mathfrak{E}(A(\tau, \Delta f_{CFO}) \times SNR) \end{aligned} \quad (3.15)$$

Even without the ICI disadvantage, a high PAPR will still limit the application of the proposed architecture due to the requirement of highly linear and low efficiency power amplifiers. Since PAPR is mainly contributed by the superposition of sub-carriers, PAPR is a function of increasing number of sub-carriers. Usually, an OFDMA system employs a large number of sub-carriers to deal with the frequency selective channel over a wide bandwidth, e.g. 256 or 1024 sub-carriers over 20MHz. From the viewpoint of multiplexing, this number of sub-carriers is far too large, so that it is impossible in practice for a scheduling algorithm to allocate sub-carriers individually. For instance, the OFDMA system allocates groups of sub-carriers together to reduce the complexity. In the multi-hop WSNs scenario considered here, the overall bandwidth is relatively narrow, e.g. only 2MHz, while the number of competing client devices within a one hop area is also limited, e.g. tens of device. Therefore, a smaller number of sub-carriers is adequate. In our experiment and analysis, 8 sub-carriers have been employed to reduce the PAPR value. This also helps to simplify the complexity of digital processing.

The system can be further designed with two dimension scalability: scaling in both the output power and the bandwidth. For instance the power consumption of the baseband processing is proportional to the bandwidth occupied. Current technology enables the ADC/DAC power to scale with the

clock frequency, which by Nyquist theory corresponds to the baseband bandwidth. Instead of using the baseband generator to generate the whole baseband signal without any awareness of the occupied bandwidth, the baseband generator will only generate the required spectral width, thereby reduce the baseband bandwidth. In this case the reduction in occupied bandwidth will lead to lower power consumption of the baseband generator, which is the second highest power consuming component of RFIC. In this case the frequency synthesiser will need to generate a carrier frequency plus baseband offset to up convert the baseband signal to its target position. We estimate the power consumption profile of this architecture, as shown in Figure 3.10. Ranveer C. et. al. in [82] also reported similar phenomena for an IEEE 802.11 device.

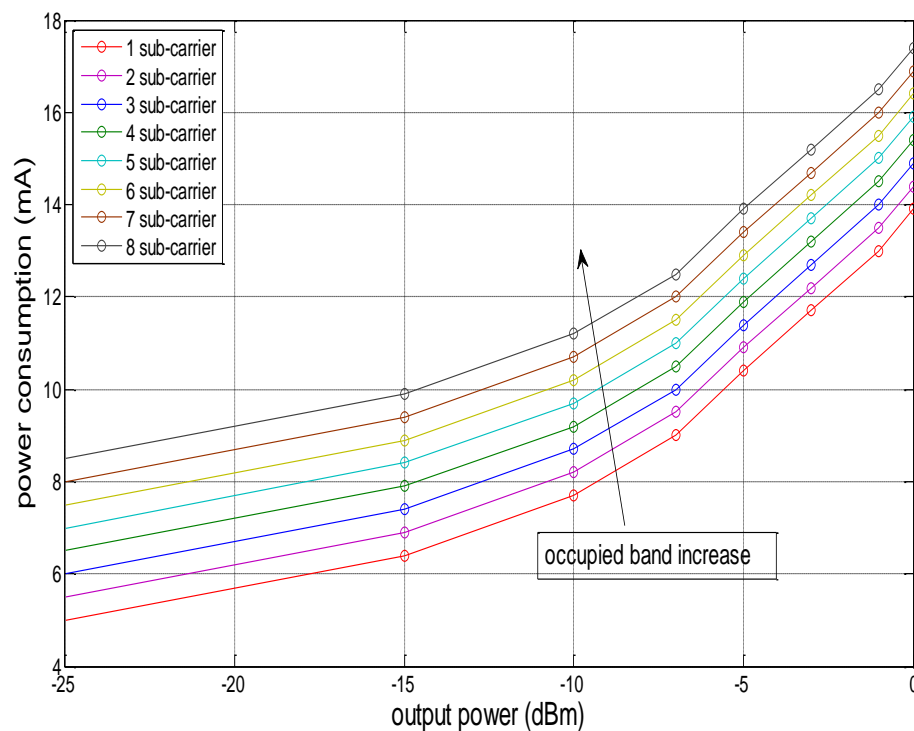


Figure 3.10. Two dimension power scalability

### 3.4 Experiment Validation

The proposed system has been evaluated by emulating the most popular transceiver in WSNs: CC2420 [20], which was designed and produced by Chipcon (now part of Texas Instrument). The functions of this

transceiver were divided into 3 parts, which will be emulated by different instruments respectively:

- Matlab for digital processing
- Agilent ESG 4432b for up-converting and as a Power Amplifier
- R&S FSQ 40 for down-converting and as an Low Noise Amplifier

Two Agilent ESG4432b were employed to emulate two independent transmitters, as well as one FSQ40 acting as the Rx device. They are all connected and controlled by GPIB. Each transmission device generates half the sub-carriers with the same output power. To simplify the experiment, it is assumed that the Rx has locked to the frequency of Tx1, while Tx2 transmits with a frequency offset of  $\Delta f_{CFO}$ . Additive noise is added at the receiver side during the digital processing to simplify the emulation. The central carrier frequency is 2.4GHz. The setup of the experiment is given in Figure 3.11, while the photo of experiment is given in Figure 3.12. A screen snapshot of the FSQ40 has been sampled and is shown in Figure 3.13 to give an example of the signal spectrum.

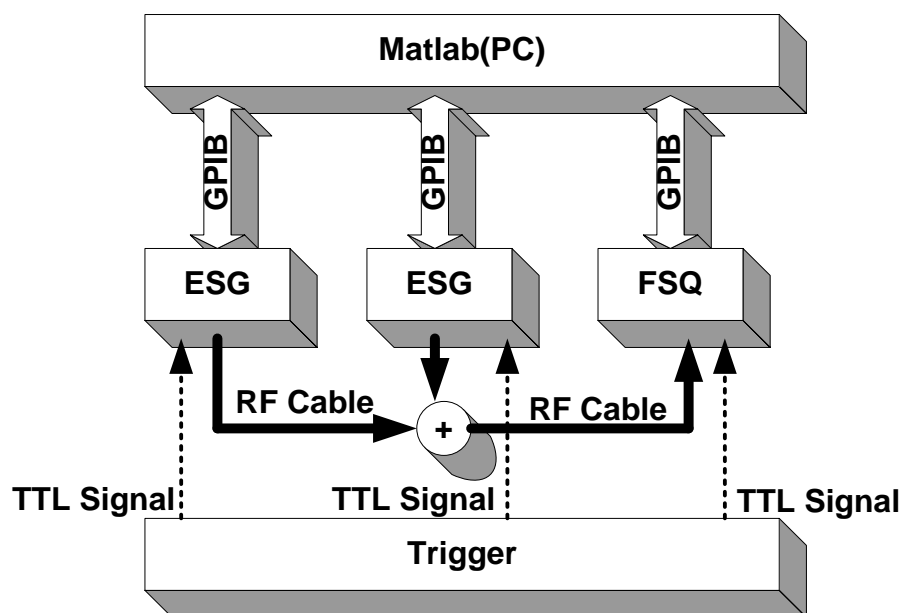


Figure 3.11. Experiment Setup of the multi-carrier base WSN architecture

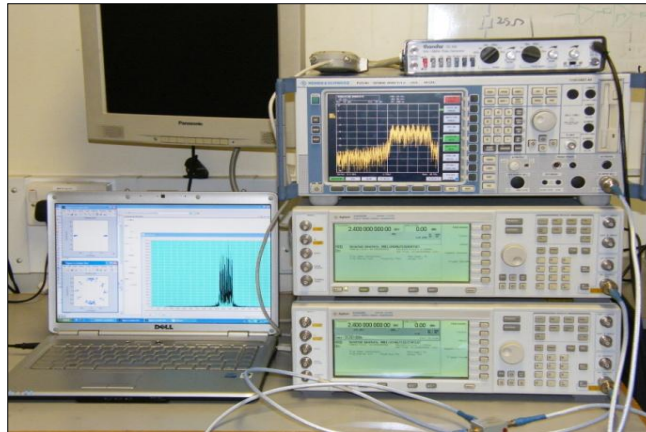


Figure 3.12. Photo of the multi-carrier base WSN Experiment

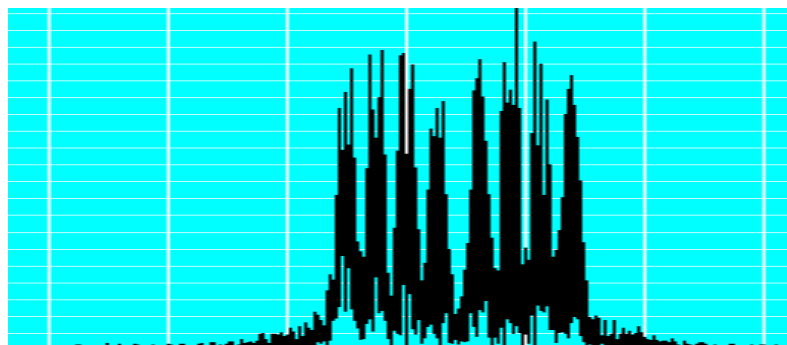


Figure 3.13. Signal Spectrum in experiment, captured from FSQ40

The results in Figure 3.14 clearly show that the error performance of the system is acceptable within  $\pm \frac{1}{4}dF$ . The tolerable CFO range for the proposed system is  $\frac{1}{2}dF$ . By carefully choosing the number of sub-carriers and the channel bandwidth, we can restrict most of the CFO within this range. In fact, by capturing the transmitting signal from a commercial IEEE 802.15.4 transceiver, it has been noticed that the CFO of the signal is around 42kHz, which is much less than  $\frac{1}{2}dF$  (125kHz).

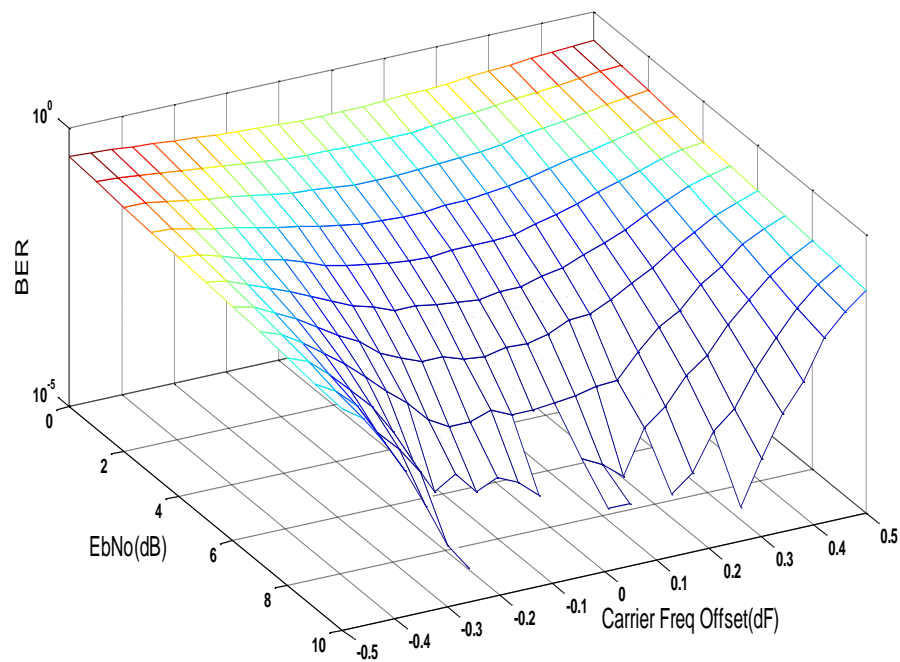


Figure 3.14. Error performance result of the multi-carrier based system

The PAPR factors of transmitted signals were monitored during the experiment. For the signal occupying all 8 sub-carriers, the PAPR factor monitored is 5.93 dB; the corresponding PAPR factor for only 4 sub-carriers is 4.42 dB. When compared to the PAPR of other popular signals, 4 dB for a QPSK signal, 7 dB for SCFDMA signal, and 12 dB for an OFDM signal (according to [83], where the signal consisted of 256 sub-carriers), this factor is only slightly worse than the QPSK signal. This suggests that high cost, linear power amplifiers will not be required, which is much preferred in WSN systems. This experiment has validated the performance of the proposed multi-carrier architecture which is suitable for adoption in the multi-hop sensor networks.

### 3.5 Performance Evaluation

In the previous section, one of the possible multi-carrier physical layer architectures has been proposed and examined through an experimental approach, which enables the devices in the wireless sensor network to use OFDMA-like multiplex with great flexibility. Differing from the traditional device (e.g. CC2420) that can only switch between independent channels,

devices with this new architecture will be able to transmit data over any number of sub-carriers at the same time allowing several devices to transmit concurrently by occupying different sub-carriers. To quantify the potential performance benefits, we have developed an analytic model, in which the overall bandwidth is equal to one channel in the traditional system, e.g. 2MHz in IEEE 802.15.4 as shown in Figure 3.15. This restriction normalises the performance gain to the improvement contributed by the increased channel sharing flexibility not due to any bandwidth increase.

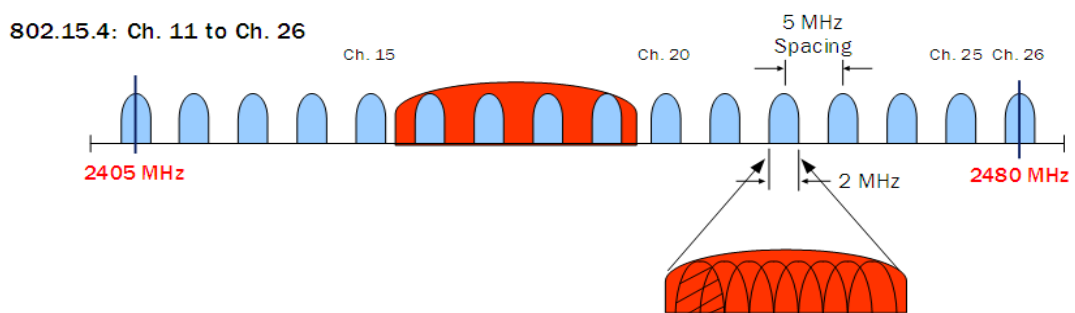


**Figure 3.15. Channel regulation for multi-carrier based system**

For the purpose of baseline analysis, Slotted Aloha is used in the proposed analytic model, as it is the simplest MAC protocol for wireless networking and can be regarded as the baseline, against which other MAC protocols can be compared. The most straightforward candidate is the CSMA based MAC approaches, which have been employed in IEEE 802.15.4 and IEEE 802.11 DCF. Within a CSMA based MAC protocol, the system will have to acquire all the sub-carrier information in the Clear Channel Assessment (CCA) operation, i.e. the device will be able to know which sub-carriers are being occupied by other devices already. Then, the device can only choose the idle sub-carrier to transmit a packet. As a result, the CSMA style MAC could benefit more from the multi-carrier scheme compared with the pure random based Slotted Aloha, since the collision probability can be further decreased (i.e. the performance further increased) by avoiding occupied sub-carriers.

### 3.5.1 Renewal process of Slotted Aloha

The analytic model was built based on the concept of a level based renewal process [84]. This approach can significantly simplify the

mathematical analysis without loss of accuracy, while other approaches e.g. Markov chain [85] are usually analytically complicated.

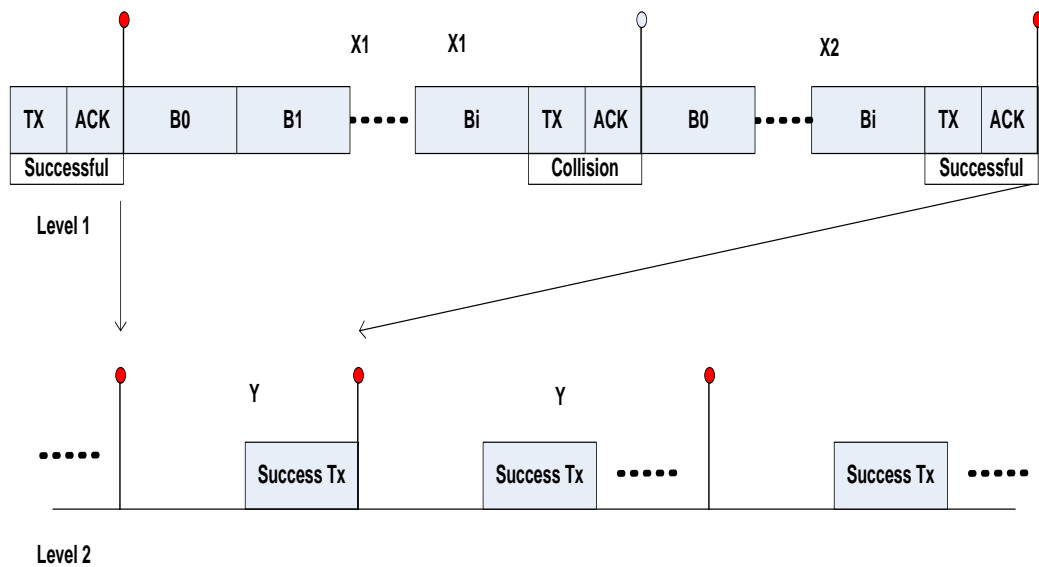


Figure 3.16. Renewal process of Slotted Aloha

Figure 3.16 shows the scheme of the renewal cycle of slotted aloha. Each time a device has a packet ready to send, it will backoff with a random number of time slots following the specified retransmission policy. After the backoff period, the device sends a packet via the wireless channel. If there is only one device sending, then this attempt will be successful (marked as X2 cycle in level 1) and the device will receive the ACK packet from the receiver later in that time slot. Otherwise this transmission attempt will be considered to fail due to a collision (marked as X1 cycle in level 1). There may be  $i$  ( $i > 0$ ) X1 cycles before one X2 cycle, where  $i$  depends on the probability of successful transmission.

From level 2's point of view, there will always be a successful transmission event in each Y cycle, while the average length of Y cycle depends on the performance of the X cycle. After the calculation of the Y cycle's average length, the throughput of the tagged node can be easily deduced as well as other performance measures.

For such a slotted aloha MAC protocol, the completion rules in the proposed multi-carrier architecture based mode will follow the main principle of slotted aloha. The only difference is in the selection of sub-carriers, where

a device takes only a subgroup of sub-carriers, assigned dynamically by the allocation algorithm. Successful transmission is conditioned on whether there is more than one device transmitting on the same subgroup of sub-carriers, rather than over the whole bandwidth. If two devices are assigned to different subcarriers, they can transmit concurrently without collision. Thus, channel competition is less fierce and the probability of collisions decreases. As a result, the average number of re-transmission is reduced which can increase the overall performance.

### 3.5.2 Analytic Model under ideal channel conditions

In this section, an analytic model of slotted aloha is developed and three retransmission policies (uniform backoff, binary exponential backoff, and geometric backoff) analysed. To simplify this analysis, all devices are considered to be placed within the transmission range of one another, so there will be no hidden terminals in the network. All the devices are randomly distributed with uniform probability around the sink device. Consider a single-cluster wireless sensor network with  $N$  devices: when a packet transmission fails, a retransmission is scheduled after a random backoff period, which is determined by a specific retransmission policy. Let  $W_i$  be the  $i$ th backoff period with units of time slots. Then the  $i$ th retransmission takes place at the beginning of the  $W_i$ th available slot after the last failed transmission.

#### 3.5.2.1 Uniform Backoff

Under a Uniform Backoff (UB) policy, all  $W_i$  are uniformly distributed in the same range from  $[0, w - 1]$ , where  $w$  is the backoff window size. The current device will start to transmit in the current slot with probability  $\tau$ , defined by:

$$\tau = \frac{1}{\bar{X}} \quad (3.16)$$

where  $\bar{X}$  is the average length of  $X$  cycle:

$$\bar{X} = T_{Bo} + T_{tx} \quad (3.17)$$

$$\begin{aligned}
&= \frac{w-1}{2} + 1 \\
&= \frac{w+1}{2}
\end{aligned}$$

We first assume that the channel is ideal, i.e. no transmission error. Then, the conditional probability that a device transmits a packet successfully in a single carrier system can be derived by equation (3.18). The extension to the realistic non-ideal channel (where packets will be corrupted with an error probability instead of perfect transmission) will be discussed later this section.

$$P_{suc} = (1 - \tau)^{N-1} \quad (3.18)$$

where  $N$  is the number of devices within the network. If none of the other  $N-1$  devices are trying to transmit in the same slot, then the current device's transmission will be successful. Hence,  $P_{suc}$  represents the ratio of X1 cycle number to X2 cycle number in level 1 within a single carrier system, which means that a level 2 cycle contains a average number of  $1/P_{suc}$  level 1 cycles with an average length of  $\bar{X}$ .

As mentioned in pervious sections, the main performance gain of the multi-carrier system in this model is contributed by increased sharing of the wireless channel, i.e. the increase of  $P_{suc}$ :

$$P_{suc}^{\wedge} = \prod_{n=1}^{N-1} \left[ (1 - \tau) + \tau \cdot \frac{B-1}{B} \right] \quad (3.19)$$

Compared with equation (3.18), the probability of successful transmission is constituted of two parts: the first part is identical to equation (3.16): the current device will not transmit in the current slot, while the second part can be understand as: the current device will transmit in the current slot, but the chosen sub-carrier from the overall  $B$  sub-carriers is different to the one chosen by the current device. Normally  $P_{suc}^{\wedge}$  is much smaller than  $P_{suc}$ , especially when the number of competing nodes is large.

Thus, the average length of a level 2 cycle is:

$$\bar{Y} = \frac{\bar{X}}{P_{suc}} \quad (3.20)$$

The throughput of the tagged device can be calculated, as only one packet can be successfully transmitted in each level 2 cycle:

$$TP_s = \frac{L}{\bar{Y}} \quad (3.21)$$

where  $L$  is the payload in one slot time.

Therefore, the network throughput at the sink node can be defined as:

$$TP = N \cdot TP_s \quad (3.22)$$

### 3.5.2.2 Binary Exponential Backoff

Considering a Binary Exponential Backoff (BEB) policy, the backoff period is uniformly distributed in a binary, exponentially expanding range. After each unsuccessful transmission, the backoff window size will be doubled. In other words,  $W_j$  is uniformly distributed in  $[0, 2^{i-1}(w-1)]$ , where  $i$  is the number of the retransmission,  $w$  is the initial backoff window size. Clearly, the length of  $X$  cannot be directly estimated as in the uniform backoff scenario, since it depends on the successful transmission rate. With a given  $P_{suc}$ , the average length of  $X$  cycle can be written as:

$$\begin{aligned} \bar{X} = & P_{suc}(T_{BO}^0 + T_{tx}) \\ & + P_{suc}(1 - P_{suc}) \frac{(T_{BO}^1 + T_{tx} + T_{BO}^0 + T_{tx})}{2} \\ & \dots \dots \dots \quad (3.23) \\ & + P_{suc}(1 - P_{suc})^{M-1} \frac{(\sum_{m=0}^{M-1} T_{BO}^m + T_{tx})}{M} \\ & + (1 - P_{suc})^M \frac{(\sum_{m=0}^{M-1} T_{BO}^m + T_{tx})}{M} \end{aligned}$$

where  $M$  is maximum retry number, after which the current device will discard the packet.  $E(T_{BO}^i)$  is the expectation of back off slot given by:

$$E(T_{BO}^i) = \frac{2^i w - 1}{2} \quad (3.24)$$

Applying  $T_{BO}^i$  to equation (3.23) gives:

$$\begin{aligned} \bar{X} = & \sum_{m=0}^{M-1} P_{suc}(1 - P_{suc})^m \frac{\sum_{i=0}^m \frac{2^i w - 1}{2} + 1}{m + 1} \\ & + (1 - P_{suc})^M \frac{\sum_{i=0}^{M-1} \frac{2^i w - 1}{2} + 1}{M} \end{aligned} \quad (3.25)$$

As we expected, the average length of  $X$  is highly dependent on the value of  $P_{suc}$ . Then, we can build a non-linear system shown in equation (3.26) by combining the equation (3.18) with equation (3.25). The performance of a single carrier based network can be obtained through the calculation of this non-linear system.

$$\left\{ \begin{aligned} \bar{X} = & \sum_{m=0}^{M-1} P_{suc}(1 - P_{suc})^m \frac{\sum_{i=0}^m \frac{2^i w - 1}{2} + 1}{m + 1} \\ & + (1 - P_{suc})^M \frac{\sum_{i=0}^{M-1} \frac{2^i w - 1}{2} + 1}{M} \\ P_{suc} = & \left(1 - \frac{1}{\bar{X}}\right)^{N-1} \end{aligned} \right. \quad (3.26)$$

Similarly, we can obtain the non-linear system for multi-carrier scenario in equation (3.27) by applying  $P'_{suc}$  from equation (3.19).

$$\left\{ \begin{aligned} \bar{X} = & \sum_{m=0}^{M-1} P_{suc}(1 - P_{suc})^m \frac{\sum_{i=0}^m \frac{2^i w - 1}{2} + 1}{m + 1} \\ & + (1 - P_{suc})^M \frac{\sum_{i=0}^{M-1} \frac{2^i w - 1}{2} + 1}{M} \\ P'_{suc} = & \prod_{n=1}^{N-1} \left[ \left(1 - \frac{1}{\bar{X}}\right) + \frac{1}{\bar{X}} \cdot \frac{B - 1}{B} \right] \end{aligned} \right. \quad (3.27)$$

Equations (3.26) and (3.27) represent a non-linear system with two unknown variables,  $\bar{X}$  and  $P_{suc}$ . For a given scenario, this non-linear system can be solved numerically [86].

### 3.5.2.3 Geometric Backoff

For a Geometric Backoff (GB) policy, the backoff period is geometrically distributed with parameter  $q$ , where the device will start transmission in the current slot with probability of  $q$ . Obviously, the expectation of  $T_{BO}$  is only determined by  $q$ , which can be expressed as  $1/q$ . Thus, the average length of the X cycle can be expressed as:

$$\begin{aligned}\bar{X} &= T_{BO} + T_{tx} \\ &= \frac{1}{q} + 1\end{aligned}\tag{3.28}$$

All the other equations needed for the GB model for both single carrier systems and multi-carrier systems are similar to the UB model discussed previously, and can be easily solved following the same approach.

### 3.5.3 Model Extension

#### A. Non-ideal channel

A non-ideal channel will cause unsuccessful reception of packets in a real deployment. In this more realistic assumption, equation (3.16) should be modified with the condition that both payload packets and ACK packets are transmitted with error probability.

$$P_{suc}^n = (1 - \tau)^{N-1} \cdot PRR_{payload}^n \cdot PRR_{ack}^n\tag{3.29}$$

where  $PRR^n$  is the Packet Receive Rate (PRR) for device  $n$ :

$$PRR_l^n = (1 - BER^n)^{8 \cdot l}\tag{3.30}$$

where the Bit Error Rate (BER) is a function of the distance between device  $n$  and sink device, which can be calculated using equation (3.13) with the condition  $\Delta f_{CF0} = 0$ .  $l$  is the length of packet in Bytes. In this condition, equation (3.19) should be rewritten as:  $\sum_{n=1}^N TP_n$  since each device will have a different BER based on their different distance from the sink device.

Obviously, this modification will make the analytic model hard to solve. With the assumption that all the devices are uniformly random distributed around the sink device, a constant value of PRR expectation can be used to instead:

$$\begin{aligned}
 TP &= \sum_{n=1}^N TP_n \\
 &= \sum_{n=1}^N \frac{L \cdot P_{suc}^n}{\bar{X}} \\
 &\cong N \cdot \frac{L \cdot P_{suc} \cdot PRR'_{payload} \cdot PRR'_{ack}}{\bar{X}} \\
 &= N \cdot TP_s \cdot PRR'_{payload} \cdot PRR'_{ack}
 \end{aligned} \tag{3.31}$$

where  $PRR'$  is a constant value which can be calculated by numerical solution.

#### B. Service delay

Service delay is defined as the duration from the time when the packet is generated to the end of its successful transmission. The average length of a level 2 cycle represents the time period between two successful transmissions. If  $M = \infty$ , in other words, a packet will never be discarded and  $\bar{Y}$  will be the exact service delay. However, a packet will be discarded after  $M$  attempts in a real deployment so that  $\bar{Y}$  should be redefined as a combination of the service time for discarded packets and the service time for the current packet.

Let  $P_{dis}$  denotes the probability that a packet will be discarded by the current device after  $M$  unsuccessful transmissions,  $P_{dis}$  can be calculated as:

$$P_{dis} = (1 - P_{suc})^M \tag{3.32}$$

We note that there will be only one successful transmitted packet in every  $\frac{1}{P_{dis}}$  attempted transmission. Thus, the average service delay  $\bar{D}$  is the average length of level 2 minus the average length contributed by discarded packets:

$$\bar{D} = \frac{\bar{X}}{P_{suc}} (1 - P_{dis}) \quad (3.33)$$

The delay distributions can also be derived from this analytic model when required, more details can be found in [87].

### C. Energy consumption

Power efficiency in this model is evaluated by the average power consumed for each of the level 2 cycles, i.e., the power consumed for each successfully transmitted packet. As stated previous, each successful transmission is based on several level 1 cycles, which are consisted of three stages: backoff, transmission and receive, with each stage, consuming power with rates:  $E_i$ ,  $E_t$  and  $E_r$  respectively. It should be noted that the power consumed in that slot will always be the same whether or not the ACK is successfully received. As a result, the power consumed in this stage has been normalised to a single rate  $E_a$  to simplify the calculation. The energy consumption for each transmission attempt can be defined as:

$$\bar{e} = T_{BO} \cdot E_i + T_{tx} \cdot E_a \quad (3.34)$$

where  $T_{BO}$  and  $T_{tx}$  are related to different scenarios, which can be derived from equations (3.17), (3.23), (3.27).

Considering that current transmission attempt is a success transmission with probability  $P_{suc}$ , then the energy consumption for each successfully transmitted packet can be defined as  $\bar{E}$ :

$$\bar{E} = \frac{\bar{e}}{P_{suc}} = \frac{T_{BO} \cdot E_i + T_{tx} \cdot E_a}{P_{suc}} \quad (3.35)$$

### 3.5.4 Performance Analyses

All three retransmission policies have been implemented in the open source network simulator OMNet++ 4.0 to validate the accuracy of proposed analytic model. In the simulation, all the devices are uniformly distributed within the  $Dmax = 40m$  area. For comparison, two RF physical modes have been implemented in the simulation for network performance evaluation: the first mode is the standard IEEE 802.15.4 PHY mode as a bench mark, where

the RF front-end occupies a bandwidth of 2 MHz and enables a 250 kbps data rate; the second one is the proposed multi-carrier system, where the 2 MHz overall bandwidth is divided into 4 groups of sharable sub-carriers, each of which has a data rate of 62.5 kbps (250kbps/4). We configured that  $\Delta f_{CFO}$  follows normal distribution with mean  $\mu = 0$  and stand deviation  $\sigma = 0.2dF$  (i.e. 50 kHz, according to the 42 kHz frequency offset monitored in an IEEE802.15.4 system through an experimental approach). Therefore the PRR expectation for the analytic model was derived from the experiment data. It is worth noting that, as discussed in [88], although the proposed multi-carrier system has acceptable performance when the frequency shift is within  $\pm \frac{1}{4} \Delta f$ , the error expectation of multi-carrier system will still be slightly worse than a single-carrier system in the same network scenario. The time slot length was set to be  $40 \cdot T_s$ , ( $T_s$  is set to be one symbol duration: 16  $\mu$ sec, according to [16]), which equates to 80 bits of data in the packet. The initial backoff window size  $W$  is set to 8, with the maximum retransmission attempts  $M=4$ , and the geometric probability  $q$  used in the GB model is set to 0.1. The transmission error performance is derived from the previous experiment results in section 3.4. Each simulation program lasts around 30min, and is repeated 10 times to give a reliable average result.

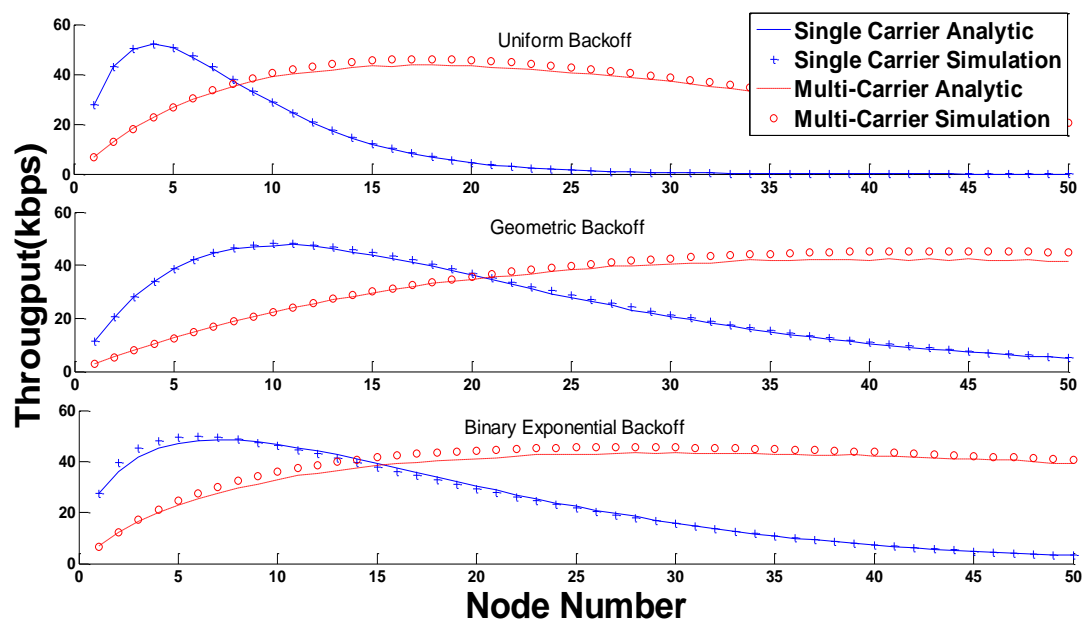


Figure 3.17. Simulation result versus Analytic result ( $W=8$ ,  $M=4$ ,  $Q=0.1$ ,  $B=4$ )

Throughput is calculated in the sink device and shows how many data packets arrived at the sink device successfully in a given period. The results in Figure 3.17 show a high degree of correlation between the simulation and the proposed analytic model. Therefore, although the throughput of the proposed system is lower than the traditional system because of the lower available traffic load with lower node numbers (since the simulation works in saturation mode, the offered traffic load is only decided by node number), the throughput of the proposed system will be greater than the standard system when the node number crosses a threshold. Furthermore, the throughput of the single-carrier system will trend to zero when the size of network is extremely large, while the proposed system still shows very good performance. The results suggest that the proposed system is more suitable for data intensive applications in large scale networks.

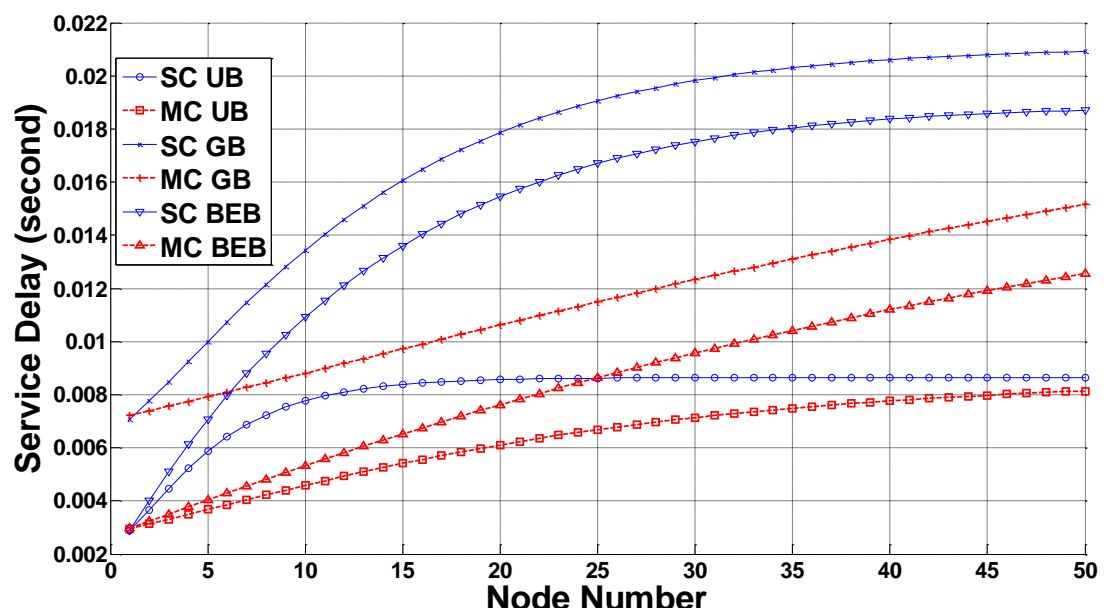


Figure 3.18. Average Service Delay

Figure 3.18 shows the average service delay of the single carrier system and the proposed multi-carrier system in the three different backoff policies. In the UB backoff, the general trends of the service delay can be described as: the service delay of single-carrier increases rapidly to the upper bound, while the delay of the multi-carrier system increases slowly and converges to the upper bound as the network size goes large. Similar trends can be seen obviously in the GB and BEB policies. However, as the average

cycle lengths in these two models are larger than the UB model, these trends have been significantly amplified.

In order to calculate the energy performance, an approximation of the power consumption of the CC2420 transceiver (as shown in Table 1) is deduced from the datasheet of the CC2420 [20]. In the CC2420, the currents are mainly drawn by four components: front-end, baseband processing, digital processing and the system basic components (i.e. clock sources, I2C bus communication and other basic functionalities). According to the datasheet, CC2420 has an idle state with power consumption of 400 $\mu$ A. Thus, the 400 $\mu$ A is regarded as the power consumption for the system basic component. However, the datasheet only provides the total power consumption of 17.4mA for Tx and 19.7mA for Rx modes without distinguishing how much of the current is consumed by each of the components. It is reasonable to approximate the power consumption of the transmitter front end at 0dBm transmission power by 9mA and the remaining 8.4mA consumption consists of 4mA by baseband processing, 4mA by digital processing and 0.4mA by the basic component. Similarly, in the Rx mode, the Rx front end power consumption is approximated by 11.3mA, and 8mA for both baseband processing and digital processing.

**Table 3.1 Power consumption settings**

	Power Consumption(mA)
Tx front-end (PA)	9 (output 0 dBm)
Rx front-end(LNA)	11.3
Baseband (DAC,ADC)	4
Digital Processing	4
Idle (CLK, bus)	0.4

Therefore,  $E_{BO}$  is set to 8.4mA and  $E_a$  is set to 18.5mA in equation (3.30). The proposed multi-carrier based WSNs system has been considered with a 1mA increase in power consumption in the digital processing component due to the additional signal processing function proposed in [7]. The result, shown in Figure 3.19, is in the form of energy consumption per cycle, which can be understood as how much energy has been consumed to successfully transmit a packet. The result demonstrates that the proposed multi-carrier system has a superior performance over the traditional single-carrier system. For instance, the energy consumption in the single carrier

system increases rapidly with increasing network size, while the multi-carrier system maintains relatively low power consumption until the network size is as large as 40. This excellent performance in energy efficiency is due to the high availability of the shared wireless channel, i.e. a higher  $P_{suc}$ .

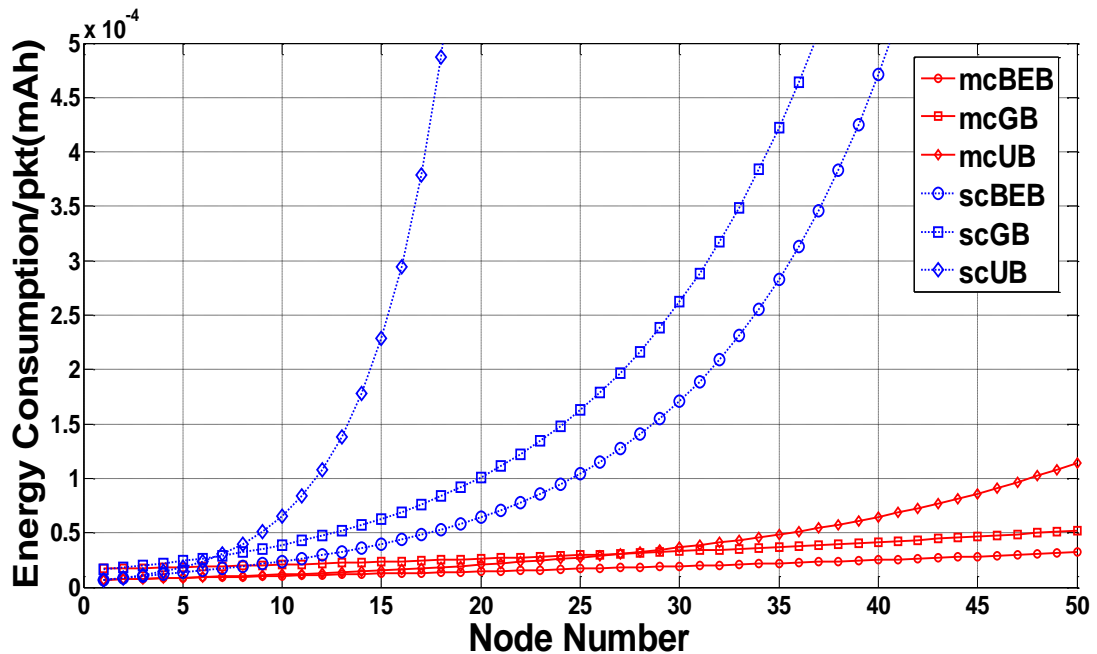


Figure 3.19. Average Energy Consumption every level 2 cycle

Although it is possible to achieve a better throughput performance of the single-carrier system for larger networks by increasing the backoff size, it is at the expense of service delay and energy consumption. Figure 3.20 provides an interesting example: by decreasing  $q$  in GB mode to  $2/33$ , the throughput performance of a single-carrier system shows a similar curve with that of a UB mode multi-carrier system with  $W=8$   $B=4$ . This demonstrates that the proposed multi-carrier system is able to increase throughput, service delay and energy consumption at the same time, which are usually conflicting performance in traditional single-carrier system.

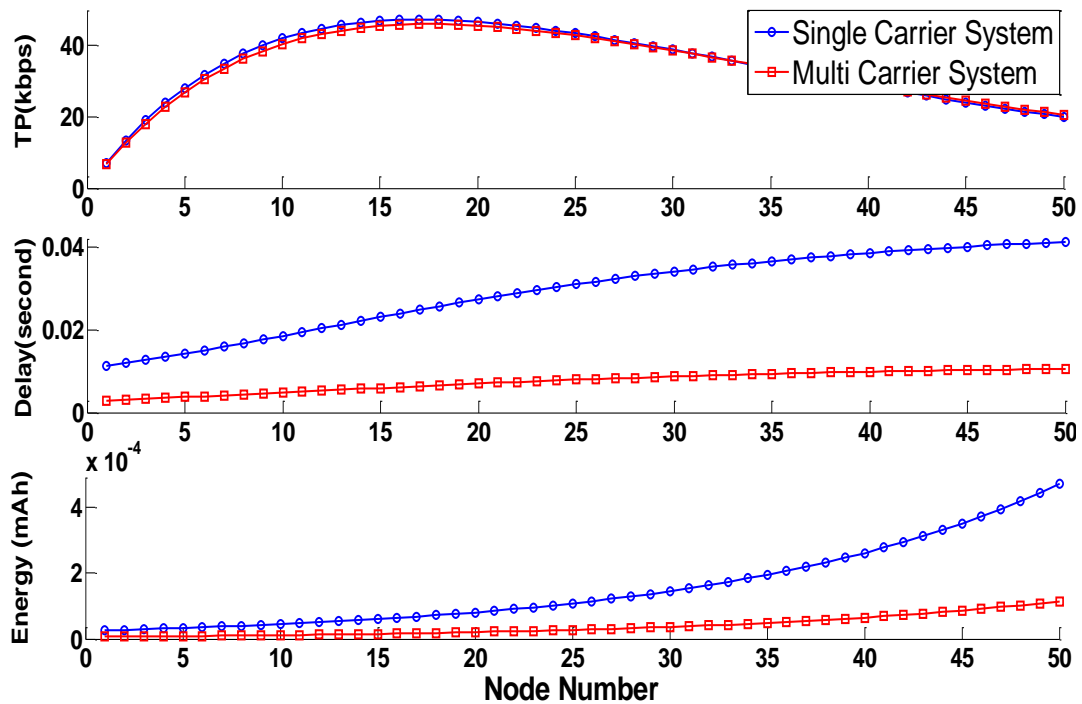


Figure 3.20. Performance for similar throughput

The experiment results verify that, although the proposed multi-carrier based WSNs may not be able to achieve a significant performance improvement in terms of network throughput, i.e. in the form of maximum achieved throughput, the proposed multi-carrier scheme does improve other important performance metrics, notably, service delay and energy efficiency without sacrificing the throughput performance. The deliverable throughput improves when exposed to heavy offered traffic load in dense networks.

To simplify the analyses, the analytic model was introduced with the stipulation that each device only occupies one sub-carrier. Then it is easy to verify that, for any device, the performance can be further improved, if one device is allowed to occupy more sub-carriers. This could be the best solution to provide different QoS service according to application requirements. However, the assignment of sub-carriers at the network level is expected to be an extremely complex optimisation problem, especially in the multi-hop network scenario. This will be studied in our future work. The system can also be designed to work with a wider overall bandwidth, (e.g. the system works across all 16 IEEE802.15.4 channels), which can be expected to give a significant performance improvement compared with the

standard IEEE802.15.4 system. Nevertheless, the proposed analytic model may still apply for these scenarios, and the extension should be very straightforward.

### 3.6 Conclusion

In this chapter, we introduced an OFDMA liked multi-carrier architecture for WSN systems intending to increase the network performance in the channel contention period. We first analysed the cause of CFO and PAPR problems for multi-carrier system, based on which a low cost solution for multi-carrier system has been proposed to mitigate these problems. Such architecture can be utilised for the intelligent bandwidth management by dividing the overall channel into several sub-carriers, which can be allocated to different WSN devices to enable concurrent transmission. Beside of this, as each sub-carrier operates in a relatively narrow band, the system will have high resistance to the frequency selective fading channel caused by multi-path effects. The proposed solution is compatible to the essential low cost and energy efficiency requirements of WSNs.

An emulation based experiment has been set up to prove the feasibility and show error performance of the proposed architecture. An analytic model has been proposed to evaluate the potential performance improvement of the proposed multi-carrier architecture for wireless networks. The performance improvement has been validated by intensive simulations in OMNet++4.0. Compared with the single carrier system, the proposed scheme demonstrates a number of benefits. First, superior energy efficiency can be achieved, because of the efficient channel contention process which reduces backoff time, collisions and retransmissions. Second, the proposed multi-carrier scheme has a better throughput performance in larger networks with intensive traffic load for the WSN applications with high traffic load. These performance improvements are the result of the significantly increased success probability of the contention period.

In addition, there is another important benefit of this proposal: dynamic bandwidth assignment for WSNs. The proposed multi-carrier system can allocate different bandwidth to devices according to their

application requirements. This flexibility allows differentiation of QoS requirements by allocating more bandwidth to the task with high priority, time critical requirement, or large quantities of data to be transferred. However, since the assignment of sub-carriers at the network level is expected to be an extremely complex problem [89;90], we defer to future work the examination of the resource allocation problem.

## Chapter 4. Error Performance Estimation for Adaptive Spreading Code Length based WSN

### 4.1 Introduction

The Direct Sequence Spread Spectrum (DSSS) technique utilised in the most prevalent wireless sensor network standard, IEEE 802.15.4, provides high reliability in high interference environments. The scheme converts each information symbol into a 32 bit chip sequence. This spreading operation utilises a wider bandwidth to suppress interference from the environment or self interference caused by multi-path effects. However, in many deployments the wireless link may provide far higher Signal to Noise Ratio (SNR) than required and therefore this spreading unnecessarily decreases the data rate. Such an operation will prolong the transmission period of packets, which reduces the throughput and wastes energy. However, as the spreading code length is adjustable<sup>7</sup>, it is possible to employ a shorter spreading code to increase the data rate in higher SNR scenarios. Therefore, we are motivated to exploit this to improve the performance of WSN systems by finding the trade-off between transmission resilience and channel quality.

There exist other approaches to achieve a similar improvement, the most popular of which is to adapt the modulation order, e.g. from 2-PSK to 8-PSK. This scheme can offer more scalability within the varying wireless channel, but also requires more complexity. In the adaptive spreading code length, the system can switch the data rate by simply changing the mapping scheme with multiple code sets in the decoding stage. In contrast, adaption of the modulation order requires several modulation and demodulation functions to be utilised, entailing the reconfiguration of the whole receiving chain rather than just the digital decoding stage. As a result, the complexity

---

<sup>7</sup> Such feature can be easily implemented with very simple modification in the mapping stage of transceiver. Several IEEE 802.15.4 transceivers from Atmel and Freescale have already supported this incompatible function.

and energy consumption will increase for adaptive modulation order approaches. Considering the low cost and low energy nature of the WSNs, the adaptive spreading code length is a more reasonable solution.

The expected system should be able to transmit packets at a data rate optimised to the SNR margin of the particular wireless link. Obviously, an optimisation process is required in the upper layer to decide when and how to adapt the spreading mode to achieve optimum performance. Such a mechanism should be able to identify the potential link capacity for each of the spreading code length modes, which is vital to utilise the adaptive spreading code length to increase the network performance. Therefore, in this chapter we try to propose an accurate estimation model for the error performance of different spreading modes in the AWGN channel. Later in Chapter 5, we will deal with how to estimate the channel quality with limited calculation resource.

To better understand these problems, we base our analysis and experiment on a Commercial off-the-shelf (COTS) platform, the ATMEL AT86RF231 [21], which supports an evolution of the adaptive spreading code length from the IEEE 802.15.4 standard [16]. The standard employs 32 chips DSSS to provide a fixed 250kbps data rate at 2Mchip/s. In the AT86RF231, three additional operating modes with spreading code lengths: 4 chips, 8 chips and 16 chips along with the standard 32 chips mode are realised, which enable the experimental demonstration of the trade off between the data rate and the error performance. It is shown that the accuracy of error performance estimation is highly dependent on the composition of the spreading code sets. We examined the error performance for different spreading code lengths through an analytic approach and proposed an accurate model to estimate the error performance of an adaptive spreading code length scheme. To validate this model, we designed an attenuator based experiment to obtain the error performance of different modes. The experimental results have been compared with the analytic results to demonstrate the accuracy of proposed model.

This chapter is organised as follows: The adaptive spreading code length technique has been briefly introduced in section 4.2. In section 4.3, we

present an analysis of the error performance of different spreading modes. An experiment based on a COTS platform is implemented to obtain the error performance for different spreading modes in section 4.4. The experimental results have been compared with the analytic model results to demonstrate the accuracy of proposed estimation model. To conclude, we summarise our findings and discuss some potential benefited applications in section 4.5.

## 4.2 Adaptive Spreading Code Length in IEEE 802.15.4 System

In this work, we outline a performance estimation model for the adaptive spreading code length based on the IEEE802.15.4 architecture, which is one of the most popular physical layer solutions for wireless sensor networks. As introduced in Chapter 2, four information bits (a symbol) are used to select one of 16 code words from a nearly orthogonal code set to be transmitted during each data symbol period in the physical layer of IEEE 802.15.4. Hence, the rate adaptation will be enabled by adjusting the length of these code words in the mapping stage, as shown in Figure 4.1. As the length of these code words increases, the data transmission rate decreases in addition to an increased SNR requirement. Such a scheme will be an evolution of the IEEE 802.15.4 solution, compliant in its basic mode and backwards compatible. The work in [50] proposed an adaptive spreading code length scheme based on this evolution and demonstrated the great potential of this technique, but due to hardware limitations a full experimental demonstration was not presented. Therefore, although proposed method in [50] is able to show the trends of different spreading code length, it may be hard to guide the practical implementation due to the loss of accuracy in error performance estimation.

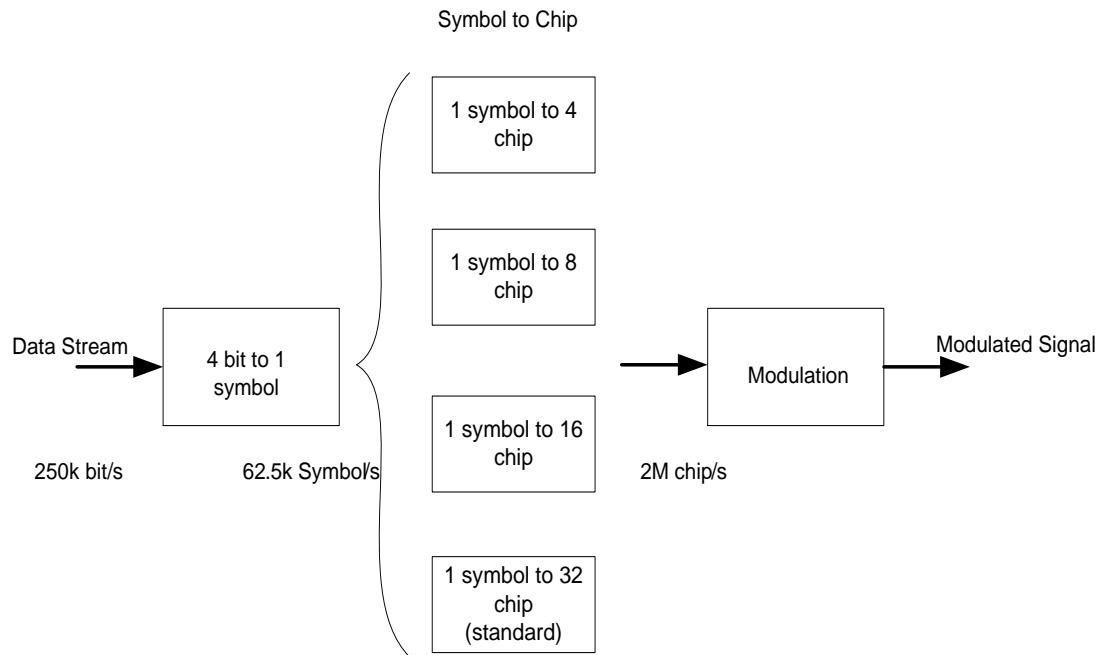


Figure 4.1. Modification in the mapping scheme of IEEE 802.15.4 standard

An accurate analytic model for the error performance of an IEEE 802.15.4 based system must consider the coding effect of DSSS. We first refer to the analytic model of transmission error performance for IEEE 802.15.4 systems coming with the standard [16], which is described by (4.1). This equation is obviously derived from the Bit Error Rate (BER) function for non-coherent 16-ary orthogonal signals using envelop detection method. As the spreading code set used by IEEE802.15.4 is not formed of a true orthogonal code set, such a model can only be considered as a roughly approximation and failed to be extended to other spreading lengths. For instance, some researchers have reported significant deviation between (4.1) and experimental results [91].

$$BER = \frac{8}{15} \cdot \frac{1}{16} \cdot \sum_{k=2}^{16} -1^k \cdot \binom{16}{k} \cdot e^{(20 \cdot SINR \cdot (\frac{1}{k} - 1))} \quad (4.1)$$

Another approach to calculate the BER performance of IEEE 802.15.4 has been proposed in [51] by expressing the spectrum spreading effect as the combination of Coding Gain (CG) and Processing Gain (PG). Processing Gain is well studied for DSSS systems, and is commonly defined as:

$$PG = \frac{n}{b} \quad (4.2)$$

where  $b$  is the number of bits carried in one symbol (in IEEE802.15.4 each symbol contains 4 bits of information) and  $n$  is the length of spreading code.

Coding gain is much more complex, and is usually defined as the reduction in the required  $E_b/N_o$  due to the error performance properties of the coding. For a soft decision based demodulator, an approximate expression of coding gain can be estimated using equation (4.3) according to [51]:

$$CG_{soft} \cong k \cdot \left( \frac{\bar{d}}{n} - \frac{\ln 2}{E_b N_o} \right) \quad (4.3)$$

where  $\bar{d}$  is the mean Hamming distance of a certain spreading code set. For the linear block code employed by IEEE 802.15.4, the Hamming distance can be bounded using the equation:

$$d_{\max} < n(1 - k/n) + 1 \quad (4.4)$$

However, coding gain in a real implementation is usually far from the upper-bound provided by equation (4.3), which is believed to be highly related to the compromises made in choosing the code set. Therefore, although this approach is able to show the trends of different spreading code length, as shown in Figure 4.2, it is still not able to guide the practical implementation.

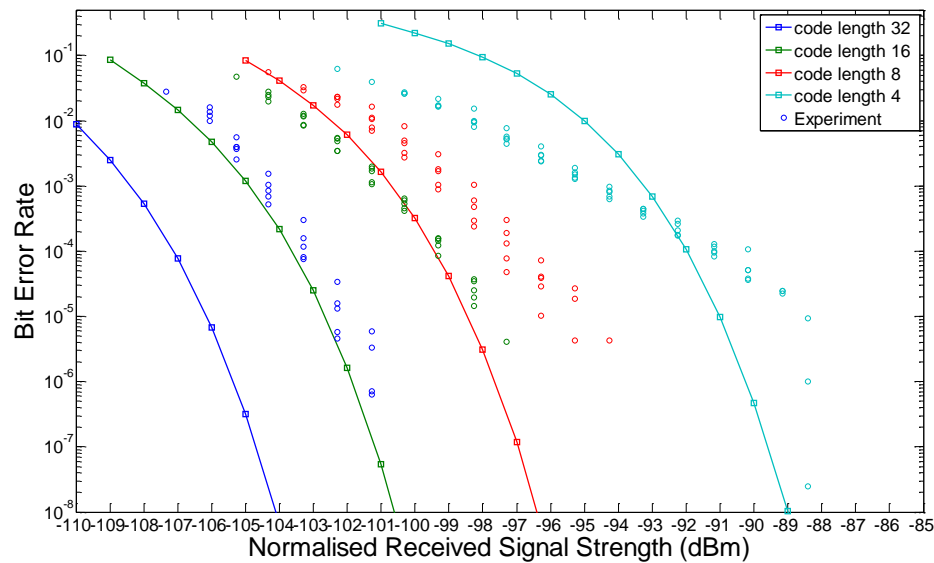


**Figure 4.2. Theoretic BER Performance estimated using hamming distance method**

In addition, a number of attempts have been published aiming to provide an error performance estimation method for IEEE 802.15.4 system [51;92] following numerical and simulation approaches. However, to the best of our knowledge, most of these estimation models either lack of accuracy or too complex to reliably guide practical implementation. Therefore, most proposed higher layers approaches calibrate the relationship between SNR and error performance by exchanging probe packets [93]. Such an operation will cause a relatively high overhead and lead to a reduction in throughput performance and energy efficiency. An accurate error performance estimation model is critical when an adaptive spreading code length is to be employed in IEEE 802.15.4 based WSNs. This motivated us to examine the error performance and propose an accurate error performance estimation model to guide the upper layer design and maximise the potential performance increase.

### 4.3 Error Performance Estimation Model for Adaptive Spreading Code Length in IEEE 802.15.4

The code set used by IEEE 802.15.4 is a linear systematic block code, which is constant for all standard compliant RFIC implementations of IEEE 802.15.4. However, the de-spreading scheme could be different for different implementations. As reported in [94;95], the implementation in the

AT86RF231 uses a hard decision scheme, which can be divided into a two step process. The first step demodulates the 32 chips before feeding them to the detector. It should be noted that the non-coherent differential MSK demodulation is usually employed instead of coherent O-QPSK demodulation to enable low cost and low complex transceiver design as discussed in [94;95]. The complexity of demodulation can be greatly simplified by removing the need for accurate frequency and phase synchronisation. It is well accepted that non-coherent demodulation for MSK system has the same error performance as non-coherent 2-FSK [96].

The demodulated chip sequence will then be correlated with all the possible code words to generate the de-coded decision in the second step. It should be noted that the non-coherent MSK demodulation mechanism is implemented by comparing the phase different between the current chip and the previous chip. In other words, the direct demodulation output can be seen as a differential encoded variation of the original chip sequence. Therefore, in the correlation stage the system can either re-code the output result or re-code the code words. The later solution has been widely adopted, since the first choice requires a dynamic re-coding process. In this case, the spreading code set provided in the IEEE 802.15.4 regulation can not be directly used in the correlation stage, and the provided code set should be re-coded in advance following the differential approach instead. Such scheme has been examined and discussed in [97]. The re-encoded code sets for the demodulator have been provided in Table 4.1. Clearly, the first step should have same error performance as a non-coherent MSK system. The coding gain and processing gain is contributed by the de-spreading process of the second step, as an incorrect decision can only be made when the number of error chips exceeds a certain threshold (defined as the largest number of chips that the code set can correct within each block of  $n$  chips, denoted as  $N_e$  for the following discussion).

A Monte Carlo simulation has been implemented in Matlab to determine the  $N_e$  performance of IEEE 802.15.4 code set. The results, shown in Figure 4.3, provide a better understanding of the effect of coding in IEEE 802.15.4:

- The  $N_e$  in this scheme is not a constant value. Instead, a normal distribution could better express the coding effect.
- There is an imbalance among the code sets. It is clear that the code set can be divided into two groups: code word 1~8 and code word 9~16. The first group has a higher mean value than the second group, as shown in Figure 4.3.

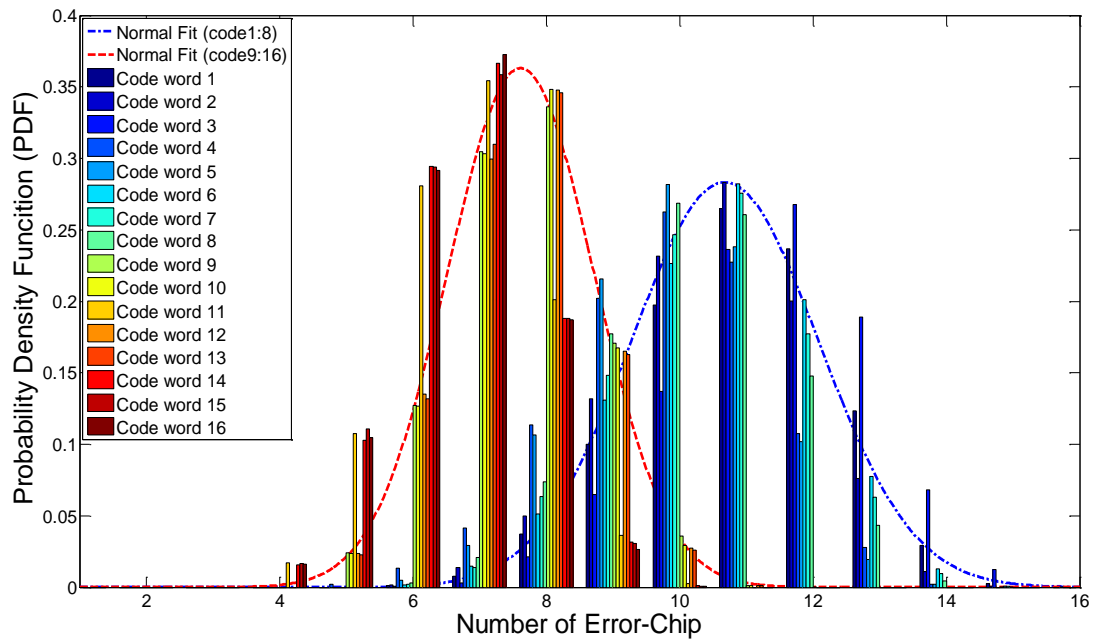


Figure 4.3. Histogram of maximum tolerant number of the error chip

We assume that the distribution of  $N_e$  is closely related to the exact composition of the code sets. Although the code set used for 250kbps mode has been provided by IEEE 802.15.4 regulation, the code sets employed by the other 3 modes are not revealed in the datasheet of AT86RF231 or any other documents. Therefore, we designed an experiment to obtain these code sets by using a Vector Signal Analyser to capture the RF signal from AT86RF231 and digitally down convert it to a baseband I-Q sequence. We then examined the baseband signal by comparing the phase difference between chips, which is a common differential MSK demodulation method. We have successfully demodulated the first 3 modes of 250kbps, 500kbps, and 1Mbps to determine the unique spreading code sets employed, which have been provided in Table 4.1. It was discovered that the 2Mbps mode

also employs a chip scrambling scheme to improve its spectral properties<sup>8</sup>, which results in different performance from the first 3 modes. Thus, it would require an entire different analytic model to predict error performance, which persuaded us to defer the study of the 2Mbps mode to future work.

**Table 4.1 Spreading code sets employed by AT86RF231 in MSK format**

Symbol	Code Length 32	Code Length 16	Code Length 8
0x0	0x 6077AE6C	0x 68C5	0x 36
0x1	0x 4E077AE6	0x 7A31	0x 1B
0x2	0x 6CE077AE	0x 5E8D	0x 0D
0x3	0x 66CE077A	0x 17A2	0x 46
0x4	0x 2E6CE077	0x 45E9	0x 63
0x5	0x 7AE6CE07	0x 317A	0x 31
0x6	0x 77AE6CE0	0x 0C5E	0x 58
0x7	0x 077AE6CE	0x 2316	0x 6C
0x8	0x 1F885193	0x 173A	0x 49
0x9	0x 31F88519	0x 05CE	0x 64
0xA	0x 131F8851	0x 2173	0x 72
0xB	0x 1931F885	0x 685C	0x 39
0xC	0x 51931F88	0x 3A17	0x 1C
0xD	0x 051931F8	0x 4E85	0x 4E
0xE	0x 0851931F	0x 73A1	0x 27
0xF	0x 78851931	0x 5CE8	0x 13
<b>Mean value of <math>N_e</math></b>	8.8	3.15	0.77

With knowledge of code sets obtained, it is now possible to build an error performance model for the adaptive spreading code length modes. In the IEEE 802.15.4 system, it is the chip stream, instead of the bit stream, that is transmitted in the channel, and received by the receiver. Therefore the energy per chip to noise spectral density ratio ( $E_c/N_o$ ) should be equal to the SNR of the wireless channel as shown in (4.5).

$$E_c/N_o = SNR \quad (4.5)$$

As discussed above, although the modulation is O-QPSK with half sine pulse shape filter, the demodulation used by the AT86RF231 is based on the non-coherent MSK system to avoid complex synchronisation. Thus, the Chip Error Rate (CER) function can be expressed as:

<sup>8</sup> This has been confirmed by the designer of this transceiver.

$$CER = \frac{1}{2} \cdot e^{(-\frac{1}{2} \cdot E_c/N_o)} \quad (4.6)$$

Therefore, a symbol is detected incorrectly only in the condition that more than  $N_e$  of the chips were demodulated in error. If  $N_e$  is a constant value, the Symbol Error Rate (SER) function can be defined as [98]:

$$SER \cong \frac{1}{n} \cdot \sum_{j=t+1}^n j \cdot \binom{n}{j} \cdot CER^j \cdot (1 - CER)^{n-j} \quad (4.7)$$

where  $n$  is the spreading code length for different modes, for instance 32, 16, 8 respectively,  $t$  is equal to the  $N_e$  of current code set, and CER is defined in equation (4.6). However, since Figure 4.3 shows that  $N_e$  is a distribution rather than a constant value in the IEEE 802.15.4 system, equation (4.7) should be modified as:

$$SER \cong \frac{1}{C} \cdot \sum_{t=1}^c \sum_{t=1}^n P_t \cdot \frac{1}{n} \cdot \sum_{j=t+1}^n j \cdot \binom{n}{j} \cdot CER^j \cdot (1 - CER)^{n-j} \quad (4.8)$$

where  $c = 16$ , is the number of code words in a code set and  $P_t$  is the Probability Distribution Function (PDF) of  $N_e$  for current code word.

We are now able to calculate the error performance for an IEEE 802.15.4 system and its adaptive spreading code length evolutions, through equations (4.6) and (4.8). As a rough approximation, equation (4.7) with the mean value of  $N_e$  can be used. The mean values of  $N_e$  for different modes have also been provided in Table 4.1, and can be rounded to the nearest integer: 9, 3, and 1 respectively.

## 4.4 Empirical Validation of the Model

### 4.4.1 Experiment setup

To collect a reliable measurement from the practical implementation, a COTS (Commercial off-the-shelf) device based experiment has been designed and constructed using an attenuator system to implement a controllable AWGN channel, where the SNR can be accurately configured and all errors are caused by the additive noise. It should be noted that, in the

real deployment, WSN networks are posed with a wireless channel with fading effects as we discussed in Chapter 2. The error estimation models for the fading channel are usually complex and environment dependent (e.g. the degree of fading is location correlated), which makes it unaffordable in the low cost WSN platform. Therefore, we only discuss the AWGN based estimation model and use a controllable AWGN channel to validate the accuracy. This does not mean this scheme is only lab applicable. To make the proposed models works with the real deployment, we will discuss a new channel indicator in the next Chapter, which will consider the fading effect and generate a new indicator equalised to SNR value in AWGN channel to achieve the same error performance. As a result, these two schemes will work closely with each other to accurately estimate the capacity of the current channel state with affordable processing cost to enable deployment in low cost WSN platforms.

Figure 4.4 describes the architecture of this experiment, while Figure 4.5 shows a photo of the experiment. The RF signal from the transmitter will be fed to the attenuator system, consisting of a 6 dB fixed attenuator and an adjustable attenuator with a range of 0dB ~ 71dB. Using a Power Combiner, an emulated environment noise signal generated from an HP ESG4432B Vector Signal Generator has been added to the transmitted signal. After that a Power Divider will split the signal to two even parts. One signal will be fed to the receiver, while another will be fed to a spectrum analyser to monitor the signal strength. Prior to the experiment, the whole transmission system has been characterised using an AGILENT 8714ET Vector Network Analyser.

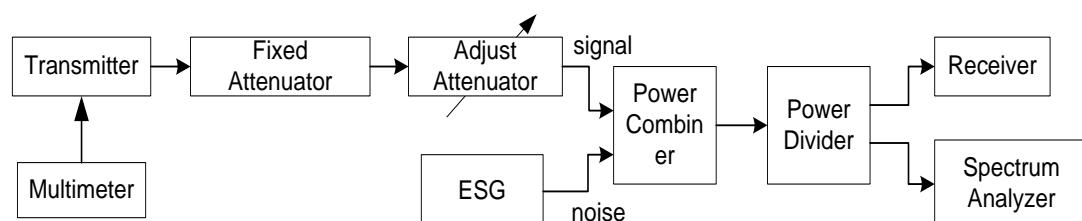


**Figure 4.4. Experiment architecture to determine the error performance in an AWGN channel**

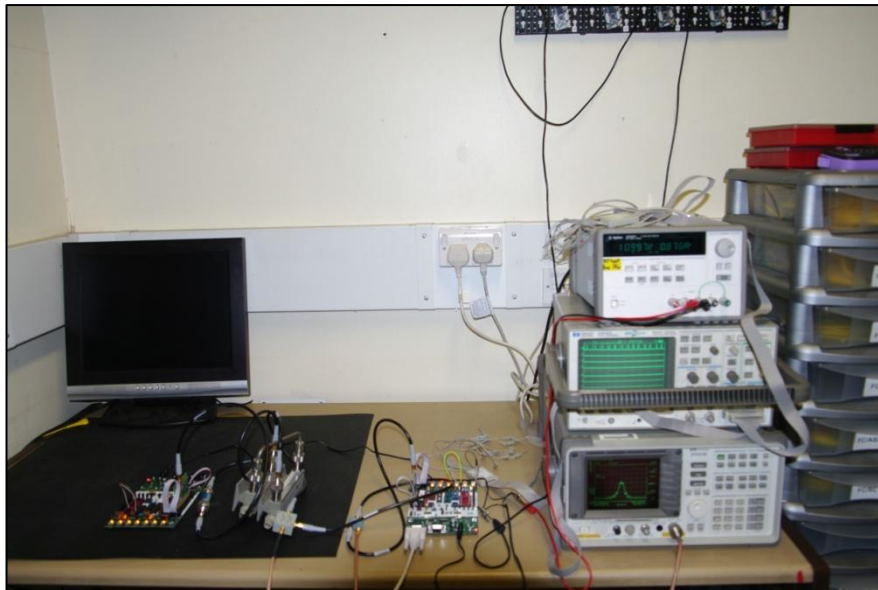


Figure 4.5. Photo of Experiment setup to determine the error performance in an AWGN channel

In the experiment, the transmitter has been configured to work in the saturated model<sup>9</sup> using the IEEE802.15.4 un-slotted MAC protocol without ACK (the scheme is shown in Figure 4.6 and discussed in Chapter 2). The **payload length** of packet, **transmitted power** and **spreading code length** are configurable parameters within the experiment. The receiver will generate the statistical information of successfully received packets during each period (default value is 5 seconds in this experiment).

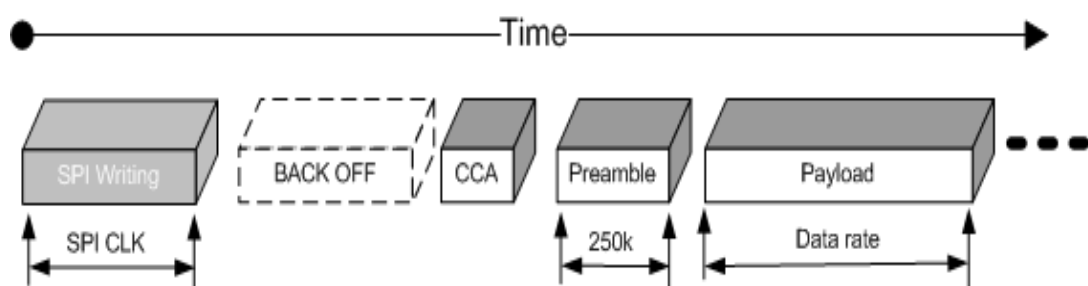


Figure 4.6. IEEE 802.15.4 un-slotted MAC scheme

#### 4.4.2 Validation of error performance estimation model

The experiment result was first presented in the form of Packet Received Rate (PRR, defined as the received packet number compared with the maximum receivable packets number, which is equal to  $1 - \text{PER}$ ) versus Received Signal Strength (RSS) as shown in Figure 4.7 by comparing the result with the maximum number of packets received per period in the

<sup>9</sup> In the saturated model, there will always be a packet ready in the queue to be sent.

experiment, e.g. the extremely high SNR scenario. Without loss of generality, all the variable of figures have been normalised to the Received Signal Strength (RSS) to simplify the comparison in this chapter. The normalised received signal strength is defined as the received signal strength to achieve the same performance without any additional environment noise. We validate our experimental results by comparison with the receiver sensitivity provided by the datasheet of AT86RF231 [21]. As shown in Figure 4.7, the thresholds of sensitivities for different modes provided by [21] show good agreement with the experiment results.

Given the fact that the experimental results are tested with different packet lengths from 20 Bytes to 100 Bytes, it will be inaccurate to validate our experiment using the PRR information. The IEEE802.15.4 standard employs a Cyclic Redundancy Check (CRC) with a length of 16 bits as the frame check to indicate bit errors [21], which means a single symbol error will flag the entire packet as in the 'error received' state. Therefore, we are able to convert the obtained PRR vectors into the form of SER versus Received Signal Strength (RSS). Then, the reliable experimental results can be compared with the output from analytic model (both accurate method and approximation) in Figure 4.8. Although the set of results at each received power value shown a variance, the overall trend for each spreading mode shows an excellent relation to the output of analytic model. These prove that our analytic model is accurate for future usage.

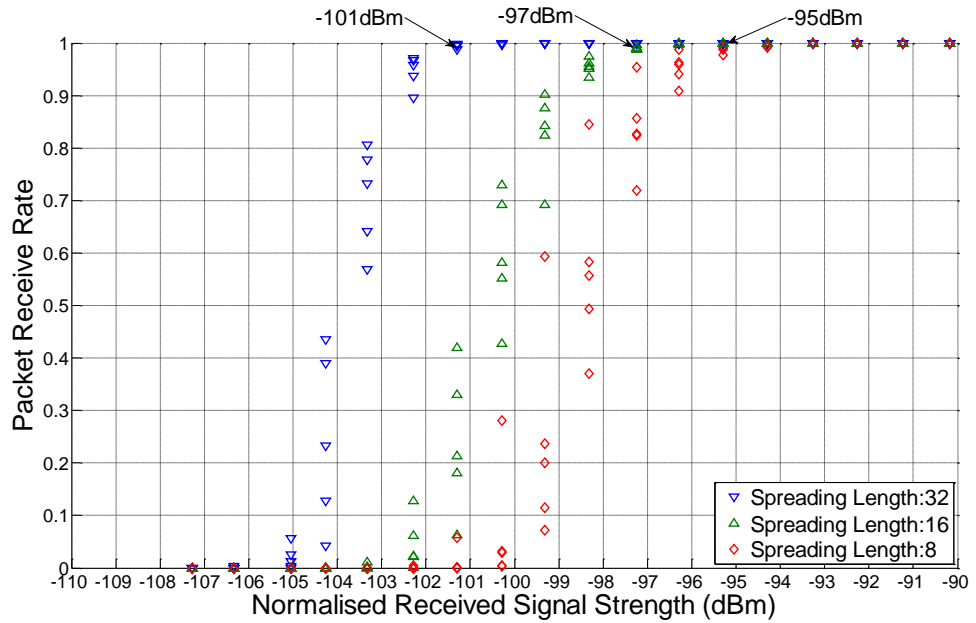


Figure 4.7. Recovered Packet Received Rate from Experiment Results

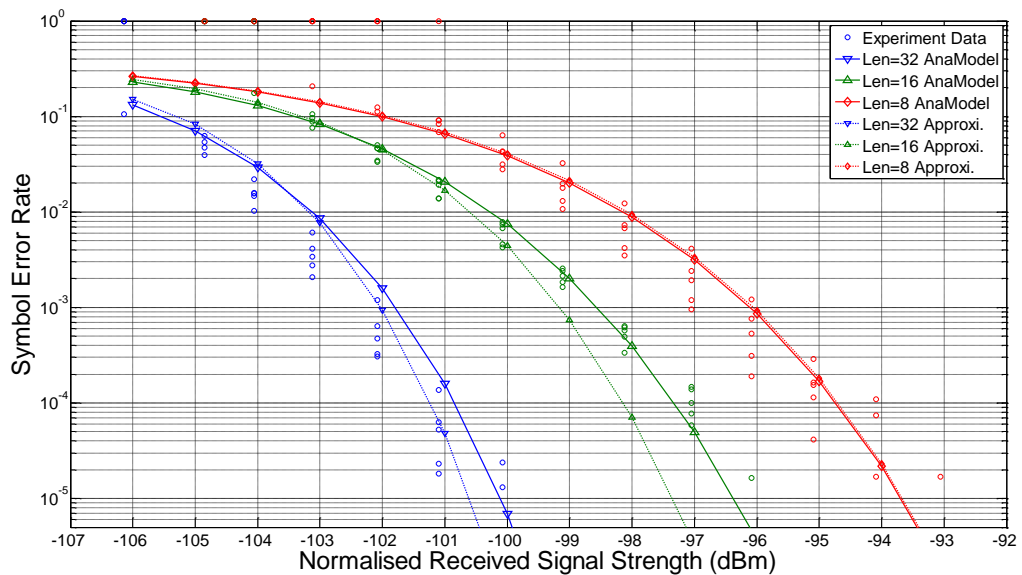


Figure 4.8. Error performances of different spreading code lengths

In order to understand how accurate the proposed analytic models could be, a Root Mean Square (RMS) of the residual, and a Standard Deviation (STD) of the residual are provided as performance criteria. Let  $\overline{SER}_a$  denote the analytic output and  $SER_e$  denote the experiment result. The residual was defined as:

$$r_k = \overline{SER}_a - SER_e \tag{4.9}$$

Then the RMS and STD for N data samples can be defined as:

$$RMS = \sqrt{\frac{1}{N} \sum_{k=1}^N r_k^2}$$

$$STD = \sqrt{\frac{1}{N-1} \sum_{k=1}^N (r_k - \bar{r}_k)^2}$$
(4.10)

where  $\bar{r}_k$  is the mean value of the  $N$  samples. The RMS, STD of the residual error for different analytic models have been provided in table 4.2.

**Table 4.2 RMS/STD of analytic model**

	Code Length 32	Code Length 16	Code Length 8
<b>RMSs</b>	9.0283e-005	1.2721e-005	8.4049e-006
<b>STDs</b>	6.7269e-007	2.2312e-006	6.5868e-007

The proposed analytic model can be employed by the upper layer protocols for the estimation of error performance. Within this usage, the calculation complexity could be an important factor when considering the relatively constrained computation resource in WSN systems. Therefore, we present a calculation cost of proposed model in table 4.3, including the analytic and approximation models. The complexity is defined by the calculation time used in Matlab. Although the absolute value is high related to the CPU, the comparison between two models can assist to understand the trade-off of these two models between accuracy and computation complexity.

**Table 4.3 Calculation complexity**

	Code Length 32		Code Length 16		Code Length 8	
<b>Calculation cost (second)</b>	Analytic	Approximation	Analytic	Approximation	Analytic	Approximation
		1.4518	0.0028	0.4637	0.0018	0.1881

#### 4.4.3 Analysis of throughput Performance

We are now able to analyse the throughput performance of the experimental results to illustrate what benefits can be expected with the adaptive spreading code length feature. Since the experimental setup only

involves a single transmission pair working in the saturated model, and with the validated error performance estimation model, the throughput performance can be easily estimated using equation (4.11):

$$TP = \frac{\text{Payload} \cdot (1 - SER)^{2 \cdot \text{payload}}}{E(T_{SPI}) + E(T_{bo}) + E(T_{CCA}) + E(T_{tx}^{\text{preamble}}) + E(T_{tx}^{\text{payload}})} \quad (4.11)$$

where SER is the symbol error rate, which can be estimated by equation (4.8) and  $E(T_{bo})$  is the expectation of the Back Off (BO) time. The value of  $E(T_{bo})$  can be calculated by  $\sum_{i=0}^{w-1} \frac{i}{w} \cdot 20 \cdot T_{symbol}$ , in which  $20 \cdot T_{symbol}$  is the period for each back off count and  $w$  is equal to  $2^{BE}$ . BE is set to 3 by default, which means that the backoff count is uniformly chosen from (0~7);

$E(T_{CCA})$  is the expectation of Channel Clear Assessment (CCA) time. According to [16], CCA period lasts 128 $\mu$ s;

$E(T_{tx}^{\text{preamble}})$  is the expectation of preamble transmitting time with the data rate of 250kbps;

$E(T_{tx}^{\text{payload}})$  is the expectation of payload transmitting time with a data rate from 250kbps to 1Mbps;

$E(T_{SPI})$  is time cost to write a packet to the AT86RF231 through SPI.

The results of throughput performance are shown in following figures. It is clear that the proposed model fits the experimental results very well. As a result of the variations in temperature, which normally affect the noise floor and the performance of the attenuator network, a random shift existed in some results but such measurement noise is usually slight less than 0.2dB for all the tested results. Generally, due to the high data rate, the spreading modes with shorter code lengths have better throughput as long as there is sufficient SNR. As the signal strength falls, the error rate will increase rapidly, which will lead to a fall in throughput in the high data rate modes. In this region the longer spreading code length based modes have better throughput performance. This trend has been shown by all the experimental results and analytic models, which demonstrates that an optimum mode exists for a given SNR condition to achieve the best system performance.

Figure 4.9 shows the results when the emulated environment noise was fixed at  $-40\text{dBm}$  and the attenuator was adjusted to reduce the signal strength. The second experiment was implemented with the signal strength fixed and the power of environment noise adjusted shown in Figure 4.10. As expected, the results show almost the same curve for each investigated case regardless of the experiment methods. These results demonstrate that the SNR is sufficient to predict the error performance in the AWGN channel.

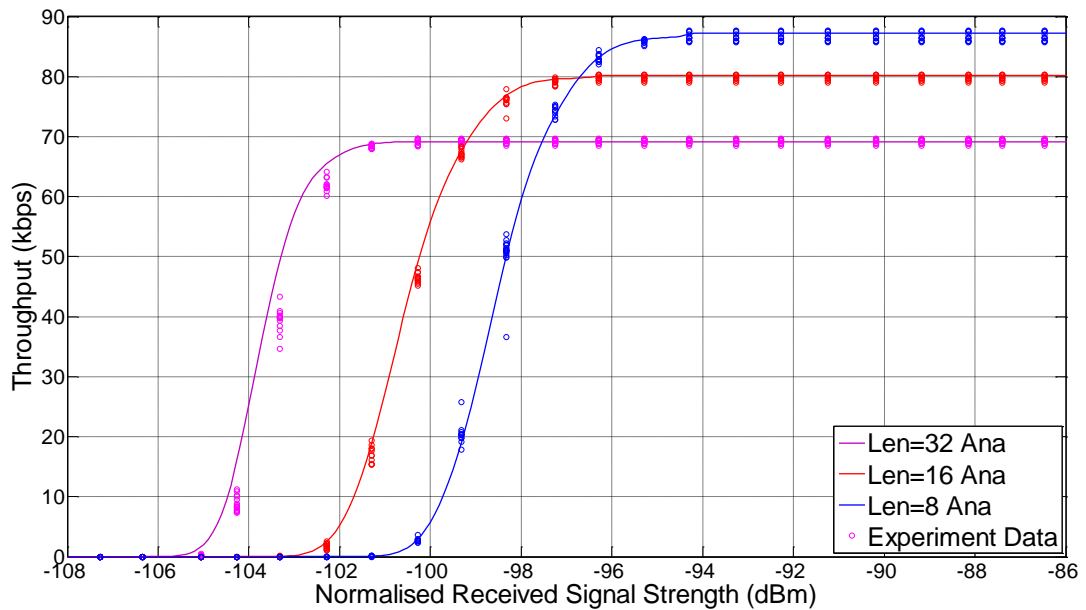


Figure 4.9. Throughput performance with variable signal strengths

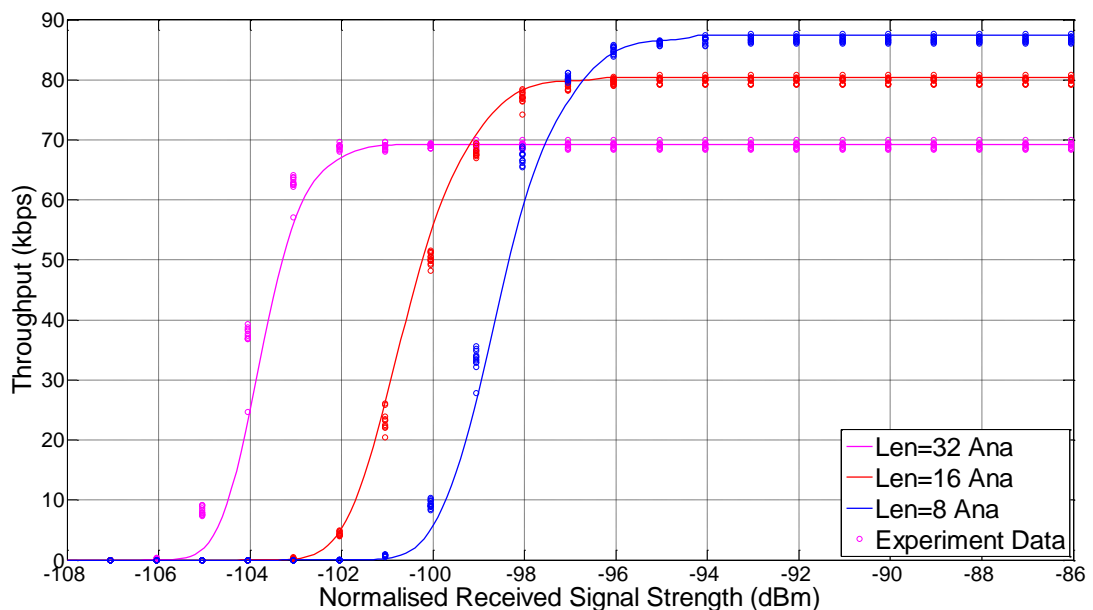


Figure 4.10. Throughput performance with variable noise levels

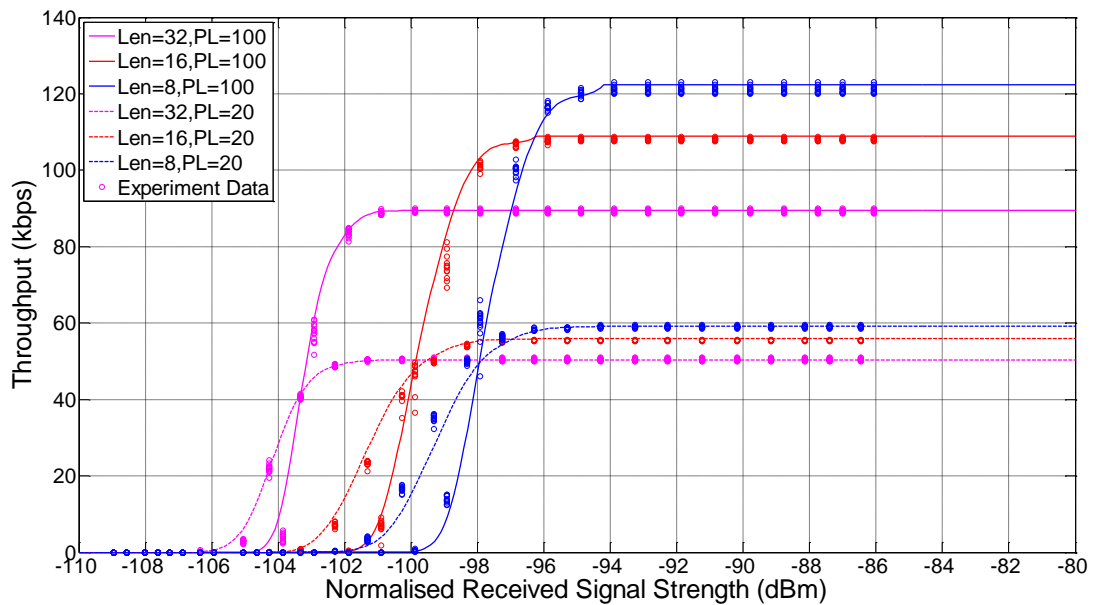


Figure 4.11. Throughput performance with varying packet lengths

As discussed in section 4.4, the preamble is transmitted with a fix data rate (250kbps), therefore the longer payload lengths can result in a higher throughput due to the decrease in the ratio between overhead and data. This effect can be observed by the comparison of Figure 4.11, which shows the differences between the performance increase of 20 and 100 Byte packet length respectively for each spreading code length. The maximum achieved throughput for a 20 Bytes packet length is around 60 kbps, while the system can provide as high as 120kbps throughput for a 100 Bytes packet length. On the other hand, the longer packet length will lead to higher error probability. It is easy to notice that all the curves have been shifted to right with a 100 Byte lengths comparing with a 20 Byte lengths. For instance, the 90% PRR threshold for the mode with a 20 Bytes packet length and 8 chips spreading length is -94.3dBm, while the corresponding value for 100 Bytes is -95.7dBm. Therefore, the length of the packet can cause the trade-off between throughput and error performance, which need to be taken into consideration in the design of upper layer protocol. This phenomenon can be predicated by employing our proposed analytic model.

Figure 4.12 and Figure 4.13 demonstrate the effect of different back-off window sizes, which is an important parameter in the IEEE 802.15.4 MAC protocol. The results shown in Figure 4.12 used  $BE=4$ , while Figure 4.13 shows the effect of increasing this to  $BE=5$ . The maximum throughput for the

3 spreading code length modes decreases to 37.31, 40.32 and 42.02 kbps respectively, compared to 53.19, 59.52, and 63.29 kbps respectively. The analysis reveals that a longer back off window size will increase the overhead per packet, hence, decreasing the throughput for a single device. At the same time, it may increase the throughput for the network as a whole due to the decreased chance of collision. Therefore, in the high layer protocols, the MAC layer parameters are usually tuneable to obtain the optimum performance. The comparisons between the experimental results and analytic model results, shown Figure 4.12 and Figure 4.13, guarantee the accuracy for the extension to the large scale network with the current MAC layer model. It is noted that although the proposed model has only been validated in the implemented experiments with the simplest network topology, it is very straightforward for it to be extended to more complex topology and MAC protocols, e.g. S-MAC or B-MAC [12;99] if desired.

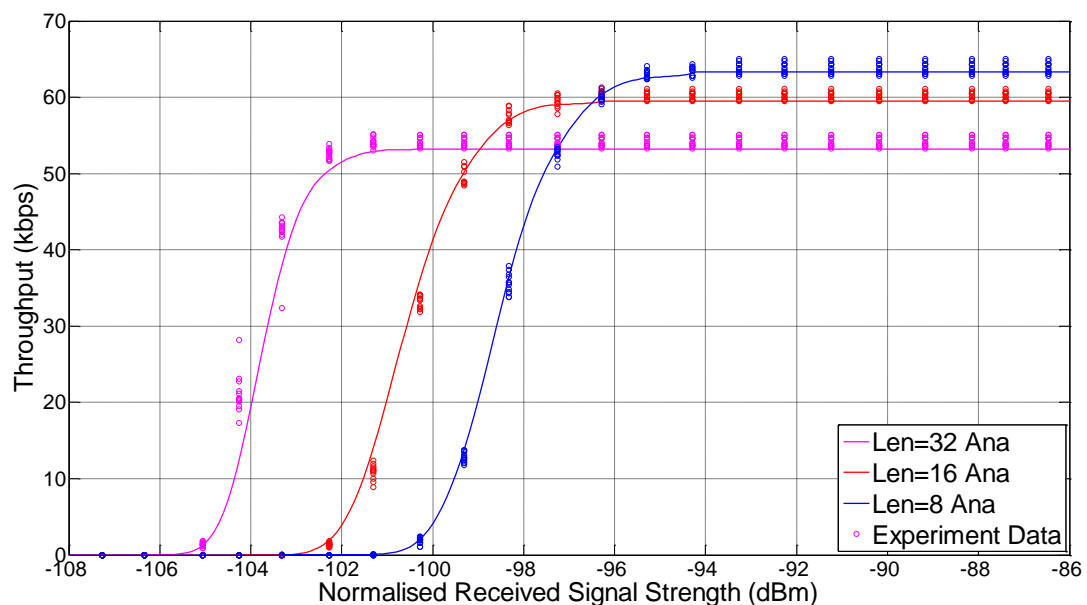


Figure 4.12. Effect of backoff window size BE=4

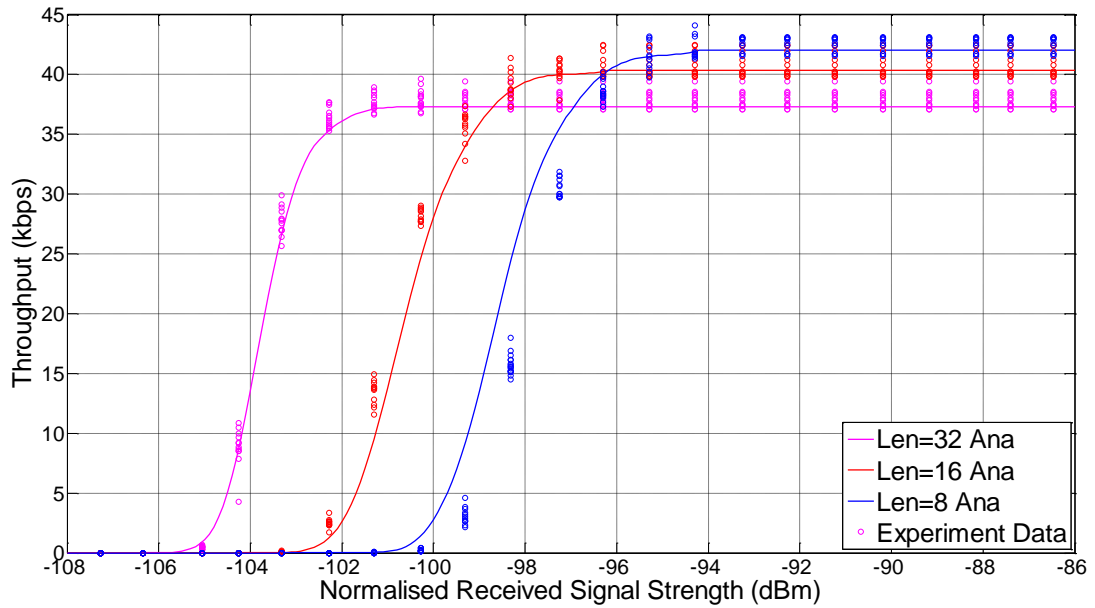


Figure 4.13. Effect of backoff window size  $BE=5$

Generally, a throughput versus distance result is more straightforward to be understood and to guide the practical deployed wireless system. Equation (4.12) is a well accepted free space propagation model for omnidirectional transmission. In [100], ATMEL demonstrated the experimental validation of this model for its low cost wireless transceiver AT86RF230. As it is widely known that AT86RF230 and AT86RF231 share most of their architecture except the spreading logical, this propagation model is believed to be also valid for the AT86RF231.

$$P_{rx} = P_{tx} \cdot \left(\frac{\lambda}{4\pi d}\right)^2 \quad (4.12)$$

where  $P_{tx}$  is the power of transmitted,

$\lambda$  is the wavelength of transmitted signal,

$d$  is the distance between transmitter and receiver,

By applying  $P_{tx} = 3dBm$  and the sensitivity of  $-101dBm$  to equation (4.12), it is possible to show an effective distance of 1.56km. We implemented an outdoor experiment over a lake environment with this transceiver, which resulted with a 1008m effective range at 5% PER. However, if we take the existence of an additional  $-4dBm$  power loss between the transceiver and antenna into consideration, the sensitivity

threshold would be reached around 1km which perfectly matches the experimental results.

It is now possible to illustrate the throughput versus distance performance in Figure 4.14 by substituting  $P_{rx}$  into equation (4.12), which shows the potential optimisation space of several hundreds meters.

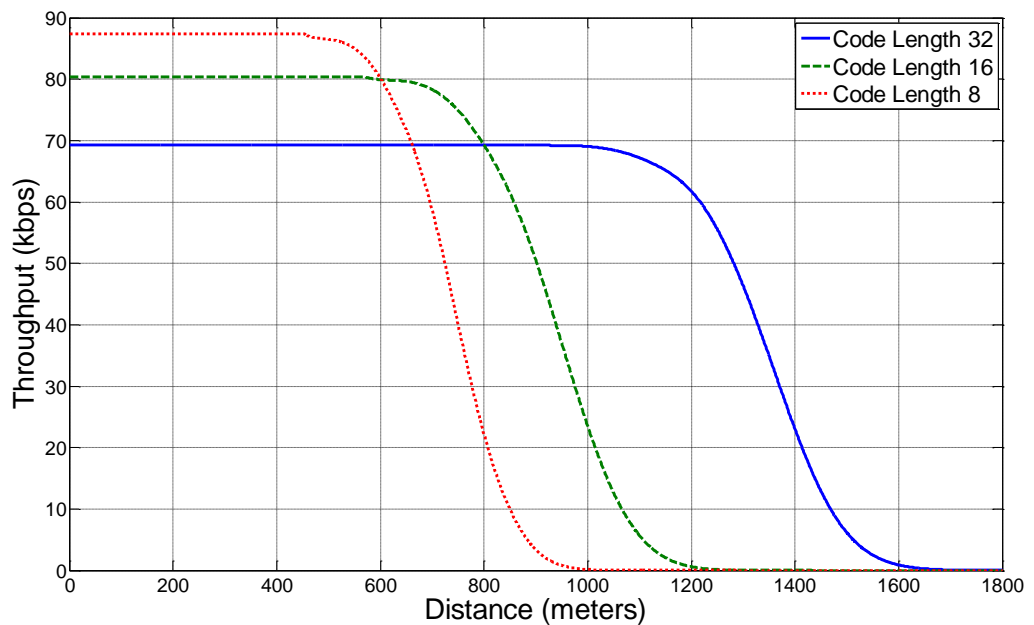


Figure 4.14. Throughput versus Distance

#### 4.4.4 Power efficiency

We now demonstrate the power consumption of a node with different spreading lengths. In the results shown in Figure 4.15, the device is configured to send the same packet with different spreading code length modes, from 32 chips to 8 chips respectively. As the chip rates are the same for all modes, we expect, as seen in Figure 4.15, the power consumption level to be the same for all modes. This gives designers the option of trading power efficiency with error performance. By employing a shorter spreading code length, the packet can be transmitted faster which leads to the less power consumption.

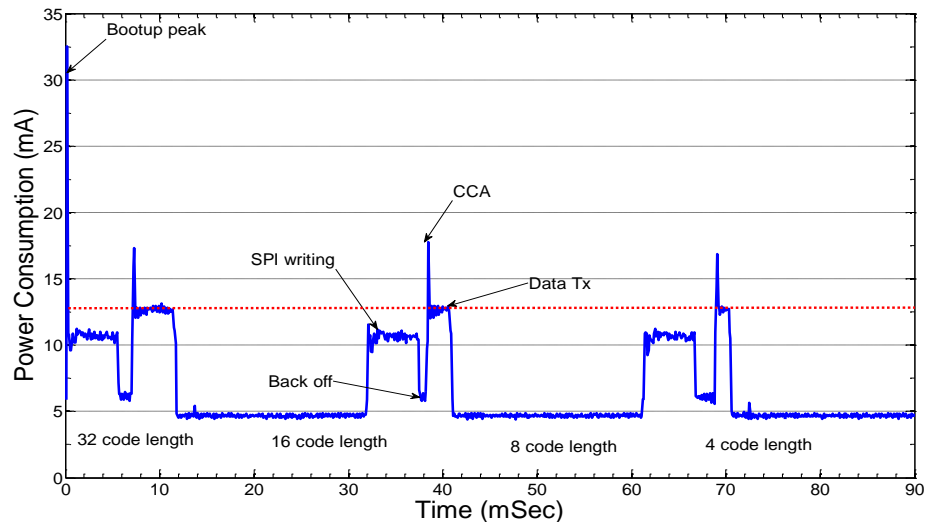


Figure 4.15. Power consumption for different spreading modes

## 4.5 Conclusion

In this chapter, we have experimentally demonstrated the use of an adaptive spreading code length to improve the throughput and energy usage performance of WSNs. However, to maximise the improvement an accurate error performance estimation model must be derived to aid the design of the upper layers. Thus, we have proposed an analytic error performance estimation model, which shows good accuracy when compared with the experimental results. Our findings can be concluded as following,

- Higher throughput performance can be achieved in regions with a high SNR.
- Error performance and throughput performance can be accurately predicted by the analytic model.
- The power consumption is independent of spreading mode.

A number of potential WSNs applications may benefit from the improvements offered by the adaptation of spreading code length. The most straightforward one is the rate adaptation protocol to increase the throughput performance, which has been well studied and widely implemented in similar standards e.g. IEEE802.11. Due to the same power consumption level for all different modes, less energy will be consumed at higher data-rates. Considering the additional energy constraints present in WSNs, such a

scheme can be expected to increase the energy efficiency as well as increasing throughput.

The particular benefit will be obtained by WSNs deployed in industrial environments, considered the largest WSNs market. In such an environment, WSNs equipped with spreading code length adaptation can be expected to automatically adjust to the RF environment to provide optimum performance against a stated requirement. With an appropriately designed upper layer protocol, i.e. MAC and Routing, such a system can also be application-aware, by assigning better Quality of Service (e.g. higher capacity and short hop numbers, etc.) to the tasks with higher priority (e.g. fault detection, gas leaking detection, etc.).

The work shown in this chapter is the foundation for the design of appropriate upper layer algorithms, which will be discussed in the following chapters.

## Chapter 5. Effective-SNR Estimation for Wireless Sensor Network Using Kalman Filter

### 5.1 Introduction

In Chapter 4, we have presented an accurate error performance estimation model for adaptive spreading code lengths in WSN systems. However, problems still exist, preventing this technology from being fully utilised by the MAC and other upper layer algorithms. In particular, the question remains of how to obtain the input parameters, i.e. the channel quality, required for the error estimation model? Furthermore, the error performance model was built considering the ideal AWGN channel, while in some cases the WSN system need to be deployed in harsh RF environments, especially for the advanced applications as discussed in Chapter 2. A harsh RF environment often possesses characteristics in terms of multi-path effects due to stationary or moving metallic structures and RF interferences from machine (i.e. power generator and motor) or other RF device. These effects contribute to the time-varying fading channel, which has been demonstrated by field tests [53;56;101] and our own investigation and can adversely affect the quality of the wireless communication. Thus, how to estimate the quality of the wireless channel in an agile and low cost manner poses the biggest challenge to the utilisation of adaptive spreading code lengths for WSNs.

As witnessed and discussed by many researchers, the raw Received Signal Strength Indicator (RSSI) provided by WSN transceivers may not be a good indicator to predict successful delivery of data packets [58], due to fading effect and device impairments. In order to improve the quality of the link estimation, a number of recently proposed methods make use of learning algorithms to estimate the link quality [93;102;103] instead of using the SNR. However, these learning based methods require that the sensor node must be active all the time to overhear all wireless transmissions, which is not

suitable for energy constrained WSNs. Other approaches calibrate the relationship between SNR and Packet Receive Rate (PRR) by exchanging probe packets. Such operation will cause a relatively high overhead, which rises rapidly with the square of the network size. At least one WSN deployment crashed due to the unexpected high volume of overhead packets [104].

As specified in the IEEE 802.15.4 standard [16], all IEEE 802.15.4 compatible devices [20;21] have to provide a Link Quality Indicator (LQI) to represent the quality of the wireless link. Usually this value results from the correlation of multiple symbols within the received packet and indicates the error performance directly. It is believed that LQI is more accurate and reliable than the SNR in representing the link quality. Our experimental results, as well as previously published results [101;105], have shown that the average LQI has a high correlation with the error performance<sup>10</sup>. This feature of IEEE 802.15.4 makes it possible to accurately estimate the link quality without the overhead of probe based calibration. Therefore, LQI is recommended by many standards including ZigBee [17], IETF 6LoWPAN WG [18]. Nevertheless, the utilisation of LQI has been challenged by many problems in this implementation. Firstly, the LQI is related to the error performance and yet only available within the transition area, i.e. PRR is less than 100%, which means it fails to show the wider link margin. Secondly, the instantaneous raw LQI is known to vary over a wide range. As a result, many algorithms rely on the average of LQI over many packets to achieve acceptable accuracy and thus fail to capture a fast changing channel. In WSN applications with high traffic load, although there could be sufficient traffic load for the average operation to give adequate performance, a fast converging indicator is usually required for high layer optimisation.

We are consequently motivated to exploit the redundancy between the LQI and SNR to assist in providing a better link quality indicator, which is

---

<sup>10</sup> Although different vendors calculated LQI in different ways, (e.g. AT86RF231 provided by ATMEL correlated with the packet error rate, while CC2420 provides an indicator of the chip error rate).

referred to as the Effective-SNR<sup>11</sup>, which should be able to provide reliable and fast estimation without additional overhead or hardware support. The proposed method is expected to be not only accurate but also easily implemented. Accordingly, several immediate questions should be addressed. Firstly, is the LQI good enough to express the link quality? Secondly, if so, is there a simple but effective approach to combine LQI and SNR to produce a trusted output? Thirdly, is the cost of such an algorithm acceptable in resource constrained WSN? To address these questions, in this chapter, we first investigate the different relationships between SNR, LQI, and PRR. Based on the analysis of experiment results, we decompose the link quality into multiple components and build an Effective-SNR model to represent the underlying relationship among these components. This model enables us to make use of mature Kalman Filter techniques to reduce the measurement noise and enhance the accuracy of the estimation. To the best of our knowledge, this is the first deployment of Kalman filter tracking of the variation of signal strength, environment noise strength, and signal impairment at the same time, while most pervious work focuses only on the signal strength using simple, average based approaches. With the help of this framework, LQI and SNR can be combined to generate a trustable Effective-SNR indicator, which provides an accurate estimation of the link quality margin to allow concurrent transmission as well as rate adaptation. In comparison with other approaches, the main advantage of our method is that it can avoid the overhead of probe packets or constant monitoring of the channel (overhearing), which makes it suitable for WSN deployment. The proposed algorithm can be easily employed by many other higher level algorithms to increase their performance. We also demonstrate that such a filter can be easily deployed with fixed-point computation and is therefore acceptable for implementation in simple 8-bit microprocessors which are widely employed by many WSN platforms.

We start in section 5.2, in which we formulise the problem and provide the general model of link quality based on empirical evidence. Section 5.3

---

<sup>11</sup> The concept of using E-SNR was originally proposed in space-time modulation systems [106] and OFDM systems [107] to predict the error performance. In this work we use this name but with an entirely new formulation for WSNs.

introduces the design of the Kalman filter and shows how to deploy the algorithm in a resource constraint platform. Section 5.4, presents experimental results based on a COTS (Commercial off-the-shelf) platform are provided to illustrate the performance of the proposed method. This chapter concludes by discussing some key issues of potential future work in section 5.5.

## 5.2 Problem Formulation

According to the discussion in Chapter 4, it can be concluded that if sensor networks are deployed in an ideal Additive White Gaussian Noise (AWGN) channel, then the capacity of the wireless link can be accurately estimated by the SNR. However, in reality the channel will include fading effects which can not be accurately represented by the SNR, due to the distortion of signals. It is still possible to estimate the system capacity in a fading channel, but this usually requires a high complexity analytic model, which can not be afforded by resource constraint WSN platforms. Therefore, we propose the estimation of Effective-SNR, by which the channel quality in harsh RF environments is simply mapped to a corresponding effective SNR in an AWGN channel. Then, the channel capacity can be obtained by substituting this indicator into a system performance model for an AWGN channel. The following section will discuss how to estimate this indicator through the analysis of the varying RF channel and by utilising existed measurements available in COTS platforms.

### 5.2.1 Notation

In this chapter, the following notation and assumptions have been used:

- Transmission Power ( $P_{tx}$ ): We define the signal power at the antenna of the transmitter as the transmission power.
- Received Signal Strength ( $P_{RSS}$ ): We define the signal power after the antenna of the receiver as the received signal strength.

- Internal Noise ( $N_i$ ): We define all the noise added to the signal after the antenna of the receiver device as internal noise. The internal noise mainly consists of thermal noise generated by the radio components, which could be influenced by the noise figure as well as temperature. It has previously been demonstrate that due to manufacturing tolerances, different devices may have different noise figures, which can be easily calibrated offline.
- Environment Noise ( $N_e$ ): We define the noise from devices outside the network as environment noise, which may be from other RF devices (i.e. WiFi, other narrow band devices working in ISM band) or the EM noise generated by machinery (i.e. power generator, motor, or microwave oven). In our application, the latter tends to be a more important issue since it is a common effect in industrial locations. Through field trials it has been shown that such noise can be as high as -30dBm around 2.4GHz in the engine test site of Rolls Royce [55;108]. Similar effects have been reported in [14] for a power plant site around 915MHz with a lower value of -64dBm.
- Interference: We define the signal from other network devices while the current transmission is ongoing as interference. This gives rise to the well known hidden terminal problem, exposed terminal problem, as well as the capture effect.
- Signal Quality Degradation (SQD): Wireless channels suffer from reflection and diffraction caused by objects in the environment or refractions in the medium. Such effects, usually termed fading effects, will cause distortion of the signal at receiver device and will further increase the error probability. Therefore, we define SQD as the degradation of signal when compared with the same signal transmitted via an AWGN channel.

### 5.2.2 Propagation Model in the Harsh RF Environment

There are two main types of propagation, depending on their effects on the different source:

1) Slowly fading, which can be further divided into pathloss and shadowing, is the largest contributor to signal loss. One of the most common radio propagation models is the log-normal shadowing path loss model [109].

2) Fast fading, often termed multipath fading or frequency selective fading, causes signal distortion. If only the strength of the received signal is considered, then the multi-path effect can be described with the same random process  $X_\sigma$ .

These relationships can be expressed by equation (5.1) according to [109].

$$\begin{aligned} P_{rss} &= P_{tx} - PL(d) + X_\sigma \\ &= P_{tx} - PL(d_0) + 10n \log_{10} \left( \frac{d}{d_0} \right) + X_\sigma \end{aligned} \quad (5.1)$$

where  $PL(d)$  is the pathloss at the distance  $d$ ,  $d_0$  is a reference distance,  $n$  is the pathloss exponent, and  $X_\sigma$  is a zero-mean Gaussian random process with standard deviation  $\sigma$  to express the shadowing effect.

$$SNR = \frac{P_{rss}}{N_i + N_e} \quad (5.2)$$

Therefore, the SNR at the receiver side can be expressed in equation (5.2) by subtracting internal noise and environment noise. If the transmitter and receiver are connected through an AWGN channel, the components of  $X_\sigma$  can be avoided, which means no variance and more importantly no distortion to the signal. Thus we can assume that the error performance can be accurately estimated by the SNR, which has been validated by the discussion in chapter 4.

The calculation of SNR requires both information on the received signal strength and the noise power at the receiver. However, due to constraints on cost and power, Received Signal Strength Indicator (RSSI) provided by IEEE 802.15.4 is generally believed to be unreliable because of the measurement noise and device impairment. Furthermore, it should also be noted that the RSSI contains both RSS and the environment noise arrived in the transceiver. Therefore, although the RSSI can be used to calculate

SNR, the calculated results are typically inaccurate. A recent study [110] has also reported such effect in an anechoic chamber environment (i.e. almost AWGN channel) and therefore, we cannot rely on pure RSSI values to obtain an accurate SNR. Due to the effects of fading and multi-path, the relationship between RSSI and the received signal strength ( $P_{RSS}$ ) and noise ( $N_e$ ) becomes a nonlinear function.

We first consider the impact of fading on RSSI. Similarly to the AWGN channel, the fading effect can be modelled as a variance of the power of the transmitted signal, as shown by equation (5.1). Aware that the RSSI measurement consists not only of the measurement noise but also of the variance caused by the fading effect, the RSSI can be expressed as following:

$$RSSI = P_{tx} - PL(d) + X_\sigma + N_i + N_e + \eta \quad (5.3)$$

where  $\eta$  is a zero-mean Gaussian distribution expressing the measurement noise. The RSSI variable only detects the received signal strength at the antenna without attempting to distinguish whether it is due to signal or noise, as the noise power of  $N_i$  and  $N_e$  also contributes to the RSSI value. In the worst case, where the noise power is high, the signal strength is masked by the noise and the value of RSSI deviates from the true RSS. The relationship between RSSI,  $P_{RSS}$  and  $N_e$  is given by equation (5.4). Let  $RSS$  denote the actual value of the real received signal strength, which can be obtained through the deduction of  $N_e$  from RSSI.

$$RSS = 10 \log_{10} \left( 10^{\frac{P_{RSS}+b}{10}} - 10^{\frac{N_e+b}{10}} \right) \quad (5.4)$$

where  $b$  is the base value of RSSI detection, which is normally around -91dBm, but calibration is required for different devices.

Although the variation factor  $X_\sigma$  has been added, the trend of received signal strength can be tracked by  $RSS$  measurement as well and therefore, the link quality can be estimated accordingly. Although this operation needs additional computations to deal with the measurement noise and small timescale fading effects, it is simple enough to be implemented in low cost

WSN nodes, for example, a moving average method has been employed in [110]. Environmental noise  $N_e$  can also be tracked using a similar approach as it still follows the propagation law of RF signals. Such an approach is being employed by IEEE 802.11k [111] to estimate the environment noise and interference. In applications without high environmental noise, e.g. remote sensing applications, the proposed architecture would be equal to a simplified tracking filter, that takes only RSSI as the input parameter, yet uses the offline measured internal noise floor to calculate the SNR. Therefore, this simplification would have the same performance as the work shown in [61].

If we consider that the measurement noise caused by the RSSI function has already been filtered, the observed  $RSS$  and  $N_e$  can be used to estimate the PRR performance by using a combination of equation (5.2) and the look up table generated from the error performance estimation model discussed in Chapter 4.

### 5.2.3 Effective-SNR model

It is well known that multipath and other factors cause signal distortion, which increases error probability. Without any doubt, such effects will make offline tested SNR-PRR measurements unreliable. For example, although a measured SNR margin is 8dB, the real margin may only be 6 dB. Based on this inaccurate indicator, the higher-level application algorithm will make an incorrect decision to decrease the system performance, e.g. allow concurrent transmissions which should not occur, or switch to a high data rate which cannot be supported, causing a decrease in capacity instead of the expected increase. In order to provide an accurate estimation of link margin, some algorithms [93;110] rely on the probe packets and online calibration to rebuild the SNR to PRR relationship in various environments, or even give an offline measurement [102]. As discussed previously, these techniques are able to mitigate this problem but suffer from several drawbacks including transmission overheads and long converge times.

In this chapter, Effective-SNR is defined as the equalised value of SNR to achieve the same error performance as would be expected in an

AWGN channel. Effective-SNR can be obtained by including all negative effects on the signal quality as factors in the Signal Quality Degradation (SQD) calculation, as shown in equation (5.5). Without loss of generality, we assume SQD is a large time-scale factor, since the multi-path effect can be roughly assumed to be constant for a static sensor network system<sup>12</sup>.

$$ESNR = SNR - SQD \quad (5.5)$$

If we have already estimated SQD and combined it with the SNR, the error performance PRR can be simply obtained through a look up table measured off-line with Effective-SNR as an input which can avoid the high overhead as well as achieve high accuracy. The only problem is how to estimate SQD in a low cost device. The straightforward calculation of SQD requires a very detailed specification of the low level demodulator employed in the RFIC. This may be possible in expensive software define radio development kits, but is impractical for low cost COTS products.

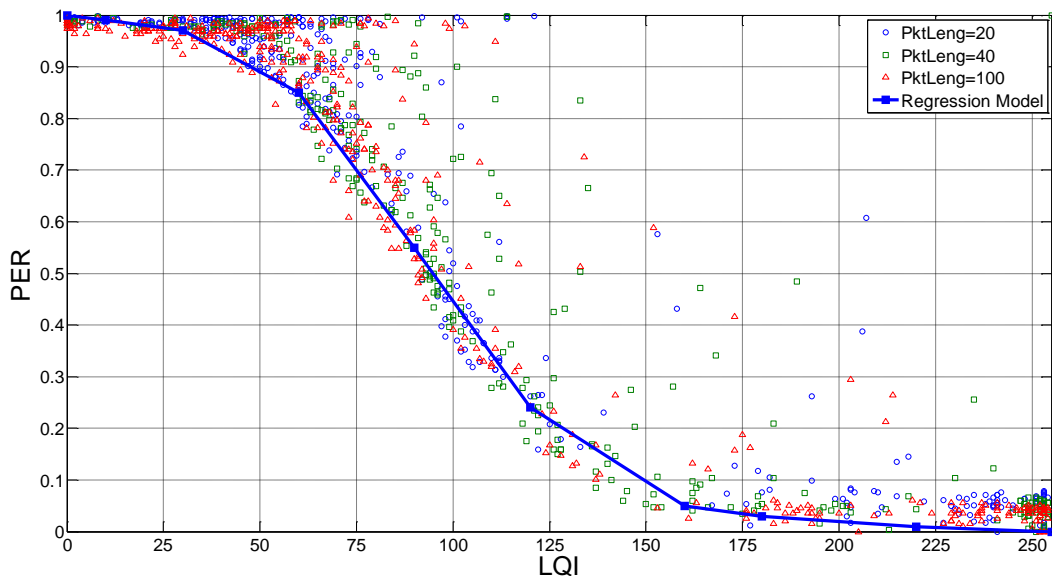


Figure 5.1. PER-LQI Empirical Result

The acquisition of SQD in widely used WSN platforms is not straightforward, because this variable is usually embedded behind the complex combination of several indicators provided by the low cost WSN system. Notwithstanding, it is possible to obtain the Effective-SNR at a low

<sup>12</sup> Most deployments of WSN system are static, although we understand that some applications require mobile WSN devices.

cost from raw LQI, one of the indicators provided by IEEE 802.15.4 system. As reported in many test reports, the output of the LQI has significant correlation with PRR. As discussed earlier, Effective-SNR is linked with PRR, which implies a correlation between LQI and Effective-SNR. However, as indicated by the vendor [21]: a reliable estimation of the packet error cannot be based on a single or a small number of LQI values. This hypothesis has been validated in our experiments with different parameters and in different environments, as shown in Figure 5.1<sup>13</sup> and Figure 5.2. The result in Figure 5.1 was provided in the format of PRR in one second versus the average LQI per second. As the LQI can be understood as the error probability of the current packet, the average LQI in one second can be considered to be the best indicator of error performance for that second. Therefore, in the results provided in Figure 5.1 show very high correlations with the PRR regardless with the different packet lengths (performances of three different lengths 20, 40 and 100 have been examined). To better understand the relationship between the averaged LQI and the instantaneous LQI, a snapshot of the experiment result has been illustrated in Figure 5.2. As expected, only the averaged LQI shows the similar trends with the channel capacity, the instantaneous LQI varies over a much wider range and less correlated with the error performance. However it should be noted that, the averaged LQI is only a *posterior* statistical value which cannot be utilised to predict the channel quality. In this context, a low cost statistical method is required to obtain a reliable *a priori* indicator, which is the motivation of this work.

The experimental results discussed above can be combined to generate a look-up table to convert the LQI input to an Effective-SNR output (i.e. corresponding SNR in AWGN channel). However, the relationship between LQI and Effective-SNR is segmented, resulting in values for SQD not always being available. Such nonlinearity increases the complexity in estimating Effective-SNR. Indeed, the system cannot rely on estimating Effective-SNR directly from LQI for each transmission. Nonetheless, aware that the SQD is mainly caused by multi-path effects, after the location of

---

<sup>13</sup> We are aware that different vendors provide LQI in different ways, e.g. RF231 provided by ATMEL is correlated with PER, while CC2420 provided by TI is correlated with BER. However, this difference can be easily fixed in implementation of algorithm.

devices has been fixed, the SQD for each tagged link can be approximated as a static value. Hence, we propose to estimate SQD through Effective-SNR in the situation where the LQI is provided. Values of SQD can be easily calculated by applying the estimated Effective-SNR to equation (5.5) with the SNR detected using the RSSI function discussed in section 5.2.2. The estimated SQD can be maintained to estimate Effective-SNR for other situations.

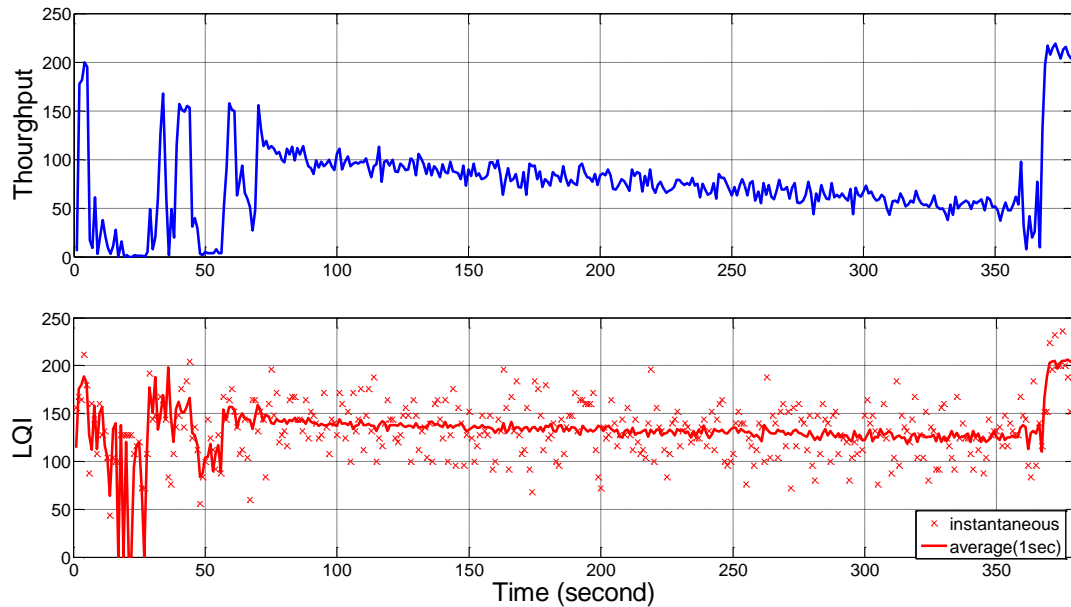


Figure 5.2. Average LQI vs Instantaneous LQI

Based on the analysis above, it can be concluded that a better estimation of SNR and the link quality margin can be achieved by using the information redundancy among RSSI, LQI, and the measured noise power  $N_e$ . In fact, we define a new variable Effective-SNR to replace the SNR, and it is expected that the Effective-SNR should give a better description of the channel condition than the original SNR directly provided by the RFIC. Furthermore, as shown in the Effective-SNR model, the information redundancy between SNR and LQI is accounted for in the estimation of Effective-SNR, where the information redundancy helps to improve the accuracy of the SNR estimation. However, due to the nonlinearity which exists in both models, it is challenging to get an accurate estimation of Effective-SNR. A carefully designed estimator is required to deal with the nonlinearity, segmentation and the measurement noise in RSSI and LQI. Beyond that, due to the nature of resource constraints in WSNs,

such an estimator must be able to be deployed on low cost devices. In this section, we will introduce the design of a Kalman Filter and show that it can be implemented to achieve higher estimation accuracy while avoiding the transmission overheads required by other techniques such as probe packets.

### 5.3 Kalman Filter Design

According to the discussion in the last section, it is clear to notice that this problem is a typical dynamic system with measurement noise. In particular, the measurement noise in WSNs is accentuated due to the low cost hardware platform used. It is necessary to improve the estimation of the channel quality by getting rid of the measurement noise. Since the mature Kalman filter has shown the ability to track (estimate) the system parameters (states) from noisy measurements, we are motivated to designing and deploying a Kalman filter to track the variation of channel quality against the measurement noise from low cost hardware platform. Other state of art approaches for similar scenarios include the moving average filter which has been deployed in a rate adaptation algorithm for WiFi systems [43] and a Geometric based solution [112]. Compared with these methods, Kalman filters typically converge much faster than moving average filters due to a better modelling and understanding of the signal relationship and measurement noise. The Kalman filter provides quantised accurate channel quality estimation<sup>14</sup> comparing with the simple good or bad result generated by the Geometric methods. Therefore, the Kalman filter is a good trade-off between the performance and the computation costs, which has motivated us choosing Kalman filter as our solution to solve this problem.

Based on the two models presented in the preceding section, a linearisation algorithm is first proposed to derive a linear model. Then, a novel Bi-KF (meaning double Kalman Filter) estimator is proposed to deal with the measurement noise and stochastic fading effects resulting in a more reliable estimate of Effective-SNR while tracking the time varying link quality with high accuracy. The advantages of using KF are threefold:

---

<sup>14</sup> The quantised estimation result is vital to be worked with the capacity estimation model discussed in Chapter 4.

(1) The link quality is a time varying variable, for example, the shadowing effects caused by a moving object have a dramatic affect on the link quality. Since the KF is good at tracking time varying systems, the proposed Bi-KF estimator is able to track the variation quickly (usually able to converge in less than ten inputs according to empirical experience).

(2) The linear KF is of low computation cost. In comparison with probe-base and learning-based methods, the proposed Bi-KF method can give an acceptable estimation of Effective-SNR without the additional probe packets or increased energy consumption.

(3) The information redundancy between signals is fully utilised by the KF. Such information redundancy contributes significantly to the accuracy of the estimation.

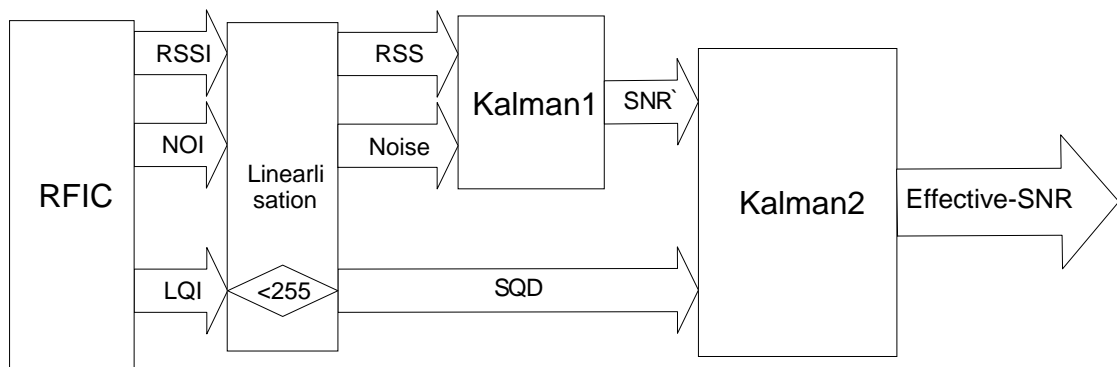


Figure 5.3. Architecture of Kalman Filter

Figure 5.3 illustrates the structure of the proposed Bi-KF estimator. The first Kalman Filter (KF1) filters the measurement noise from the RSSI-SNR model while the second Kalman Filter (KF2) generates Effective-SNR using  $SNR^*$  and SQD as input parameters. KF2 aims at using the information redundancy between SNR and LQI to improve the Effective-SNR estimation. KF1 uses the RSSI and environment noise reading (denoted NOI in the rest of this chapter) from RFIC as the input. Since the RSSI and NOI readings are immediately available when a packet arrives, KF1 provides a filtered SNR value once a packet is received. Because of the availability of SQD, KF2 only updates the value of Effective-SNR when the received packet's LQI is less than 255. Whereas, when the LQI is saturated (equal to 255), KF2 does not

update the observed equation of KF2. In this situation the estimation is only updated by the state equations of KF2.

### 5.3.1 Linearisation of the measurements

Based on the discussion in section 5.2, we note that the object system is nonlinear. For a nonlinear system, an improved version of Kalman Filter, referred as an Extended Kalman Filer (EKF), has to be designed. However, the design of an EKF requires higher computation costs, which is not suitable for WSN nodes with low computation recourses.

In order to build a linear estimator with lower computation requirements, the nonlinear system has to be transformed into a linear system. It is worth noting that, although the system defined in (5.4)-(5.5) is highly nonlinear, the nonlinearity exists only in the system inputs and the main dynamics of the system can be described by a linear system. Such a nonlinear system can be fitted by the Hammerstein model [113], where a pre-linearisation process is employed to convert the nonlinear system into a linear system. Therefore, the system state can be easily estimated using a linear Kalman filter at lower computation cost, instead of a complex Extended Kalman Filter. The nonlinearity embedded in the RSSI and NOI can be easily eliminated with the help of equation (5.4). Meanwhile the process of LQI is rather complex. As shown in Figure 5.1, the LQI shows a significant correlation with PRR, and thus a one to one mapping function can be set up to obtain PRR probability of the current packet through LQI. As specified in the standard, IEEE802.15.4 employs a Cyclic Redundancy Check (CRC) with a length of 16 bits as the frame check to indicate bit errors [21], which means a single symbol error will flag the entire packet as in the error received state.

$$PRR = (1 - SER )^{2 \cdot PacketLength} \quad (5.6)$$

Therefore, once the PRR value is ready, a SER value can be calculated using equation (5.6) and the packet length. The packet length is also provided once a packet was successfully received. By indexing the empirical data (shown in Figure 5.1), it will be easy to find out the equalised

signal to noise ratio in an AWGN channel, which is the expected Effective-SNR. In addition, it is also easy to notice that all these processes can be calculated offline to build a two-dimension look up table, thus avoiding the computation costs of floating point calculations. Hence, in the online process, once a packet has been successfully received, the Effective-SNR can be simply obtained through searching the look up table with the index of LQI and packet length.

### 5.3.2 Kalman Filter Design

The design of KF1 is to address the variation of signal strength (RSS and environment noise) by filtering the measurement noise. Although the function of KF1 is similar to the average filtering method, KF may give higher accuracy with faster tracking ability. Considering that the packet transmission and environment noise are subjected to the fading effects,  $RSS$  and  $N_e$  can be assumed to be slowly changing variables. Therefore, the system can be modelled as:

$$\begin{cases} RSS_k \approx RSS_{k-1} + w_{s,k} \\ N_{e,k} \approx N_{e,k-1} + w_{n,k} \end{cases} \quad (5.7)$$

where  $w_s$  and  $w_n$  represent the impact of fading on the signal and the environment noise, respectively.  $w_s$  and  $w_n$  are assumed independent with zero mean Gaussian distributions.

For the sake of compact notation, equation (5.7) can be rewritten in vector form, which gives the following state evolution equation:

$$x_k = A \cdot x_{k-1} + w_k \quad (5.8)$$

where  $x = \begin{bmatrix} RSS \\ N_e \end{bmatrix}$  is the state variable of the dynamic system,  $A = \begin{bmatrix} 1 & 0 \\ 0 & 1 \end{bmatrix}$ ,  $w = \begin{bmatrix} w_s \\ w_n \end{bmatrix}$ . In the RSSI-SNR model, it can be seen that the state variable can be observed by the RFIC<sup>15</sup> directly and subject to measurement noise. Therefore the observation equation can be written as:

<sup>15</sup> To obtain the environment noise indicator may involve a carefully design in MAC protocol to avoid the effect of interference, especially for the application which intends to enable concurrent

$$y_k = H \cdot x_k + v_k \quad (5.9)$$

where  $y = \begin{bmatrix} P_{rss} \\ \text{NOI} \end{bmatrix}$ ,  $H = \begin{bmatrix} 1 & 0 \\ 0 & 1 \end{bmatrix}$ , and  $v_k = \begin{bmatrix} v \\ v \end{bmatrix}$ .  $v$  is the measurement noise vector caused by the impairment of hardware

Once the state space model has been setup by equations (5.7~5.9), the associated Kalman filter is straightforward [114].

$$\text{Priori Update:} \quad x_k^- = A \cdot x_{k-1}^- \quad (5.10)$$

$$\text{Priori Error covariance:} \quad P_k^- = A \cdot P_{k-1}^- \cdot A^T + Q \quad (5.11)$$

$$\text{Kalman Gain:} \quad K_k = (P_k^- \cdot H^T) \cdot (H \cdot P_k^- \cdot H^T + R)^{-1} \quad (5.12)$$

$$\text{Posteriori Update:} \quad x_k = x_k^- + K_k \cdot (y_k - H \cdot x_k^-) \quad (5.13)$$

$$\text{Posteriori Error covariance:} \quad P_k = (I - K_k \cdot H) \cdot P_k^- \quad (5.14)$$

where  $x_k^-$  is the *a priori* estimation of state,  $x_k$  is the *a posteriori* estimation of state,  $P_k^- \in R^{2 \times 2}$  is the *a priori* estimated error covariance,  $P_k \in R^{2 \times 2}$  is the *a posteriori* estimated error covariance.  $K_k \in R^{2 \times 2}$  is the Kalman gain,  $Q$  is the variance of state noise,  $R$  is the variance of measurement noise. Since the initial value  $P$  does not affect the optimal value of  $K$ , a non-zero matrix can be assigned to  $P$  as the initial value, and  $K$  will automatically converged to the optimal value. The appropriate values of  $P$  and  $Q$  will be determined empirically and discussed in the next section.

Unlike the first Kalman filter, the second Kalman filter can only be triggered if the LQI of received packet is less than 255. Once the second Kalman filter has been activated, it will use the output of the first Kalman filter as one of its measurements through a simply deduction of two states variables. As discussed in section 5.3, the SQD can be approximated to be a static variable over short time-scales. Hence, the estimated SQD rather than Effective-SNR can be more useful in this Kalman filter design, because the

---

transmission. In this chapter, as only one transmission pair was employed, we simply start an additional energy detection operation just after the receiving interrupt of packet to obtain the NOI.

maintained variable could be used to estimate Effective-SNR when the LQI is not provided. Then the state equation is given by (5.15).

$$x_{2k} = A_2 \cdot x_{2k-1} + w_{2k} \quad (5.15)$$

where  $x_2 = \begin{bmatrix} SNR \\ SQD \end{bmatrix}$ ,  $A_2 = \begin{bmatrix} 1 & 0 \\ 0 & 1 \end{bmatrix}$ , and  $w_2 = \begin{bmatrix} w_{snr} \\ w_{sqd} \end{bmatrix}$ .  $w_{snr}$  and  $w_{sqd}$  represent the variations of the SNR and SQD, from the view of the signal strength degradation and signal distortion, respectively. Theoretically, these two noises depend on the environment and channel status, but change following different models as discussed in section 5.2, which can be assumed to be independent. However, in the implementation, the SQD is calculated through a linear process from SNR and LQI, making these two noises correlated. As a result, the independence between  $w_{snr}$  and  $w_{sqd}$  is not met to some degree, which will degraded the tracking performance. However, our preliminary experiments show that the correlation between these two noises is relatively small. In order to reduce the computation costs, it is assumed that these two noise are independent. Although the assumption may degrade the performance, the performance drop is slight. This is verified by our experiments where the proposed Kalman filter system can still converge and track the system variation.

Then the observation equation can be written in equation (5.16).

$$y_{2k} = H_2 \cdot x_{2k} + v_{2k} \quad (5.16)$$

where  $y_2 = \begin{bmatrix} SNR \\ ESNR \end{bmatrix}$ ,  $H_2 = \begin{bmatrix} 1 & 0 \\ 1 & -1 \end{bmatrix}$ , and  $v_2 = \begin{bmatrix} v_{SNR} \\ v_{LQI} \end{bmatrix}$ .  $v_{SNR}$  and  $v_{LQI}$  are the measurement noise caused by tolerances in the hardware design, which are independent and with zero mean Gaussian distributions.

In common with the evolution of KF1, the second Kalman Filter can be solved by applying equation (10)~(14) to the model described in (15)-(16) . Note that, the parameter matrices of KF1 (i.e.,  $A, B, C, D, P, Q$ , etc.) in (10)-(14) should be replaced by the parameter matrices of KF2, respectively.

Therefore, the overall estimation algorithm can be described by Algorithm 5.1.

**Algorithm 5.1:** Effective-SNR estimation Algorithm

```

Trigger: Receive a packet
{
y[0] = read_RSSI();
y[1] = measure_NOI();
Linearisation(y);
SNR = Kalman_One(y);

LQI = read_LQI();
If(LQI<255)
{
PL = read_Packet_Length();
ESNR = Look_up_table(LQI,PL);
y[0] = SNR;
y[1] = ESNR;
ESNR_hat=Kalman_two(y,&SNR_hat,&SQD_hat);
}
else
{
ESNR_hat = SNR-SQD_hat;
}
return ESNR_hat;
}

```

**5.3.3 Estimating the covariance matrices**

It is well known that the performance of a Kalman Filter depends on the accuracy of the parameter matrices, particularly the process noise covariance matrix  $Q$  and the measurement noise covariance matrix  $R$ . In the practice, the selection of  $Q$  and  $R$  play an important role on the evaluation of Kalman Filter. Since the measurement noises are device dependent, different hardware platforms may have different noise features and the theoretic derivation of these covariance matrices may not be accurate enough for all platforms. This is particularly true of low cost WSN platforms. In practice, it is more straightforward and accurate to obtain these covariance matrices from carefully designed experiments in an offline fashion before the deployment. In the following sections, we will describe the process of

obtaining these parameters for one hardware platform although the same process can be applied to other platform as well.

### 5.3.3.1 Measurement noise

The variance of the measurement noise can be accurately calculated through an AWGN based experiment discussed in Chapter 4. In this experiment the values of  $P_{tx}$  and  $PL$  are set manually, external noise removed and fading can be negated. Therefore, it is reasonable to consider this as the true value of received signal strength. This can be validated with standard measurement equipment, i.e. spectrum analysers.

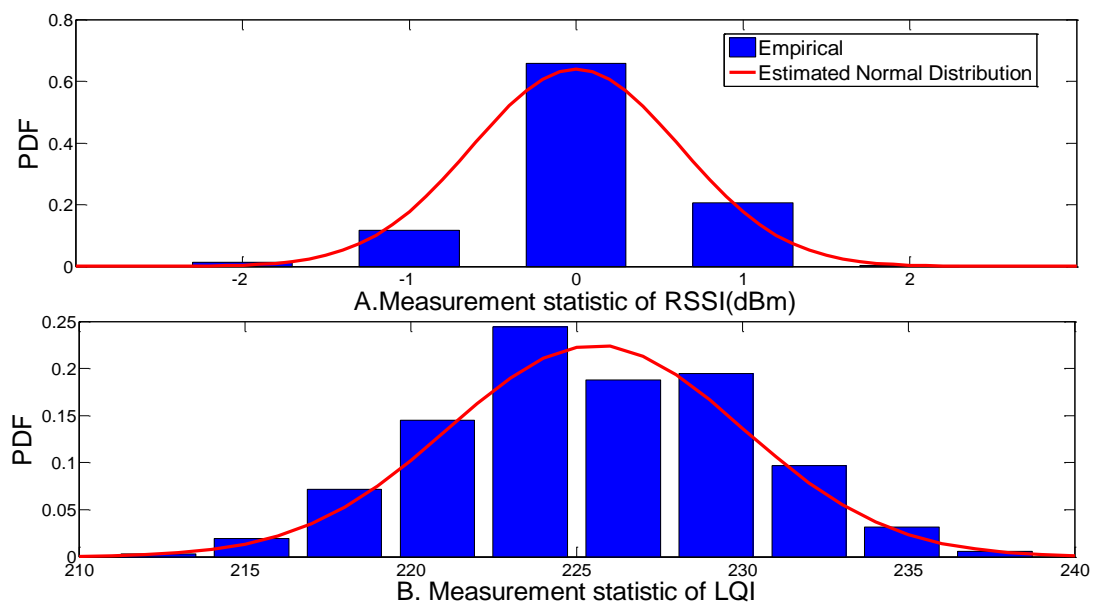


Figure 5.4. Measurement noise

We are then able to determine the measurement noise through a comparison between the RSS measured and the RSSI measurement produced. Using statistical methods on 20000 measurement samples over around 30 minutes, it is straightforward to calculate the variance  $R$  as shown in sub-figure A of Figure 5.4. As the measurement of RSSI and NOI are obtained using the same method at different time points, the variances should be same. Due to manufacturing and component tolerances, the devices used exhibit slightly differing performance parameters. As shown in the sub-figure B of Figure 5.4, a similar method can be employed to determine the variance of the LQI detection and finally calculate the measurement variance of the Effective-SNR. Differing from the RSSI

measurement, the detection of LQI is only based on the correlation of symbols inside the data frame and thus can expect to be hardware independent.

### 5.3.3.2 Process noise

Unfortunately, the process noise in the proposed Kalman filter is caused by the fading channel, hence, its variance will be highly dependent on the deployed location of the WSNs system. Similar effects have been reported in [110], which implemented the experiment in different locations and showed variance changes between 1.9 dB and 12.34 dB. Due to the implementation limitation, the noises on  $SNR$  and  $SQD$  are correlated and the off-diagonal entries of the covariance matrices are non-zero. However, according to our implementation experience, their correlation is relatively small which means that the off-diagonal entries are close to zero. Thus it is convenient to assume they are independent and adopt diagonal covariance matrices for the purpose of reducing the computation costs of Kalman filter.

Although some methods has been proposed to estimate the unknown process noises<sup>16</sup>, their computation complexity make them not applicable to the WSN devices with limited computational resources. To determine an initial value of  $Q$  to start the Kalman process, we developed an experimental set up in an anechoic chamber with several metal devices positioned to cause multi-path reflections. The process noise can be observed by calculating the statistical distribution of the received packet number compared with the maximum possible value (i.e. when LQI is equal to 255). The training sequence has been shown in Figure 5.5. The process noise required by the Bi-KF system can be obtained by applying PRR into system models.

---

<sup>16</sup> As reported in [115], High Gain Observer (HGO), an evolved form of Kalman filter, is able to detect and estimate the change of process noise. However, the computational cost is also expected to be higher and thus the implementation is deferred to future work.

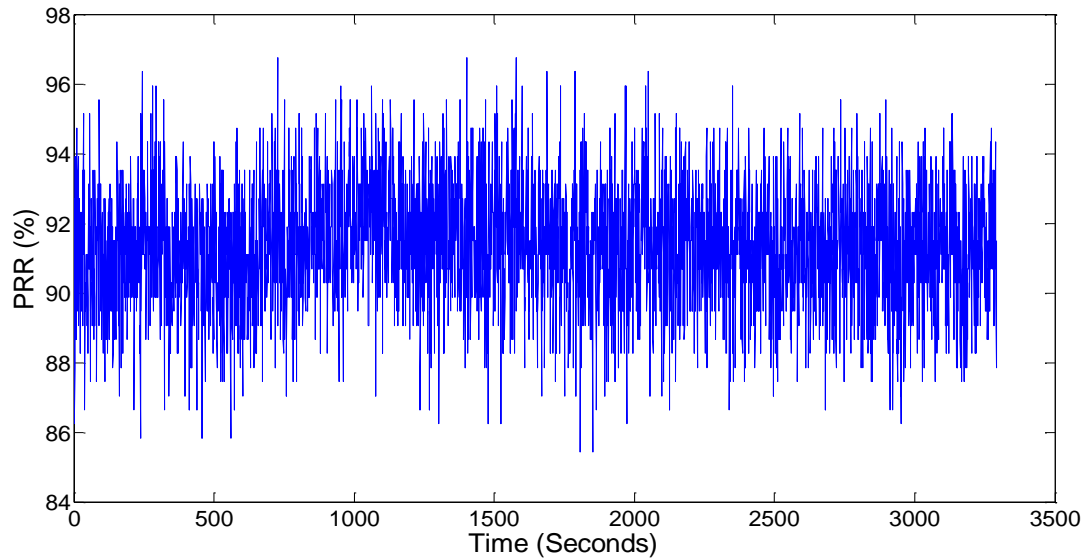


Figure 5.5. Training Sequence of PRR

### 5.3.4 Simplified implementation of Kalman filter

From our experiment, it was seen that the dynamic range of the metric used in the Kalman filter is relatively small and bounded as shown in Figure 5.6. Therefore, we suggest that it is unnecessary to employ floating point numbers in this implementation. Without significant loss of accuracy, the 16-bit fixed point method with a scale of 128 (i.e. a measurement of 1 will be scaled to 128, giving a resolution around 0.01 and the full-scale of [-256~256]) was employed.

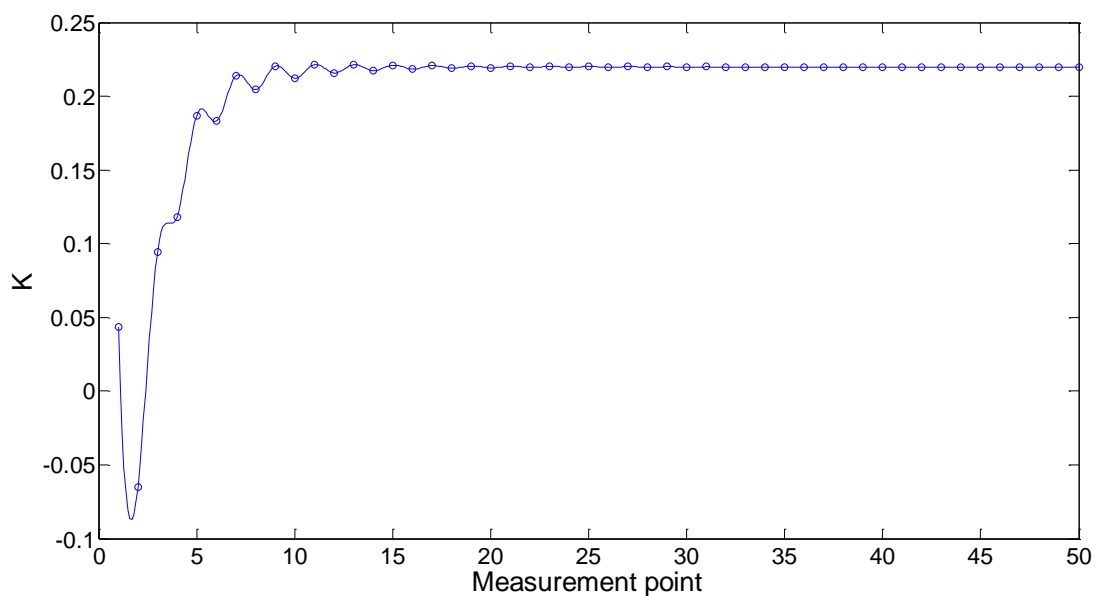


Figure 5.6. Converge Process of K

Given that the two states in equation (5.5) are independent of each other, the vector Kalman filter can be decomposed into two independent scalar Kalman filters, thus transforming the matrix inverse operation in equation (5.11) into a simple fixed-point divide operation that greatly decreases the calculation cost. However, unlike the 1st Kalman filter, the calculations used in the second Kalman filter cannot avoid complex matrix operations, e.g. product and inverse. This consumes most of the calculation cycles required by this algorithm. Nevertheless, fixed point calculations can still be used for the second Kalman filter and result in a decrease in the computation time from 2.14ms to 0.2ms in our implementation. Considering that the normal interval between two packets even in the saturation mode of standard IEEE 802.15.4 MAC (i.e. the average time cost for back off and CCA) is around 1.2ms, such cost of computation and time can be well accepted in WSNs.

#### 5.4 Experiment Results

We have implemented the proposed estimation algorithm in a COTS platform, where the MCU is ATmega128 working at 8MHz, without a float accelerator. The transceiver employed in this experiment is AT86RF231 which is the same as that used in Chapter 4. Such a configuration is comparable with most of the WSNs platforms (e.g. MicaZ, TelosB.) while some platforms supported higher computation capacity (i.e. IMote2 equipped a PXA271 which can work at 103MHz with a mathematic co-processor). We therefore suggest that the proposed algorithm is capable of being implemented on almost all WSN platforms.

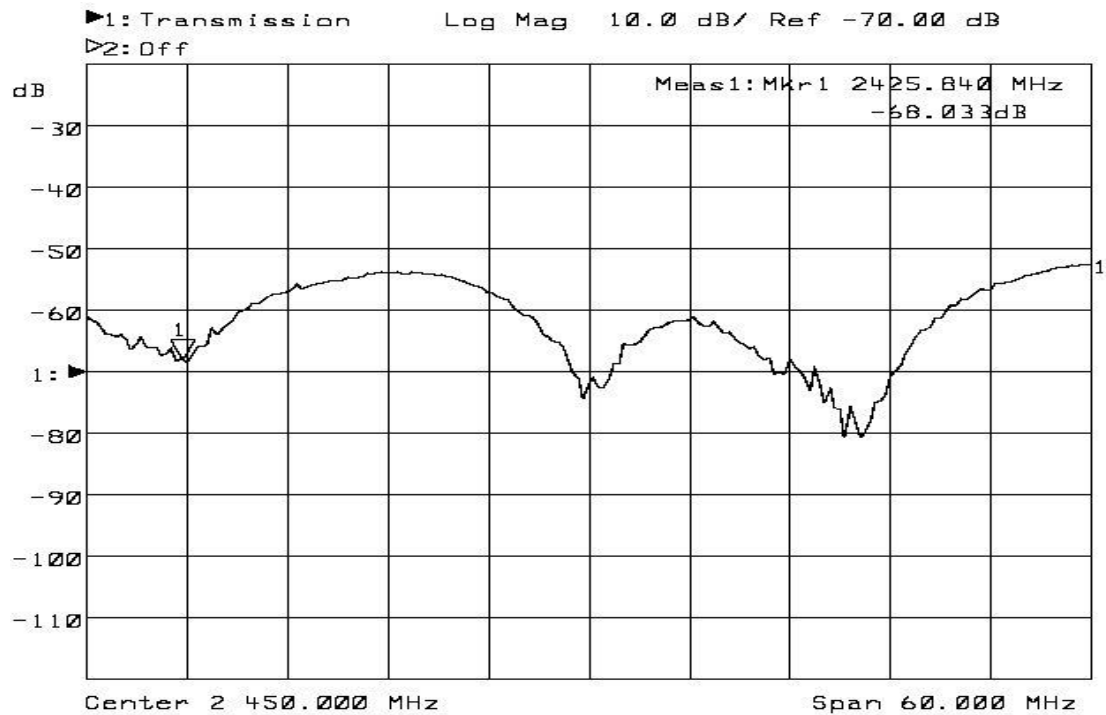
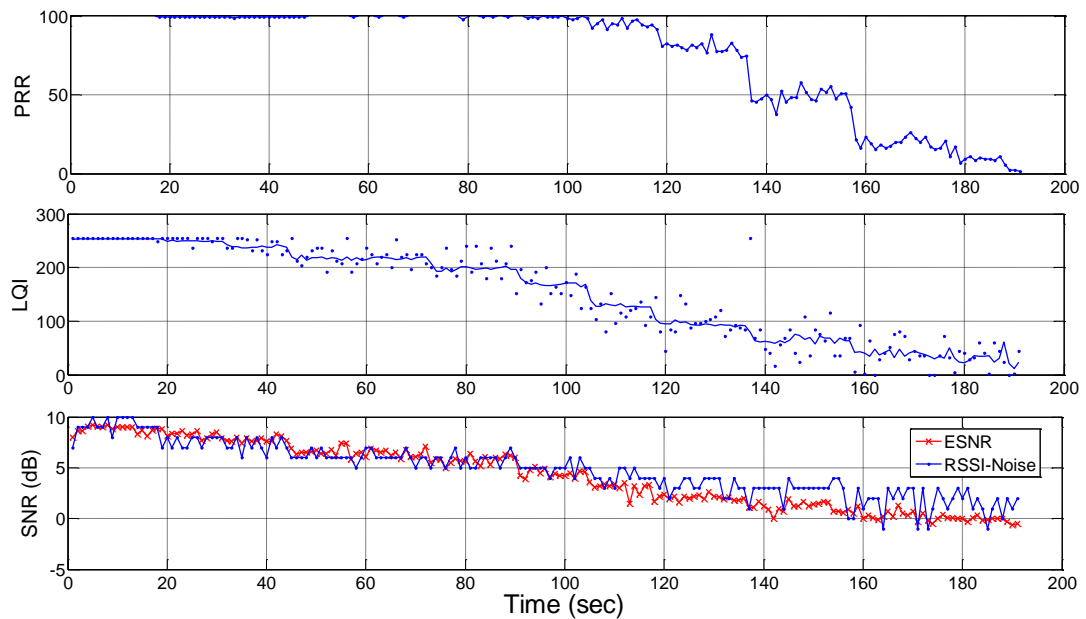


Figure 5.7. Frequency selective channel for Effective-SNR estimation experiment

The experiment has been setup in our laboratory, which contains instruments and workbenches with metal surface. As it is expected, such environment can cause fading effect, for instance, the frequency selective fading channel (tested using a RF network analyser as shown in Figure 5.7).

In the experiment, the transmitter was configured to work in saturation mode, meaning there is always a packet ready in the queue to be sent. A wideband RF source and antenna was located near the receiver and was used to generate noise in the wireless channel. Each packet contained a 100 Bytes information payload. The receiver recorded several metrics including: the number of packets it received at one second intervals, the averaged LQI for the period, instantaneous values of LQI and estimated Effective-SNR and SNR` (i.e. calculated through the deduction of RSSI and NOI) at the start of the period. It should be noted that the averaged LQI cannot be employed in the real application as it is an *a posteriori* statistic value, and we provide it only as the upper-bound of the *a priori* indicators.



**Figure 5.8. Experiment result in time sequence under indoor environment with varying environment noise**

The experiment results shown in Figure 5.8 were undertaken in the presence of adjustable environment noise from a wideband signal generator. The signal generator has been manually adjusted from  $-39\text{dBm}$  to  $-28\text{dBm}$ . As a result, the link quality of the wireless channel will inevitably be affected, which can be observed by the decrease in the number of successfully received packets. To simplify the illustration, we normalised the received packet number to give a Packet Receive Ratio (PRR) by comparing each result with the maximum number of received packet number, which has been provided in the first sub-plot. The averaged and instantaneous LQI performance is shown in the second sub-plot. In the third sub-plot of Figure 5.8, we provided the raw SNR calculated from the quantised RSSI. As can be seen from the recorded time sequence result shown in Figure 5.8, all the channel indicators are changing accordingly with the adjusted environment noise strength.

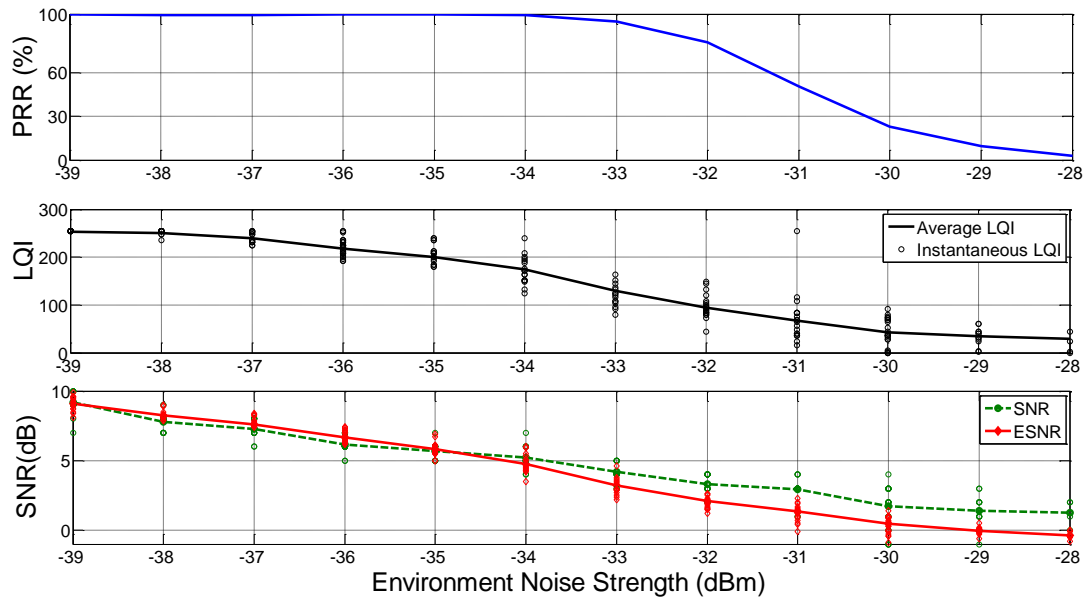


Figure 5.9. Experiment result in varying noise strengths under indoor environment

Obviously, the results shown in Figure 5.8 are indirect to provide the information of how accurate the channel indicator is. Then, the sampled results have been statistical processed and illustrated in Figure 5.9 in the format of PRR and different indicators versus the environment noise strength. The PRR can be seen to decrease steadily with increasing environment noise strength as shown in Figure 5.9. In the second sub-plot of Figure 5.9, both LQI and instantaneous LQI decreased nonlinearly, while the later one demonstrates a very high degree of variance. In the third sub-plot of Figure 5.9, the estimated Effective-SNR and raw SNR have been shown with trend lines to illustrate the averaged values. These two indicators also decreased with increasing environment noise, while the Effective-SNR has much less variance and better linearity than the SNR. It is easy to understand that the lower the variance, the more reliable the estimation.

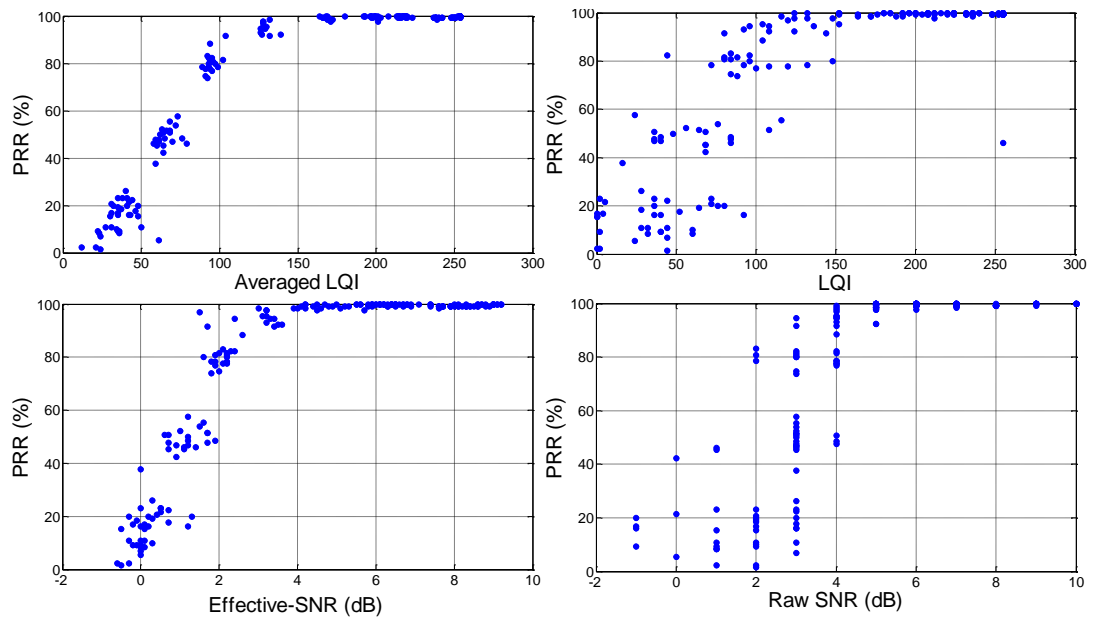


Figure 5.10. Correlation results under indoor environment with varying environment noise

To highlight the degree of variance, the experimental data has been further processed to show the correlation between the indicator and the PRR result, which have been illustrated in Figure 5.10. Clearly, the Effective-SNR shows the smallest variance among the three indicators, only slightly worse than the chosen upper-bound; the averaged LQI. The instantaneous LQI values tend to show much wider variance than the Effective-SNR, while the quantized RSSI based indicator is loosely correlated with the PRR with lower resolution.

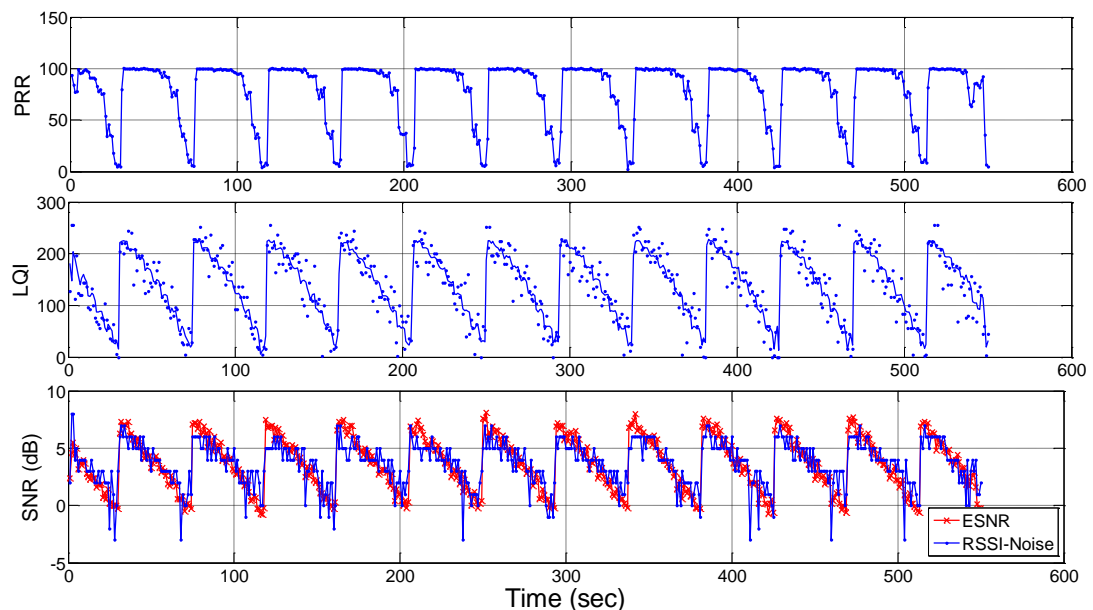


Figure 5.11. Experiment result in time sequence with varying transmitting signal strengths

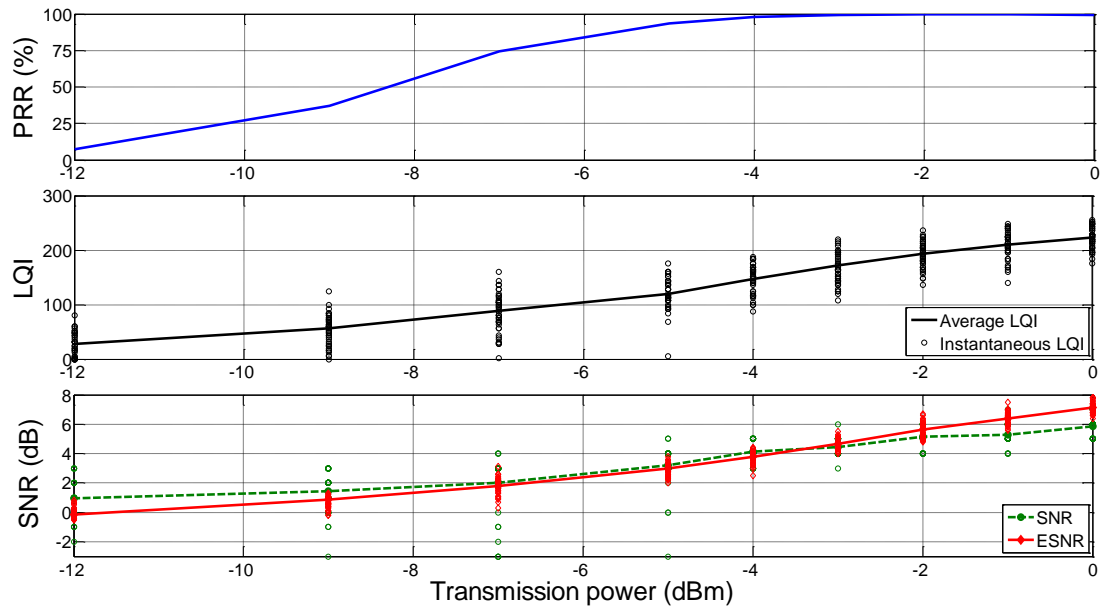


Figure 5.12. Experiment result in varying transmitting signal strengths

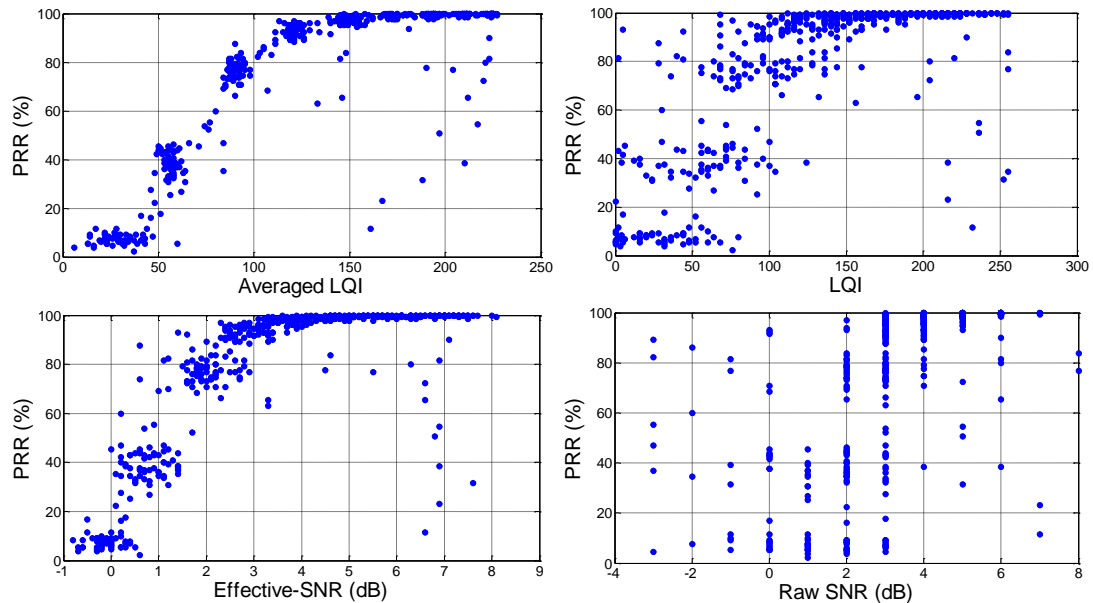


Figure 5.13. Experiment result under indoor environment with varying transmit power

In the Figure 5.11 to Figure 5.13, we presented the collected results from the second experiment, where the transmitter power was varied at transmitter from -12 dBm to 0 dBm and has been repeated for several cycles. The experimental results in the second experiment results show almost the same trends with the first experiment, i.e. all the channel indicators are changing with the PRR according but with different variations. Easy to notice from Figure 5.12 and Figure 5.13, the Effective-SNR has the smallest variation and highest correlation with the PRR, which demonstrate that the

accuracy of proposed indicators and its independent of the cause of channel quality change.

It is clear that in both experiments the Effective-SNR indicator shows very high correlation with the PRR, demonstrating the suitability of Effective-SNR as a channel performance indicator. To further examine the accuracy of applying indicators to estimate the channel capacity, a program has been implemented in MATLAB, which utilise the indicators obtained to estimate the error performance in the corresponding time period with the help of the error estimation model discussed in chapter 4. In order to better understand the comparison between different estimated results, a Root Mean Square (RMS) and a standard deviation (STD) of the residual are proposed as performance criteria.

Let  $\overline{PRR}_k$  denotes the estimated PRR, the residual was defined as:

$$r_k = \overline{PRR}_k - PRR_k \quad (5.17)$$

Then The RMS and STD for N data samples can be defined as:

$$RMS = \sqrt{\frac{1}{N} \sum_{k=1}^N r_k^2} ; STD = \sqrt{\frac{1}{N-1} \sum_{k=1}^N (r_k - \bar{r}_k)^2} \quad (5.18)$$

where  $\bar{r}_k$  is the mean value of the N samples.

Table 5.1 RMS/STD of the different residuals

Condition	Average LQI		Effective-SNR		LQI		SNR	
	RMSs	STDs	RMSs	STDs	RMSs	STDs	RMSs	STDs
Adjust Noise	0.0343	0.0296	<b>0.0544</b>	<b>0.0486</b>	0.1181	0.1067	0.1425	0.1291
Adjust Tx. Power	0.0492	0.0415	<b>0.0570</b>	<b>0.0452</b>	0.1171	0.0951	0.2377	0.2101

The RMS and STD of the residual error for different estimation methods are provided in Table 5.1. In general, the proposed Kalman estimator method significantly outperforms other methods. The performance of the averaged LQI is provided for reference. These results validate the effectiveness and improvement gained by the proposed Kalman filter based estimation method. In which a more reliable Effective-SNR is generated without high transmission overhead in WSNs.

## 5.5 Conclusion

In order to utilise the maximum capacity of WSNs in advanced applications, the availability of a simple yet accurate estimation of the RF channel quality is vital. However, due to measurement noise in the low cost devices and fading effects in the time-varying wireless channel, it is usually estimated through probe or learning based methods, which result in high energy consumption or high overheads. This chapter proposes to make use of information redundancy among indicators provided by the IEEE 802.15.4 system to improve the estimation of the link quality. A Kalman Filter based solution is used due to its ability to give an optimal estimate of the un-measurable states of a dynamic system subject to observation noise.

In this chapter we presented an empirical study showing that an improved indicator, termed Effective-SNR, can be produced by combining SNR and LQI with minimal additional overhead. The estimation accuracy is further improved through the use of Kalman Filtering techniques. Finally, experimental results demonstrate that the proposed algorithm can be implemented on resource constraints devices typical in WSNs, while the estimation accuracy can be increased through the proposed Effective-SNR solution. The estimated error performances of wireless link have shown that the accuracy of estimation has been increased 160% compared with raw SNR, and 120% when compared with the instantaneous LQI. The link quality estimator can be implemented in conjunction with a variety of the upper-layer algorithms in sensor networks. Within the context of this thesis, the proposed low cost Effective-SNR is able to estimate the channel capacity accurately in harsh RF environments with the help of the error performance model discussed in Chapter 4. It is possible to design an optimisation based MAC protocol to utilise the adaptive spreading code length, which will be discussed in the next chapter.

---

## Chapter 6. Utilising the Adaptive Spreading Code Length for the MAC Protocol Design of WSNs

### 6.1 Introduction

This chapter presents the design of a MAC protocol aiming to utilise the adaptive spreading code length feature to achieve better performance in WSN systems by ways of improving link reliability, or by increasing throughput and energy efficiency. The motivation comes from the advanced WSNs applications discussed in Chapter 2, where deployed WSN system have to deal with the challenge of intensive traffic load as well as harsh RF environments. We suggest that the use of adaptive spreading code length in wireless sensor networks could be one of the most suitable candidates for these applications. Aided by the adaptive spreading code length feature, the WSN system will be able to automatically adjust the spreading code length to deliver the highest throughput for the current wireless link margin. In the case of a harsh RF environment, the system can also deliver robust service by increasing the spreading code length, while the system can decrease the spreading length to deliver information in opportunistic high data-rate mode. The WSN system deployed in ordinary RF environment can also be significantly benefited from the utilisation of adaptive spreading code length, since the system will be able to deliver much higher throughput comparing with the standard IEEE 802.15.4 based WSN system. We have named the proposed MAC protocol *Adaptive Spreading – MAC*, briefly noted as *AS-MAC* for the following discussions.

The design of the proposed *AS-MAC* will be grounded on the findings discussed in previous chapters, 4 and 5. In detail, we experimentally identified the error performance of different spreading length modes, based on which, an analytic model has been proposed to accurately estimate the error performance in the AWGN channel. Since we cannot expect the ideal AWGN channel in most deployments of WSNs, we proposed a new link

indicator named Effective-SNR which is able to normalise the link quality in a fading channel into an equalised Effective-SNR in an AWGN channel with the aid of a two layer Kalman filter. Due to the nature of Kalman filter, such an indicator is able to track the condition of the time varying wireless channel much faster than other approaches, e.g. moving average. Using this technique the receiver can easily calculate the optimum spreading code length for the current transmission link. However, one problem remains, which we will investigate in this chapter: only the transmitter can configure the spreading code mode for current packet, while the optimisation can only be calculated based on the information provided by the receiver. Then, clearly, the design question will be based on how to exchange this information between the transmitter and receiver; a feature which is not provided in the standard IEEE 802.15.4 MAC or its variants typically used in WSNs e.g. B-MAC.

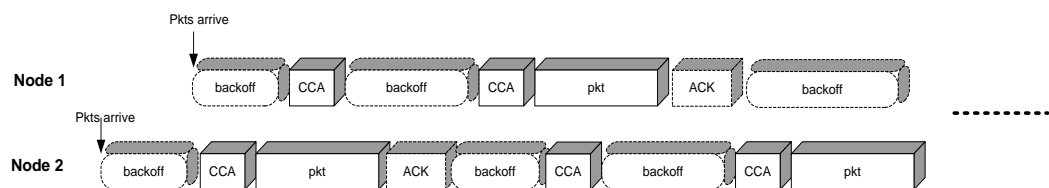


Figure 6.1. IEEE 802.15.4 MAC protocol

Obviously, the four way hand-shake scheme currently employed by the IEEE 802.11 DCF is one of the candidates to solve this problem. However, unlike the IEEE 802.11 DCF, the maximum packet length supported by the physical layer of IEEE 802.15.4 is much smaller: only 128 Bytes. The overhead cost of RTS and CTS packets for this short packet could be too high to be afforded by the WSN system. This problem can be mitigated in the scenario with heavy offered traffic load through the aggregation of packets from the application layer. As shown in Figure 6.2, instead of directly sending out packets from the application layer, the MAC layer will buffer the packets until a block of packets are waiting for transmission and can be transmitted together in one four way hand-shake procedure.

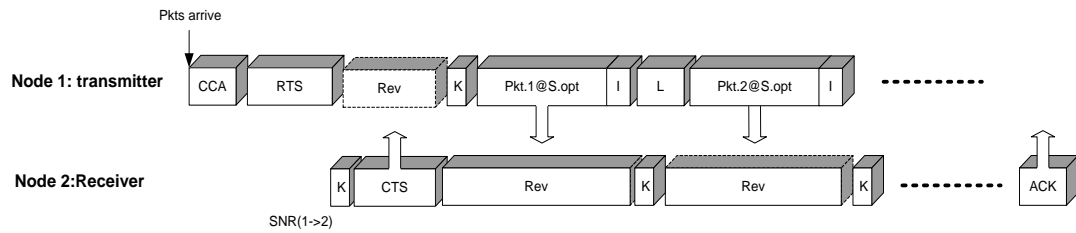


Figure 6.2. Four way hand-shake based protocol

Beyond this, the principle of this protocol design should also be compatible with both traditional applications with a low duty cycle and advanced applications with intensive data transmission tasks. It should be noted that even data intensive applications can consist of hybrid tasks, i.e. the intensive data transmissions are only triggered in a burst pattern, the network will still need to be able to deal with single and short packets at all other time. Therefore, any proposed algorithms should consider the requirements for both kinds of transmission.

As observed previously, there will always be a large number of packets transmitted in high throughput applications and thus, we are motivated to wonder whether we could use the first packet of the queue as an RTS packet, and utilise its ACK packet as the CTS packet to exchange the optimisation result generated in receiver side. If there are other packets in the queue, they could be transmitted at a faster data-rate (depend on the link quality); whereas if this is the only packet waiting to be sent, the cost can be controlled, since there is no overhead in this procedure (the same as standard IEEE 802.15.4 MAC: one data packet and one ACK packet). In this chapter we will analyse this new protocol to see if it is able to fulfil the requirements of WSN applications with high traffic load, i.e. provides higher throughput while keeps the energy efficiency with low-cost design fashion.

In section 6.2, we will discuss the detail design of the *AS-MAC* from a number of different perspectives, which will enable the optimisation of the adapted spreading code length mode. The proposed *AS-MAC* has been implemented in a COTS platform to evaluate the performance. A standard IEEE802.15.4 MAC has also been implemented in the same platform as a comparison. The recorded performance results will be provided in section 6.3

to demonstrate the advantage of proposed *AS-MAC*. Finally, our findings will be concluded in section 6.4.

## 6.2 Design of *AS-MAC* protocol

The details of the protocol will be described in this section. Different aspects in the implementation will be discussed separately first and the overall architecture of the proposed *AS-MAC* will be presented at the end of this section.

### 6.2.1 Modifications to Carrier Sense

The design of the standard IEEE 802.15.4 MAC is very similar to the IEEE 802.11 DCF protocol but with further simplification. Such simplification derived from the characteristics of the traditional WSNs system, i.e. low traffic load and low power oriented. For instance, the IEEE 802.11 DCF will freeze the backoff timer when the channel is busy and only decrease the backoff timer when the channel is detected to be idle. Obviously, this scheme will require the transceiver to be active to monitoring and report the wireless channel during the whole carrier sense process and will continually consume power. Therefore, in the design of the IEEE 802.15.4 MAC, such operation has been significantly simplified: as soon as a packet arrives, the MAC protocol will start the backoff timer following the same exponential manner. Unlike the IEEE 802.11 DCF scheme, the radio transceiver will be set to idle in this process to save energy and the backoff timer will continually decrease. The IEEE 802.15.4 MAC will only sense the channel after the backoff period for a fixed time slot (192  $\mu$ s), and the feedback of this measurement will determine whether the channel is free or not. As a result, the IEEE 802.15.4 MAC gives up the possibility to learn what's going on in the wireless channel<sup>17</sup>.

As these random backoffs were employed to de-synchronise the channel competition for different devices, such a scheme works fine in extremely low offered traffic load scenarios to provide acceptable

---

<sup>17</sup> IEEE 802.11 DCF does not try learn the transmission activity as well, but the backoff scheme keeps the possibility while the IEEE 802.15.4 standard MAC eliminate such possibility.

performance. However, as discussed in chapter 2, the WSN system has been more and more employed in advanced applications, where the character of the tasks will be slightly different. Although the overall offered traffic loads may still be in low level in these applications, there could be heavy offered traffic load concentrated in a short period which will cause high competition in the wireless channel, e.g. in the sample burst. In this case, such a simplified MAC scheme will greatly decrease the delivered system throughput due to less obtained information of the wireless channel and increased power consumption due to the higher retry and retransmission rate.

The second issue is about the carrier sense operation which originates in wired systems. In such a scheme, the physical layer will enable the radio front-end for a fixed period and record the power readings of the detected signal. If the readings exceed a pre-configured threshold, a channel busy result will be reported. In a wired system, the channel can be assumed as a perfect media, therefore having only two states: occupied or free. Such a system still works fine in fully connected wireless systems (e.g. each devices in the network can communicate with each other), but will lose performance in real wireless networks due to the quantisation of the wireless channel status instead of the simple on and off wired channel.

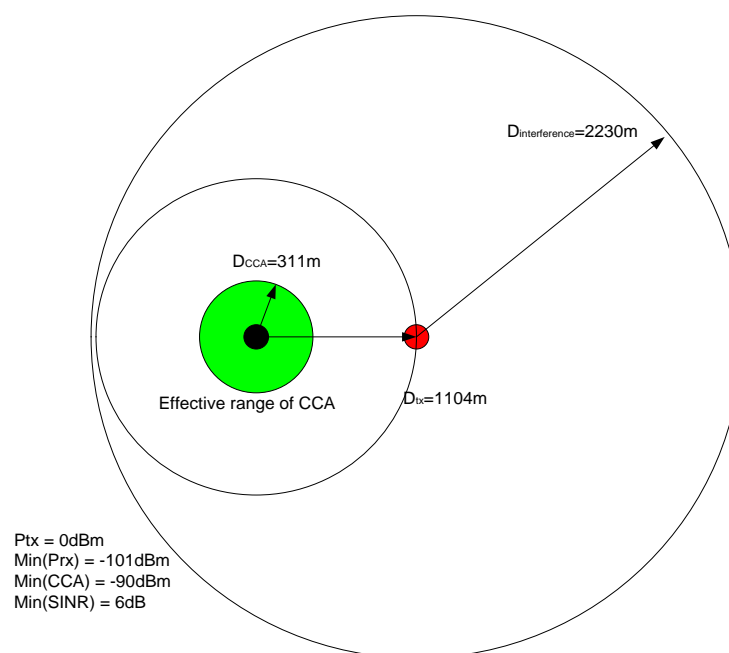
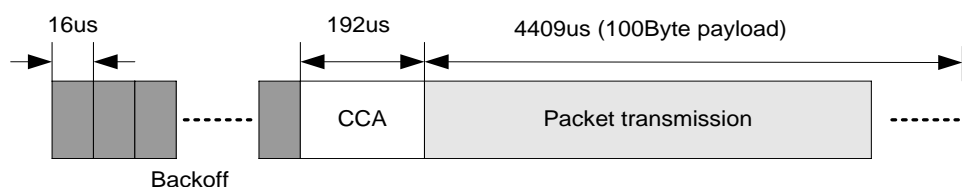


Figure 6.3. Effect of carrier sense

An example has been shown in Figure 6.3 based on the transceiver we are currently using for our experiments, but similar effects can also be expected for other IEEE802.15.4 radio transceivers. Assuming each node transmits a packet with 0dBm transmission power, the potential receiver located inside the medium cycle in Figure 6.3 can form a stable wireless link giving the condition that the minimum receiving sensitivity is -101dBm and the propagation model is the standard free space model [91]. According to [21], the minimum energy reading for the incoming signal is -90dBm, therefore the CCA can only be effective to in avoiding collisions with a competitor if it is located within the smallest cycle highlighted in green. Furthermore, considering that the minimum SINR requirement for a stable wireless link is 6dB, if the receiver is located in the red pot shown in the figure, any node located between the smallest circle and the biggest circle can interrupt the transmission link.

It is easy to notice that the effect of current carrier sense operation in IEEE 802.15.4 MAC is very limited. If a higher spreading mode was employed, the SINR requirement will be further increased which has been demonstrated in Chapter 4. As a consequence, the wireless link will be more vulnerable to competitors in the network. Therefore, we are motivated to modify the current carrier sensing operation of the IEEE 802.15.4 MAC to improve the overall performance for an adaptive spreading code length based WSNs system. In the proposed protocol, once packets arrive from the application layer, the MAC layer will start the exponential backoff timer as well. However, the MAC protocol will set the transceiver to the receiving state instead of the idle state. In other words, we prefer the system to learn as much channel information as it can rather than saving small amount energy.



**Figure 6.4. Time constraints of the carrier sense operation**

We now demonstrate that the energy consumed in this operation is relatively small compared with the whole energy consumed for a packet

transmission. According to [16], the backoff period is uniformly distributed in a binary, exponentially expanding range. In detail, the backoff period is uniformly distributed in  $[0 \sim 2^{i-1}(w-1)]$ , where  $i$  is the number of the retransmission and  $w = 8$  is the initial backoff window size. As shown in Figure 6.4, each backoff slot lasts  $16 \mu\text{s}$  and the CCA operation after the backoff period lasts  $192 \mu\text{s}$ . Then, considering that the collision probability in the traditional low traffic scenarios can be assumed to be zero, the backoff period can be approximated as  $2^{i-1}(w-1)/2$ . Now, we have all the parameters needed to calculate the proportion of power consumption in the backoff period within the traditional scenario, for example only 1.23% of the energy can be saved if the packet has a payload of 100 Bytes and was transmitted with the default power of 0dBm. It is easy to notice that keeping the transceiver idle in this operation only contributes a small proportion of the overall energy consumed. Therefore, forcing the transceiver to enter the receiving state in the backoff period will not cause significant power consumption, but this modification will assign the system more flexibility in determining the channel information. The AS-MAC will keep reading the energy detection value from the transceiver to gain information on the channel. If the channel is free, the first packet in the block will be transmitted after the backoff period. In this case, the recorded energy detection value can be assumed to be the environment noise with accumulated far away interference and will be fed to the Kalman filter as the statistic of the environment noise.

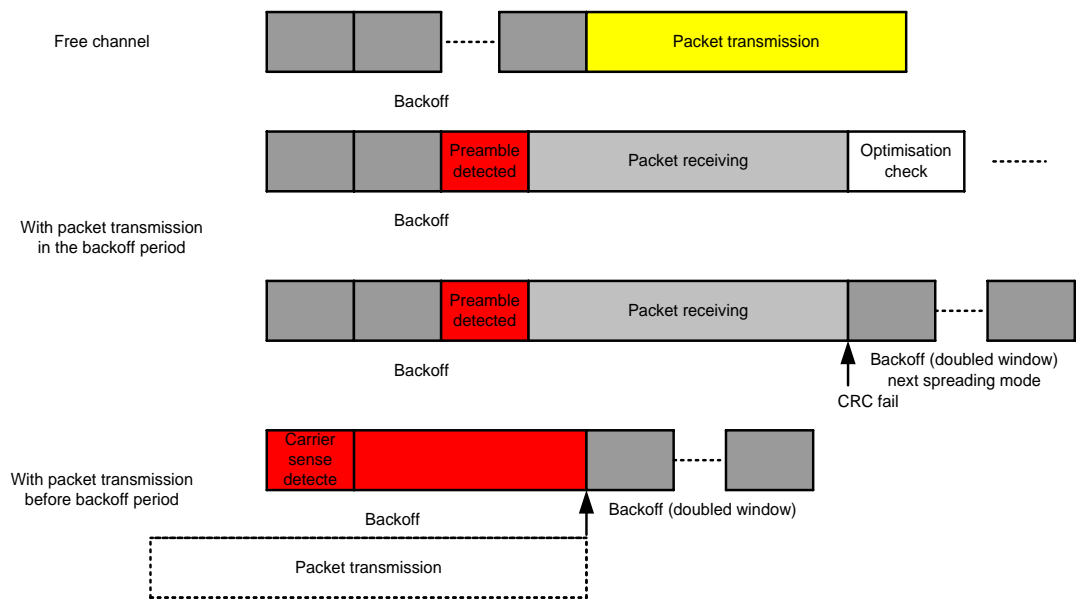


Figure 6.5. Carrier sense modification in AS-MAC

If there are other activities in the channel (e.g. another transmission link is ongoing), two potential feedbacks can be expected. First, if such transmission was initialised during the backoff period, the preamble of that packet can be captured. Then the system will receive this packet until it finished. The signal strength and the packet information with the link parameters will be passed to Kalman filter to update the link status metric. Since the preamble lasts  $192 \mu\text{s}$ , we also modify the backoff slot to last  $192 \mu\text{s}$  rather than  $16 \mu\text{s}$  to enable the carrier sensing have enough time to capture the preamble. As a consequent, the protocol can determine the channel as busy and double the back off window. Second, if the transmission was started before the backoff period, the carrier sense can still report detection of the IEEE 802.15.4 signal, but due to the limitation of the current hardware implementation, we cannot force the transceiver to decode packet without recognition of the preamble. In this case, we simply assume the channel is busy and double the backoff window, and increasing the probability of capturing the preamble in the next backoff period. It is also noted that, in both cases, since different spreading modes can be employed in this protocol, the received packet may report a CRC failure due to the un-synchronized spreading mode. When a packet has been received but reported as a CRC failure, the protocol will be cycled to the next spreading

mode for the next potential transmission. The scheme has also been shown in Figure 6.5.

We understand that it is possible to enable concurrent transmission to achieve even higher network performance. However, the current transceiver implementation will synchronise to any detected preamble even though there could be a higher SNR packet arriving later. Therefore we limited this possibility in this version of protocol and defer it to our future investigation.

### 6.2.2 Packets Aggregation

Once the channel is free, the MAC layer will attempt to send the first packet in the buffer queue. In the traditional WSN applications, it is most likely that the first packet is also the only packet waiting in the queue. In this case, just like the default IEEE 802.15.4 MAC, the packet will be sent out immediately. Since there is no other pending packets waiting to be sent, the receiver will also process this packet in the default IEEE 802.15.4 way and send the ACK packet. The only difference is that the proposed *AS-MAC* will feed the signal strength of received packet to the Kalman filter to enable it tracking the channel quality trend, if any, of the current transmission link.

However, in advanced sensor network applications, the throughput demands from the upper layers could be much higher in the sample period than the rest of time. For instance, in the structure health monitoring application discussed in Chapter 2, the system samples the vibration sensor with a 1 kHz sample rate, thus, every second there will be around 60 packets (with payload length = 100 Bytes) arriving from the upper layers. Another example could be multi-media based applications. Considering a system equipped with a standard 300×200 digital camera and recording static pictures every second, the raw data (i.e. BMP format) generated could be as large as 240kB. Even if the data can be locally processed with a JPEG algorithm, the data needing to be transferred via the network can still exceed 12kB (assuming 5% compression ratio), which will be converted to an offered traffic load of more than 120 packets per second. In traditional WSN applications with simple sensor inputs, the existence of aggregation congestion (i.e. the close to the sink device, the more aggregated packets

from previous hops will occur) can result in congestion of data packets in the MAC layer. These packets used to cause congestion in the traditional wireless sensor networks, but with the aid of adaptive spreading code length, the *AS-MAC* will be able to utilise higher bandwidth to increase the performance of WSNs in advanced applications.

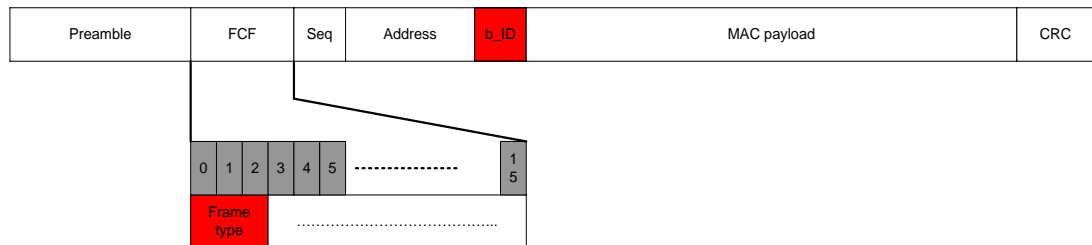


**Figure 6.6. Modification of the packet structure in AS-MAC**

In the case where there is more than one pending packet in the queue, the *AS-MAC* will process them as a block, i.e. a series of packets will be transmitted in one hand shaking process. The first packet in the queue will be sent out as a probe packet. To indicate to the receiver this unique packet type, we have reused the frame type subfield in the Frame Control Field (FCF) of the IEEE 802.15.4 packet structure. Value of 0,1,2,3 have been used by the standard IEEE 802.15.4 to indicate the beacon, data, ACK, and command packets respectively. Then we define the frame type of 4 as the probe packet, which is the first packet in the block. After the receiving of probe packet, the receiver will start the optimisation algorithm based on learned information about the current wireless link and environment, and return the optimised result within the ACK packet. However, this special ACK packet will contain different and more important information than the standard ACK packet, thus we assign it a frame type of 5 to distinguish it from standard ACKs. After successfully decoding the first ACK, the transmitter will send the other packets in the block using the optimised configuration. These packets will be indicated with a frame type of 6. After the whole block has been transmitted, the receiver will terminate the link with a final ACK packet, which will contain the packet lost information, if any, and will be flagged with a frame type of 7. Finally, the transmitter will re-buffer the lost packets into the queue and start another cycle as long as the queue is non-empty.

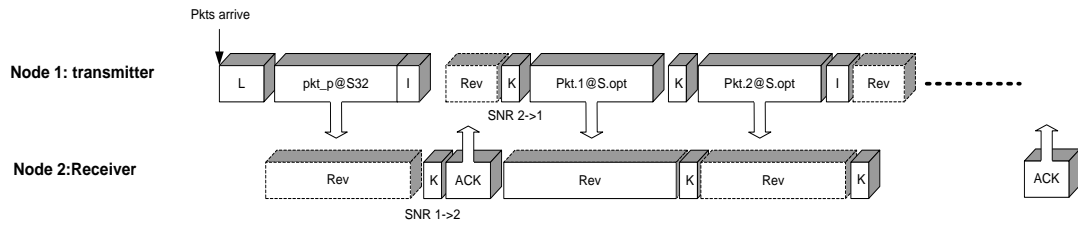


Figure 6.7. Basic scheme of AS-MAC

Besides the frame type, the *AS-MAC* will also need to know the block-ID for each packet in the block, e.g. to check if the packet is lost. We then have to add one more Byte in the MAC header just before the payload as shown in Figure 6.6. This block\_ID will be counted from high to low, i.e., the block\_ID of the probe packet will be equal to the block size, and the last packet in the block will have a block\_ID of one. Therefore, the proposed *AS-MAC* will only increase the overhead over the standard IEEE802.15.4 MAC by one Byte, which is affordable for the low-cost and resource constraint designs.

### 6.2.3 Optimisation of the spreading code length

Once the receiver has detected a probe packet, the *AS-MAC* will first check the frame type field. If the frame type of the packet is equal to the probe packet type, the optimisation process will be triggered. The optimisation process's aim is to maximise the deliverable throughput in the current wireless link without interrupting any existed wireless link. This target can be achieved theoretically by maximising the following function:

$$\operatorname{argmax}_{r \in R} \text{Throughput}(r) \quad (6.1)$$

where  $R$  is the set of the data rates for all possible spreading code length modes.

According to the discussion in Chapter 4, given the SINR and the packet length for the current link request, equation (6.1) can be derived into the following equation (6.2), i.e. minimising the packet error rate by choosing the right spreading code length.

$$\operatorname{argmin}_{r \in R} \text{PER}(r) \quad (6.2)$$

Nonetheless, the first step in the optimisation process is to estimate the link quality. However, recent published measurements [58] have shown that solely measuring the SINR during a short time scale, e.g. the duration of a packet, may not be a good predictive method to estimate the quality of wireless link. As discussed in Chapter 5, the Kalman filter can be one of the best candidates in this scenario. Firstly, it can provide an accurate estimation of the current wireless link. Secondly, the estimation is not only based on the current link states but also the historic statistic. Thirdly, a Kalman filter can follow changes in link quality very rapidly, e.g. in the implementation, the system can converge with less than 10 inputs. Furthermore, the Effective SNR processed by the Kalman filter has normalised the effect of the fading effect, thus, it will be more straightforward to calculate the best spreading code length mode with the Effective SNR measure in an AWGN channel model, rather than with SNR in a fading channel model. Therefore the Kalman filter has been employed to generate the link estimation rather than the simple moving average method used in some other rate adaptive protocols.

**Table 6.1 Pseudo code of the optimisation process**

```

Spreading_code_length_optimisation(Effective-SNR, Packet_length)
{
  minPER = 1;
  best_r = -1
  if (converge_Kalman()!=1)
  {
    return 0;
  }
  for all r∈R
  {
    SER= get_SER(Effective-SNR);
    PER=(1 - SER )2·packet_length;
    if (PER < minPER)
    {
      minPER = PER;
      best_r = r;
    }
  }
  return best_r;
}

```

As shown in Table 6.1, once the *AS-MAC* has detected a probe packet and triggered the optimisation process, it will first check whether the Kalman filter has converged. If not, the optimisation process will return the default spreading code length mode, i.e. 250 kbps. The optimisation will only have effect when the Kalman filter has converged, i.e. it is able to provide an accurate estimation. Then the *AS-MAC* will use the estimated Effective-SNR to get the corresponding Symbol Error Rate (SER). The SER can be obtained following the analytic method discussed in Chapter 4, however for reasons of simplicity, the results have been pre-generated off-line and saved into a look up table. In the online process, the *AS-MAC* will simply index the look up table with estimated Effective-SNR and get the corresponding SER. The next step is to go through all four possible spreading code length modes, calculate the Packet Error Rate (PER) with the SER and packet length. It should be noted that different packet lengths will affect the error performance due to the CRC scheme. Finally, the spreading mode with minimised PER will be returned as the optimised spreading code length mode.

As discussed in Chapter 5, the Kalman filter implemented in our system will also track the change of environment noise in addition to the signal strength. Therefore, the Effective-SNR estimation will reflect the variation of both the signal strength and the environment noise. Obviously, the adaptation is not only optimised for the link quality but is also aware of changes in the environment noise, which will make the *AS-MAC* appropriate to be deployment in industrial locations with harsh RF environments where it will be able to track the change of environment noise strength, and deliver higher throughput when higher Effective-SNR exists in an opportunistic manner.

The optimisation result will be embedded into an ACK packet and sent back to the transmitter. The receiver will then be configured to the optimised spreading mode while waiting for the upcoming packet block. Since the ACK packet may also have the possibility of error, *AS-MAC* will start a timeout timer with the upper-limit of two packet intervals. In the case that the ACK packet is lost the timeout event will be triggered where the *AS-MAC* will stop

the current receiving process and switch back to the idle state with the default spreading mode.

#### 6.2.4 Overall protocol architecture

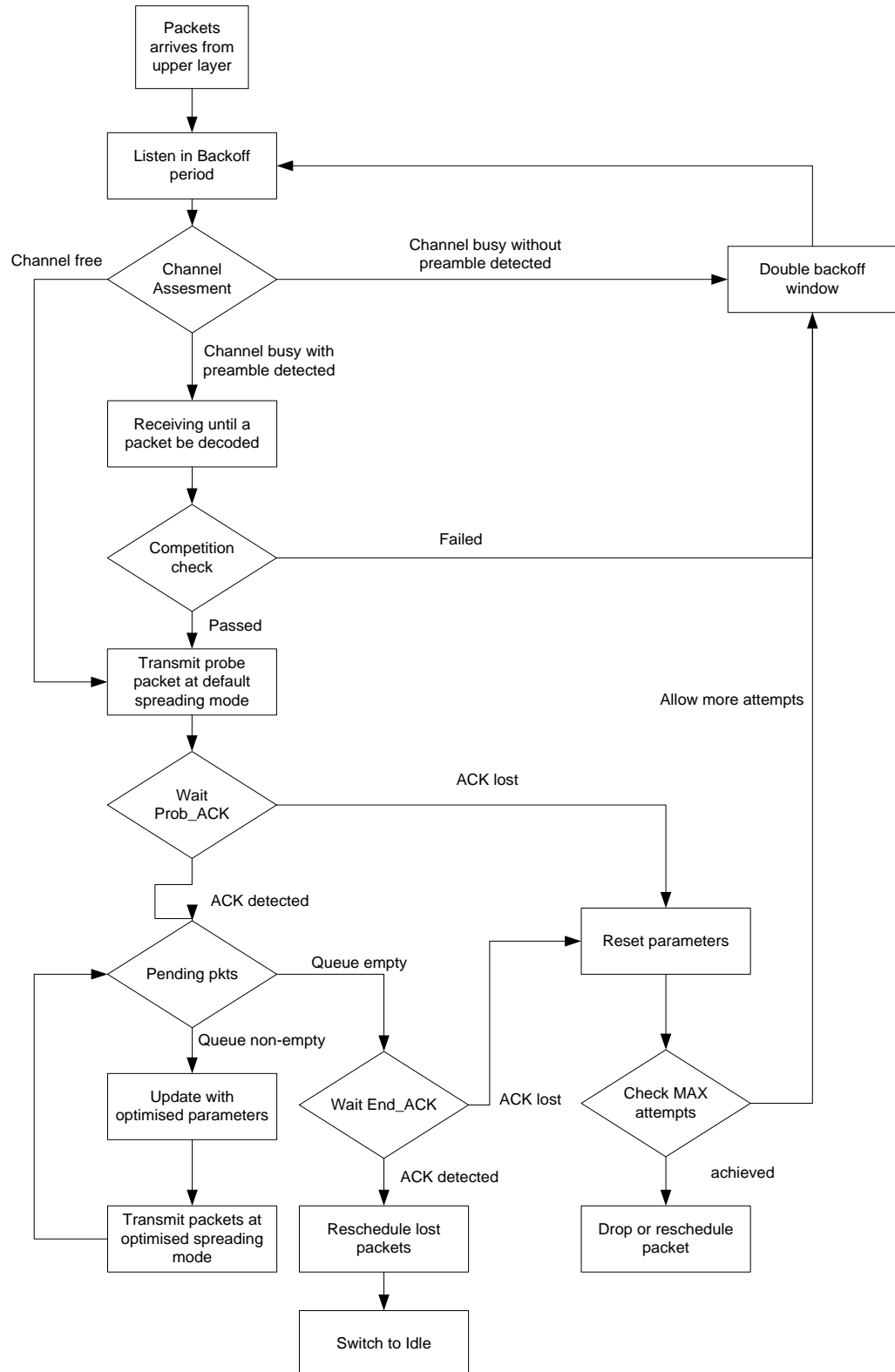
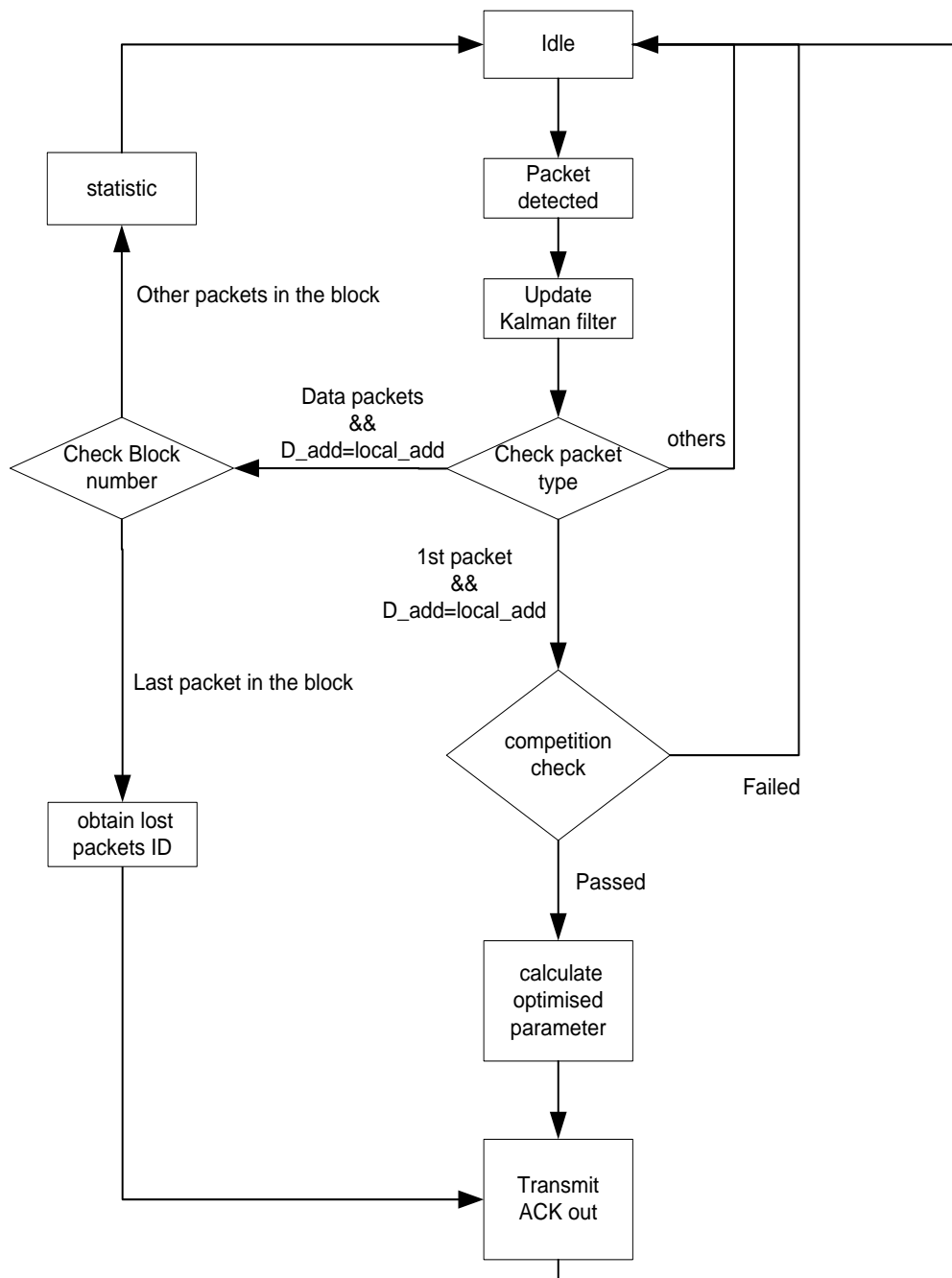


Figure 6.8. Algorithm for transmission operation



**Figure 6.9. Algorithm for receiving operation**

Here we will provide a description of the overall protocol architecture outlined by the algorithms in Figure 6.8 and Figure 6.9, for the transmission and receiving operation respectively. The system will be able to track and predict the change of link quality by employing a Kalman filter. In the case the Kalman filter has not converged, the system will work with the default, most robust spreading code length. As soon as the Kalman filter converges, the system carries out the optimisation process and uses the optimised

spreading code to deliver as high a throughput as possible, which will, of course, decrease the latency and reduce the energy consumption. It should also be noted that such a scheme should have almost the same energy efficiency with low offered traffic loads, but can trade the energy consumption for a better channel utilisation with heavy offered traffic loads. We will experimentally demonstrate the system performances using this approach in the next section.

### 6.3 Performance Evaluation using Experimental approach

The proposed *AS-MAC* protocol has been implemented in the same COTS platform employed in chapter 4 and 5. This platform is comparable with most common WSNs platforms (e.g. MicaZ, TmoteSky.) in terms of MCU frequency and memory space. As a consequence, the proposed protocol implemented here should also be able to be implemented and work with almost all other WSN platforms. The standard IEEE 802.15.4 MAC protocol has been implemented as well to provide a direct comparison of the *AS-MAC* performance. The experiment location is an ordinary in-door environment, which suffers from the multi-path effect due to reflections. Similarly to previous experiments, a vector signal generator, ESG4432B has been employed to generate the variable environment noise.

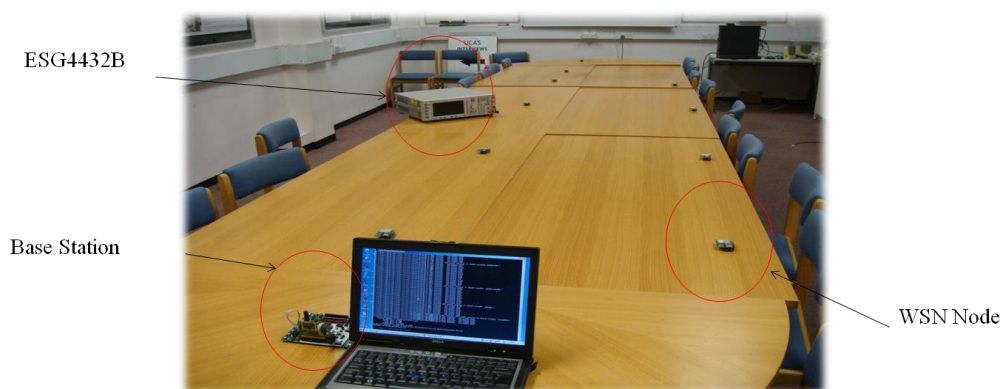


Figure 6.10. Photo of the *AS-MAC* experiment setup

A series of experiments have been conducted to evaluate the proposed MAC protocol. The packet arrival rate was pre-configured before the experiment following a Poisson distribution with a mean value of  $\lambda$ . Note that the default block contains 20 packets and the default payload length of a

packet is 100 Bytes unless otherwise specified. In all the experiments, both the IEEE 802.15.4 MAC protocol and the *AS-MAC* have been configured with the default MAC parameters: the initial backoff window size  $W$  was set to 8, maximum retransmission attempts  $M$  is set to 4. To simplify the analyses, we disabled the retransmission scheme in both protocols, i.e. the protocol will drop the current packet in the event of ACK\_Timeout being exceeded instead of re-adding it to the buffer queue for retransmission. As a result of this regulation, the offered traffic loads were determined only by the data arrival rate.

### 6.3.1 Throughput performance

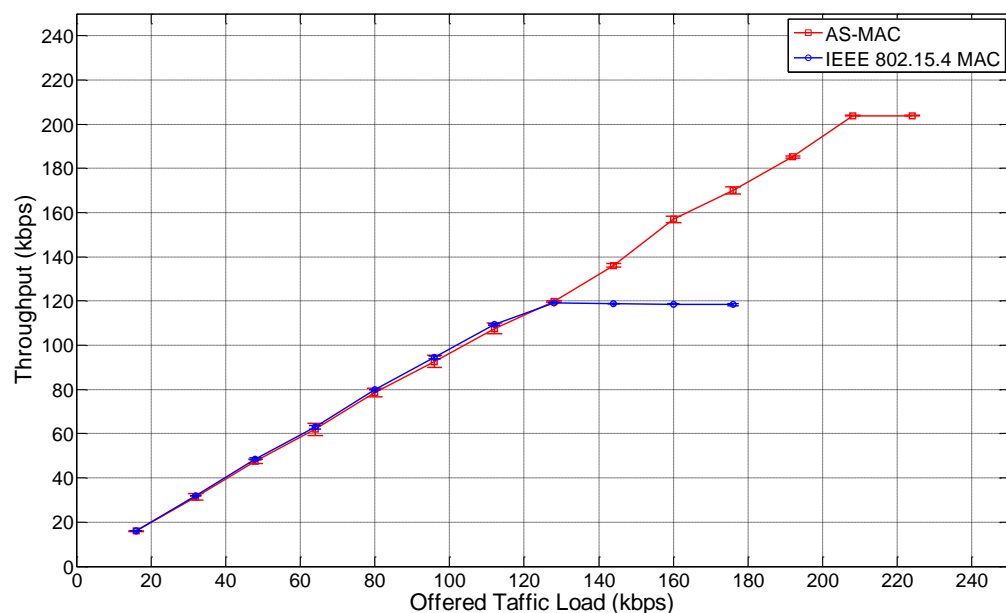
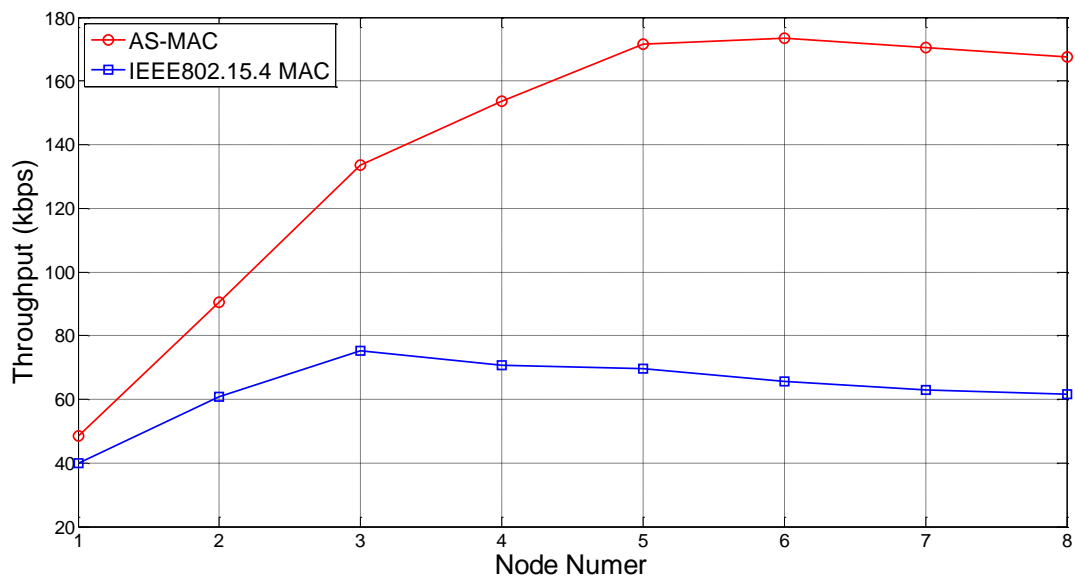


Figure 6.11. Capacity comparison between the proposed AS-MAC and standard IEEE 802.15.4 MAC

We first explore the potential throughput capacity of the proposed *AS-MAC* by deploying only one transmission pair, where the channel collision probability can be eliminated. During the experiment, we increased the data arrival rate for the transmitter, i.e. increasing the offered traffic load in the system, until the system saturated. As expected, the standard IEEE 802.15.4 MAC is saturated at a packet arrival rate of 160 packets per second (pps), where the system is able to provide the throughput of 118kbps. Only the payload of a packet will be treated as the effective throughput, i.e. the header

of MAC layer and preamble of PHY layer have been excluded when calculating the throughput performance. Therefore, the illustrated throughput in our work will be slight less than the offered traffic loads shown in Figure 6.11, and may also be less than the reported value in other publications due to this calculation method. Then, as shown in Figure 6.11, by enabling the adaptive spreading code length, the proposed *AS-MAC* allows increased throughput enabling the system to cope with an increasing offered traffic load of up to 260 pps (around 208 kbps). The maximum achieved throughput provided by *AS-MAC* could be as high as 204 kbps, which is a 76% performance improvement comparing with the standard IEEE 802.15.4 MAC.



**Figure 6.12. Throughput performance in Star topology**

The throughputs shown in Figure 6.11 were monitored with a zero probability of collision in the wireless channel. As a result, the network throughput should be less than the maximum throughput shown in Figure 6.11 when more nodes join the network and compete for the wireless channel. Therefore we deployed the protocol within a more realistic scenario to produce Figure 6.12, where a certain number of nodes formed a fully connected topology. All nodes will transmit packet to a central device, which can be understood as the sink device or the cluster head. The packet arrive rate in each node has been configured to a fixed rate of 60 pps (48 kbps). Obviously, each newly joined node will increase the offered traffic load for the whole network and increase the collision probability. In the results shown

in Figure 6.12, the delivered throughput of the IEEE 802.15.4 MAC increased until the network exceeded 3 nodes and achieved a maximum throughput of 72.3 kbps. After this point, due to the increasing collision probability, the network throughput started to decrease with increasing network size. If we deployed the proposed *AS-MAC* protocol within the same network scenario, as expected, the *AS-MAC* was able to support a higher offered traffic load, not peaking until the network reached 6 nodes. At this point, the *AS-MAC* delivered a throughput of 173.3 kbps which is a 139.7% improvement over the standard IEEE802.15.4 MAC. Furthermore, if the results are compared with the capacity without collisions as shown in Figure 6.11, it is seen that the standard IEEE 802.15.4 can only achieve 61.3% of the capacity while *AS-MAC* is able to achieve higher ratio of 84.8%, which means the proposed *AS-MAC* can utilise the wireless channel in a more efficient way.



Figure 6.13. Two flow topology. Node 1 and 3 are exposed terminals

We have also examined the protocol performance in a multi-hop scenario. We first investigated the typical exposed terminal topologies consisting of two flows. In the topology shown in Figure 6.13, node 1 and node 3 were transmitters and deployed within each other's transmission range. It should be noted that all devices in this experiment have been equipped with a 20dB attenuator to decrease the transmission range to simplify the experiment setup without loss of any accuracy. Therefore, through careful calibration node 0 has been deployed out of the effect range of node 3, i.e. node 0 cannot sense or receive any packet from 3. Following the same principle, node 2 has been deployed out of the effect range of node 1.

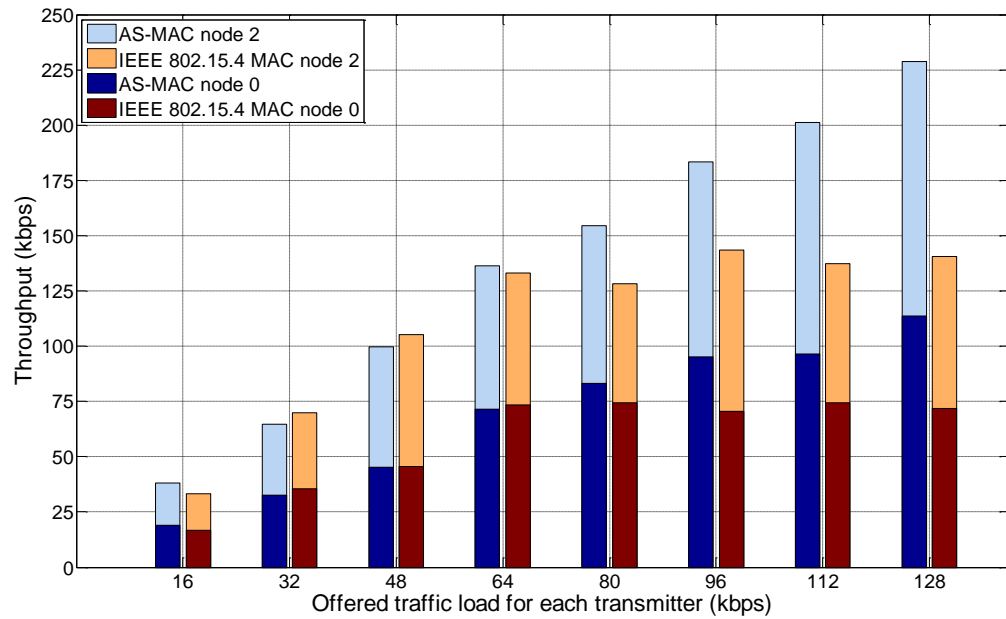


Figure 6.14. Throughputs in exposed terminal scenario

As shown in Figure 6.14, when the offered traffic load increases at both transmitters, the successfully delivered throughputs of flow 1->0 and flow 3->2 increase as well. However, due to the capacity of protocol, the IEEE802.15.4 MAC was saturated when the data arrival rate is 80 pps (64 kbps). After this point, the delivered throughput cannot maintain the offered traffic load and remains at a constant level. As a comparison, the AS-MAC can steadily increase until 160 pps (128 kbps), therefore increasing the total network throughput by 60.7%. It should be noted that the total network throughput cannot go beyond the maximum throughput of a single flow in an ideal channel. However, in the experiment, the false channel sense assessment may enable the exposed terminals to transmit concurrently, slightly increasing the total system throughput delivered.



Figure 6.15. Two flow topology. Node 3 is the hidden terminal of node 0

We now deploy the experiment with the topology shown in Figure 6.15, aiming to evaluate the throughput performance in the hidden terminal scenario. Similarly to the topology shown in Figure 6.13, both 1->0 and 3->2 flows have been deployed with great enough link margin to achieve

maximum throughput, while node 3 and 1 have been deployed out of the range of each other to replicate the hidden terminal scenario. In the standard IEEE 802.15.4 MAC, the carrier sensing scheme in node 1 may fail to detect the hidden terminal activity of node 3, as a result the node 1 could access the channel with the false result and increase the collision probability in the channel. Therefore, the delivered throughput shows an unfair pattern in Figure 6.16 for the IEEE 802.15.4 MAC, i.e. the throughput of Node 0 has been limited to a relatively low value with respect to the total system throughput. As discussed in section 6.2, the introduction of a competition check in the *AS-MAC* is able to aid Node 3 to successfully avoid the interruption of the transmission in link 1->0 by monitoring actions occurring in link 0->1. Therefore, as shown in Figure 6.16, the system throughput can achieve an almost fair throughput performance among both flows, while the overall system throughput is also higher than standard IEEE 802.15.4 MAC because of the high data rate achieved by the shorter spreading code length nodes.

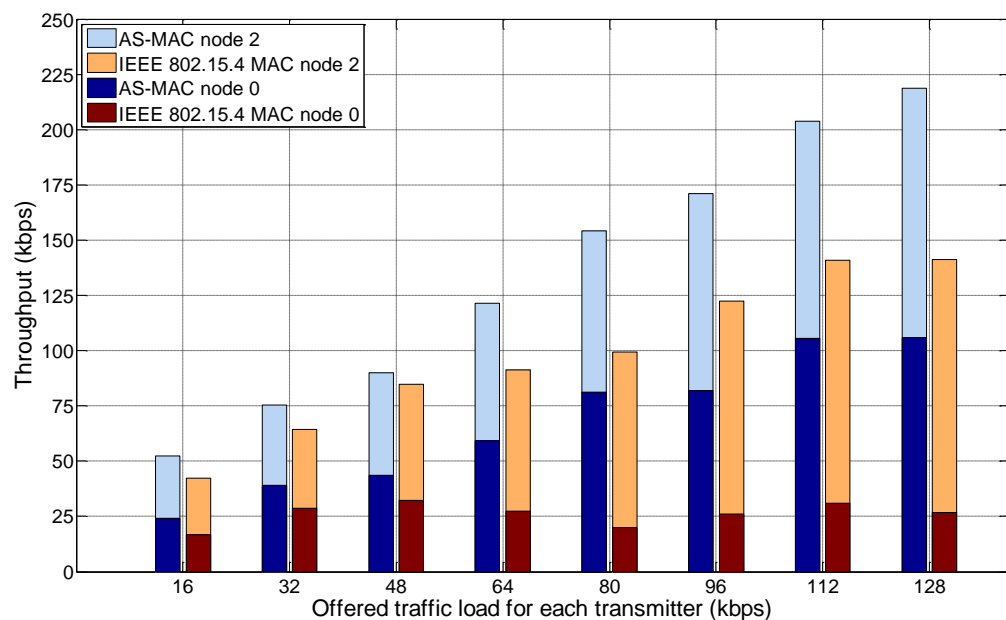
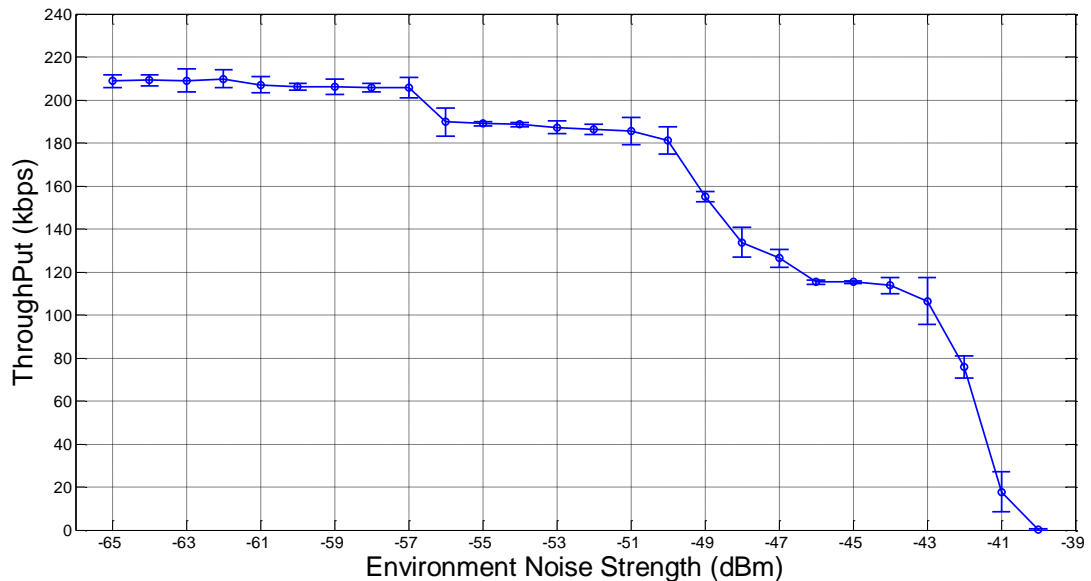


Figure 6.16. Throughputs in the hidden terminal scenario

### 6.3.2 Throughput performance with variable environment noise

To evaluate the performance of the *AS-MAC* under the condition of channel noise, a vector signal generator ESG4432B has been employed to

generate environment noise. The ESG4432B has been equipped with a 2.4GHz 0dBi antenna to feed noise directly into the wireless channel.



**Figure 6.17. Throughput performance of AS-MAC with variable environment noise**

Similarly, we first evaluated the performance of single transmission flow with variable environment noise strengths. The transmitter has been configured with a fixed packet arrival rate 260 pps (208 kbps), which is almost the saturated state. The strength of environment noise is adjusted and the number of received packets at the receiver side recorded to calculate the throughput. The results are provided in Figure 6.17. The delivered throughput remains at its highest level of around 204 kbps until the environment noise exceeds -57dBm. It is assumed that before this point, the SNR was high enough for the transmission pair to work with the shortest spreading code length mode which can lead to the highest datarate. Consequently, when the environment noise was higher than -57dBm, the Kalman filter could learn this change in the environment and signal the AS-MAC to switch to the next spreading code length. This caused the degradation of the delivered throughput to around 185 kbps. However, the third spreading mode was relatively hard to track in Figure 6.17, since the SNR region for this mode is only 1dB (around -48dBm). Then, it is easy to notice the standard spreading mode of IEEE802.15.4 around 118 kbps from -46dBm to -43dBm. Beyond this point, although the system can still determine the decrease of the SNR margin, the system was fixed in this mode until the

throughput trends to zero since there are no other modes for lower SNR margins. According to the motivation behind this protocol design, the experiment successfully demonstrates the ability of the protocol to be cognitive to the environment change and adjust itself to the best operating mode to maintain a reliable transmission link.

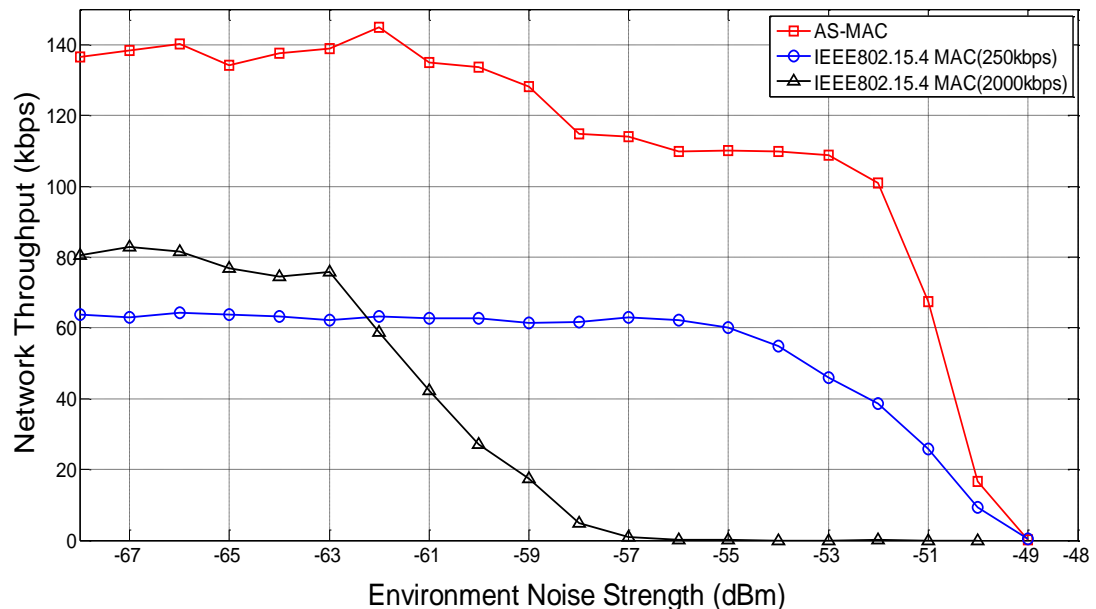


Figure 6.18. Throughput performance of AS-MAC with environment noise under star topology

We now evaluate the performance under environment noise in the more general star topology. The configuration of this experiment was almost the same as the previous experiment except the network consisted with three nodes with a packet arrival rate of 60 pps (48 kbps). Since there are three links in total deployed in different locations, the link status will change in an uncorrelated fashion among nodes. Therefore, the combination of delivered throughputs shown in Figure 6.18 is slightly different to the result shown in Figure 6.17. The overall deliverable throughput has been kept around 140kbps when the environment noise is lower than -62dBm. Then along with the increasing of environment noise to -58dBm, the delivered throughput decrease slowly to 110 kbps. In the last stage, the throughput is going to decrease rapidly toward zero, when the environment noise is higher than -53dBm. Generally, although the cognitive process of the *AS-MAC* is not as clear as the single device experiment, the system still shows the adaptively along with the changing environment noise, while the standard

IEEE 802.15.4 MAC has kept a relatively lower throughput around 60 kbps just before reducing to zero. As a comparison, we also implemented another protocol which maintains the standard IEEE 802.15.4 MAC, except that the datarate has been forced to the highest rate. The result of this mode is shown as the black curve in Figure 6.18. It demonstrates that without a carefully designed protocol, simply increasing the datarate cannot deliver consistently higher throughput.

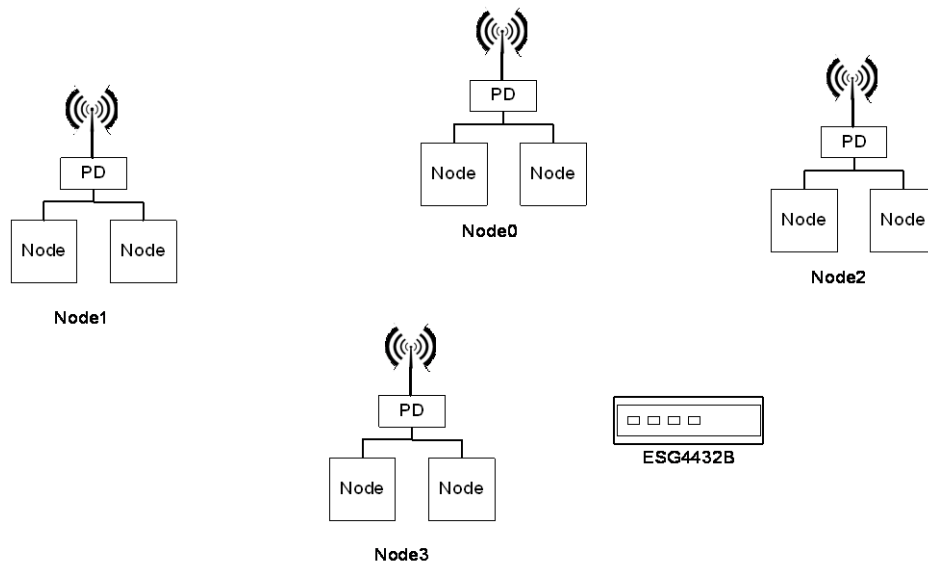


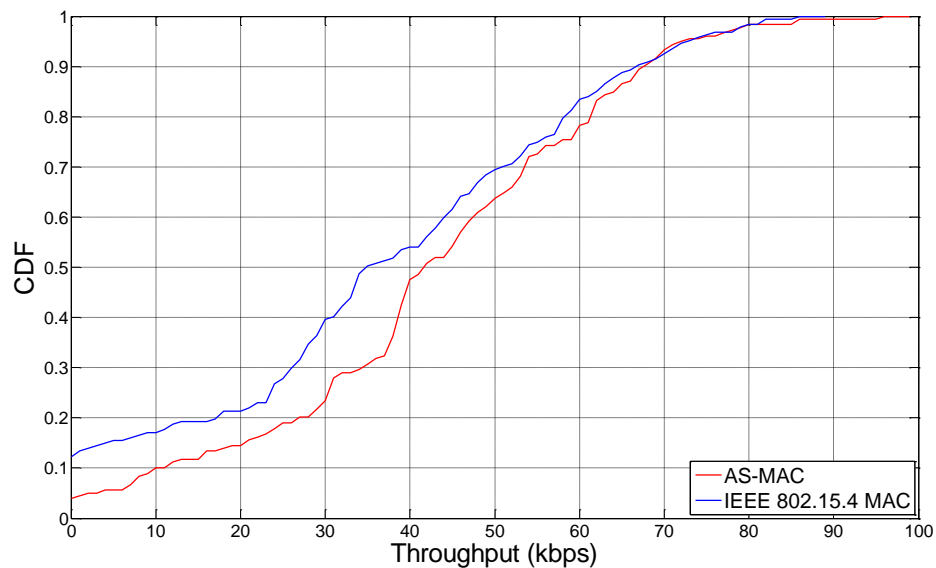
Figure 6.19. Experiment setup for protocol comparison with variable environment noise



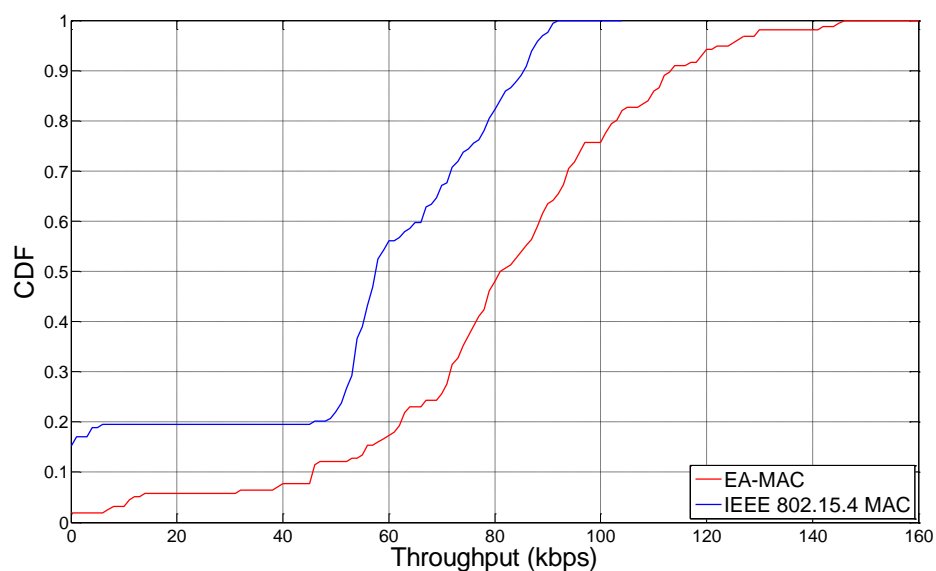
Figure 6.20. Experiment photo for protocol comparison with variable environment noise

The performance of the multi-flow scenario with environment noise was evaluated, as shown in Figure 6.19 and Figure 6.20. Devices configured for the AS-MAC and IEEE802.15.4 MAC have been deployed together,

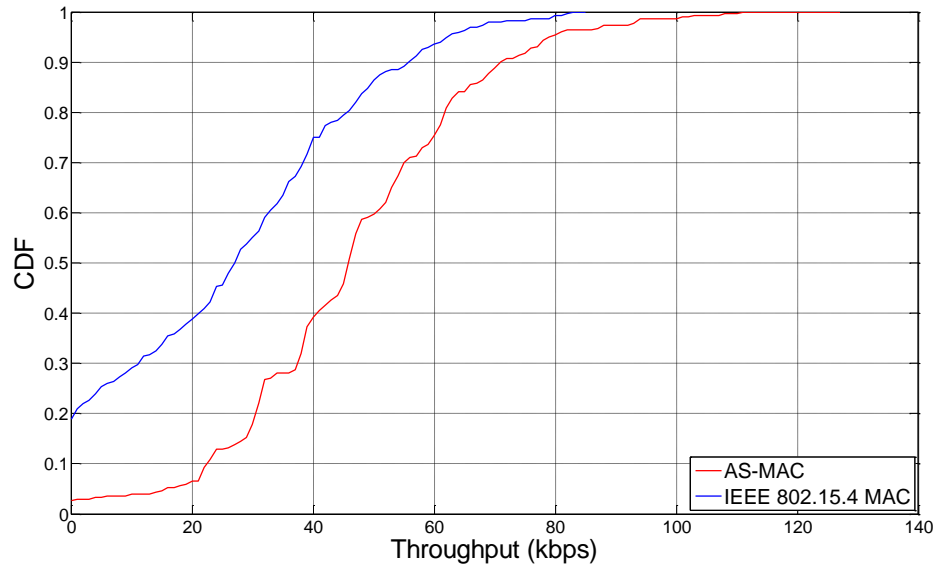
connected via a 2.4GHz Power Combiner/Divider to a single antenna to ensure that each pair of devices posed with an identical wireless channel (with a 3dB degradation in transmit power due to the Combiner/Divider). The two nodes have been configured with the same ID but working in different RF channels. Consequently, the ESG4432B has been configured to generate an environment noise covering both channels.



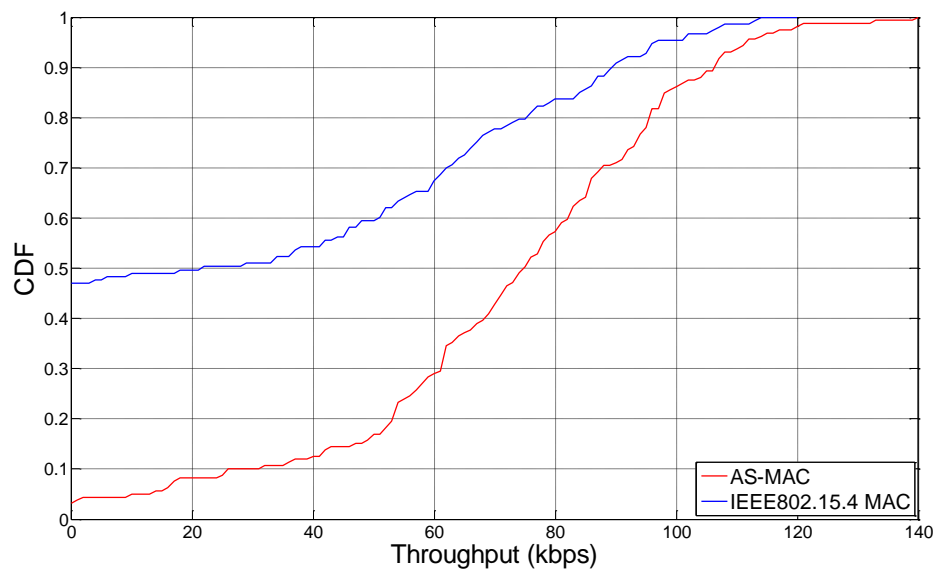
(a) packet arrival rate = 60 pps, spreading length = 32



(b) packet arrival rate = 120 pps, spreading length = 32



(c) packet arrival rate = 60 pps, spreading length = 4



(d) packet arrival rate = 120 pps, spreading length = 4

**Figure 6.21. Throughput performance with environment noise in the multi-flow scenario**

A series of experiments have been implemented with this setup. Each of them was carried out with different MAC configurations, i.e. the offer traffic load and spreading code lengths. During each experiment, the strength of the environment noise was slowly adjusted from low to high and then reversed with the process being repeated for several times. The receivers recorded and calculated the Cumulative Distribution Function (CDF) of the delivered throughput, which has been presented in Figure 6.21. It should be

noted that since these experiments will involve manual manipulation of the experimental set-up (e.g. the physical process of connecting nodes to allow the uploading of new programmes may cause small movements of the devices location), we are unable to guarantee that the experiment conditions are exactly same for each of the four experiments. However, within each experiment the condition has be exactly the same for the two implemented protocols.

When the offered traffic load was low, i.e. 60 pps packet arrival rate, as the experiment result in Figure 6.21 (a) shows, the delivered throughputs of *AS-MAC* and IEEE802.15.4 MAC show almost the same performance. However, when higher traffic load exists, as high as 120 pps shown in Figure 6.21 (b), the *AS-MAC* can achieve higher throughput than the standard IEEE802.15.4 MAC. In the result shown in Figure 6.21 (c) and (d), we compared the *AS-MAC* with the standard IEEE 802.15.4 MAC with the shortest spreading code length. We see that this protocol can achieve higher throughput than the standard protocol but is still not able to deliver the throughput of the *AS-MAC*. This demonstrates that simply increasing the datarate could, in some circumstances expose the transmission link to a degraded link quality.

### 6.3.3 Energy efficiency

In this section, we will show the energy efficiency performance of the proposed *AS-MAC*. As discussed in previous sections, the *AS-MAC* should be able to achieve better energy efficiency by reducing the transmit time. To demonstrate this, a NI DAQ card (PCI 6209 with sample rate 10 kHz) has been employed to capture the current draw of the device during different operations. The integration of the recorded current allow us to derive the overall energy consumed by device in that period, which is one of the most accurate ways to evaluate the energy efficiency of different MAC protocols.

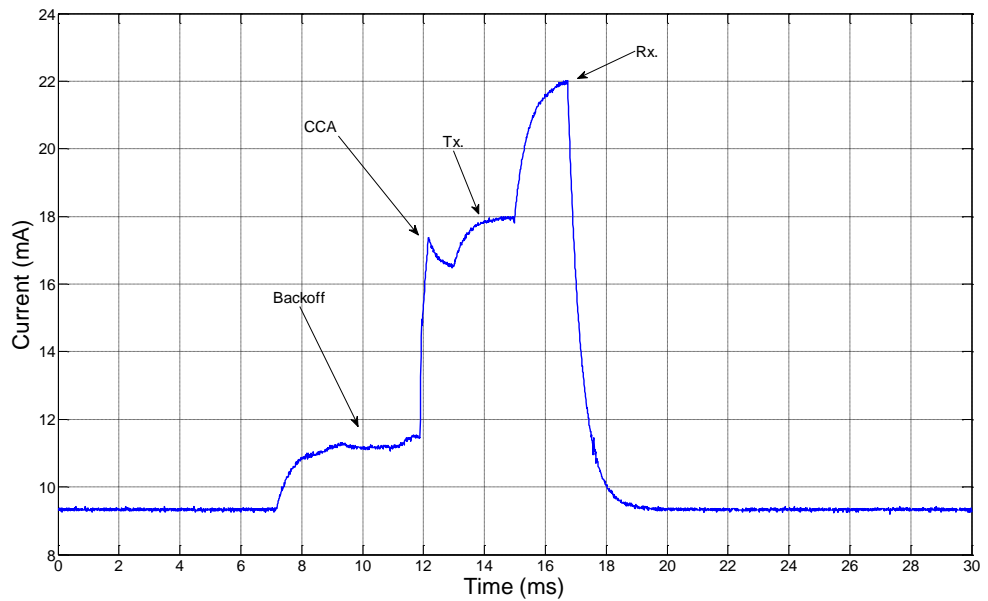


Figure 6.22. Power consumption of IEEE802.15.4 MAC

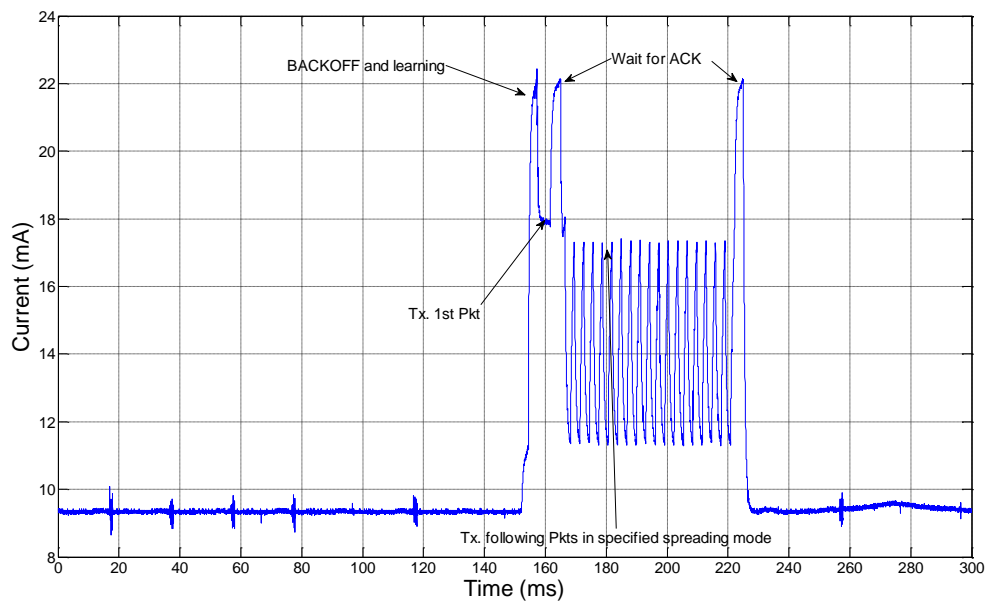


Figure 6.23. Power consumption of AS-MAC

Figure 6.22 and Figure 6.23 show the current consumption of IEEE 802.15.4 MAC and AS-MAC respectively. The devices we employed for experiment are equipped with capacitors to filter noise on the power lines which also leads to a low-pass filtering effect in the current monitoring system, i.e. a gradual transition between states. However, it should be noted that this effect will not degrade the accuracy of the analysis of energy

efficiency. For the IEEE 802.15.4 MAC, we show the current drawn during the transmission of one packet: the device first enters the BACKOFF state for a random period, and then switch to the CCA state. If the CCA returns with a free channel event, the device will send the packet and then enter the RX state waiting for the ACK packet. Instead of one packet, we will show the power consumption of a block of packets for the AS-MAC which is more common in this protocol. As discussed in previous sections, the system also first enters the BACKOFF state, the different is the AS-MAC will enable receiving during its time in the BACKOFF state to gain as much as the channel information as possible, e.g. the exchange of packets. After the BACKOFF state, the MAC uses the information learned and historical data to decide whether the device can start the transmission. If it decides that the channel is free, the device will send the first packet in the block as a probe packet. The receiver will then calculate the optimised spreading mode and reply with the ACK containing the optimisation result. After receiving this ACK, the transmitter will send out the subsequent packets in the block with the optimised spreading code length. Then the transmitter will wait for the final ACK to report whether there have been any packets lost in this operation and arrange the retransmission if any.

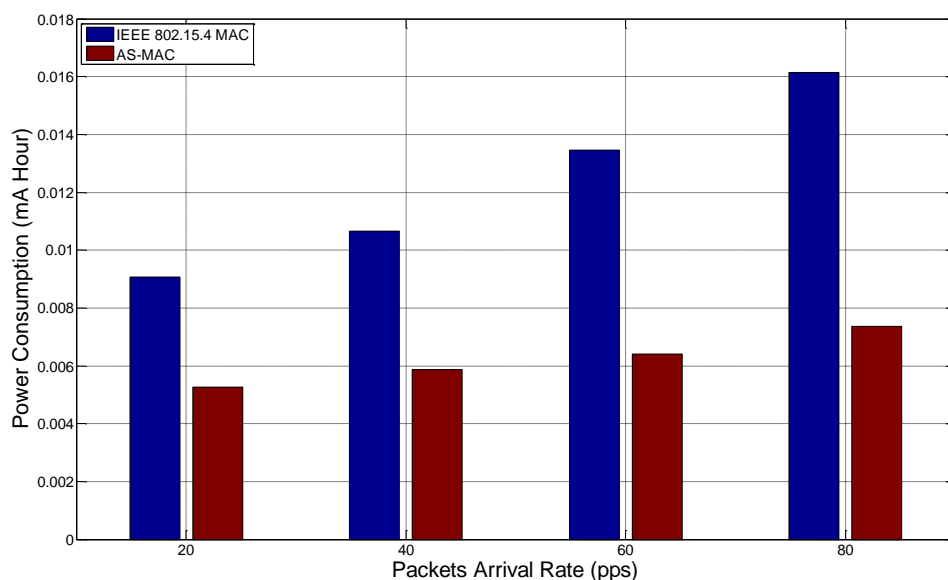


Figure 6.24. Power consumption with increased packets arrival rate for 10 min

Following the other experimental results analysed in this section, we first evaluated the power consumption for a single transmission link. The offered traffic load has been increased from 20 pps to 80 pps, with each experiment lasting 10 minutes to record an average value of power consumption. As shown in Figure 6.24, as the offered traffic load increases, the power consumption of the standard IEEE 802.15.4 MAC increases rapidly. As a comparison, the power consumption of *AS-MAC* increases much more slowly. For instance, when the packet arrival rate is 80 pps, the *AS-MAC* can save 54.3% of the energy used by the IEEE 802.15.4 MAC.

**Table 6.2 Power Consumption for 1 hour in extremely low traffic load,  
Block\_Size = 1 and packet arrival rate = 1 pps.**

	IEEE802.15.4 MAC	AS-MAC
Power Consumption (mA Hour)	0.0197	0.0202

In section 6.2, we claimed that the *AS-MAC* should be compatible with the traditional applications, i.e. the system offers extremely low traffic load (for example, 1 pps). Therefore, we evaluated the energy performance in this scenario, through the configuration of Block\_Size = 1 and packets arrival rate of 1 pps. The experiment lasted one hour for both protocols, and the two protocols show almost the same performance as shown in Table 6.2: *AS-MAC* consumed 0.0202 mAh, only slightly higher than the 0.0197 mAh of IEEE 802.15.4 MAC. If both systems were equipped with a standard 2000 mAh battery, the system with IEEE 802.15.4 MAC can last 11.75 years, while the system with *AS-MAC* can last 11.45 years. The additional power is consumed by the increase in energy used in the BACKOFF state. However, due to the extremely low offered traffic load, the probability of channel contention has been limited as well. Therefore, the energy consumed by the BACKOFF state can be regulated to an affordable level as we discussed in section 6.2.

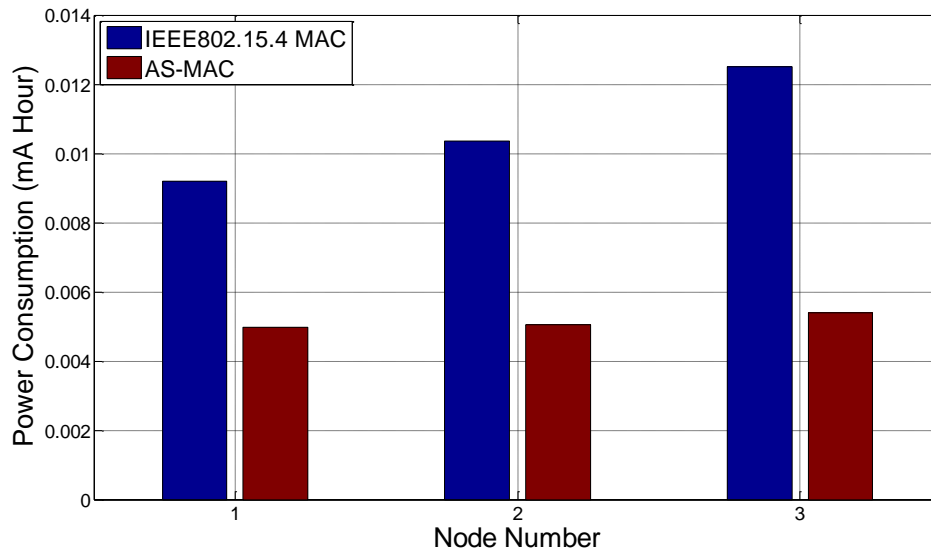


Figure 6.25. Power consumption with increased node number, 20 pps for 10 min

Then now evaluate the energy efficiency of the proposed *AS-MAC* in a general star topology. Due to the experimental limitations<sup>18</sup>, we only recorded the power consumption for only a small number of devices. To compensate, we increase the packet arrival rate to increase the offered traffic load in the network, which will cause competition and collisions. Also it is believed the trend of power consumption will scale with the node number. In the results shown in Figure 6.25, both systems were offered a traffic load of 20pps. In this scenario, the IEEE 802.15.4 MAC consumed more energy when the competition probability was increased due to the scaling of the network size. As a comparison, the energy consumed by *AS-MAC* can be kept at almost the same level. For example, the *AS-MAC* only consumed 43% of the energy consumed by IEEE802.15.4 MAC when the network size was 3. This demonstrates that the *AS-MAC* has better energy efficiency as well as ability to handle increased competition in the network.

To further validate this hypothesis, the offered traffic loads have been increased to 80 pps in the experiment shown in Figure 6.26. Because of the heavy offered traffic load, the competition probability also increased to a higher level, and therefore the *AS-MAC* consumed more energy in the BACKOFF state. However, if we recall the results shown in Figure 6.12, we

<sup>18</sup> We used a 8-channel ADC card, and 8 devices for the experiment. However, two of them are acting as the sink node, which means only three pairs of nodes can be monitored in these experiments.

can conclude that *AS-MAC* can trade this increase in energy usage for a better channel utilisation which guarantees the delivered throughput in a high competition scenario. Even in this condition, *AS-MAC* still shows better energy efficiency than the IEEE 802.15.4 MAC, i.e. *AS-MAC* consumed only 84.7% of IEEE 802.15.4 MAC when the network size was 3.

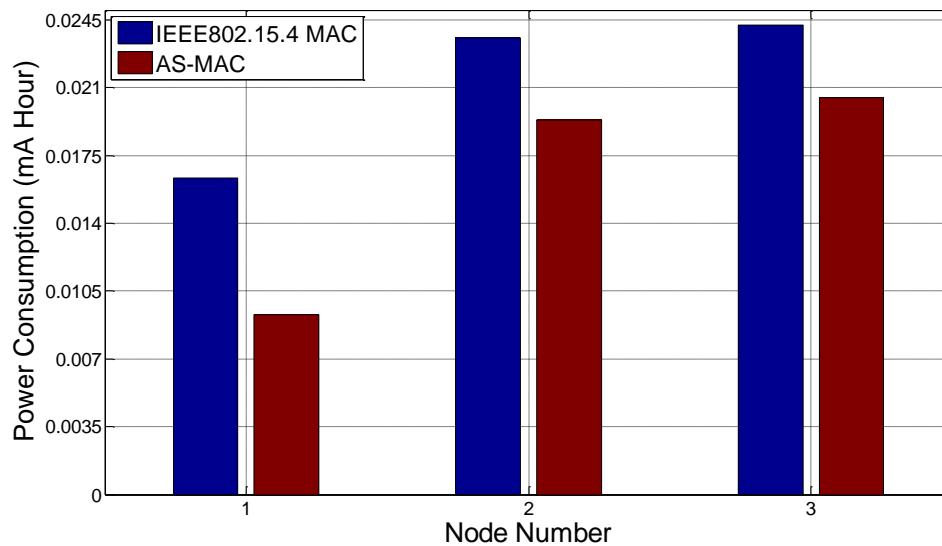


Figure 6.26. Power consumption with increased node number, 80 pps for 10 min

## 6.4 Conclusion

The proposed protocol jointly considers the signal strength, environment noise and competitors in the network to calculate the optimised spreading mode for the wireless sensor network. Our experimental results show that, in ordinary scenarios the *AS-MAC* can use less than half the energy to deliver more than double the throughput.

The advantages of proposed *AS-MAC* can be summarised as follows:

- The protocol will be able to deliver 139% higher throughput as well as save more than half of the power consumption for the standard IEEE 802.15.4 system.
- The protocol is robust to harsh RF environments by adapting the spreading code length to match the available link quality.
- The protocol is backwards compatible, e.g. it offers support for both extremely low duty cycle and data intensive scenarios.

- The implementation of the protocol is very low cost within resource constrained nodes.

Despite these benefits, the system based on the *AS-MAC* will also be able to provide multi-constraint QoS for the WSN systems which have different QoS requirements for different tasks running within one network. For instance, the MAC will report the current link capacity to the route layer, thus, the route protocol could assign links with higher capacity to packets with higher priority. Since the link capacity will be adapted from time to time, the routing protocols will need to be able to self-learning. The investigation of compatible routing protocol will be a possible direction for future work.

## Chapter 7. Utilising the battery recovery effect in WSN with high traffic load applications

### 7.1 Introduction

Many applications of wireless sensor networks require batteries as energy source for the sensors. However, the small form factors of devices often prohibit the use of large and long lasting batteries. Also, the ad-hoc deployment of sensor networks and the inconvenience of sensor collection usually constrain frequent replacements of batteries. Hence, the design of energy saving algorithms and protocols has become a crucial topic in WSNs. There are a variety of energy optimisation studies in the literature that mostly consider batteries as ideal energy reservoirs, from which energy can be drained at a constant discharging voltage, and can be halted and resumed at anytime to regain the same voltage. However, most commercial batteries are governed by complex non-linear internal chemical reactions to provide energy. Such chemical reactions are known by chemical engineers to be dependent on a variety of environmental factors and operational parameters (e.g. discharge duration, discharge current, memory of past discharge profiles).

Particularly, there is a subtle phenomenon named *battery recovery effect*, which refers to the process whereby the active chemical substances in a battery will replenish themselves if left idling for a sufficient period of time, and hence, the deliverable energy of a battery can, to some extent, be recharged. Thus, we are motivated to exploit battery recovery effect as a viable approach of energy optimisation for sensor networks. Even in the early age of WSN, battery recovery effect had already been reported [116]. As we discussed in the chapter 2, in the traditional working pattern of WSN, the duty cycle is pretty low, e.g. less than 1%. Therefore, the battery effect can be automatically maximised without any specify design. However, as the application requirement changes in advanced sensor network applications,

the offered traffic load could be much heavier and the work pattern be much more complex, i.e. bursts of data in vibration and ECG monitoring systems. Thus, we have to examine the effect of battery recovery and design an algorithm to benefit from the battery recovery gain in the high traffic load sensor applications.

There are several immediate questions. First, is the battery recovery effect sufficiently significant to extend battery runtime? Second, if so, is there a simple but effective approach to take advantage of battery recovery effect in sensor networks? Third, does such an approach affect the performance of sensor networks and if so, how will the induced performance (e.g. latency of data delivery) be affected?

To address these questions, we first empirically examine the gain in battery lifetime due to the battery recovery effect, through extensive test-bed experiments on COTS sensors platforms. Since radio transceivers consume a significant proportion of the available energy (even in listening mode), as compared to processing and sensing activities, we focus on measuring the battery lifetime in the presence of duty cycled radio operations. We found that there is a gain of up to 25% ~ 45% of the normalised battery lifetime between cycled and continuous radio operations. Moreover, we empirically study some key characteristics of the battery recovery effect with respect to different duty cycle schedules. We observe that there exists a saturation threshold, beyond which an increased idle time will have little contribution to battery recovery. The immediate ramification to sensor networking is that if we carefully adjust the sleep time period of device before reaching the saturation threshold, the system may benefit from the battery recovery effect without exacerbating the latency of data delivery. Through simulation in a large scale multi-hop network, we demonstrated such possibility, which shows the network life time can be increased by 20% by using the battery recovery aware design. This suggests that a system may be able to maximise such benefits by an adaptive duty cycle algorithm, which would be discussed in our future work.

## 7.2 Experiment demonstration of battery recovery effect in WSN platforms

In this section, we present the experimental results from our sensor network test-bed to show the significance of the battery recovery effect. These experiments were carried out on two types of commercial sensors from Crossbow: TelosB and Imote2. Both are popular models for wireless sensor networking. The TelosB consists of an MSP430 MCU and a CC2420 radio transceiver. The Imote2 consists of a PXA271 CPU and a CC2420 radio transceiver. The TelosB allows more energy-saving settings with low energy consumption, whereas Imote2 is equipped with more computation ability and therefore higher energy consumption. We mainly studied the effectiveness of battery recovery effect on the TelosB nodes.

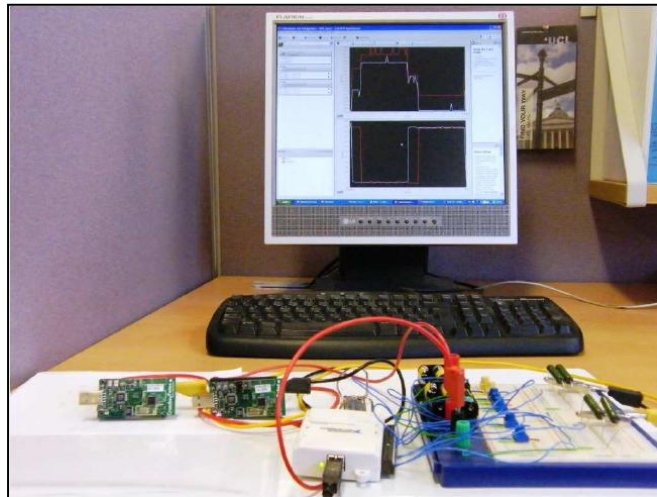


Figure 7.1. The experiment setup of battery recovery effect

In the experiments, we use an analogue-to-digital conversion (ADC) interface card and LabVIEW software to measure and record the discharge profiles of a pair of communicating sensors (see Figure 7.1). Each sensor is powered by standard AAA NiMH 600 mAh batteries (TelosB has two and Imote2 has three). When the supply voltage of the battery is lower than a certain threshold (called the stop voltage), the device can no longer operate, which is considered as completely discharged. We set different duty cycle rates on the sensors by putting the radio transceiver in active and sleep modes periodically and measuring the induced battery runtime. The duty cycle rate is defined as the fraction of the active time period.

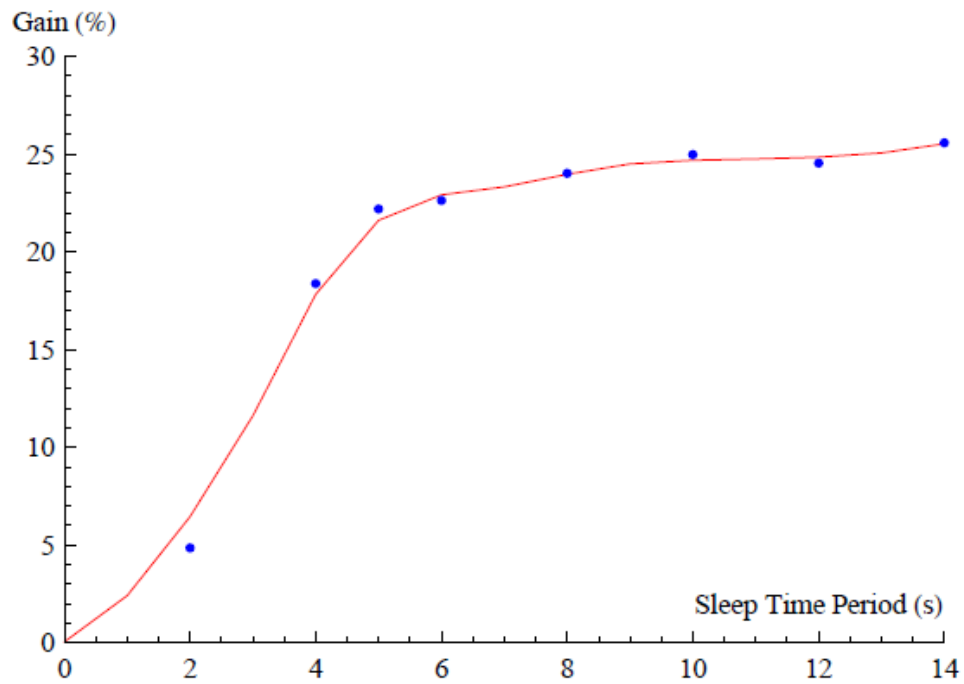


Figure 7.2. The normalised lifetime gain with constant active time

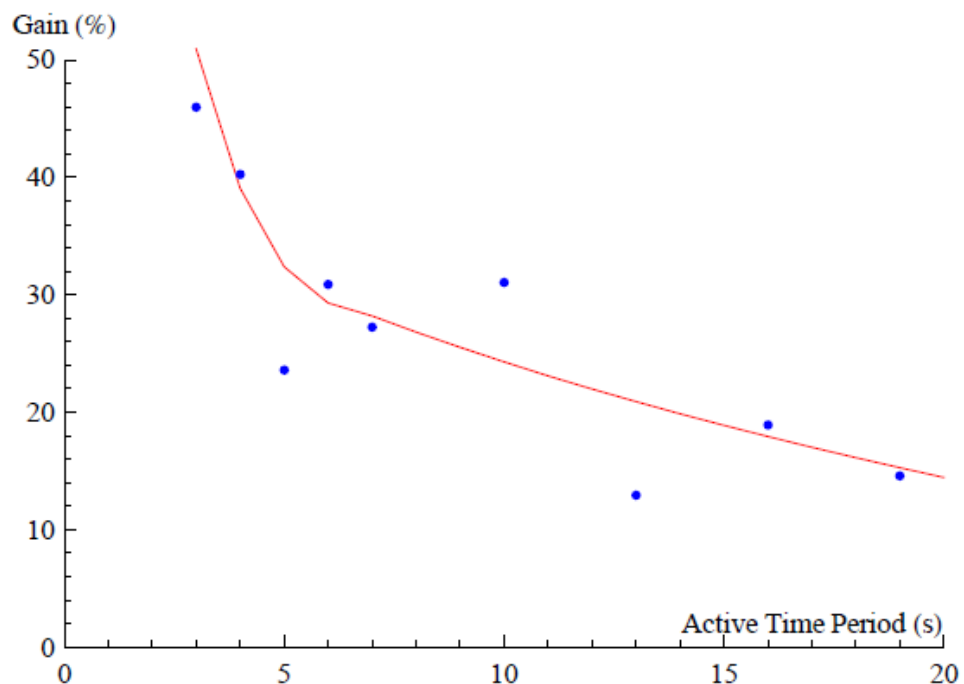


Figure 7.3. The normalised lifetime gain with constant sleep time

The result presented in Figure 7.2 has been obtained from an experiment using the TelosB platform. The devices have been set with a 10 seconds fixed active period, while the length of sleep period has been adjusted from 0 to 14 seconds. The *normalised gain* was obtained by first multiplying the measured system lifetime with the duty cycle rate, and then compared with the continuous radio operation (i.e. always on). Along with the

prolonged sleep time, the deliverable energy increases rapidly until the sleep time is equal to 5 seconds. After this point, although the lifetime gain is still increasing, the trend is much slower. The lifetime gain with 5 seconds sleep time is around 22.3%, while the lifetime gain with 14 seconds sleep time is just 25%.

Similarly, we show the performance for the TelosB with a constant sleep time (5 seconds) and variable active time from 3 seconds to 19 seconds in Figure 7.3. The lifetime gain decreases rapidly with increased active time, again with the trend slowing after 6 seconds of active time. The performance of the Imote2 platform has been shown in Figure 7.4. Although the power consumptions and experiment configurations for Imote2 are quite different to those of the TelosB platform, a very similar trend to Figure 7.2 can be found in Figure 7.4.

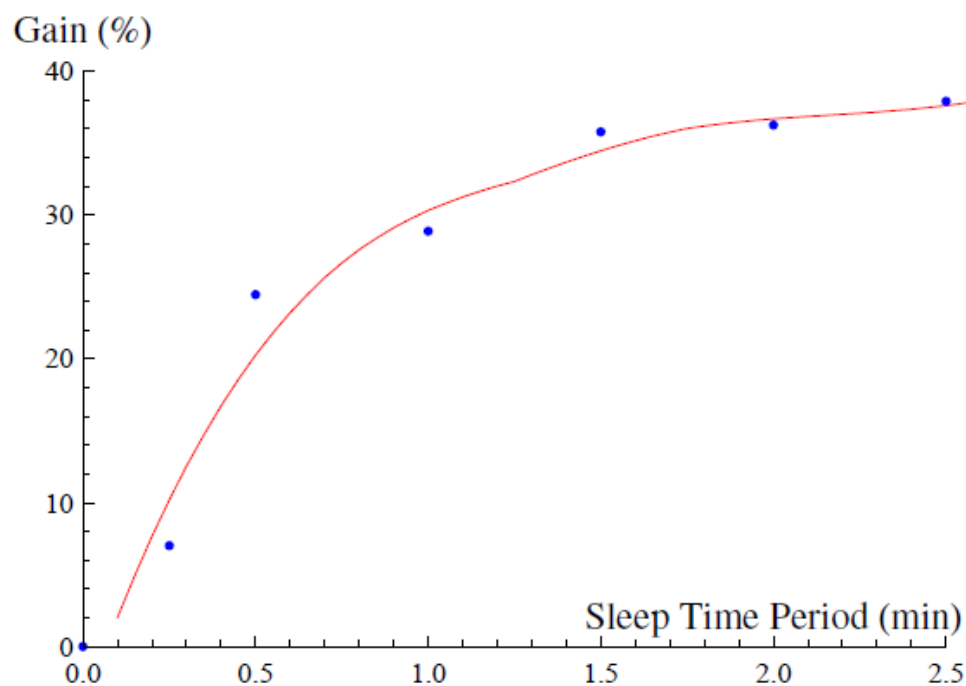


Figure 7.4. The normalised lifetime gain of Imote2 with constant active time

There are a number of key observations from the experiments:

- 1) There are clear signs of battery recovery effect. With the same active time period, a longer sleep time period induces a longer normalised battery runtime and hence a larger deliverable energy from the battery.

2) The effect of the sleep time period is non-linear. It appears that sleep time periods greater than a certain threshold will contribute much less to battery recovery, which we call a *saturation threshold*.

3) The effect of the active time period is also non-linear. Very small active time periods appear to cause a large gain in normalised battery runtime (up to 45% in TelosB).

4) Even if the sensor is in sleep mode on the radio transceiver, there is still energy consumption due to the timer and other processing activities. The TelosB consumes 6.1  $\mu\text{A}$  in sleep mode, whereas Imote2 consumes 0.38mA. We observe that battery recovery can take place under low battery consumption, and the impact of background consumption is not substantial to battery recovery.

Note that the actual battery runtime is much longer than the normalised battery runtime (which is multiplied by the duty cycle rate). Hence, duty cycle schedules not only prolong the network lifetime by placing the node in a sleep mode, but also increase the deliverable energy by allowing battery recovery.

Although our measurement of the gains due to the battery recovery may differ in other environmental settings (e.g. different temperature, different battery type), the insights revealed by our experiments will still be useful to the modelling and optimisation of battery recovery in sensor networks. In general, under a duty cycled discharge profile, a battery is able to recover charge during idle time periods, which effectively increases the deliverable energy of the battery. However, the effectiveness of battery recovery is critically determined by the active and sleep time periods. The presence of a saturation threshold appears universal in different duty cycle schedules. We envisage that one can evaluate the saturation threshold (in some intervals) for certain environments in *a priori* manner through experiments.

### 7.3 Lifetime and latency trade-off in large scale sensor network

Due to the effects witness previously, we are motivated to design networking protocols to exploit battery recovery by taking the estimated saturation threshold as a parameter. In multi-hop sensor networks, duty cycles are always employed to regulate the transceiver, i.e. in sleep mode the radio is off, while in active mode the radio is on for all operations. This can reduce unnecessary energy consumption and harness battery recovery. As a result, it is possible to design an algorithm which can maximise the battery recovery effect by adjusting the duty cycle pattern. In this section, we will present the analysis of the proposed algorithm and examine its performance in large scale multi-hop scenarios.

#### 7.3.1 Introduction of the simplified battery model

Our experiments corroborated the presence of battery recovery effect and saturation threshold. It is useful to employ a simple model to capture these essential characteristics qualitatively, which enables further analysis and larger scale simulation on various battery consumption patterns. Hence, combining the previous well accepted battery model described in [117;118] and the analysis of experimental results, a simplified battery model has been presented [119]. The state of a battery is characterised by a tuple  $\langle n, c, t \rangle$ , where  $n, c$  are non-negative integers.  $n$  is the theoretical capacity determined by the amount of chemicals in the electrode and electrolyte.  $c$  is the nominal capacity determined by the amount of available active chemicals for chemical reactions in the battery.  $t$  is the number of idle slots (time is discretised as slots here) since the last discharging. The use of  $\langle n, c \rangle$  follows the previous definition in [117;118], while the introduction of  $t$  is first presented in this model and related to the saturation threshold.

In the discharging process, both  $n$  and  $c$  are decreasing. The amount of available active chemicals constrains the energy a battery can deliver, despite the presence of unused chemicals in the battery. Thus, we require  $n \leq c$ , but when the battery stops discharging, there is a recovery process, as a diffusion process between electrode and electrolyte to replenish available active chemicals, effectively increasing  $n$ , which, however, cannot increase

beyond the theoretical capacity  $c$ . There is a saturation threshold  $t_{sat}$  for  $t$ , such that more consecutive idle slots  $t > t_{sat}$  will not contribute additional recovery. Here, the units of  $n$  and  $c$  have been normalised, at each idle slot,  $n$  can be recovered by only one unit. More detail discussion about this model can be found in [119].

### 7.3.2 Battery recovery awareness design in large scale WSN

In a multi-hop sensor network, we rely on the simulation implemented in OMNet++ to study the network performance. We implemented the simple discrete battery model discussed in section 7.3.1 for each sensor. We assumed that the data arrival rates of all sensors follow an independent Poisson distribution. The transmission will follow the block transmission protocol discussed in Chapter 6, except, we assumed the wireless channel in this simulation is ideal, without any environmental noise.

Without the battery recovery awareness design, in the synchronised wake up time slot, the transmission pair will attempt to send all the packets in the buffer queue through one hand-shake process. To extend this scheme by considering the battery recovery effect, we propose a simple scheme of forced sleep. This scheme is a two-folder action applied in both the transmitting operation and receiving operation. The first step is simple: suppose the receiver determined from the probe link after the rate optimisation that current operation could be active for more than  $B_{max}$  busy slots, then the ACK packet will be sent back to notify the transmitter to send only  $N_{max}$  packets in this block. In the second step, the device, either as a transmitter or receiver, will check the active time slot at the end of each block transmission. The active time can be contributed by one large block or several small blocks in different roles. If a device has been active for more than  $B_{max}$  consecutive slots before the current slot, then it must go to sleep for the next  $S_{buf}$  slots for some  $S_{buf} \leq t_{sat}$ . This allows sufficient battery recovery to improve the deliverable energy of a battery. After  $S_{buf}$  slots, the device will resume normal active schedule.

Inevitably, this scheme will decrease the deliverable throughput and increase the latency while increasing the network lifetime by utilising the

battery recovery effect. However, if we carefully chose the sleep time periods within the saturation threshold, we can maximise battery recovery without exacerbating the latency of data delivery. Parameters will be adjusted in the simulation to investigate the impact of battery recovery aware design on network performance, for instance, throughput, latency and energy efficiency. By simulation, we will compare the network lifetime of battery-aware schemes with the normal operation which has the best throughput and latency performance. To demonstrate the effectiveness, we select some typical parameters, i.e.  $t_{slot}=100\text{ms}$ ,  $c = 2500$  and  $n = 1000$ .

### 7.3.3 Analysis of simulation results

We first demonstrate the performance of the proposed battery aware algorithm in a single transmission pair. The offered traffic load in the network has been steadily increased from 2 pps to 26 pps. The network has been configured in three modes: without battery aware mode, battery aware model with  $B_{max}=5$ , and battery aware model  $B_{max}=3$ .  $S_{buf}$  has been set to be equal with  $t_{sat} : 1$ . As shown in Figure 7.5, the proposed battery aware algorithm is sufficient to deliver similar traffic load as the non-aware system in all situations. Now, we will analyse the energy efficiency and latency performance.

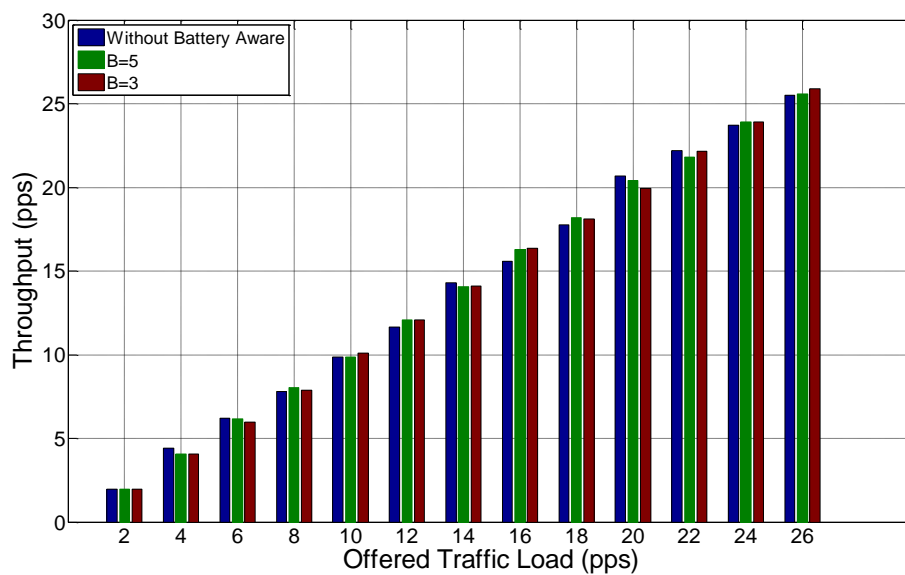
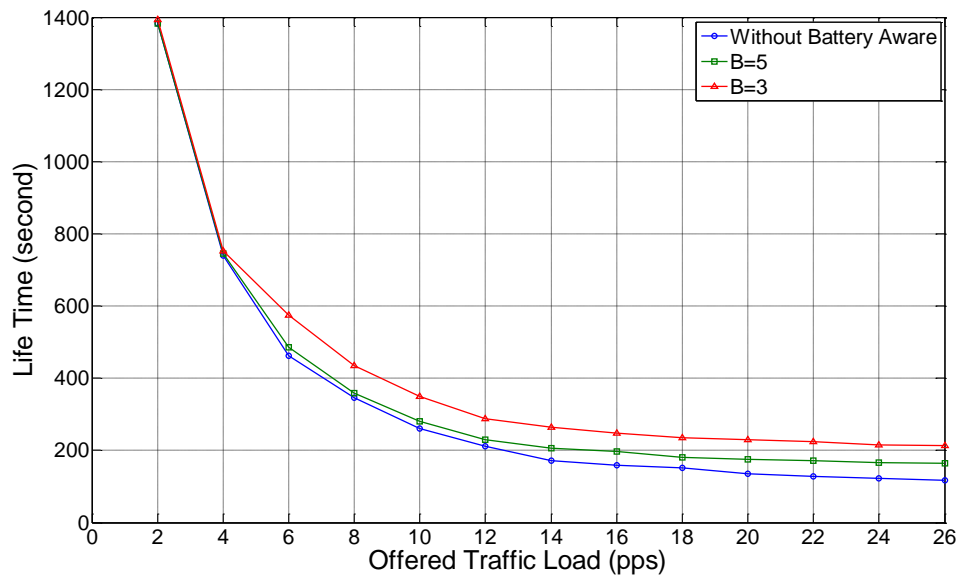


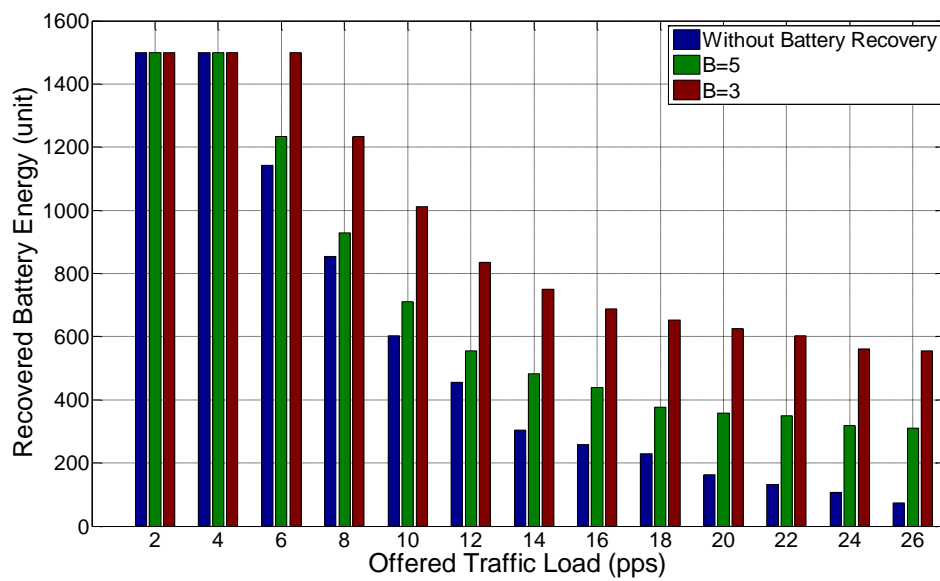
Figure 7.5. Throughput performance of single transmission pair

The lifetimes of the network with different configurations have been illustrated in Figure 7.6.a, while the recovered battery energies have been provided in Figure 7.6.b. With low offered traffic load, all three systems can automatically maximise the battery recovery effect, which can be demonstrated by the fact that performance is almost the same with 2 and 4 pps. As the offered traffic load increases, the system lifetimes show different trends. The lifetime of system without battery recovery aware design decreases rapidly. Without battery recovery aware algorithm, the recovered energy only contributes when there are no packets waiting to be sent. The probability of this situation will trend to zero with increasing offered traffic load. However, if the system is configured to be battery recovery aware, the system will be forced into sleep when it has been working for more than  $B_{max}$  time slots. Therefore, even with heavy traffic loads, the system can still benefit from the battery recovery effect. It is clear that the recovered energy will tend to a constant bound rather than zero.

It can also be seen that performance will be dependent on the setting of the  $B_{max}$ , i.e. a shorter  $B_{max}$  will provide better energy efficiency. For example, when the offered traffic load is 26 pps, the system with  $B_{max} = 3$  recovered 556 units of energy and increased system lifetime by 214 seconds (82% gain, compare with the system without battery recovery aware). With the same traffic load, the system with  $B_{max} = 5$  is only able to recover 164 units of energy resulting in a 40% extension of the lifetime.



(a). Lifetime of the system



(b). Recovered battery energy

Figure 7.6. Energy performance of the battery recovery aware algorithm

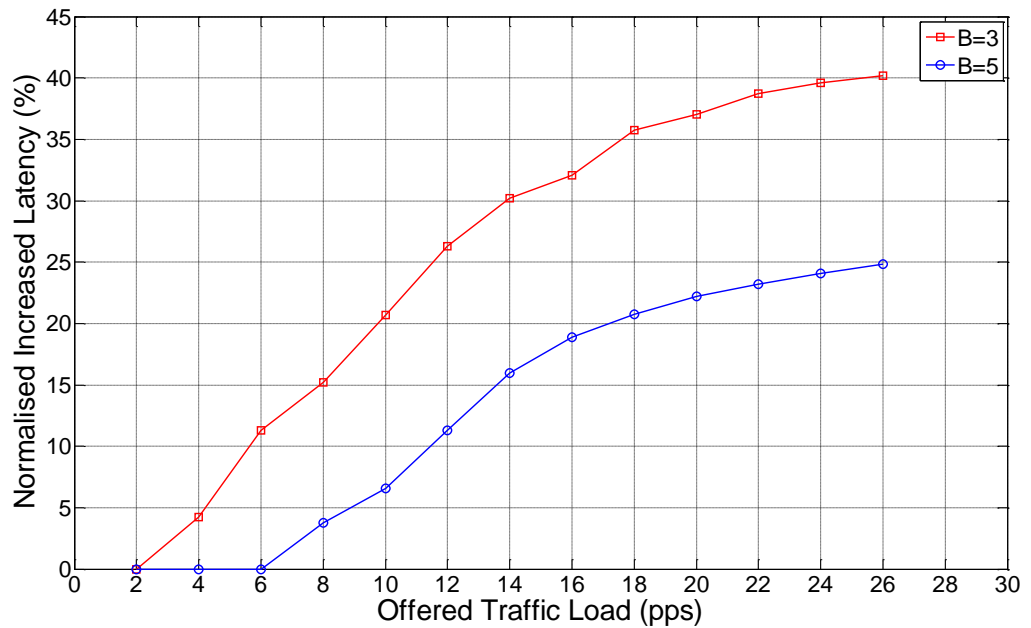


Figure 7.7. Latency performance of the battery recovery aware algorithm

However, it is very important to note that a shorter  $B_{max}$  time not only contributes to the increased deliverable energy but also increased packet delivery latency, which has been illustrated in Figure 7.7. The packet delivery latency here has been normalised to a ratio comparing with the system without battery recovery aware design. Similarly, when the offered traffic load is low, the system latencies are almost equal to the traditional system. After that, the packet delivery latencies will both increase with different speeds and bounds, with a shorter  $B_{max}$  bringing a higher latency. This phenomenon is easy to understand: the more frequent the system is forced to sleep, the more time the packet will have to wait. However, this increase in latency does show an exponential characteristic, converging to a constant value. In conclusion, the battery recovery aware algorithm with  $B_{max} = 3$  trades 40% increase latency with 82% lifetime gain, while the  $B_{max} = 5$  mode trades 26% latency with 40% lifetime.

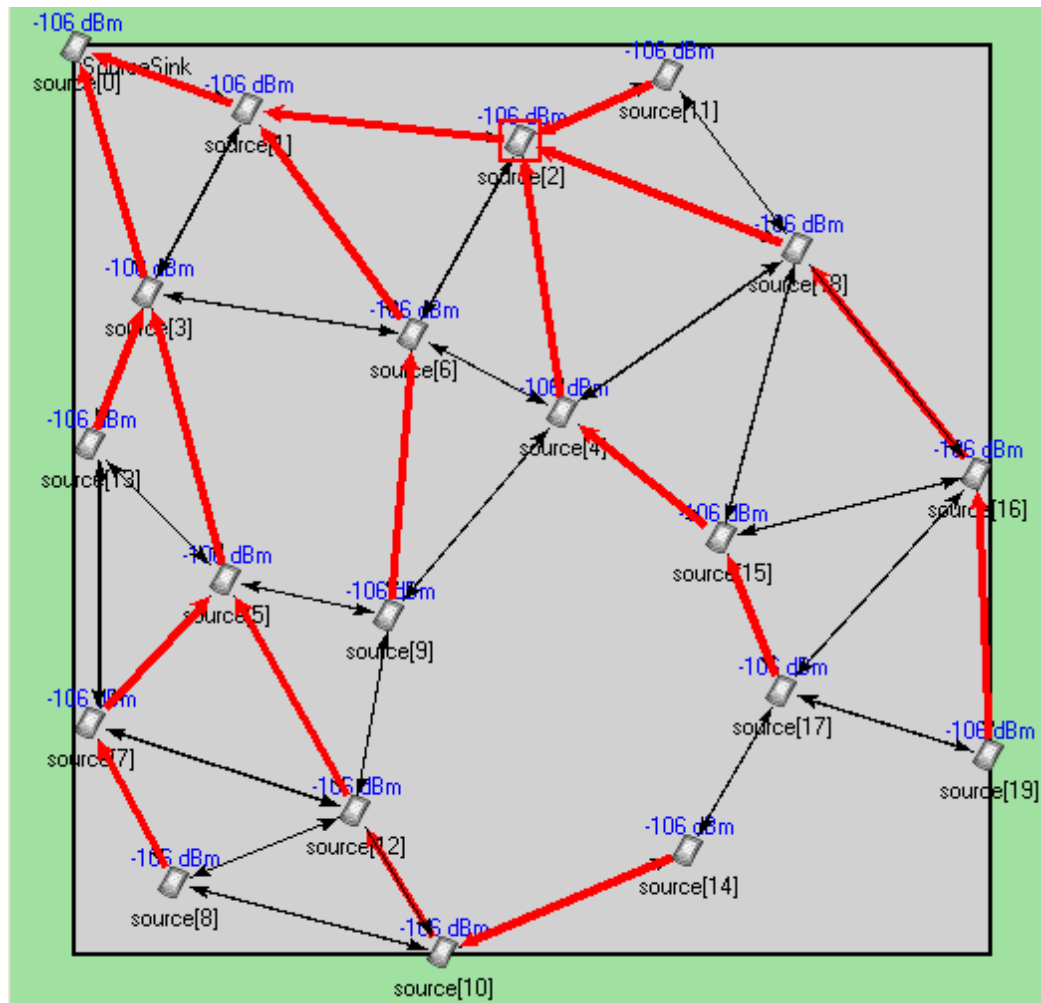
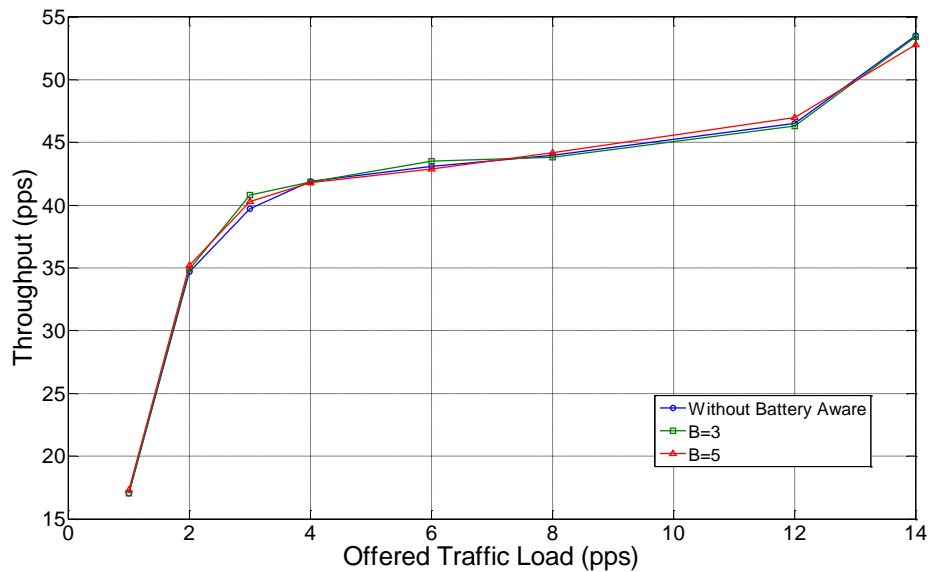


Figure 7.8. Network topology of the multi-hop simulations

We now extend the network into a multi-hop topology and demonstrate the network performance in such scenario. As shown in Figure 7.8, 20 devices have been randomly generated and located in the network. It should be noted that all the connections in the topology figure are only indications of the pre-fixed route; the actual packet transmissions will follow the propagation mode discussed in Chapter 5, which considers pathloss and slow fading effects. To create a more realistic simulation environment, we implemented accumulative interference in this simulation. For example, although the signal transmitted by device 1 cannot be demodulated by device 16 in the tail of the topology, the signal still has an effect on device 16. Clearly, the accumulation of this kind of interferences will cause a decrease of SINR in devices. All the PER calculations and power consumption are sourced from the experimental results discussed in Chapter 4.



**Figure 7.9. Throughput performance of multi-hop scenario**

As shown in Figure 7.9, the system is still able to deliver almost identical throughput with and without battery recovery aware design in the multi-hop scenarios. In other words, the forced sleep scheme does not have a significant effect on the deliverable throughput, which is believed to be limited by the congestion and pre-fixed route. Beyond this, it worth noting that the successfully delivered throughput is around 17 packets per second when the offered traffic load is 1pps per node (i.e. 20 packets will be generated in the whole network per second). Therefore, the system is already close to saturation in certain routes even with the traffic load as low as 1pps.

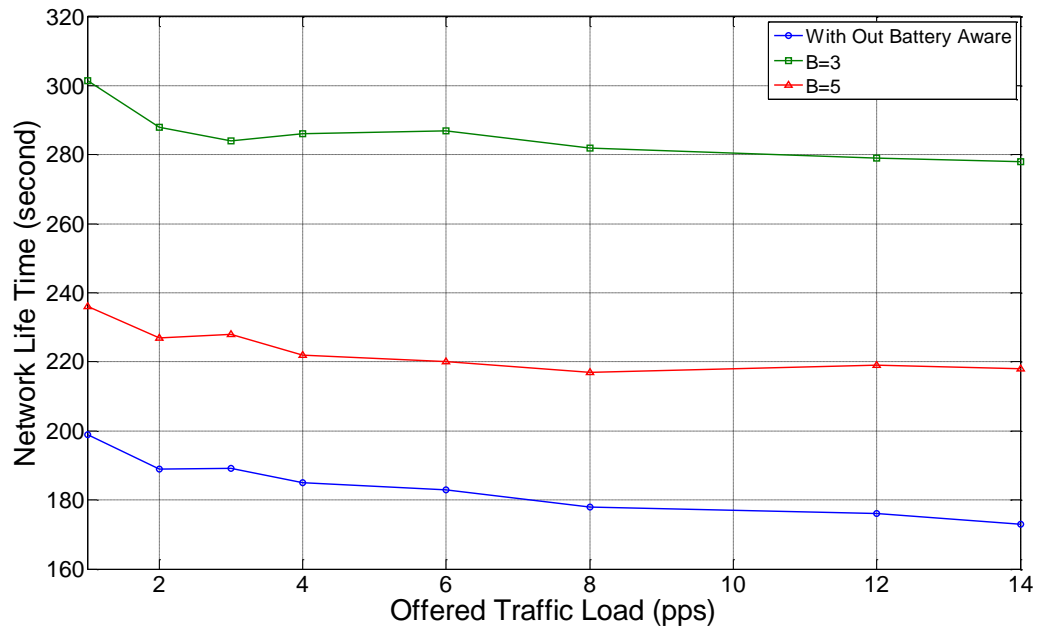


Figure 7.10. Lifetime performance of multi-hop scenario

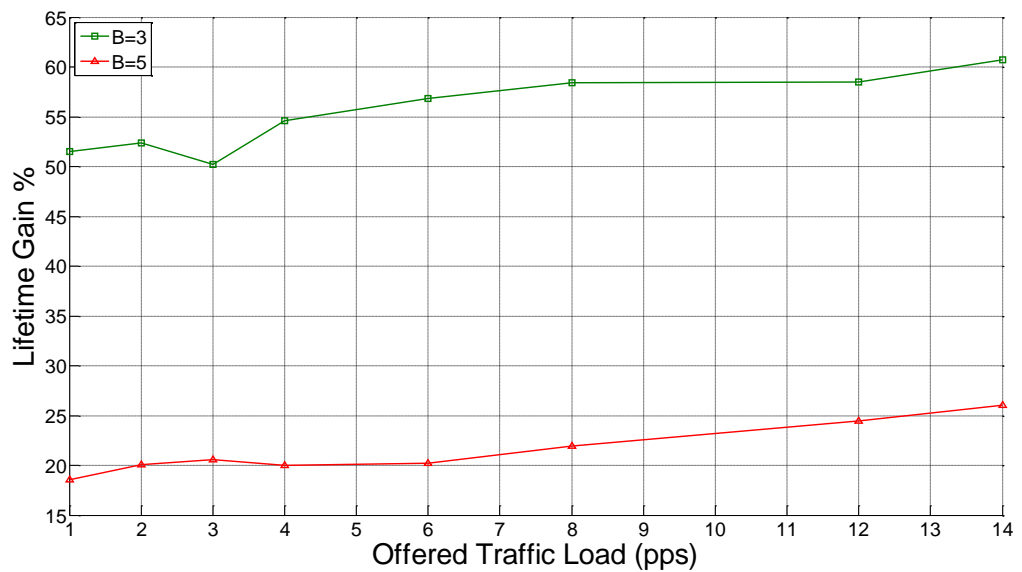


Figure 7.11. Normalised lifetime gain of multi-hop scenario

Figure 7.10 demonstrates the performance of system lifetime. As already stated the system is almost saturated even with 1pps traffic load, the lifetime performance only show moderate change. For the normal system without battery recovery aware algorithm, when the offered traffic load increased from 1pps to 14pps, the lifetime decreased from 200 seconds to around 178 seconds. Similarly the simulation results with  $B_{max} = 3$  and  $B_{max} =$

5 are decreased from 300 seconds to 278 seconds, and 236 seconds to 218 seconds respectively. The recorded results have been further processed to generate the lifetime gain for different  $B_{max}$ , which have been provided in Figure 7.11. Clearly, the battery recovery aware algorithm does increase the system lifetime significantly. Due the congestion problem, the effective traffic load will not increase rapidly with the increased packet generation rate. Therefore, unlike the single transmission pair, the system will not show a steady increase in the lifetime gain, instead the lifetime gain increased from 51% to 60% for  $B_{max} = 3$  and 18% to 26% for  $B_{max} = 5$ .

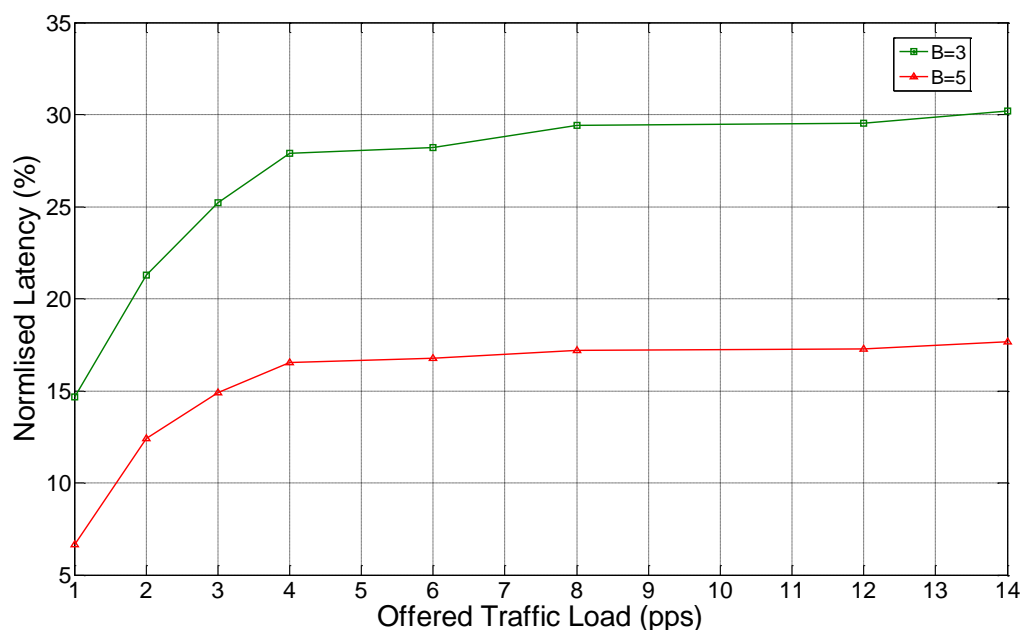


Figure 7.12. Normalised latency of multi-hop scenario

The normalised, per hop packet latencies have been illustrated in Figure 7.12, which are calculated from the end to end packet latency and averaged by the number of passed hops. Similar to the single transmission pair scenario, the multi-hop scenario also gains from the trade off between the network lifetime and the packet latency. When  $B_{max} = 3$ , the system trades a 30.9% increase in packet latency with a 60.6% increase in lifetime. When  $B_{max} = 5$ , the system trades 18.8% increase in packet latency with 26% increase in lifetime.

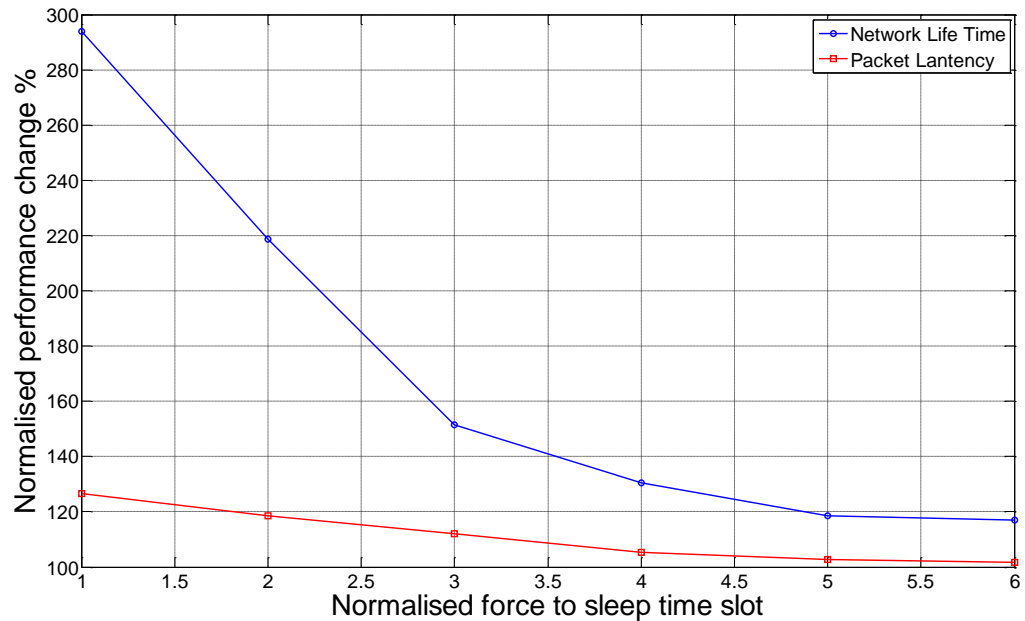


Figure 7.13. Performance change with varied  $B_{max}$

We are now motivated to examine how this profit changes with different  $B_{max}$  configurations, which have been demonstrated in Figure 7.13. In this simulation, the offered traffic load has been fixed to 1pps for each device, then the force to sleep time slot  $B_{max}$  has been adjusted from 1 to 6. The lifetime and latency have been recorded and compared with the standard system performance without the battery recovery aware algorithm. The comparison of these results is shown in Figure 7.13. This information provides the following hints. Firstly, a generic optimised may not exist but will only be determined by the system requirements. The lifetime gain is scalable with the delivery latency, i.e. higher lifetime gain comes with higher latency. Secondly, if we define the ratio between the lifetime and the latency as the profit ratio, then the profit ratio increases with decreasing force to sleep time, i.e.  $B_{max} = 1$  has the best profit ratio in the tested scenarios. However, this configuration also means the largest packet delivery latency. Finally, the implementation of the battery recovery aware algorithm should consider the maximum tolerable packet delivery latency according to the QoS requirements of the application layer. Based on that, the system can calculate the optimised duty cycles to achieve the best profit ratio without exceed the QoS requirement.

## 7.4 Conclusion

WSN systems usually rely on the duty cycle (i.e. active and sleep pattern) to prolong the network lifetime. In traditional applications, due to the low traffic load, systems are usually configured with very long sleep periods, where the systems achieve excellent energy performance. Such energy efficiency is contributed by two factors: firstly, the system only consumes energy for short active periods during the whole life time; and secondly, in the long sleep period, the battery recovery effect has been fully utilised automatically. However, this has also resulted in a failure to consider battery recovery effects. In WSN applications with high traffic load, the system is usually configured to deliver a large number of packets with specific QoS requirements and long active periods while still having high energy efficiency expectations. We were then motivated to consider whether it is possible to divide the long active period into several small duty cycles to utilise the battery recovery effect.

In this chapter, through a series of experiments, we first demonstrate the existence of the battery recovery effect. Moreover, we found that appropriate duty cycle schedules may increase the deliverable energy of a battery without significantly increasing the latency of data delivery. This is particularly useful to sensor network systems with energy and latency constraints in WSN applications with high traffic load. The simulation results for a multi-hop network scenario show that if we carefully set the duty cycle, the battery recovery effect can be utilised while guaranteeing acceptable packet delivery latency even with heavy traffic loads.

The analytical results in this chapter provide an insight into the battery recovery effect and demonstrate the possibility to utilise this effect for the WSN applications with high traffic loads. The network can significantly benefit from the battery recovery effect by carefully setting the duty cycle ratio, but the duty cycle ratio should be configured according to the traffic load and QoS requirement. Therefore, in the future work, the designer may consider an online adaptive duty cycle algorithm to maximise this effect, e.g. the device should consider the local traffic load (both generated and

forwarded), and the QoS of this traffic load to set its duty cycle ratio dynamically.

## Chapter 8. Conclusion and Future Work

### 8.1 Conclusion

Recently, there has been growing interest in and demand for modern WSN applications with high traffic loads, including structure health monitoring systems, multimedia surveillance systems, health care systems and intelligent manufacturing systems. We first analysed the system characters of these applications, which shown that the wireless system are generally expected to deliver intensive throughput in harsh RF environments in these scenarios. Most of the previous studies in the WSN area focused on traditional applications and are optimised for extremely low traffic loads with almost ideal RF environments for indoor or remote scenarios. As a result, the newly posed challenges are usually beyond the ability of traditional WSN technologies (represented by the IEEE802.15.4 standard and Berkeley 'Mica' Mote platform). Therefore, a new architecture of WSN system has been proposed in this thesis aiming to improve the performance in advanced scenarios while keeping compatibility with the essential energy efficiency, low cost and distributed nature of sensor networks.

Many applications of wireless sensor networks require batteries as energy source for the sensors. However, the small form factors of devices often prohibit the use of large, long-lasting batteries, which means that energy efficiency is always a crucial topic in WSNs. As addressed by many researchers, energy can be saved by using a very low sleep-active duty cycle. However, it can be shown that traditional architectures make very inefficient use of energy when devices wake up in the active period. Typically, WSN devices have to listen for some time before accessing the network, which is termed as the channel contention stage. Traditional WSN architecture employed a simplified random access scheme, which works fine with extremely low traffic loads. However, it was noticed that the network performance drops rapidly with intensive traffic load, as false channel busy assessment and collision probabilities significantly increase. As a result, devices have to wait longer to access the channel. In fact, most energy and

time are consumed in the channel contention period not, as is widely believed, in the transmission period. It was also noticed that typically packets are transmitted at a fixed data-rate often much above the required SNR margin in the traditional WSN architecture. Since the wireless channel is time varying, even harsh industrial environments can support higher data-rates most of the time. Therefore, the fixed modulation is rather an inefficient scheme to utilise the wireless channel.

In chapter 3, we argued that the efficiency of the channel contention stage can be increased by introducing the multi-carrier approach. To be compatible with the distributed scalability, the wireless system should be able to allocate and utilise the sub-carriers independently. However, the well documented CFO problem acts as a barrier to this feature in the multi-user scenarios. Therefore, we have analytically examined the cause of the CFO problem and presented a low cost mitigation solution for WSNs. An emulation based experiment has been implemented to validate the proposed solution showing that the error performance is acceptable when the CFO is within  $\pm \frac{1}{4}dF$ . The problem of high PAPR caused by multi-carrier architectures is well known and typically requires high quality RF front ends to avoid signal distortion. However, as only a small number of carriers have been employed, the experiment results demonstrated that the PAPR has only been slightly increased. Therefore, the proposed architecture can still work with the low-cost front-ends typical of sensor systems, since most of the modifications have been limited in the digital processing part.

An analytic model has been used to evaluate the MAC performance of WSNs with such a multi-carrier based architecture. The result of which was shown to compare well with the simulation results. The most significant benefit of this scheme is the superior energy efficiency, due to the efficient channel contention process, which reduces backoff times, collisions, and retransmissions. Secondly, due to the reduced channel contention period, the proposed multi-carrier scheme can deliver a higher throughput under intensive traffic loads. These performance improvements are the results of the significantly increased efficiency of the contention period.

In chapters 4 to 6, we implemented and analysed a novel system utilising adaptive spreading code length for opportunistic high data-rate transmission, which is expected to increase the efficiency of channel utilisation. This solution was proposed to improve throughput as well as provide reliable service within harsh RF environments. To utilise this feature, there is a need for an optimisation algorithm that can accurately detect the channel quality as well as estimate the current channel capacity. Although analytic models exist to estimate performance in fading channels, their complexity is typically too high for a low cost WSN platform. Therefore, we are motivated to propose a simpler way to estimate the system capacity to accurately enable the selection of the appropriate spreading mode.

The study first examined the error performance of variable spreading lengths before proposing an analytic error performance model for an AWGN channel. An emulated experiment was employed to validate the accuracy of the proposed model. A series of experiments were then conducted with a standard IEEE802.15.4 MAC protocol but different spreading modes deployed to demonstrate the potential throughput and power consumption advantages. The experiment results demonstrate the possibility to utilise adaptive spreading code length to increase the network performance during the packet transmission stage.

We then proposed a new channel indicator in chapter 5, which will work closely of the analytic model proposed in chapter 4 to inform the optimisation algorithm with the potential link capacity. This indicator has been named Effective-SNR, defined as the required SNR value to achieve the same error performance as in an AWGN channel. The indicator is based on a two layer Kalman filter to take advantage of the redundancy between the standard channel indicators: SNR and LQI. Due to the nature of the Kalman filter, the system also showed good performance against measurement noise and successfully tracked varying channel quality. The error residue shows that proposed scheme achieves 160% better accuracy comparing with the raw SNR and 120% comparing with instantaneous LQI.

Finally, in chapter 6 we combined these two innovations and designed a MAC protocol capably of fully utilising the new indicator and adaptive

spreading codes. The design of this protocol has considered both the requirements of traditional WSN application and WSN applications with high traffic load. Under low traffic load the system operation is very similar to the standard IEEE 802.15.4 system. However, once the system detected increased traffic load, the system can automatically enable the adaptive spreading code length mode to opportunistically utilise channel conditions to deliver packets as efficiently as possible. The protocol has been implemented in a COTS platform with the experimental results demonstrating a significant performance increase, in detail more than 200% of the deliverable throughput than IEEE 802.15.4 system, as well as save more than 50% of the power consumption.

In chapter 7, we presented an investigation of the battery recovery effect. This is a natural effect of chemical batteries, previously ignored in the WSN area as the extremely long duty cycles typical of traditional WSNs automatically utilise this feature. However, in heavy offered traffic load, a carefully designed algorithm can be employed to take advantage of this effect without decreasing performances, especially the latency of packet delivery. A series of experiments have been implemented to demonstrate the potential increase of more than 25% deliverable energy when the battery recovery effect is utilised. Then we try to demonstrate that by carefully design the duty cycle parameters, the large scale network can benefit from the battery recovery effect. The simulation results shown that the system can increase the network lifetime by more than half without exacerbating the latency of data delivery.

## 8.2 Suggestion for Future Works

In this thesis, we have proposed an improved architecture for WSN applications with high traffic load. Due to equipment limitations, we have to investigate the performance of different aspects separately. An obvious next stage would be to implement an integrated prototype with all the features proposed and demonstrate its performance in network scenarios. Designing an ASIC based wireless transceiver could be both costly and lack flexibility. Such a solution is not affordable for academic research purpose. Therefore,

we plan to seek help from the Software Define Radio (SDR) platform to implement the integrated prototype. The GNU radio, unlike the previous SDR platforms, does not require any knowledge of FPGA or DSP programming. The hardware of GNU radio is only responsible for the front end processing and the down-converted baseband signal will be transmitted back to the computer via USB for the signal processing. Therefore, the complex digital signal processing algorithms can be implemented in the computer using standard C++ within an open source framework, which maximises the flexibility of the transceiver design and testing.

The integrated system is expected to have high flexibility in the allocation of both channel bandwidth and spreading code length. As described in Chapter 2, unlike the traditional WSN applications, modern, advanced applications usually consist of various tasks with differing QoS requirements. Therefore, we suggest that our proposed architecture may be able to deliver differential QoS by utilising flexibility in bandwidth assignment and adaptive spreading coding length. We understand that an optimisation can usually only be achieved with information from the whole network. Therefore, the corresponding algorithm is usually implemented in a centrally controlled fashion. However, unlike WiFi or WiMax which forms a one-hop star topology, WSN are formed in a large scale, multi-hop topology which means all the algorithms should be distributed for ease of deployment. In a distributed algorithm, all the devices normally have only local information and partial information from neighbours, therefore optimisation is hard to achieve. Instead, distributed machine learning can be employed to achieve a sub-optimisation with the help from local convex optimisation and the global gradient problem formed by the Q-Learning based routing selection. The expected architecture will not only be able to increase the overall network performance but also provide differential QoS support for WSN applications with high traffic load.

## References List

- [1] G. Tolle, J. Polastre, R. Szewczyk, D. Culler, N. Turner, K. Tu, S. Burgess, T. Dawson, P. Buonadonna, and D. Gay, "A macroscope in the redwoods," in *Proceedings of the 3rd ACM International Conference on Embedded Networked Sensor Systems (Sensys)*, 2005, pp. 51-63.
- [2] A. Cerpa, J. Elson, D. Estrin, L. Girod, M. Hamilton, and J. Zhao, "Habitat monitoring: Application driver for wireless communications technology," *ACM SIGCOMM Computer Communication Review*, vol. 31, no. 2 supplement, p. 41, 2001.
- [3] K. Sukun, S. Pakzad, D. Culler, J. Demmel, G. Fenves, S. Glaser, and M. Turon, "Health Monitoring of Civil Infrastructures Using Wireless Sensor Networks," in *Proceedings of 6th International Symposium on Information Processing in Sensor Networks(IPSNS), 2007*, pp. 254-263.
- [4] M. Rahimi, R. Baer, O. I. Iroezzi, J. C. Garcia, J. Warrior, D. Estrin, and M. Srivastava, "Cyclops: in situ image sensing and interpretation in wireless sensor networks," in *Proceedings of the 3rd ACM International Conference on Embedded Networked Sensor Systems (Sensys) 2005*, p. 204.
- [5] D. Malan, T. Fulford-Jones, M. Welsh, and S. Moulton, "Codeblue: An Ad Hoc sensor network infrastructure for emergency medical care," in *Proceedings of International Workshop on Wearable and Implantable Body Sensor Networks (BSN)*, 2004.
- [6] L. Krishnamurthy, R. Adler, P. Buonadonna, J. Chhabra, M. Flanigan, N. Kushalnagar, L. Nachman, and M. Yarvis, "Design and deployment of industrial sensor networks: experiences from a semiconductor plant and the north sea," in *Proceedings of the 3rd ACM International Conference on Embedded Networked Sensor Systems (Sensys)*, 2005, p. 75.
- [7] I. Johnstone, J. Nicholson, B. Shehzad, and J. Slipp, "Experiences from a wireless sensor network deployment in a petroleum environment," in *Proceedings of ACM International Conference on Wireless Communications and Mobile Computing*, 2007, p. 387.
- [8] J. Ansari, X. Zhang, and P. Mähönen, "Multi-radio medium access control protocol for wireless sensor networks," in *Proceedings of the 5th ACM International Conference on Embedded networked sensor System (Sensys)*, 2007, p. 404.
- [9] M. Kohvakka, T. Arpinen, M. Hännikäinen, and T. D. Hämäläinen, "High-performance multi-radio WSN platform," in *Proceedings of the 2nd ACM International Workshop on Multi-hop Ad Hoc Networks*, 2006, p. 97.

- 
- [10] M. Kodialam and T. Nandagopal, "Characterizing the capacity region in multi-radio multi-channel wireless mesh networks," in *Proceedings of the 11th Annual International Conference on Mobile Computing and Networking (MobiCom)*, 2005, pp. 73-87.
- [11] A. Woo, T. Tong, and D. Culler, "Taming the underlying challenges of reliable multi-hop routing in sensor networks," in *Proceedings of the 1st International Conference on Embedded networked sensor systems (Sensys)*, 2003, pp. 14-27.
- [12] W. Ye, J. Heidemann, and D. Estrin, "Medium access control with coordinated adaptive sleeping for wireless sensor networks," *IEEE/ACM Transactions on Networking*, vol. 12, no. 3, pp. 493-506, 2004.
- [13] B.Villaverde, S.Rea, and D.Pesch, "InRout-A QoS aware route selction algorithm for industrial wireless sensor networks," *Ad Hoc Networks*, 2011.
- [14] Crossbow Technology, "Avistar RF Site Survey Report,"2007.
- [15] I. F. Akyildiz, D. Pompili, and T. Melodia, "Challenges for efficient communication in underwater acoustic sensor networks," *ACM Sigbed Review*, vol. 1, no. 2, p. 8, 2004.
- [16] IEEE Std.802.15.4 Std, "Wireless Medium Access Control (MAC) and Physical Layer (PHY) specifications for low-rate wireless personal area networks (LR-WPANs)", 2003.
- [17] Zigbee Std, "<http://www.zigbee.org/>," 2005.
- [18] 6lowpan charter, "<http://www.ietf.org/html.charters/6lowpan-charter.html>," 2011.
- [19] Wireless Hart Std, "<http://www.hartcomm.org/>," 2004.
- [20] Texas Instruments, "CC2420 Datasheet," 2008.
- [21] Atmel Co.Ltd., "AT86RF231 Datasheet," 2009.
- [22] C. Y. Wan, S. B. Eisenman, and A. T. Campbell, "CODA: congestion detection and avoidance in sensor networks," in *Proceedings of the 1st ACM International Conference on Embedded Networked Sensor Systems (Sensys)*, 2003, pp. 266-279.
- [23] B. Hull, K. Jamieson, and H. Balakrishnan, "Mitigating congestion in wireless sensor networks," in *Proceedings of the 2nd ACM International Conference on Embedded Networked Sensor Systems (Sensys)*, 2004, pp. 134-147.
- [24] C. T. Ee and R. Bajcsy, "Congestion control and fairness for many-to-one routing in sensor networks," in *Proceedings of the 2nd ACM*

---

*International Conference on Embedded Networked Sensor Systems (Sensys)*, 2004, pp. 148-161.

- [25] S. Rangwala, R. Gummadi, R. Govindan, and K. Psounis, "Interference-aware fair rate control in wireless sensor networks," in *Proceedings of the Conference on Applications, Technologies, Architectures, and Protocols for Computer Communications (SigComm)*, 2006, p. 74.
- [26] E. Gelenbe and C. H. N. Edith, "Adaptive QoS Routing for Significant Events in Wireless Sensor Networks," in *Proceedings of 5th IEEE International Conference on Mobile Ad Hoc and Sensor Systems (MASS)*, 2008.
- [27] C. Na and Y. Yang, "MRSD: Multirate-based Service Differentiation for the IEEE 802.15. 4 Wireless Sensor Network," in *Proceedings of IEEE Global Telecommunications Conference, (GLOBECOM)*, 2009.
- [28] D. Kipnis, A. Willig, J. H. Hauer, and N. Karowski, "The ANGEL IEEE 802.15. 4 enhancement layer: Coupling priority queuing and service differentiation," in *Proceedings of 14th European Wireless Conference (EW)*, 2008.
- [29] E. C. H. Ngai, E. Gelenbe, and G. Humber, "Information-aware traffic reduction for wireless sensor networks," in *34th IEEE Conference on Local Computer Networks (LCN)*, 2009, pp. 451-458.
- [30] C. Bisdikian, "On sensor sampling and quality of information: A starting point," in *Proceedings of the Fifth IEEE International Conference on Pervasive Computing and Communications*, 2007, pp. 279-284.
- [31] M. D. Jovanovic and G. L. Djordjevic, "TFMAC: Multi-channel MAC Protocol for Wireless Sensor Networks," in *Proceedings of 8th International Conference on Telecommunications in Modern Satellite, Cable and Broadcasting Services*, 2007, pp. 23-26.
- [32] T. ElBatt and A. Ephremides, "Joint scheduling and power control for wireless ad hoc networks," *IEEE Transactions on Wireless Communications*, vol. 3, no. 1, pp. 74-85, 2004.
- [33] M. a. N. T. Kodialam, "Characterizing achievable rates in multi-hop wireless networks: the joint routing and scheduling problem," in *Proceedings of the 9th ACM Annual International Conference on Mobile Computing and Networking (MobiCom)*, 2003, pp. 42-54.
- [34] M. J. Neely, E. Modiano, and C. E. Rohrs, "Dynamic power allocation and routing for time-varying wireless networks," *IEEE Journal of Selected Areas on Communications*, vol. 23, no. 1, pp. 89-103, Jan.2005.

- 
- [35] J. Redi, S. Kolek, K. Manning, C. Partridge, R. Rosales-Hain, R. Ramanathan, and I. Castineyra, "JAVeLEN - An ultra-low energy ad hoc wireless network," *Ad Hoc Networks*, vol. 6, no. 1, pp. 108-126, Jan.2008.
- [36] A. Nasipuri, J. Zhuang, and S. R. Das, "A multichannel CSMA MAC protocol for multi-hop wireless networks," in *Proceedings of IEEE Wireless Communications and Networking Conference (WCNC) 1999*, pp. 1402-1406.
- [37] A. Nasipuri and S. R. Das, "Multichannel CSMA with signal power-based channel selection for multihop wireless networks," in *Proceedings of 52nd IEEE Vehicular Technology Conference (VTC) 2000*, pp. 211-218.
- [38] M. Caccamo, L. Y. Zhang, S. Lui, and G. Buttazzo, "An implicit prioritized access protocol for wireless sensor networks," in *Proceedings of 23rd IEEE Real-Time Systems Symposium (RTSS) 2002*, pp. 39-48.
- [39] G. Zhou, C. Huang, T. Yan, T. He, J. A. Stankovic, and T. F. Abdelzaher, "MMSN: Multi-Frequency Media Access Control for Wireless Sensor Networks," in *Proceedings of 25th IEEE International Conference on Computer Communications (INFOCOM) 2006*, pp. 1-13.
- [40] J. Shi, S.Theodoros, and W. Knightly, "Starvation mitigation through multi-channel coordination in CSMA multi-hop wireless networks," in *Proceedings of the 7th ACM International Symposium on Mobile Ad Hoc Networking and Computing (MobiHoc) 2006*, pp. 214-225.
- [41] A. Kamerman and L. Monteban, "WaveLAN?II: a high-performance wireless LAN for the unlicensed band," *Bell Lab Technical Journal*, vol. 2, no. 3, pp. 118-133, 1997.
- [42] G. Holland, N. Vaidya, and P. Bahl, "A rate-adaptive MAC protocol for multi-hop wireless networks," in *Proceedings of the 7th Annual International Conference on Mobile Computing and Networking (MobiCom)*, 2001, pp. 236-251.
- [43] M. Lacage, M. H. Manshaei, and T. Turletti, "IEEE 802.11 rate adaptation: a practical approach," in *Proceedings of the 7th ACM International Symposium on Modelling, Analysis and Simulation of Wireless and Mobile Systems (MSWim)*, 2004, pp. 126-134.
- [44] M. Vutukuru, H. Balakrishnan, and K. Jamieson, "Cross-layer wireless bit rate adaptation," *ACM SIGCOMM Computer Communication Review*, vol. 39, no. 4, pp. 3-14, 2009.

- 
- [45] J. Zhang, K. Tan, J. Zhao, H. Wu, and Y. Zhang, "A practical SNR-guided rate adaptation," in *Proceedings of the 27th IEEE Conference on Computer Communications (INFOCOM)*, 2008, pp. 2083-2091.
- [46] L. J. Chen, R. Kapoor, M. Y. Sanadidi, and M. Gerla, "Enhancing Bluetooth TCP throughput via link layer packet adaptation," in *Proceedings of IEEE International Conference on Communications (ICC)*, 2004.
- [47] B. S. Kim, Y. Fang, and T. F. Wong, "Rate-adaptive MAC protocol in high-rate personal area networks," in *Proceedings of IEEE Wireless Communications and Networking Conference (WCNC) 2004*.
- [48] K. Balachandran, S. R. Kadaba, and S. Nanda, "Channel quality estimation and rate adaptation for cellular mobile radio," *IEEE Journal of Selected Areas on Communications*, vol. 17, no. 7, pp. 1244-1256, 1999.
- [49] E. Esteves, P. J. Black, and M. I. Gurelli, "Link adaptation techniques for high-speed packet data in third generation cellular systems," in *Proceedings of European Wireless Conference (EW) 2002*.
- [50] S. Lanzisera, A. M. Mehta, and K. S. J. Pister, "Reducing Average Power in Wireless Sensor Networks Through Data Rate Adaptation," in *Proceedings of IEEE International Conference on Communication (ICC) 2009*.
- [51] S. Lanzisera and K. S. J. Pister, "Theoretical and Practical Limits to Sensitivity in IEEE 802.15.4 Receivers," in *Proceedings of IEEE International Conference on Electronics Circuits and Systems (ICECS) 2007*, pp. 1344-1347.
- [52] L. Tang, K. C. Wang, Y. Huang, and F. Gu, "Radio channel characteristics of zigbee wireless sensors in machine shop for plant floor process monitoring," in *Proceedings of ASME 2006 International Manufacturing Science and Engineering Conference (MSEC)*, 2006.
- [53] J. Slipp, C. Ma, N. Polu, J. Nicholson, M. Murillo, and S. Hussain, "WINTeR: Architecture and Applications of a Wireless Industrial Sensor Network Test-bed for Radio-Harsh Environments," in *Proceedings of the IEEE Communication Networks and Services Research Conference*, 2008, pp. 422-431.
- [54] Anritsu, "Radio Frequency Interference in Hospitals," 2011.
- [55] EUROCAE ED-14E, "A Joint EUROCAE RTCA Achievement, "The European Organisation for Civil Aviation Equipment, 2005.
- [56] D. Sexton, M. Mahony, M. Lapinski, and J. Werb, "Radio channel quality in industrial wireless sensor networks," in *Proceedings of Sensor for Industry Conference 2005*.

- 
- [57] K. Remley, G. Koepke, C. Holloway, D. Camell, and C. Grosvenor, "Measurements in harsh RF propagation environments to support performance evaluation of wireless sensor networks," *Sensor Review*, vol. 29, no. 3, pp. 211-222, 2009.
- [58] D. Aguayo, J. Bicket, S. Biswas, G. Judd, and R. Morris, "Link-level measurements from an 802.11 b mesh network," in *Proceedings of the Conference on Applications, Technologies, Architectures, and Protocols for Computer Communications (SigComm)* ACM, 2004, pp. 121-132.
- [59] D. Son, B. Krishnamachari, and J. Heidemann, "Experimental study of concurrent transmission in wireless sensor networks," in *Proceedings of the 4th ACM International Conference on Embedded Networked Sensor Systems (Sensys)* 2006, p. 250.
- [60] K. Jamieson and H. Balakrishnan, "PPR: Partial packet recovery for wireless networks," in *Proceedings of the 2007 Conference on Applications, Technologies, Architectures, and Protocols for Computer Communications (SigComm)*, 2007, p. 420.
- [61] M. Senel, K. Chintalapudi, D. Lal, A. Keshavarzian, and E. J. Coyle, "A kalman filter based link quality estimation scheme for wireless sensor networks," in *Proceedings of IEEE Global Telecommunications Conference (GLOBECOM)* 2007, pp. 875-880.
- [62] D. Linden, *Handbook of batteries and fuel cells* McGraw-Hill Book Company, 1984.
- [63] C. Park, K. Lahiri, and A. Raghunathan, "Battery discharge characteristics of wireless sensor nodes: An experimental analysis," in *Proceedings of 2nd Annual IEEE Communications Society Conference on Sensor and Ad Hoc Communications and Networks (SECON)*, 2005, pp. 430-440.
- [64] R. Rozovsky and P. R. Kumar, "SEEDEX: A MAC protocol for Ad Hoc networks," in *Proceedings of the 2nd ACM International Symposium on Mobile Ad-Hoc Networking & Computing*, 2001, p. 75.
- [65] Y. Sun, O. Gurewitz, and D. B. Johnson, "RI-MAC: a receiver-initiated asynchronous duty cycle MAC protocol for dynamic traffic loads in wireless sensor networks," in *Proceedings of the 6th ACM conference on Embedded network sensor systems (Sensys)*, 2008, pp. 1-14
- [66] Y. Sun, S. Du, O. Gurewitz, and D. B. Johnson, "DW-MAC: a low latency, energy efficient demand-wakeup MAC protocol for wireless sensor networks," in *Proceedings of the 9th ACM International Symposium on Mobile Ad-Hoc Networking and Computing (MobiHoc)*, 2008, pp. 53-62.

- [67] S. Jayashree, B. S. Manoj, and C. Murthy, "On using battery state for medium access control in ad hoc wireless networks," in *Proceedings of the 10th ACM Annual International Conference on Mobile Computing and Networking (MobiCom)*, 2004, p. 373.
- [68] M. Dhanaraj, S. Jayashree, and C. S. R. Murthy, "A Novel Battery Aware MAC Protocol for Minimizing Energy x Latency in Wireless Sensor Networks," in *Proceedings of 12th International Conference on High Performance Computing (HiPC)* Springer, 2005.
- [69] Dust Networks, "<http://www.dustnetworks.com/>," 2011.
- [70] B. H. Liu, N. Bulusu, H. Pham, and S. Jha, "CSMAC: A novel DS-CDMA based MAC protocol for wireless sensor networks," in *Proceedings of IEEE Global Telecommunications Conference Workshops*, 2004.
- [71] H. Steendam and M. Moeneclaey, "The Effect of Carrier Frequency Offsets on Downlink and Uplink MC-DS-CDMA," *IEEE Journal on Selected Areas in Communications*, vol. 19, no. 12, pp. 2528-2536, 2001.
- [72] J. Deng, Y. S. Han, and Z. J. Haas, "Analyzing split channel medium access control schemes," *IEEE Transactions on Wireless Communications*, vol. 5, no. 5, pp. 967-971, 2006.
- [73] Y. S. Han, J. Deng, and Z. J. Haas, "Analyzing multi-channel medium access control schemes with ALOHA reservation," *IEEE Transactions on Wireless Communication*, vol. 5, no. 8, pp. 2143-2152, 2006.
- [74] R. Haas and J. C. Belfiore, "A Time-Frequency Well-localized Pulse for Multiple Carrier Transmission," *Wireless Personal Communications*, vol. 5, no. 1, pp. 1-18, 1997.
- [75] P. H. Moose, "A technique for orthogonal frequency division multiplexing frequency offset correction," *IEEE Transactions on Communications*, vol. 42, no. 10, pp. 2908-2914, 1994.
- [76] T. M. Schmidl and D. C. Cox, "Robust frequency and timing synchronization for OFDM," *IEEE Transactions on Communications*, vol. 45, no. 12, pp. 1613-1621, 1997.
- [77] I. Kanaras, A. Chorti, M. R. D. Rodrigues, and I. Darwazeh, "Spectrally Efficient FDM Signals: Bandwidth Gain at the Expense of Receiver Complexity," in *Proceedings of IEEE International Conference on Communication (ICC)*, 2009, pp. 1-6.
- [78] T. Ihalainen, Y. Yuan, and M. Renfors, "Filter bank based frequency-domain equalizers with diversity combining," in *Proceedings of IEEE International Symposium on Circuits and Systems (ISCAS)* 2008, pp. 93-96.

- [79] H. H. Nguyen, "Effect of chip waveform shaping on the performance of multicarrier CDMA systems," *IEEE Transactions on Vehicular Technology*, vol. 54, no. 3, pp. 1022-1029, 2005.
- [80] H. Nikookar, B. G. Negash, "Frequency offset sensitivity reduction of multi-carrier transmission by wave-shaping," in *Proceedings of IEEE International Conference on Personal Wireless Communications*, 2000, pp. 444-448.
- [81] W. Kozek and A. F. Molisch, "Non-orthogonal pulse-shapes for multicarrier communications in doubly dispersive channels," *IEEE Journal on Selected Areas in Communications*, vol. 16, no. 8, pp. 1579-1589, 1998.
- [82] R. Chandra, R. Mahajan, T. Moscibroda, R. Raghavendra, and P. Bahl, "A case for adapting channel width in wireless networks," *ACM SIGCOMM Computer Communication Review*, vol. 38, no. 4, pp. 135-146, 2008.
- [83] H. G. Myung, J. Lim, and D. J. Goodman, "Single carrier FDMA for uplink wireless transmission," *IEEE Vehicular Technology Magazine*, vol. 1, no. 3, pp. 30-38, 2006.
- [84] L. Xinhua, C. Yu, J. W. Mark, and S. Xuemin, "A Renewal Theory Based Analytical Model for the Contention Access Period of IEEE 802.15.4 MAC," *IEEE Transactions on Wireless Communications*, vol. 7, no. 6, pp. 2340-2349, 2008.
- [85] G. Bianchi, "Performance analysis of the IEEE 802.11 distributed coordination function," *IEEE Journal on Selected Areas in Communications*, vol. 18, no. 3, pp. 535-547, 2000.
- [86] V. I. Istratescu, *Fixed point theory an introduction*, 7 ed Dordrecht, Holland, 1982.
- [87] Y. Yang and T. S. P. Yum, "Delay distributions of slotted ALOHA and CSMA," *IEEE Transactions on Communications*, vol. 51, no. 11, pp. 1846-1857, Nov.2003.
- [88] F. Qin, Y. Yang, and J. Mitchell, "Performance Increase Through the Use of Multiple Sub-carriers in WSN," in *Proceedings of 7th ACM International Symposium on Mobility Management and Wireless Access (MobiWAC) 2009*.
- [89] S. J. Kim, X. D. Wang, and M. Madhian, "Optimal resource allocation in multi-hop OFDMA wireless networks with cooperative relay," *IEEE Transactions on Wireless Communications*, vol. 7, no. 5, pp. 1833-1838, May2008.
- [90] G. Lin, W. Xinbing, and X. Youyun, "Multi-radio Channel Allocation in Multi-hop Wireless Networks," *IEEE Transactions on Mobile Computing*, vol. 8, no. 11, pp. 1454-1468, 2009.

- 
- [91] D. O'Rourke, S. Fedor, C. Brennan, and M. Collier, "Reception region characterisation using a 2.4 GHz direct sequence spread spectrum radio," in *Proceedings of the 4th ACM Workshop on Embedded Networked sensors*, 2007, p. 72.
- [92] M. Petrova, J. Riihijarvi, P. Mahonen, and S. LaBell, "Performance study of IEEE 802.15. 4 using measurements and simulations," in *Proceedings of IEEE Wireless Communications and Networking Conference (WCNC)*, 2006, pp. 487-492.
- [93] M. Sha, G. Xing, G. Zhou, S. Liu, and X. Wang, "C-MAC: Model-driven concurrent medium access control for wireless sensor networks," in *Proceedings of the 28th Annual IEEE International Conference on Computer Communications (INFOCOM)*, 2009.
- [94] M. Schmidt and F. Poegel, "A Low-Complexity 802.15. 4 Digital Receiver Front End," in *Proceedings of IEEE International Conference on Communications (ICC)*, 2006.
- [95] W. Kluge, F. Poegel, H. Roller, M. Lange, T. Ferchland, L. Dathe, D. Eggert, and D. Atmel, "A Fully Integrated 2.4-GHz IEEE 802.15. 4-Compliant Transceiver for ZigBee Applications," *IEEE Journal of Solid-State Circuits*, vol. 41, no. 12, pp. 2767-2775, 2006.
- [96] J. G. Proakis and M. Salehi, *Digital communications* McGraw-hill New York, 1995.
- [97] J. Notor, A. Caviglia, and G. Levy, "CMOS RFIC architectures for IEEE 802.15.4 networks," *Cadence Design Systems, Inc*, 2003.
- [98] B. Sklar, "Defining, designing, and evaluating digital communication systems," *IEEE Communications Magazine*, vol. 31, no. 11, pp. 91-101, 1993.
- [99] J. Polastre, J. Hill, and D. Culler, "Versatile low power media access for wireless sensor networks," in *Proceedings of the 2nd International Conference on Embedded Networked Sensor Systems (SenSys)* 2004, pp. 03-05.
- [100] D. Eggert, S. Beyer, and F. Poegel, "IEEE 802.15.4 Systems and Related Propagation Characteristics," in *Atmel European Develop Conference*, 2008.
- [101] L. Tang, K. C. Wang, Y. Huang, and F. Gu, "Channel characterization and link quality assessment of IEEE 802.15. 4-compliant radio for factory environments," *IEEE Transactions on Industrial Informatics*, vol. 3, no. 2, pp. 99-110, 2007.
- [102] M. Vutukuru, K. Jamieson, and H. Balakrishnan, "Harnessing exposed terminals in wireless networks," in *Proceedings of the 5th USENIX Symposium on Networked Systems Design and Implementation*, 2008, pp. 59-72.

- 
- [103] A. Acharya, A. Misra, and S. Bansal, "Design and analysis of a cooperative medium access scheme for wireless mesh networks," in *Proceedings of 1st International Conference on Broadband Networks (BroadNets) 2004*.
- [104] K. Langendoen, A. Baggio, and O. Visser, "Murphy loves potatoes: Experiences from a pilot sensor network deployment in precision agriculture," in *Proceeding of 20th IEEE International Parallel and Distributed Processing Symposium*, 2006, p. 8.
- [105] S. Kannan and L. Philip, "RSSI is under appreciated," in *Proceedings of the 3rd Workshop on Embedded Networked Sensors, Cambridge, Massachusetts: Harvard University*, 2006, pp. 1-5.
- [106] C. B. Peel and A. L. Swindlehurst, "Effective SNR for space-time modulation over a time-varying Rician channel," *IEEE Transactions on Communications*, vol. 52, no. 1, pp. 17-23, 2004.
- [107] S. He and M. Torkelson, "Effective SNR estimation in OFDM system simulation," in *Proceedings of IEEE Global Telecommunications Conference*, 1998.
- [108] K. Sasloglou, I. A. Glover, P. Dutta, R. Atkinson, I. Andonovic, and G. Whyte, "A Channel Model for Wireless Sensor Networks in Gas Turbine Engines," in *Loughborough Antennas & Propagation Conference*, 2009.
- [109] M. Zuniga and B. Krishnamachari, "Analyzing the transitional region in low power wireless links," in *Proceedings of 1st IEEE Conference on Sensor and Ad Hoc Communications and Networks (SECON) 2004*, pp. 517-526.
- [110] G. Judd, X. Wang, and P. Steenkiste, "Efficient channel-aware rate adaptation in dynamic environments," in *Proceedings of the 6th International Conference on Mobile Systems, Applications, and Services (MobiSys) ACM*, 2008, pp. 118-131.
- [111] S. Mangold, Z. Zhong, G. R. Hiertz, and B. Walke, "IEEE 802.11 e/802.11 k wireless LAN: spectrum awareness for distributed resource sharing," *Wireless Communications and Mobile Computing*, vol. 4, no. 8, pp. 881-902, 2004.
- [112] Carlo Alberto Boano, Marco Antonio Zúñiga, Thiemo Voigt, Andreas Willig, and ay Romer, "The Triangle Metric: Fast Link Quality Estimation for Mobile Wireless Sensor Networks," in *Proceedings of 19th International Conference on Computer Communications and Networks (ICCCN)*, 2010, pp. 1-7.
- [113] L.Ljung, *System Identification: Theory for the User*, 2ed, Prentice Hall PTR, 2010.

- 
- [114] R. E. Kalman, "A new approach to linear filtering and prediction problems," *Journal of basic Engineering*, vol. 82, no. 1, pp. 35-45, 1960.
- [115] X. Dai, Z. Gao, T. Breikin, and H. Wang, "Estimation Delay Compensation in High-gain Observer-based Parameter Identification," in *Proceedings of the 48th IEEE Conference on Decision and Control (CDC) 2009*, pp. 8212-8217.
- [116] E. Callaway, "Low Power Consumption Features of the IEEE 802.15.4/ZigBee LR-WPAN Standard," *Mini-tutorial, ACM Sensys*, 2003.
- [117] C. F. Chiasserini and R. R. Rao, "Improving battery performance by using traffic shaping techniques," *IEEE Journal on Selected Areas in Communications*, vol. 19, no. 7, 2001.
- [118] C. F. Chiasserini and R. R. Rao, "Energy efficient battery management," *IEEE Journal on Selected Areas in Communications*, vol. 19, no. 7, 2001.
- [119] C.Chau, F.Qin, S.Samir, M.Wahab, and Y.Yang, "Harnessing Battery Recovery Effect in Sensor Networks: Experiments and Analysis," *IEEE Journal on Selected Areas in Communications*, vol. 28, no. 7, 2010.